Titre: Title:	Dynamique d'écoulement et pellétisation dans un granulateur à rotor
Auteur: Author:	Jonathan Bouffard
Date:	2012
Type:	Mémoire ou thèse / Dissertation or Thesis
Référence: Citation:	Bouffard, J. (2012). Dynamique d'écoulement et pellétisation dans un granulateur à rotor [Thèse de doctorat, École Polytechnique de Montréal]. PolyPublie. https://publications.polymtl.ca/723/

UNIVERSITÉ DE MONTRÉAL

DYNAMIQUE D'ÉCOULEMENT ET PELLÉTISATION DANS UN GRANULATEUR À ROTOR

JONATHAN BOUFFARD

DÉPARTEMENT DE GÉNIE CHIMIQUE

ÉCOLE POLYTECHNIQUE DE MONTRÉAL

THÈSE PRÉSENTÉE EN VUE DE L'OBTENTION

DU DIPLÔME DE PHILOSOPHIAE DOCTOR (Ph.D.)

(GÉNIE CHIMIQUE)

JANVIER 2012

UNIVERSITÉ DE MONTRÉAL

ÉCOLE POLYTECHNIQUE DE MONTRÉAL

Cette thèse intitulée:

DYNAMIQUE D'ÉCOULEMENT ET PELLÉTISATION DANS UN GRANULATEUR À ROTOR

présentée par : BOUFFARD Jonathan

en vue de l'obtention du diplôme de : Philosophiae Doctor

a été dûment acceptée par le jury d'examen constitué de :

M.LEGROS Robert, Ph.D., président

M.CHAOUKI Jamal, Ph.D., membre et directeur de recherche

M.BERTRAND François, Ph.D., membre et codirecteur de recherche

M.TAVARES Jason R., Ph.D., membre

M.BRITO DE LA FUENTE Edmundo, Ph.D., membre

Une découverte consiste à voir ce que tout le monde a vu et de penser à ce que personne n'a pensé.

Albert Szent-Györgi

Dans les champs de l'observation, le hasard ne favorise que les esprits préparés.

Louis Pasteur

À mes parents

REMERCIEMENTS

Je remercie mes directeurs de thèse, Jamal Chaouki et François Bertrand, pour m'avoir donné l'opportunité de collaborer avec eux au sein de leur groupe de recherche, ainsi que pour m'avoir encouragé tout au long de la poursuite de mes travaux. Leurs conseils judicieux m'ont permis d'amener ma réflexion un peu plus loin non seulement sur cette thèse, mais sur bien d'autres sujets.

Je tiens aussi à remercier mon ancien superviseur chez Merck Frosst, Hubert Dumont, pour m'avoir offert un stage il y a de cela quelques années au sein du groupe PR&D. C'est l'événement déclencheur qui m'a poussé à entreprendre ce doctorat.

J'aimerais remercier les membres du département de Génie Chimique qui m'ont fait assez confiance pour contribuer aux activités d'enseignement, une expérience enrichissante. Gino Robin, Martine Lamarche, Jean Huard, Daniel Dumas et Robert Deslisle, merci pour votre aide précieuse. La contribution d'un collègue, Alexandre Cabana, ainsi que de la professeure Suzanne Giasson doit aussi être mentionnée pour l'obtention de certaines données expérimentales.

Bien entendu, tout cela aurait été bien moins captivant sans la présence de Jocelyn Doucet, Olivier Dubé, Marc Lemieux, Louis-Alexandre Leclaire et Jean-Philippe Laviolette, des collègues mais bien avant tout des amis.

Je tiens aussi à dire merci à Nadia et Pascal avec qui j'ai passé plusieurs moments agréables et, peut-être sans qu'ils ne le sachent, m'auront aidé à conserver ma motivation durant ces études qui maintenant arrivent à leur aboutissement.

Finalement, je remercie les membres de ma famille qui m’ont toujours supporté et encouragé et sans qui tout ce cheminement parcouru jusqu’à aujourd’hui aurait été sûrement beaucoup plus difficile.

La thèse a été financée en partie par une bourse de doctorat (ES-II) du conseil de recherche en science naturelle et génie (CRSNG) ainsi qu’avec la collaboration de Merck et Ratiopharm pour l’obtention de matériel et d’équipements.

RÉSUMÉ

Cette thèse propose différentes approches permettant de quantifier l'évolution de la dynamique d'écoulement particulaire dans un procédé de granulation et évaluer son impact sur celui-ci. Plusieurs types d'équipement permettent d'effectuer la granulation. Pour ce travail, un granulateur à rotor a été sélectionné puisqu'il permet de produire un écoulement de particules relativement simple à caractériser. Le choix de ce granulateur a aussi été basé sur le fait qu'il a été très peu étudié par rapport aux mélangeurs à cisaillement élevé ou les lits fluidisés. Le sujet de cette thèse est approché selon trois angles différents :

- La caractérisation et la quantification des patrons d'écoulement et de ségrégation particulaire dans un sphéroniseur modifié (granulateur à rotor);
- Le développement d'une méthode originale qui permet de contrôler l'intensité des forces interparticulaires dans un écoulement de particules à l'intérieur d'un sphéroniseur modifié;
- Le développement d'un modèle multi-échelle prenant en compte le mouvement des particules afin de prédire la distribution de taille granulaire dans un procédé de granulation à rotor.

Dans un premier temps, l'étude d'un écoulement dense d'un mélange de particules de 2 et 4 mm dans un sphéroniseur est effectuée. Pour y arriver, l'emploi d'une méthode par éléments discrets (DEM), une méthode numérique basée sur la seconde loi de Newton, permet de caractériser le déplacement des particules à l'intérieur de l'équipement. Le mélange des particules est analysé à l'aide d'indices de mélange ayant été développés par Doucet et al. (2008) afin de caractériser la ségrégation se produisant dans le domaine de particules. Cette partie du travail permet de montrer que le niveau de remplissage ainsi que la vitesse du disque (rotor) ont un effet significatif sur le phénomène de ségrégation observé. Pour des vitesses de disque variant entre 20 et 100 rad/s, le lit de particules prend la forme d'un tore où deux zones distinctes de ségrégation sont apparentes. Au fur et à mesure que la vitesse du disque augmente, les petites particules ont tendance à migrer de la zone localisée au centre du domaine toroïdal vers la deuxième zone localisée à la paroi du

sphéroniseur. Les coefficients de corrélation spatiale employés pour le calcul de l'indice de mélange corroborent cette migration des petites particules. De plus, l'importance de prendre en compte l'intensité du cisaillement pour expliquer ces patrons de ségrégation est aussi exposée. Les deux zones de ségrégation associées à une concentration élevée de petites particules correspondent à l'emplacement où les taux de cisaillement sont les plus faibles. D'un autre côté, une corrélation considérant le niveau de cisaillement est développée afin de prédire le profil des vitesses azimutales des particules dans le sphéroniseur. Cette corrélation permet d'améliorer sensiblement la prédiction des profils de vitesses lorsque l'intensité du cisaillement est élevée.

La deuxième partie de cette thèse présente le développement d'une nouvelle approche qui permet de simplifier l'introduction et le contrôle des forces interparticulaires de manière homogène dans un lit de particules en mouvement. Cette approche utilise un copolymère de PEA/PMMA qui, lorsqu'il est soumis à une augmentation de température au-dessus de sa température de transition vitreuse, cause l'apparition de forces cohésives entre des particules qui en sont enrobées. La relation entre les forces interparticulaires induites par le copolymère et l'écoulement des particules enrobées est établie avec l'aide d'un appareil de mesure de surface, plus communément appelé *surface force apparatus* (SFA). Cet équipement met en évidence l'augmentation linéaire des forces interparticulaires entre 10°C et 50°C. Les forces interparticulaires induites par cette nouvelle approche, comparées avec d'autres types de forces fréquemment rencontrées dans les procédés de granulation, permet de mettre en valeur la large étendue d'intensité de cohésion pouvant être obtenues. Par la suite, l'écoulement de particules cohésives est étudié pour deux applications différentes. La première application considère un écoulement dense de particules normalement observé pendant la granulation humide à l'intérieur d'un sphéroniseur modifié. La deuxième application montre la possibilité de pouvoir reproduire l'écoulement des particules observées dans les lits fluidisés à haute température avec l'avantage de pouvoir les opérer près de la température ambiante.

La troisième partie de cette thèse utilise spécifiquement la méthode d'introduction des forces interparticulaires précédemment proposée afin de caractériser les écoulements de particules cohésives dans un sphéroniseur modifié. En contrôlant le niveau d'intensité des forces

interparticulaires, quatre différents états d'écoulement sont obtenus. Le premier état est caractérisé par un écoulement libre des particules, lequel est observé près de la température ambiante. Le deuxième état est associé à l'apparition d'agglomérats à la surface du lit de particules, lesquels augmentent de taille à mesure que la température est haussée. Le troisième état fait référence à la formation d'une seconde couche de particules agglomérées dont le volume change de manière périodique en fonction du temps. Le quatrième état est caractérisé par un écoulement en masse produit par l'agglomération quasiment complète des particules. L'emploi d'un profileur laser permet de quantifier les différents états d'écoulement en mesurant la forme du tore obtenu ainsi que la variabilité de la position du profil de la surface du lit de particules. À la suite des résultats obtenus, un diagramme des états d'écoulement est construit. Ce diagramme montre le potentiel de cette approche pour imiter les écoulements cohésifs propres aux procédés de granulation humide. En conséquence, il est recommandé que la granulation humide soit opérée dans des conditions permettant d'obtenir le deuxième état d'écoulement décrit précédemment. Ceci est expliqué par le fait que les forces interparticulaires permettent d'induire la formation d'agglomérats sans toutefois nuire au mélange granulaire qui est essentiel pour obtenir un produit homogène.

La quatrième partie de cette thèse utilise un modèle multi-échelle qui fait intervenir un bilan de population résolu à l'aide d'une méthode de Monte-Carlo commandée par événement. Ce bilan de population est utilisé pour simuler la granulation humide dans un sphéroniseur modifié. Il prend en compte l'échelle particulaire en considérant trois mécanismes de granulation qui sont le mouillage des particules, la coalescence et le bris. D'autre part, à l'échelle du granulateur, l'intégration du mouvement granulaire est prise en compte à l'aide d'une compartimentation du lit de particules. À l'aide d'une approche utilisant une chaîne de Markov à temps continu, les mouvements de particules entre les zones peuvent alors être considérés. La construction des propriétés de la chaine de Markov, soient le temps de séjour dans les zones et la matrice indiquant la probabilité de transition des particules entre celles-ci, est effectuée grâce aux résultats ayant été obtenus à l'aide de la DEM dans la première partie de cette thèse. Une fois le modèle multi-échelle mis en place, celui-ci est comparé à un modèle utilisant un bilan de population qui ne tient pas compte du déplacement des particules. Les résultats de simulation obtenus sont comparés aux expériences de granulation afin de voir les améliorations obtenues

avec le modèle multi-échelle. Il apparaît que pour des conditions où le taux de mouillage est modéré, la considération du mouvement des particules permet d'améliorer les résultats de la modélisation. La distribution de taille des particules en fonction du temps correspond mieux à la tendance observée expérimentalement qu'avec un bilan de population conventionnel. Par contre, pour un taux de mouillage élevé, le modèle multi-échelle et le bilan de population conventionnel donnent sensiblement les mêmes résultats.

ABSTRACT

This thesis proposes different approaches to quantify particle flow dynamics effects for granulation processes. Different types of granulation equipment exist. The rotor granulator has been selected for the simplicity of its design which produces easy to characterize particle flow patterns. The rotor granulator has also several advantages of the high shear mixers and fluid bed granulators but it has not been extensively covered in the literature compared to these granulators. The particle flow dynamics in the rotor granulator is investigated following three different points of view:

- The characterization and quantification of the flow and segregation patterns in a modified spheronizer, which is similar to a rotor granulator;
- The development of a new approach to control the intensity of the interparticle forces within the particle flow inside a modified spheronizer;
- The development of a multiscale model which takes into account the motion of particles in order to predict the particle size distribution during granulation with a modified spheronizer.

The first part of this thesis studies the dense granular flow of a 2 and 4 mm particle blend inside a spheronizer. The use of the discrete element method (DEM), a particulate model that can simulate the particle motion based on Newton's second law of motion, allows characterizing the particle flow behavior inside the equipment. The particle mixedness state is assessed with the help of mixing indexes that have been developed by Doucet et al. (2008) in order to quantify the segregation occurring inside the particle bed. This study shows that the fill level and the disc rotational speed have a significant impact on the segregation phenomena observed. For a disc speed varying between 20 and 100 rad/s, the particle bed takes the form of a torus within which two distinct segregation zones are observed. As the disc speed increases, the small particles tend to migrate from a zone located at the center of the torus toward another zone which is observed near the spheronizer wall. This transfer of small particles is confirmed by the coefficients of correlation used by the mixing index, which relate the particle size and spatial coordinates.

Moreover, the distribution of the shear rate in the particle domain explains the appearance of the segregation patterns. The two zones characterized by a high concentration of the smallest particles are correlated with the areas of the particle bed associated to a low shear rate. On the other hand, a correlation which considers the shear rate was developed to predict the azimuthal speed of the particles inside the spheronizer. This correlation improves the velocity profile predictions when the particle flow is characterized by high shear rate values.

The second part of this thesis develops a new approach to incorporate and control interparticle forces homogeneously in the context of particle flow applications. This approach uses particles coated with a PEA/PMMA copolymer. When submitted to an increase of temperature above the copolymer glass transition state, the interparticle forces increase. A relationship between the interparticle forces created by the copolymer and the flow of coated particles is characterized with a surface force apparatus (SFA). This equipment shows that the cohesion forces increase linearly when the temperature in incremented from 10°C to 50°C. The interparticle forces obtained are in the same range as other common forces encountered frequently in granulation processes such as the capillary and the van der Waals forces. The flow behavior of the cohesive coated particles is applied to two different applications. The first application considers a dense particle flow normally encountered during a wet granulation with a modified spheronizer. The second application shows the possibility to mimic the particle flow behavior that would be obtained in high temperature fluidized beds but with the advantage of operating them near ambient conditions.

The third part of this work uses the polymer coating approach proposed in the second part of the thesis to characterize the flow behavior of cohesive particles inside a modified spheronizer. By controlling the level of intensity of interparticle forces with the increase of temperature, four different flow states are observed. The first state is characterized by a free-flowing behavior of the particles, which is observed near ambient temperature. The second flow state is associated with the appearance of agglomerates at the surface of the torus of particles. These agglomerates increase in size as the temperature is incremented within this state. The third flow state refers to the appearance of a secondary layer formed by agglomerated particles the volume of which

changes periodically with respect to time. The fourth state is characterized by a solid mass motion of the particle bed which is produced following the complete agglomeration of the particles. The use of a laser profiler helps to quantify the particle flow behavior observed for the different flow states by measuring the torus shape obtained and the variability associated with the surface profile position. These results help to construct a flow map representing the different flow behaviors observed. The flow map shows the potential use of the polymer coating approach to mimic the interparticle forces observed in wet granulation applications. Based on this flow map, it is shown that it is preferable to operate the wet granulation processes within the second flow state. This is explained by the fact that interparticle forces in this flow state induce the formation of agglomerates without preventing a good particle mixedness state that ensures the production of a uniform product.

The fourth part of this thesis develops of a multiscale model based on an event-driven Monte-Carlo based population balance. It is used to simulate wet granulation in a modified spheronizer. The model takes into account the particle scale with three different granulation mechanisms, which are the wetting, the coalescence and the breakage of the particles. On the other hand, the granulator scale integrates the particle motion with a compartmental approach which divides the particle bed into different zones, each of which is associated with a granulation mechanism. The use of a continuous-time Markov chain allows representing the motion of the particles between the different zones. The properties of the Markov chain, which are the residence time in the different zones and the matrix containing the probabilities of transition between the zones, are built with the DEM simulation results of the particle flow in the spheronizer presented in the first article. Once the multiscale model is defined, it is compared to a conventional population balance that does not take into account particle motion. These two population balance models are then tested against granulation experiments with the modified spheronizer. The results show that for a low spray rate, the multiscale model improves results obtained with the conventional population balance without motion. On the other hand, the multiscale model and the conventional population balance give similar results when the spray rate is high. In this case, the granulation mechanisms overcome the effect of the particle flow pattern and the advantage of the proposed multiscale model is less apparent.

TABLE DES MATIÈRES

LISTE DES TABLEAUX

LISTE DES FIGURES

LISTE DES SIGLES ET ABRÉVIATIONS

Chapitre 2

a	Rayon d'une particule (m)
	Flux de surface des particules (m^{-2})
A_H	Constante d'Hamaker (J)
	Nombre de particule formée suite au mécanisme de bris (m^{-3})
	Noyau de bris (s^{-1})
	Constante du taux de consolidation (s^{-1})
	Diamètre des gouttelettes (m)
	Moyenne harmonique du diamètre des particules (m)
	Coefficient de restitution
	Module de Young (MPa)
	Module de Young ajusté (MPa)
	Composante normale de la force appliquée sur la particule (N)
	Composante tangentielle de la force appliquée sur la particule (N)
F_{cap}	Force capillaire (N)
F_{VdW}	Force de van der Waals (N)
	Taux d'entrée des particules dans le domaine (s^{-1})

Taux de sortie des particules dans le domaine (s^{-1})

Constante gravitationnelle ($m\ s^{-2}$)

h Distance de séparation particulaire (m)

Dimension caractéristique des aspérités de surface (m)

Épaisseur de la couche de liquide liant (m)

Moment d'inertie de la particule ($kg\ m^2$)

Noyau de nucléation ($m^{-6}\ s^{-1}$)

Nombre de concentration particulaire par intervalle de volume (m^{-6})

Masse de la particule (kg)

Moyenne harmonique de la masse des particules (kg)

Probabilité de créer une particule suite au mécanisme de bris

Rayon de la particule (m)

Rayon des pores des particules (m)

Saturation maximale des pores

Nombre de déformation de Stokes

Nombre de déformation de Stokes maximal

Nombre de viscosité de Stokes

Nombre de viscosité de Stokes maximal

Temps (s)

Temps de circulation des particules (s)

Vitesse relative initiale des particules (m s^{-1})

Volume d'une particule fictive (m^3)

Débit volumétrique du liant (m^3 s^{-1})

Volume de gouttelettes (m^3)

Ratio de la masse de liquide sur la masse de solide granulaire

Position de la particule

Y Position de l'interface du pont capillaire (m)

Contrainte de cisaillement limite (MPa)

Lettres grecques

Noyau d'agglomération (m^3 s^{-1})

Taux de cisaillement (s^{-1})

Tension de surface (N m^{-1})

Volume de la particule générée suite à la nucléation (m^3)

Δp Pression de Laplace (Pa)

Déformation plastique permanente (m)

Porosité des granules

Porosité minimale des granules

Porosité du lit de granule

Indice d'écoulement

Angle de contact dynamique

θ Angle de contact

Viscosité du liquide liant (Pa s)

Masse volumique du liquide liant (kg m^{-3})

Masse volumique du solide granulaire (kg m^{-3})

Couple de résistance au roulement de la particule par rapport à (kg m^2 s^{-2})

Temps de pénétration adimensionnel des gouttelettes

Facteur de contrainte (MPa)

Ratio de Poisson

ϕ Position polaire du point de contact du pont liquide

Flux d'atomisation adimensionnel

Vitesse angulaire de la particule (s^{-1})

Chapitre 5

Constantes de régression

Composante normale de la force appliquée sur la particule (N)

Composante tangentielle de la force appliquée sur la particule (N)

Constante gravitationnelle ($m\ s^{-2}$)

Hauteur dans le tore (m)

Moment d'inertie de la particule ($kg\ m^2$)

Masse de la particule (kg)

Probabilité de mesure

Position radiale dans le tore (m)

Position de la surface du tore (m)

Rayon du sphéroniseur (m)

Rayon de la particule (m)

Temps (s)

Ensemble des propriétés particulaires

Vitesse azimutale adimensionnelle

Vitesse azimutale des particules ($m\ s^{-1}$)

Position de la particule

Lettres grecques

Taux de cisaillement (s^{-1})

Tenseur adimensionnel de cisaillement (s^{-1})

Position radiale adimensionnelle (m)

Couple de résistance au roulement de la particule par rapport à ($kg\ m^2\ s^{-2}$)

Hauteur adimensionnelle

Vitesse de rotation du disque (s^{-1})

Vitesse angulaire de la particule (s^{-1})

Chapitre 6 et Chapitre 7

a	Rayon d'une particule (m)
A_H	Constante d'Hamaker (J)
	Champ magnétique ($kg\ s^{-1}\ C^{-1}$)
Bo	Nombre de Bond
	Constante de régression
De	Nombre de Deborah
	Coefficient de diffusion de la reptation ($m^2\ s^{-1}$)
	Module de Young (MPa)
	Force d'adhésion (N)
F_{cap}	Force capillaire (N)
F_{mag}	Force magnétique (N)

F_P	Force de séparation interfaciale (N)
F_{VdW}	Force de van der Waals (N)
h	Distance de séparation particulaire (m)
h_0	Épaisseur initiale de la couche de polymère (m)
	Masse d'une particule (kg)
	Rayon des particules et (m)
	Rayon de giration des chaines de polymère (m)
	Température (°C)
	Temps de contact (s)
	Vitesse de séparation des particules (m s^{-1})
	Vitesse de collision normale des particules (m s^{-1})
	Énergie d'adhésion (N m^{-1})
	Énergie d'adhésion maximale (N m^{-1})
Y	Position de l'interface du pont capillaire (m)

Lettres grecques

	Taux de cisaillement (s^{-1})
Δp	Pression de Laplace (Pa)
	Perte de charge mesurée et perte de charge théorique (Pa)

Déformation maximale (m)

θ Angle de contact

Constante magnétique (kg m A^{-2} s^{-2})

Perméabilité magnétique du fluide (kg m A^{-2} s^{-2})

Perméabilité magnétique des particules (kg m A^{-2} s^{-2})

Masse volumique de la particule (kg m^{-3})

Contrainte sur la couche de polymère (Pa)

Temps de reptation (s)

Ratio de Poisson

ϕ Position polaire du point de contact du pont liquide

Flux d'atomisation adimensionnel

Vitesse angulaire de la particule (s^{-1})

Chapitre 8

Nombre de particules formées suite au mécanisme de bris (m^{-3})

Noyau de bris (s^{-1})

Constante du noyau de bris (s^{-1})

Distribution cumulative des temps de résidence

Composante normale de la force appliquée sur la particule (N)

Composante tangentielle de la force appliquée sur la particule (N)

Taux d'entrée des particules dans le domaine (s^{-1})

Taux de sortie des particules dans le domaine (s^{-1})

Constante gravitationnelle ($m\ s^{-2}$)

Moment d'inertie de la particule ($kg\ m^2$)

Noyau de nucléation ($m^{-6}\ s^{-1}$)

Nombre de concentration particulaire par intervalle de volume (m^{-6})

Taux d'addition des gouttelettes (s^{-1})

Nombre de particules fictives

Masse de la particule pour la DEM (kg)

Masse de liquide dans la particule pour la PBM (kg)

Masse du lit de particules réelles (kg)

Nombre de particules réelles initial

Ratio du nombre de particules contenant un nombre de particules primaires

Nombre de particules en mouvement simultané

Matrice des probabilités de transition entre les zones

Probabilité d'occurrence d'un événement

Ratio du volume d'une particule par rapport au volume d'une particule

primaire

Nombre aléatoire de distribution uniforme entre 0 et 1

Fréquence d'un événement à l'itération (s^{-1})

Fréquence de l'événement mouillage (s^{-1})

Fréquence de l'événement coalescence (s^{-1})

Fréquence de l'événement bris (s^{-1})

Fréquence de l'événement de déplacement des particules (s^{-1})

Taux de bris (s^{-1})

Temps (s)

Temps de résidence (s)

Volume d'une particule fictive (m^3)

Volume de la plus petite particule fictive permise (m^3)

Volume moyen des particules (m^3)

Volume adimensionnel des particules

Volume adimensionnel des particules en régime permanent

Volume du domaine simulé (m^3)

Nombre de particules réelles représentées par une particule fictive

Position de la particule

Lettres grecques

Noyau d'agglomération ($m^3\ s^{-1}$)

Noyau EKE ($m^{0.5}$)

Constante du noyau EKE ($m^{2.5}.s^{-1}$)

Probabilité de créer une particule suite au mécanisme de bris

Volume de la particule générée suite à la nucléation (m^3)

Fréquence de visite d'une particule (s^{-1})

Masse volumique des gouttelettes ($kg\ m^{-3}$)

Temps caractéristique de bris (s)

Temps caractéristique de coalescence (s)

Couple de résistance au roulement de la particule par rapport à ($kg\ m^2\ s^{-2}$)

Pas de temps pour l'itération (s)

Ratio de saturation en liquide

Ratio critique de saturation en liquide

CHAPITRE 1 INTRODUCTION

1.1 Les procédés de granulation

La granulation, aussi appelé pellétisation, est le nom générique désignant un processus qui consiste à élargir la taille de particules en les fusionnant par le biais de différentes approches. Les domaines miniers, agroalimentaires, plasturgiques et pharmaceutiques utilisent la granulation afin d'en tirer les mêmes avantages : prévenir la ségrégation d'un mélange de poudre, améliorer les propriétés d'écoulement et atténuer les risques potentiels (pertes de matériel, inhalation ou explosions) associés à la présence de poussières fines (Iveson, 2002; A. D. Salman, Hounslow, & Seville, 2007). Le concept de granulation couvre un champ très large de méthodes qui ont été regroupées en classes (Sherrington & Oliver, 1981) comme indiquées dans la Figure 1-1. Ces classes peuvent être regroupées en les qualifiant de méthode de granulation sèche (compression, nodulisation et frittage) ou de méthodes de granulation humides (extrusion, agglomération et globulation). Le choix d'une méthode de granulation dépend de différents critères. Le mode d'opération (cuvée ou continu), la méthode de croissance pouvant être utilisée (sèche ou humide), l'espace et les besoins énergétiques requis, les propriétés des particules alimentées ainsi que les caractéristiques du produit final en sont quelques exemples (Pietsch, 2002).

Les procédés recourant à l'agitation d'un mélange de poudre, combiné à l'agglomération particulaire, sont fréquemment utilisés en industrie. Cette classe de granulation nécessite l'utilisation d'une substance liquide qui est ajoutée progressivement durant l'opération afin d'engendrer l'agglomération des particules.

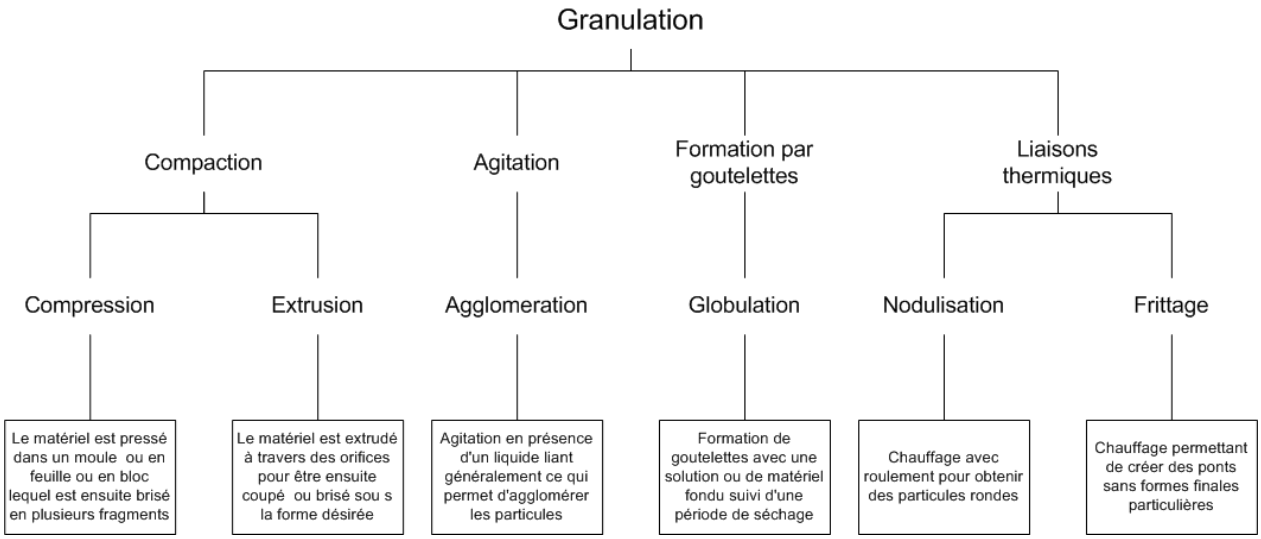

Figure 1-1: Classes et sous-classes des procédés de granulation (Sherrington & Oliver, 1981).

Pour réaliser cette granulation humide, quatre principaux types d'équipement peuvent être employés, soit le mélangeur à cisaillement élevé, le granulateur à tonneau, le granulateur à plateau ou le granulateur à lit fluidisé (Iveson, 2002; A. D. Salman, Hounslow, & Seville, 2007). Toutefois, il existe des équipements hybrides qui combinent certaines caractéristiques associées à ces types de granulateur. Le lit fluidisé avec rotor (granulateur à rotor ou FBRG) en est un exemple. Celui-ci fait intervenir une agitation mécanique comme pour le mélangeur à cisaillement élevé en utilisant un rotor plutôt qu'un agitateur à pales. D'autre part, il utilise un flux d'air introduit au bas de l'équipement afin de permettre de sécher les particules comme pour un lit fluidisé conventionnel (Gu, Liew, & Heng, 2004). Le caractère hybride de ce granulateur fait en sorte qu'il peut produire des granules dont la densité et la sphéricité sont élevées, tout en ayant l'avantage de pouvoir sécher les granules résultants au sein du même équipement. L'écoulement particulaire induit par la force mécanique fait en sorte que le lit de particules prend la forme d'un tore qui suit une trajectoire hélicoïdale comme le montre la Figure 1-2. L'atomiseur servant à ajouter le liant aux particules peut être localisé dans le lit ou peut aussi être positionné de telle manière à ce qu'il atomise le liquide à la surface de celui-ci.

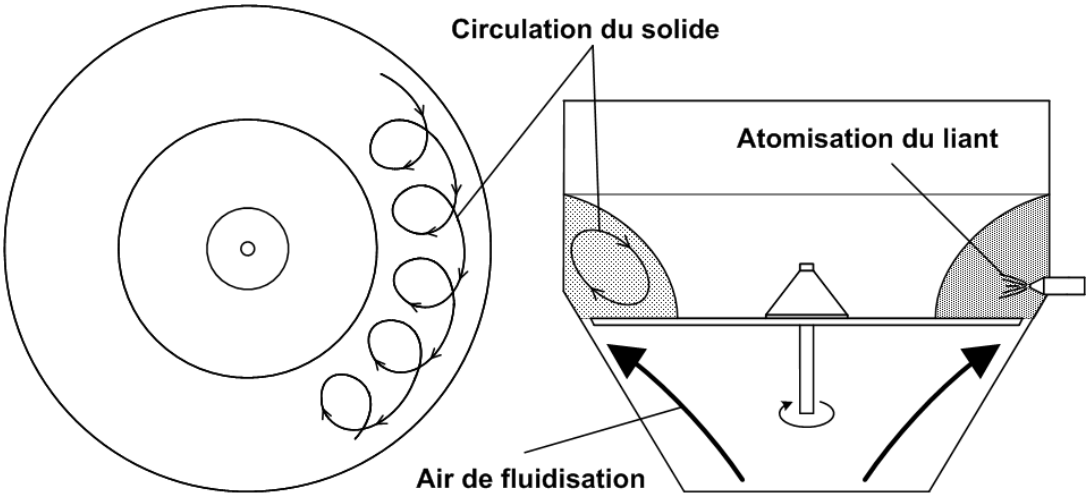

Figure 1-2: FBRG en opération avec la circulation du solide granulaire.

1.2 La granulation et les forces interparticulaires

Les forces interparticulaires impliquées dans les procédés de granulation peuvent provenir de différents mécanismes tels que la formation de ponts solides entre les particules ou la présence de forces de cohésion par exemple. Les forces interparticulaires jouent un rôle primordial dans le processus de granulation puisqu'elles initient le fusionnement des particules pour former des granules de plus grandes tailles. Pour la granulation humide, la force capillaire est généralement la force interparticulaire dominante à moins que des forces de cohésion soient induites par une importante viscosité du liant liquide. Ces deux forces changent d'intensité avec l'ajout du liant liquide (Muguruma, Tanaka, & Tsuji, 2000; Richefeu, El Youssoufi, Peyroux, & Radjai, 2008) et sont aussi affectées par le changement de taille des granules (Seville, Willett, & Knight, 2000).

Au début du processus de granulation, les particules sont généralement de faibles tailles et ne contiennent qu'une quantité marginale en eau. Cette faible quantité de liant ne permet pas de créer des ponts liquides entre les particules. À ce stade de la granulation, les forces de van der Waals ou d'origine électrostatique sont dominantes. Par contre, ces forces n'engendrent pas une agglomération des particules qui permet de changer leur distribution de taille. La coalescence des

particules devient possible seulement au moment où le liant liquide est ajouté. Elles commencent alors à être liées par les forces capillaires engendrées par la présence des ponts liquides. À mesure que le niveau de saturation en eau des granules augmente, jusqu'à atteindre une valeur maximale, les forces de cohésion augmentent et favorisent la coalescence des particules. Ce phénomène fait augmenter la taille moyenne des particules et modifie la distribution qui lui est associée. Pour une saturation plus élevée que la valeur maximale, la cohésion entre particules commence à diminuer par l'apparition d'effets de lubrification (Fournier, et al., 2005; Xu, Orpe, & Kudrolli, 2007).

Les forces capillaires, pour des interactions de types binaires avec deux particules ou entre une particule et un plan, ont été étudiées extensivement. Ainsi, les phénomènes qui interviennent dans ce type d'interaction sont bien compris. Par contre, la caractérisation des forces capillaires pour des lits de particules représente encore un défi important aujourd'hui. D'une part, la force capillaire est généralement étudiée pour des particules dont les matériaux sont insolubles dans le liant utilisé (ex : le verre, sable, etc.). Les propriétés intrinsèques de ces particules (ex : masse volumique, forme, porosité ou rigidité) ne sont pas nécessairement représentatives de celles observées dans les procédés de granulation humide. Toutefois, celles-ci ont l'avantage de ne pas s'agglomérer en présence du liant liquide et ainsi leur utilisation permet d'étudier le comportement d'un lit de particules de manière stable. D'autre part, la distribution non-homogène du liquide à l'intérieur des lits de particule rend difficile l'étude des forces capillaires qui ne sont pas réparties uniformément dans le milieu granulaire (Soulie, El Youssoufi, Cherblanc, & Saix, 2006). Ainsi, le développement d'une approche pouvant générer des forces interparticulaires de manière homogène, sans affecter les propriétés intrinsèques des particules, pourrait permettre de mieux comprendre le comportement des lits granulaires en présence de telles forces.

1.3 La granulation et les écoulements particulaires

En plus d'induire l'agglomération des particules, les forces interparticulaires ont aussi un impact significatif sur leur écoulement à l'intérieur d'un équipement de granulation (Forrest, Bridgwater,

Mort, Litster, & Parker, 2003; Forsyth, Hutton, & Rhodes, 2002; Rognon, Roux, Naaim, & Chevoir, 2008). Celles-ci sont reconnues pour affecter les propriétés d'écoulement dans le cadre de plusieurs applications, telles que le changement de l'angle de repos des piles solides (Forsyth, Hutton, Rhodes, & Osborne, 2001), la modification des patrons d'écoulement (B.F.C Laurent, 2005; Paul R, 2009; Saito, Fan, Ingram, & Seville, 2011) ou la réduction/accentuation de la ségrégation particulaire dans les équipements (Figueroa, Li, & Mccarthy, 2009; Forrest, Bridgwater, Mort, Litster, & Parker, 2003; H. M. Li & McCarthy, 2005, 2006). Pour la granulation, les patrons d'écoulement ainsi que la présence potentielle de ségrégation sont des paramètres dont l'importance est de plus en plus mise en évidence depuis quelques années (Forrest, Bridgwater, Mort, Litster, & Parker, 2003; Ben Freireich, Li, Litster, & Wassgren, 2011; Iveson, 2002). Il apparaît que la caractérisation de ces phénomènes devient de plus en plus importante afin de bien comprendre la dynamique de granulation observée. Ceci est d'autant plus vrai lorsque l'on considère la mise à l'échelle de ces procédés du laboratoire vers des unités industrielles de plus grandes dimensions (Mort, 2009).

Par contre, l'étude des écoulements de particules dans le contexte d'un procédé de granulation humide n'est pas une tâche simple. D'une part, les granules obtenus voient leur distribution de taille changer continuellement tout au long de la granulation. La modification de cette propriété granulaire affecte directement la manière dont les particules se déplacent à l'intérieur du granulateur, et peut générer de la ségrégation. Les caractéristiques des patrons de ségrégation changent avec l'évolution de la distribution de taille mais sont aussi affectées par les forces capillaires. Comme il a été indiqué précédemment, les forces capillaires dépendent elles aussi de la distribution de taille des granules. Il apparait donc que tous ces paramètres sont liés les uns aux autres et qu'il est donc difficile d'isoler leurs effets de manière indépendante sur l'écoulement granulaire.

Dans un autre ordre d'idée, jusqu'à maintenant, les approches pour modéliser la granulation considère généralement le lit de particules comme un ensemble parfaitement mélangé. La considération du mouvement des particules est alors prise en compte dans la représentation des mécanismes de granulation où on y retrouve des caractéristiques rhéologiques telles que le taux

de collisions des particules ou la distribution de vitesses d'impact. La résolution de problèmes spatialement non-homogènes est depuis longtemps prise en compte pour d'autres types d'applications ne faisant pas intervenir les écoulements denses de particules. Pour les phases liquides et les phases gazeuses, le développement des équations de Navier-Stokes a permis de pouvoir développer de nombreux modèles permettant de prédire ou d'estimer l'écoulement pour diverses applications industrielles. Pour les écoulements de particules concentrés, comme c'est le cas pour la granulation humide agitée, les phénomènes rhéologiques les régissant ne sont pas encore bien définis. Ceci empêche l'obtention d'une relation phénoménologique pour expliquer le comportement des écoulements observés jusqu'à maintenant. Par contre, les méthodes de simulation par élément discret (DEM) ou l'utilisation de méthodes de mesures non-invasives ont permis, depuis les dernières années, de faire des avancées significatives à ce sujet.

En regard des problèmes mentionnés précédemment, on peut donc définir l'objectif principal de cette thèse.

1.4 Objectif principal de la thèse

L'objectif principal de la thèse est de clarifier l'impact des propriétés de l'écoulement de particules (ou d'agglomérats de particules) en présence de forces interparticulaires sur la distribution de taille de granules dans un sphéroniseur modifié.

CHAPITRE 2 REVUE DE LITTÉRATURE

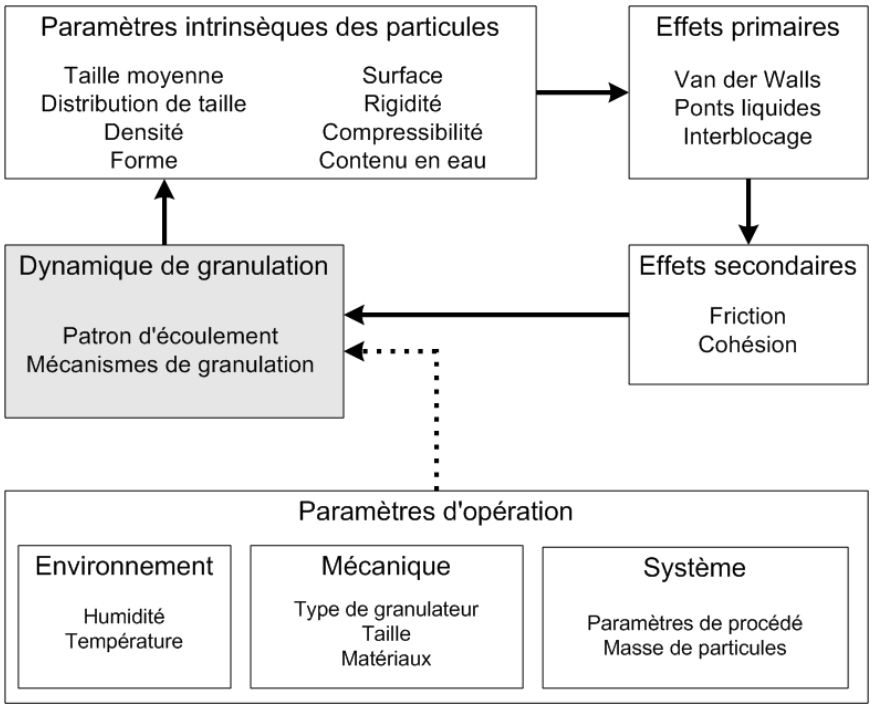

Figure 2-1: Paramètres qui affectent la dynamique de la granulation humide.

Les paramètres qui influencent la dynamique de granulation, tels que présentés à la Figure 2-1, peuvent être classés en deux groupes principaux : 1) les propriétés intrinsèques des particules et 2) les paramètres d'opération du système de granulation. La dynamique de granulation est généralement reliée aux mécanismes de granulation (nucléation/mouillage, coalescence ou bris des particules) ainsi qu'aux écoulements granulaires (profil de vitesse et distribution de temps de séjour des particules). Les deux premières sections font une revue des mécanismes de granulation et des études ayant été effectuées sur les écoulements granulaires. La dernière section fait un résumé des différentes approches numériques pouvant être employées afin de modéliser les procédés de granulation.

2.1 Mécanismes de la granulation humide

Iveson et al. regroupent en trois familles les mécanismes principaux qui influencent la granulation humide (Iveson, Litster, Hapgood, & Ennis, 2001) telles qu'énumérées à gauche de la Figure 2-2. Cette section présente brièvement chacune de ces familles.

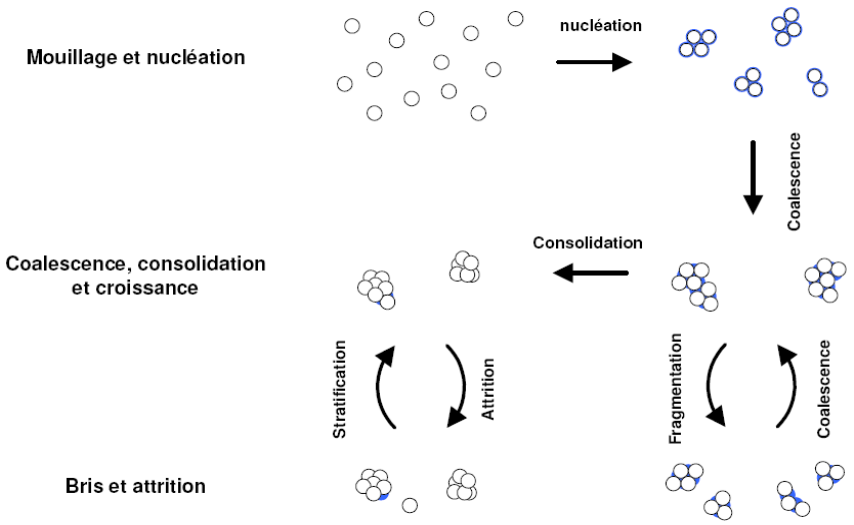

Figure 2-2: Mécanismes de la granulation humide (Iveson, Litster, Hapgood, & Ennis, 2001).

2.1.1 Mouillage et nucléation

La nucléation est un mécanisme qui est associé à la formation des premiers granules qui sont le résultat de l'interaction entre les gouttelettes de liant et la poudre sèche (Iveson, Litster, Hapgood, & Ennis, 2001). La nucléation est la première étape conduisant à la croissance des particules via d'autres mécanismes tels que la coalescence. Deux processus affectent principalement la nucléation (Hapgood, Litster, & Smith, 2003; Wildeboer, Litster, & Cameron, 2005), soit celui contrôlé par les gouttelettes de liant qui dépend des propriétés thermodynamiques et cinétiques de mouillage et celui contrôlé par la dispersion du liant liquide dans la poudre, lequel dépend des paramètres du procédé.

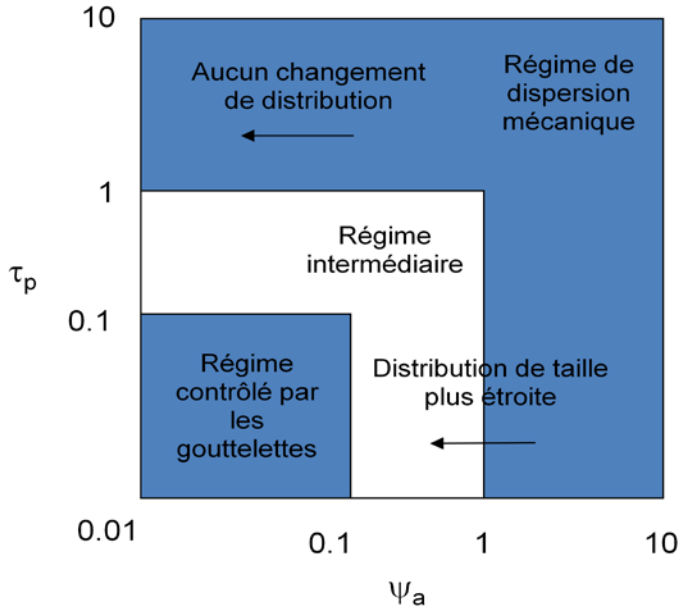

Figure 2-3: Diagramme de nucléation (Hapgood, Litster, & Smith, 2003)

La Figure 2-3 présente le diagramme du mécanisme de nucléation. Celui-ci permet d'identifier les différents régimes qui sont observés en fonction du temps de pénétration adimensionnel des gouttelettes de liant et du flux d'atomisation adimensionnel décrits par :

(2-1)

où est le volume de gouttelettes, la porosité du lit de particule, le rayon des pores granulaires et , et sont la viscosité, la tension de surface et l'angle de contact dynamique du liant liquide, est le temps de circulation correspondant au délai de temps avant qu'une particule sorte et entre de nouveau dans la zone d'ajout du liant, et par :

(2-2)

où est le débit volumétrique du liant, le flux de surface des particules traversant la zone d'ajout du liant liquide et est le diamètre des gouttelettes. Le régime contrôlé par les gouttelettes est présent lorsque la taille de ces dernières est supérieure à celles des particules.

Pour ce régime, la taille du noyau nouvellement formé est alors du même ordre que la dimension des gouttelettes. Par contre, pour le régime de dispersion mécanique, la taille des particules est beaucoup plus grande et dans ce cas le liant se retrouve distribué à leur surface. En fait, même si ce régime est considéré comme de la nucléation, en réalité la formation du noyau correspond à un mécanisme de coalescence qui se produit suite au mouillage des particules primaires atomisées par le liant (Le, Avontuur, Hounslow, & Salman, 2011).

2.1.2 Consolidation et coalescence

Durant le processus de granulation, les particules qui entrent en collision peuvent s'agglomérer à condition d'avoir une concentration suffisante en liant. L'agglomération successive des particules entraîne la croissance de taille des granules. Ceux-ci peuvent aussi se consolider suite à une collision avec les parois de l'équipement ou une collision avec un autre granule qui n'aboutit pas à leur coalescence.

2.1.2.1 Consolidation des granules

La consolidation est un mécanisme qui réduit la taille ainsi que la porosité des granules dû aux impacts qu'ils subissent. La quantité de liant liquide dans les agglomérats, la nature de ce liant, la taille des particules, la vitesse ainsi que le type d'équipement utilisé sont des facteurs influençant significativement le taux de consolidation (Iveson, Litster, Hapgood, & Ennis, 2001). La relation suivante permet d'approximer le taux de consolidation particulaire (Iveson & Litster, 1998a; Iveson, Litster, & Ennis, 1996; Verkoeijen, Pouw, Meesters, & Scarlett, 2002) :

— (2-3)

où et correspondent à la porosité et la porosité minimale pouvant être atteinte respectivement, est le temps et est la constante du taux de consolidation. La constante

semble dépendre de l'intensité de l'agitation dans le granulateur malgré qu'aucune corrélation claire n'a pu être établie jusqu'à aujourd'hui (Poon, Immanuel, Doyle, & Litster, 2008). Durant la granulation humide, plusieurs autres mécanismes influencent l'évolution des propriétés granulaires et il est donc difficile, voire impossible, d'isoler l'effet de la consolidation et d'ajuster les paramètres et de l'équation (2-4). En effet, l'ajustement de ces paramètres est actuellement fait rétroactivement suite aux simulations des procédés de granulation qui font entrer en jeu d'autres mécanismes de granulation. En réalité, la consolidation est souvent considérée afin de pouvoir modifier les distributions de taille simulées de telle manière à bien représenter l'évolution expérimentalement observée de la granulation humide.

2.1.2.2 Coalescence des granules

La coalescence résulte de la collision entre des particules conduisant à une nouvelle particule de plus grande taille. Le succès de la coalescence est fonction de plusieurs facteurs tels que la taille particulaire, les propriétés du liant liquide et de la poudre ainsi que des paramètres du procédé. Afin d'expliquer l'agglomération des particules, différents modèles théoriques ont été développés, lesquels sont résumés par (Iveson, Litster, Hapgood, & Ennis, 2001). Ceux-ci ont été regroupés en deux classes (Iveson, 2001). La classe 1 considère que les particules sont libres de bouger dans l'espace et que les propriétés élastiques des granules dominent. Pour qu'il y ait coalescence, il faut que l'énergie cinétique soit complètement dissipée lors de la collision car, dans le cas contraire, les particules rebondissent. On considère ici que si l'impact initial conduit à l'agglomération des particules, celles-ci seront indivisibles. La classe 2 prend en compte les mêmes critères que la classe 1, mais considère qu'un lien se forme entre les particules et que celui-ci peut se briser éventuellement. Ainsi une agglomération permanente est atteinte si le lien entre les particules est capable de soutenir les collisions subséquentes et les forces de cisaillement présentes dans le granulateur.

Un critère de coalescence pour la classe 1 a été développé par (Ennis, Tardos, & Pfeffer, 1991). Celui-ci considère une approche se basant sur le nombre de viscosité de Stokes ( ),:

(2-4)

où et correspondent à la moyenne harmonique de la masse et du diamètre des particules respectivement, est la vitesse relative initiale des particules et la viscosité du fluide. Afin qu'il y ait coalescence des particules, doit être inférieur à un nombre de viscosité de Stokes critique ( ) lequel est donné par l'équation suivante :

(2-5)

où est le coefficient de restitution, est l'épaisseur de la couche de liquide liant à la surface des granules, et est la dimension caractéristique des aspérités de surface des granules.

Certaines limitations sont toutefois associées à l'analyse du problème selon une approche de classe 1 car les granules sont considérés comme étant purement élastiques et non poreux, ce qui signifie que le liant liquide se trouve en surface (Litster & Ennis, 2004). En réalité, le liant liquide arrive à pénétrer à l'intérieur de la structure granulaire, ce qui sature partiellement l'agglomérat. Les granules ont aussi tendance à se déformer plastiquement, absorbant par le fait même une partie de l'énergie cinétique de collision. Considérant les limitations du modèle de classe 1, l'incorporation de la déformation plastique des granules possédant une couche liquide en surface permet de considérer la coalescence de classe 2 telle que présentée à la Figure 2-4.

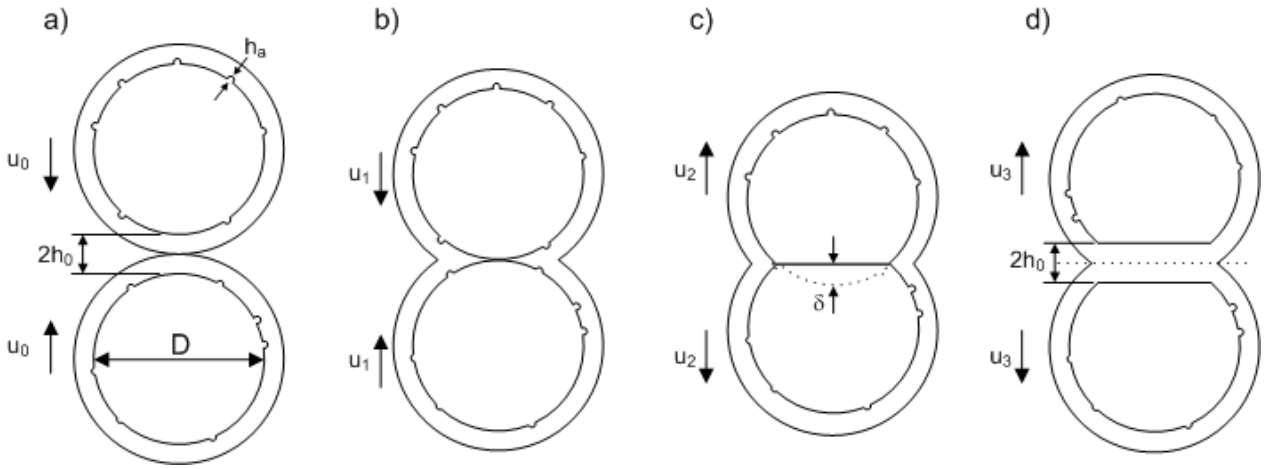

Figure 2-4: Collision entre des granules déformables et saturés en liant a) Approche; b) Déformation; c) Séparation initiale; d) Séparation des couches liquides.

Pour la coalescence de classe 2 (L. Liu & Litster, 2002), on considère que celle-ci survient lorsque l'énergie cinétique est non seulement dissipée par la couche de liant liquide en surface, mais aussi par la déformation plastique des granules. L'introduction du nombre de déformation de Stokes permet de prendre en compte le ratio de l'énergie cinétique d'impact et de la déformation plastique :

(2-6)

où est la contrainte de cisaillement limite. La Figure 2-5 montre les régions propres aux deux classes de coalescence pour un système donné. Pour la classe 1, les granules sont freinés totalement par la dissipation visqueuse se produisant au niveau de la couche de liant en surface. Ainsi, cette situation se produit en dessous d'une valeur critique de , et ce de manière indépendante à , car les propriétés mécaniques des granules ne jouent aucun rôle. Cette frontière correspond à l'équation suivante :

(2-7)

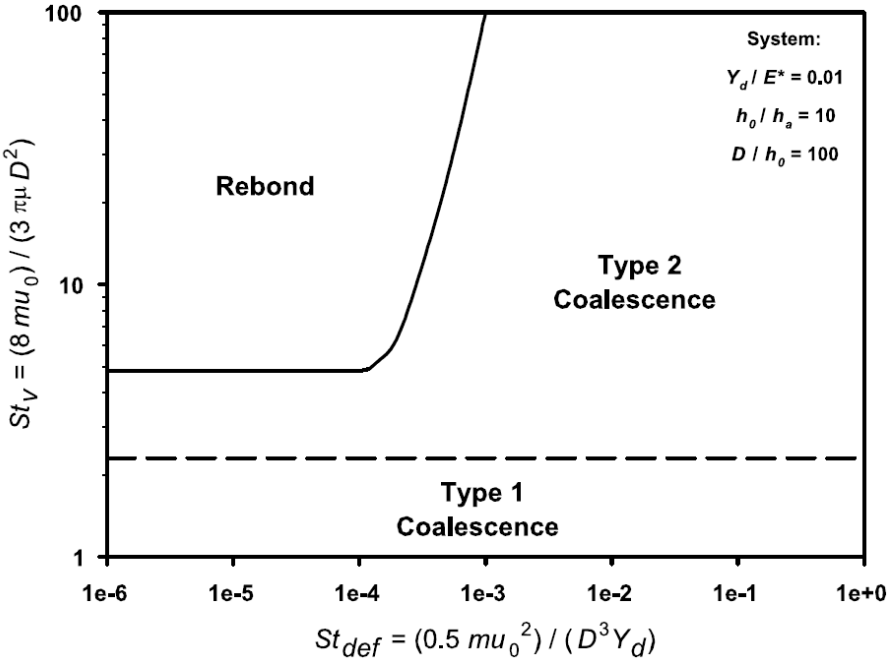

Figure 2-5: Représentation des classes de coalescence en fonction de et (L. X. Liu, Litster, Iveson, & Ennis, 2000). Les frontières sont indiquées par rapport à un système dont les propriétés sont mentionnées dans le graphique.

La frontière associée à la coalescence de classe 2 est plus complexe à obtenir que la précédente. Le développement de cette relation est traitée en détail dans (L. X. Liu, Litster, Iveson, & Ennis, 2000) et ici on ne présente que l'expression finale :

(2-8)

avec la déformation plastique permanente exprimée par :

(2-9)

et le module de Young ajusté est donné par l'expression suivante :

(2-10)

où et sont les modules de Young des deux granules et et sont leurs ratios de Poisson respectifs. La coalescence correspondant à la classe 2 est possible à obtenir avec des granules dont la surface est sèche. Pour ce faire, le liant liquide interne doit être comprimé vers la surface lors de la collision et respecter les critères suivant (Litster & Ennis, 2004):

1. Le contenu en liquide est près de la valeur critique de saturation pour que celui-ci puisse apparaître en surface ;
2. Il y a une aire de contact significative formée durant la collision (élevé) ;
3. Le liquide migre rapidement vers la zone de contact (viscosité faible et taille de pore assez large).

La considération de granules dont la surface est sèche modifie légèrement les expressions (2-8) et (2-9) étant donné qu'il n'est plus nécessaire de considérer la phase d'approche à travers la couche liquide lors du contact des particules (Litster & Ennis, 2004).

Un autre paramètre important à considérer est le niveau de saturation en liquide (liant) des granules, car celui-ci affecte l'évolution des granules durant le procédé. Iveson et al. ont étudié l'évolution de la distribution de taille des granules obtenus d'expériences caractérisées par différents niveaux de cisaillement (Iveson, et al., 2001). Leur analyse a permis de classifier divers comportements de croissance des granules qui sont présentés à la Figure 2-6. Ce diagramme

présente différentes frontières approximatives délimitant les types de croissance en fonction de la capacité de déformation des granules ainsi que du niveau de saturation. La saturation maximale des pores y est définie comme le ratio entre la masse de liquide pouvant occuper la totalité du volume des pores sur la masse du granule lorsque les pores sont complètement vides :

(2-11)

où est le ratio de la masse de liquide sur celle du solide, et sont les masses volumiques du liquide et du solide respectivement. Lorsque le niveau de saturation est plus faible que , le liquide se retrouve emprisonné à l'intérieur des granules et ceux-ci doivent être compressés afin de pouvoir faire sortir le liquide à la surface. Pour une valeur de saturation supérieure à , une partie du liquide remplie complètement les pores des granules tandis que la quantité résiduelle se retrouve à la surface. Dans la Figure 2-6, les particules sèches pouvant s'écouler librement apparaissent lorsqu'une faible quantité de liquide est présente tout en ayant de larges forces de déformation appliquées sur les granules. Lorsque le niveau de liquide est augmenté dans le lit de granules et que les déformations demeurent grandes, les granules peuvent commencer à se briser et causer la diminution de la taille moyenne des particules dans le système. Si cette quantité de liquide est encore augmentée à un niveau de saturation plus grand que , les larges déformations présentent font apparaître un état de surmouillage qui peut aller jusqu'à l'obtention d'une masse de particules cohésives.

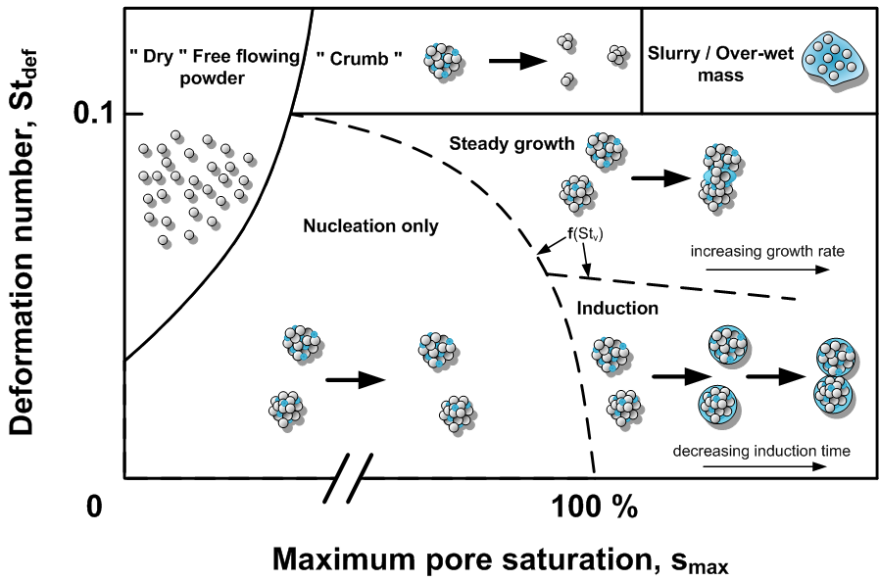

Figure 2-6: Diagramme de la granulation humide (Iveson, et al., 2001)

Lorsque le niveau de déformation est plus faible, d'autres types de croissance granulaire peuvent être obtenus, dont la nucléation qui a été expliquée dans la Section 2.1.1. Brièvement, la nucléation est toujours observée lorsque le niveau de saturation est faible et qu'il ne dépasse pas la valeur maximale pouvant être atteinte. À partir d'une valeur de saturation approchant , deux états peuvent survenir tels que présentés à la Figure 2-7, soit la croissance à taux constant ou la croissance inductive (Iveson & Litster, 1998b). La croissance à taux constant apparait lorsque les granules sont malléables et qu'ils subissent une déformation importante suivant une collision. Dans ce cas, de larges surfaces de contact entre les particules sont formées et le liquide qui se trouve à l'intérieur des granules est alors pressé à la surface, ce qui favorise la coalescence. Ce type de croissance est à peu près linéaire par rapport au temps d'opération et est observé pour des liquides liants à basse viscosité. Dans le cas de la croissance granulaire inductive, les granules concernés sont rigides et un impact avec un autre granule ne les déforme pas suffisamment pour rendre le liquide liant disponible pour les agglomérer. On assiste alors à une phase de croissance granulaire nulle appelée la période inductive. La longueur de cette période décroit avec l'augmentation du contenu en liquide liant dans les granules. Ce type de comportement apparaît fréquemment pour des systèmes avec de fines particules, avec ou sans liant liquide visqueux (Iveson & Litster, 1998b).

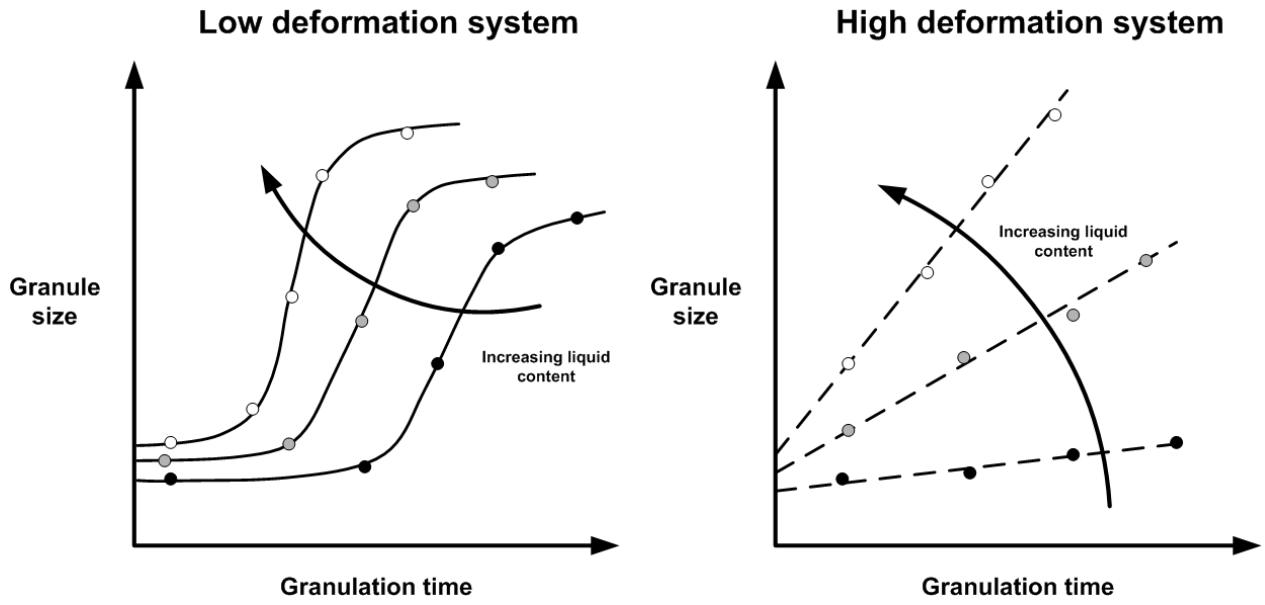

(a) Croissance par induction (b) Croissance à taux constant

Figure 2-7: Types de croissance granulaire rencontrés pour la granulation humide (Iveson & Litster, 1998b)

2.1.3 Bris et attrition

Le processus de bris des particules est un mécanisme dont l'importance peut varier selon le type d'équipement utilisé. Par contre, cet aspect de la granulation a été peu traité dans le passé et c'est seulement depuis quelques années que l'intérêt porté à ce sujet a commencé à croître. Plusieurs facteurs influencent la manière dont une particule peut se briser (Ramachandran, Immanuel, Stepanek, Litster, & Doyle Iii, 2009; Reynolds, Fu, Cheong, Hounslow, & Salman, 2005): le type de liant liquide et sa quantité dans la structure granulaire, la taille et la forme des particules primaires, le patron d'écoulement du lit de particules et l'historique des entités granulaires. L'attrition des granules est caractérisée par de petites particules qui se détachent de l'agglomérat, généralement en surface. Le bris est davantage associé au mécanisme inverse de la coalescence et concerne la séparation d'un granule en deux ou plusieurs parties qui possèdent une taille similaire (Agba D. Salman, Ghadiri, & Hounslow, 2007). Étant donné la complexité du mécanisme de

bris/attrition, la théorie existante est assez limitée (Gantt & Gatzke, 2005). Une relation a été proposée afin de quantifier ce phénomène, laquelle considère qu'un granule peut briser si son énergie cinétique surpasse un certain niveau critique (Tardos, Khan, & Mort, 1997). Cette relation est donnée en fonction du nombre de déformation de Stokes surpassant cette valeur critique :

(2-12)

où est altéré afin d'introduire un nouveau facteur de contrainte qui est plus général que la contrainte de cisaillement limite :

(2-13)

où est le nouveau facteur de contrainte décrit par le modèle de Hershel-Buckley :

(2-14)

Dans l'équation précédente, est la viscosité apparente du système particulaire, est le taux de cisaillement et est l'indice d'écoulement. Afin de parvenir à identifier des modèles de bris plus élaborés, des études expérimentales peuvent être employées. Les études expérimentales peuvent être divisées en deux classes : 1) les études portant sur l'évolution de la taille particulaire en fonction des paramètres de procédé (Iveson, Litster, Hapgood, & Ennis, 2001; P. C. Knight, Johansen, Kristensen, Schaefer, & Seville, 2000) et 2) les études identifiant le bris directement (ex. addition d'un traceur coloré) et permettant d'extraire un mécanisme en fonction de conditions d'opération spécifiques (Pearson, Hounslow, & Instone, 2001; Ramaker, Jelgersma, Vonk, & Kossen, 1998; Tan, Salman, & Hounslow, 2004). La première classe ne permet pas d'isoler les changements des propriétés granulaire en fonction du bris uniquement, car il est impossible de faire abstraction de la coalescence ou de la consolidation (Iveson, Litster, Hapgood, & Ennis, 2001) et c'est pourquoi la deuxième classe d'étude est la plus souvent rencontrée dans les études récentes (Tan, Salman, & Hounslow, 2004; Tan, Salman, & Hounslow, 2005).

En somme, plusieurs modèles mécaniques plus ou moins complexes ont été développés afin de considérer les divers mécanismes de granulation. Les modèles les plus récents requièrent un effort intense de paramétrisation puisque plusieurs termes physiques ont besoin d'être définis dans les diverses équations présentées précédemment. Une des difficultés importantes pour paramétrer ces modèles vient de leur interdépendance avec d'autres facteurs macroscopiques tels que les caractéristiques d'écoulement qui affectent la vitesse des granules, leur taux de collision et leur déplacement entre différentes zones du granulateur.

2.2 Écoulement granulaire

L'incompréhension associée aux écoulements granulaires peut amener des difficultés significatives au niveau du choix des granulateurs et le contrôle des processus de granulation. En effet, comme indiqué par (P. Knight, 2004), la caractérisation des écoulements particulaires à l'intérieur des granulateurs est un sujet de recherche clé pour le développement de nouveaux designs de granulateur ainsi que l'identification des points d'opération optimaux. Depuis les dernières années, différentes études concernant le mélange granulaire ont été menées. La majorité d'entre elles ont mis l'accent sur les matériaux granulaires non cohésifs. Les différentes études concernant les écoulements granulaires peuvent être regroupées selon deux approches, soit la dynamique d'écoulement et les processus de mélange/ségrégation.

2.2.1 Dynamique des écoulements granulaires

L'étude de la dynamique des écoulements granulaires a pour objectif de développer des modèles rhéologiques permettant d'expliquer de quelle manière les particules se déplacent en fonction des régimes d'écoulement. Le fait qu'un ensemble de particules puisse se comporter comme un solide (une pile de particules), un liquide (écoulement dans un silo) ou un gaz (lit fluidisé) représente une difficulté majeure pouvant expliquer l'absence d'une description telle que l'équation de Navier-Stokes avec les liquides (de Gennes, 1998). Pour les deux régimes extrêmes

(comportement fluidisé et solide), des lois constitutives ont été proposées. Celles-ci reposent sur la théorie cinétique des gaz pour les écoulements granulaires collisionnels rapides (Jenkins & Savage, 1983) ou la mécanique des sols pour les écoulements lents plastiques (Sokolovskii, 1965). Par contre, le régime intermédiaire, communément appelé écoulement granulaire dense, ne possède pas le même niveau d'avancement que les autres régimes. Ce fait a motivé plusieurs études dans la dernière décennie (Campbell, 2006; Jop, Forterre, & Pouliquen, 2006; MiDi, 2004; Rognon, Roux, Naaim, & Chevoir, 2008).

2.2.1.1 Écoulement granulaire rapide

Depuis les 20 dernières années, les écoulements granulaires rapides ont menés à de nombreuses recherches afin que des lois constitutives puissent expliciter leur comportement (Campbell, 1990; Goldhirsch, 1999). La théorie cinétique des gaz fournit des équations constitutives dans le cas où les particules interagissent par le biais de collisions binaires. Le milieu possède alors un comportement similaire à un gaz dans lequel de l'énergie est dissipée lors des collisions. À partir de ces considérations, il est alors possible d'obtenir un ensemble d'équations qui ressemble à la relation constitutive de Navier-Stokes pour les fluides. Campbell indique que la théorie cinétique fonctionne relativement bien dans le cas où les concentrations de solide sont faibles, le coefficient de restitution des particules est élevé (> 0.9) et lorsqu'on peut considérer qu'aucune corrélation existe pour la vitesse et la position des particules en collision (Campbell, 2006). Ainsi, la considération de l'écoulement granulaire rapide ne peut se faire que dans les conditions précédemment mentionnées et ne peuvent donc pas être appliquées au cas où un écoulement dense se produit.

2.2.1.2 Écoulement granulaire dense

Le régime d'écoulement dense correspond au moment où les forces inertielles des particules deviennent importantes (MiDi, 2004). Ce type d'écoulement est aussi caractérisé par la présence

de chaînes de contacts (*Force chains*) qui se propagent à travers le milieu granulaire. Jop et al. ont développé récemment une loi constitutive permettant d'expliquer le comportement des écoulements granulaires denses sur un plan incliné (Jop, Forterre, & Pouliquen, 2006). Malgré le fait que l'expression a pu être généralisée pour des cas tridimensionnels concernant l'écoulement sur un plan, celle-ci n'a pas pu être appliquée pour des écoulements plus complexes, comme c'est le cas dans la majorité des mélangeurs ou granulateurs. C'est pour cette raison que les méthodes de modélisation numériques, comme en dynamique moléculaire ou la méthode des éléments discrets (DEM), sont toujours très utilisés pour étudier des phénomènes particuliers de ces écoulements comme la ségrégation par exemple (Bertrand, Leclaire, & Levecque, 2005; Zhu, Zhou, Yang, & Yu, 2007).

2.2.2 Mélange et ségrégation

Le mélange et la ségrégation sont des phénomènes résultant des écoulements granulaires, mais peuvent prendre une plus grande importance que l'écoulement lui-même (Sundaresan, Eaton, Koch, & Ottino, 2003). Ceux-ci surviennent avec des matériaux secs, humides ainsi qu'avec des suspensions concentrées. Plus spécifiquement, la ségrégation apparaît lorsque les particules possèdent des différences au niveau de leurs propriétés physiques (ex. taille, densité ou forme) (Ottino & Khakhar, 2000). La plupart du temps, le mouvement interparticulaire va causer une migration préférentielle des particules dans des zones spécifiques du contenant employé, comme présentée à la Figure 2-8..

La ségrégation a majoritairement été étudiée avec des mélangeurs culbuteurs caractérisés par la présence de cisaillement faible avec des particules non cohésives (Alexander, Muzzio, & Shinbrot, 2003; Lemieux, et al., 2007; Ottino & Khakhar, 2000) et cohésives (H. M. Li & McCarthy, 2003; McCarthy, Khakhar, & Ottino, 2000). Les mélangeurs cylindriques avec agitateur ont été peu étudiés en ce qui concerne les possibilités d'occurrence de la ségrégation. Conway et al. ont montré que, selon le taux de cisaillement, différents patrons de ségrégation peuvent être observés avec un mélangeur cylindrique à quatre pales (Conway, Lekhal, Khinast, &

Glasser, 2005). Cette étude indique donc qu'il faut porter attention à l'occurrence de la ségrégation, même dans le cas où le procédé utilisé (ex. mélangeur, granulateur) emploie des taux de cisaillement élevés.

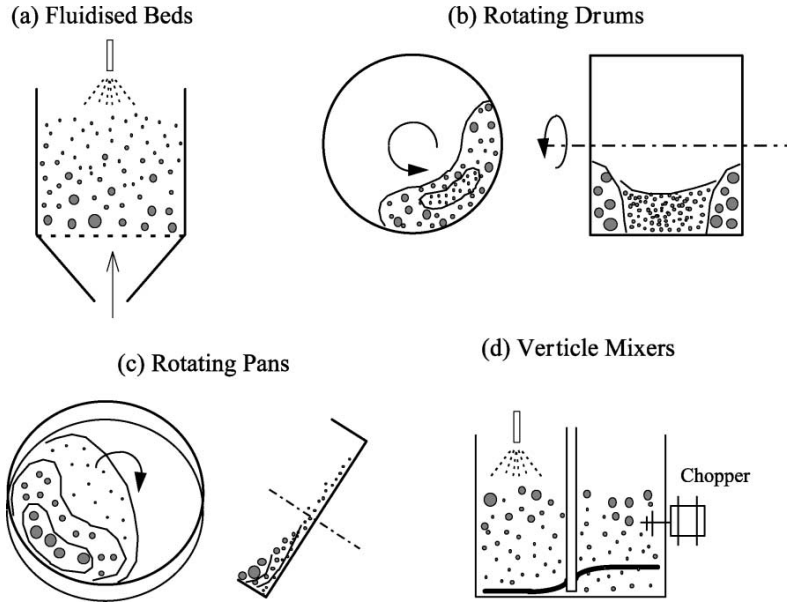

Figure 2-8: Ségrégation potentielle des granules pour différents types de granulateur (Iveson, 2002).

Afin de décrire la ségrégation, il est nécessaire de connaître l'écoulement et de disposer de modèles constitutifs pour estimer les flux de migration en fonction des états d'écoulement (Sundaresan, Eaton, Koch, & Ottino, 2003). Actuellement, l'estimation de ces flux de migration dans des écoulements particulaires denses a été effectuée à l'aide de techniques numériques telle que la méthode des éléments discrets (DEM) (H. M. Li & McCarthy, 2003; Ottino & Khakhar, 2000) ou bien par le biais d'expérimentations ciblées via des techniques de visualisation de particules (PIV ou PEPT) (B.F.C Laurent, 2005; B. F. C. Laurent, Bridgwater, & Parker, 2002). De plus, l'identification des patrons de ségrégation et le calcul du flux de migration des particules dans un environnement 3D demeurent toujours des sujets intensifs de recherche.

2.2.3 Forces interparticulaires et écoulement granulaire

Les forces interparticulaires sont importantes pour le procédé de granulation puisque celles-ci initient l'agglomération des granules. Il existe différents types de forces interparticulaires, lesquelles peuvent être regroupées en familles telles que présentées dans la Figure 2-9. Ces forces de cohésion ou d'adhésion n'ont pas seulement une influence sur le processus de coalescence des granules, mais elles ont aussi un impact déterminant sur la manière dont les écoulements s'établissent dans un équipement. Puisque les caractéristiques des écoulements granulaires ont un effet sur l'évolution des processus de granulation, il est donc facile de voir qu'il existe une interdépendance entre les mécanismes de granulation présentés précédemment et les écoulements granulaires. La suite de cette section fait un résumé des forces interparticulaires les plus fréquemment rencontrées dans les systèmes de granulation humide soit : les forces de van der Waals, les forces capillaires et les forces électrostatiques. Afin de donner une idée de l'importance relative de ces forces entre elles, ainsi que par rapport au poids des particules en fonction de leur taille, celles-ci sont représentées à la Figure 2-10.

Les force de van der Waals ont un impact significatif sur les interactions entre particules fines. La force de cohésion est directement proportionnelle à la taille des particules suivant l'équation suivante (Butt & Michael, 2010; Hamaker, 1937):

$$F_{VdW} = \frac{A_H a}{12h^2} \tag{2-15}$$

où A_H est la constant d'Hamaker, a est le rayon de la particule et h est la distance de séparation entre les surfaces des deux particules, laquelle correspond à la distance la plus faible entre les deux particules en contact. Lorsque les particules deviennent plus larges que 100 μm (Forsyth, Hutton, Osborne, & Rhodes, 2001), les forces de van der Waals commencent à perdre de l'influence par rapport aux forces inertielles et gravitationnelle. Pour des systèmes particulaires tels que ceux rencontrés dans les procédés de granulation, ces forces n'ont pratiquement pas

d'influence et leurs effets sur l'écoulement sont minimes. Pour le cas de la granulation humide par exemple, on a recours à l'ajout d'un liant liquide pour créer les forces cohésives nécessaires à l'agglomération. La formation de ponts capillaires créés par la présence du liquide interstitiel se trouvant entre les granules a aussi un impact significatif sur les écoulements granulaires pendant la granulation et peuvent changer diamétralement les patrons d'écoulement observés.

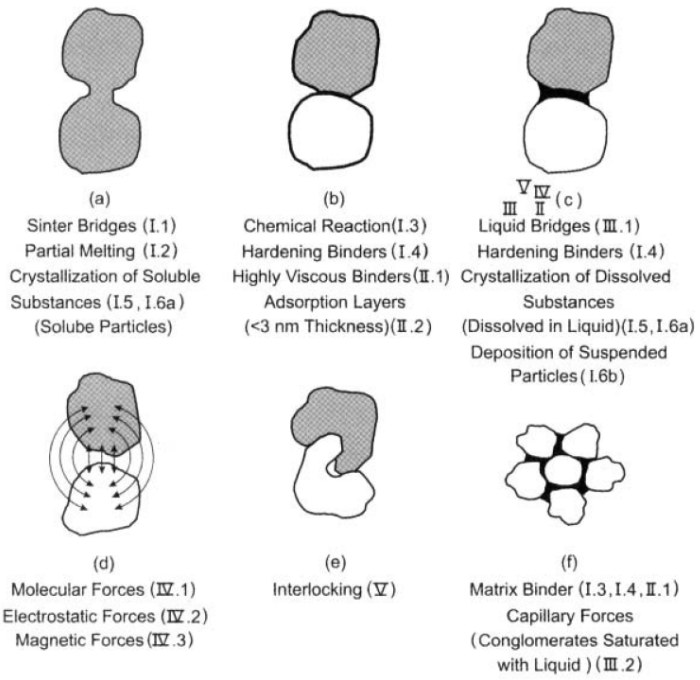

Figure 2-9: Représentation schématique des mécanismes cohésifs impliqués dans les procédés d'agglomération (Pietsch, 2002) : I) Ponts solides, II) Adhésion et forces de cohésion, III) Tension de surface et pression capillaire, IV) Forces d'attraction entre solides, et V) Forces d'interférence (interlocking).

La force capillaire dépend de la tension de surface et du différentiel de pression entre l'interface air-liquide et est représentée par la relation suivante (Soulie, El Youssoufi, Cherblanc, & Saix, 2006):

$$F_{cap} = 2\pi\gamma_{LV} a \sin\phi \sin(\phi+\theta) + \pi a^2 \Delta p \sin^2\phi \tag{2-16}$$

où ϕ est la position polaire du point de contact du pont liquide relativement au centre de la particule et l'axe de référence horizontal, θ est l'angle de contact et est la tension de surface. La pression de Laplace dépend du volume de liquide entre les particules, laquelle est exprimée par le biais du profil de l'interface du pont liquide, :

$$\frac{\Delta p a}{\gamma_{LV}} = \frac{\ddot{Y}}{(1+\dot{Y}^2)^{3/2}} - \frac{1}{Y(1+\dot{Y}^2)^{1/2}} \tag{2-17}$$

Cette expression est valide en autant que le niveau de saturation en liquide permet d'obtenir des ponts liquides qui sont caractéristiques du régime pendulaire (Iveson, Beathe, & Page, 2002). Dans cet état, les ponts liquides lient deux particules seulement. Le régime pendulaire existe tant que le niveau de saturation ne dépasse pas 1 à 3 % sur une base volumique (Weigert & Ripperger, 1999). Lorsque l'état de saturation dépasse ce niveau, les états funiculaires et finalement capillaires sont atteints et on observe alors des ponts liquides liant plusieurs particules simultanément. Pour l'étude des écoulements de particules cohésives, lorsqu'on utilise les forces capillaires, la distribution du liquide de manière uniforme pose souvent problème (Iveson, Beathe, & Page, 2002). La mauvaise homogénéisation des forces interparticulaires qui en résulte, complexifie l'étude des écoulements granulaires cohésifs qui utilisent ces forces (Radjai & Richefeu, 2009).

Récemment, une méthode alternative a été utilisée afin d'utiliser les interactions électromagnétiques afin de générer des forces cohésives dans des lits de particules (Lumay & Vandewalle, 2010; Peters & Lemaire, 2004). Un des avantages d'utiliser ces forces vient de l'absence de liquide à distribuer dans lit de particules. Par contre, le comportement de l'écoulement observé est différent par rapport aux applications industrielles, dont la granulation,

étant donné que les forces sont alignées avec le champs magnétique utilisé pour induire la cohésion. Afin d'étudier les écoulements particulaires dans un procédé de granulation, cette méthode de génération des forces interparticulaires ne permet donc pas d'imiter le comportement qui y serait normalement rencontré.

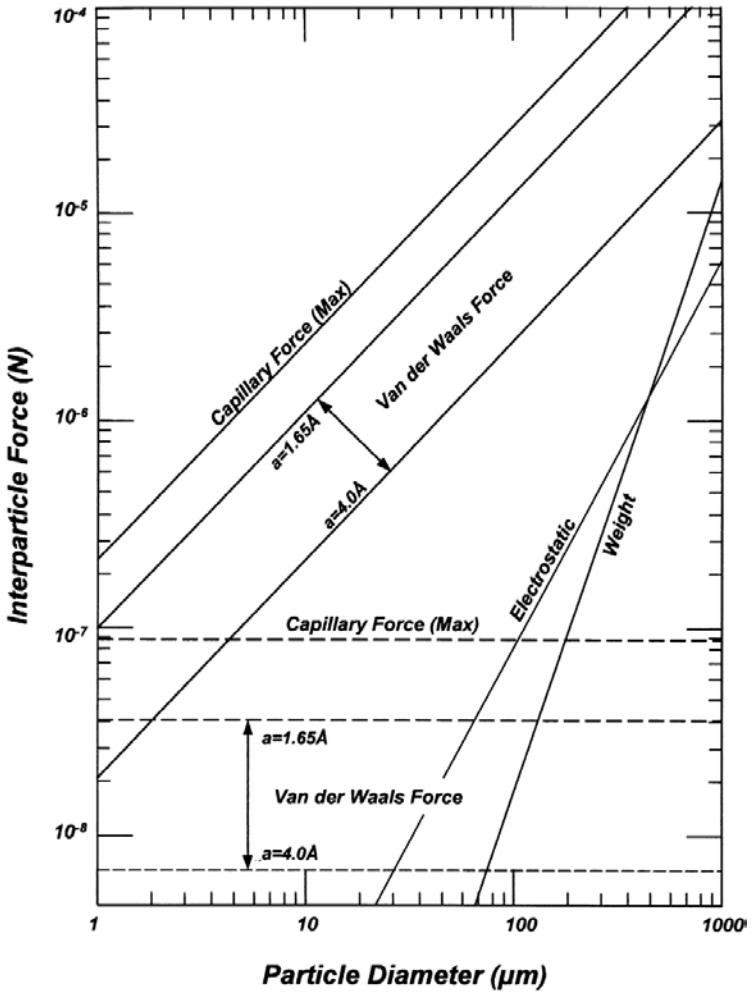

Figure 2-10: Comparaison de l'intensité de différentes forces interparticulaires en fonction de la taille des particules. Les lignes tiretées tracent la force correspondant à l'interaction entre une particule et une surface plane (Seville, Willett, & Knight, 2000). Les différentes forces interparticulaires considèrent un seul point de contact entre des particules sphériques dans l'air. Le poids des particules est comparé aux forces de van der Walls (A_H = 6.5 × 10^{-20} J) pour deux séparations particulaires, à la force capillaire maximale pour de l'eau (= 72.8 × 10^{-3} N.m^{-1}) ainsi que des

forces électrostatiques maximales ($C^2\ N^{-1}\ m^{-2}$ et densité de charge = 10 µC m^{-2}).

2.3 Modélisation des procédés de granulation

Il existe différentes approches permettant de modéliser la granulation humide. Toutefois deux d'entres elles se démarquent par le fait qu'elles peuvent inclure les mécanismes de granulation précédemment décrits, soit les modèles basés sur les bilans de population (PBM) et la méthode des éléments discrets (DEM). Ces deux approches sont discutées dans cette section.

2.3.1 Méthode des éléments discrets (DEM)

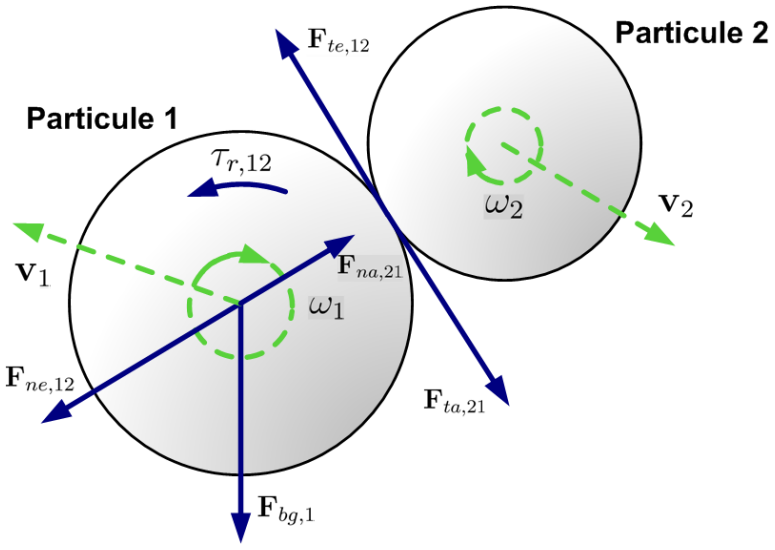

Figure 2-11: Schéma présentant les modèles de force pour la DEM

La DEM est un modèle permettant de simuler le mouvement des particules et de prendre en compte les collisions entre des particules voisines ou avec des parois d'équipement de manière

explicite. La méthode calcule le mouvement de chaque particule en intégrant numériquement la deuxième loi de mouvement de Newton, ce qui permet de considérer les forces agissant sur celle-ci :

—— (2-18)

—— (2-19)

où , , , , et sont la masse, le rayon, le moment d'inertie, la position, la vitesse angulaire et le couple de résistance au roulement de la particule suivant la collision avec la particule , et où représente le vecteur gravitationnel. À chaque pas de temps, la méthode donne la position de chaque particule ainsi que sa vitesse. Les collisions entre les particules ou une particule et une surface du domaine de calcul sont considérées comme inélastiques et sont représentées à l'aide d'un modèle de type ressort-amortisseur avec des contributions normales et tangentielles. et représentent les composantes normale et tangentielle de la force totale exercée par toutes les particules dans l'environnement immédiat de la particule . Ce modèle qui est décrit en détail dans (Bertrand, Leclaire, & Levecque, 2005), est basé sur les travaux de Cundall et Strack (Cundall & Strack, 1979) et de Zhou et al. (Zhou, Wright, Yang, Xu, & Yu, 1999). Il est à noter que d'autres forces hydrodynamiques (ex. les effets de traînée) ou non-hydrodynamiques (ex. les forces colloïdales) peuvent être ajoutée au bilan de force présenté dans (2-18) et (2-19).

La DEM possède des avantages par rapport aux bilans de population présentés à la suite de cette section. En effet, cette méthode permet d'inclure des interactions complexes et de décrire le déplacement des particules à l'intérieur d'un équipement, ce qui est plus difficile à faire pour la PBM. La DEM, une fois bien paramétrée à l'aide de mesures expérimentales pour le système considéré, peut très bien représenter les patrons d'écoulement pouvant être observé à l'intérieur d'un équipement tel qu'un granulateur (Ben Freireich, Li, Litster, & Wassgren, 2011; B.

Freireich, Litster, & Wassgren, 2009). Cependant, la DEM est très exigeante au niveau du temps de calcul comparativement à la PBM. Ceci vient du petit pas de temps normalement requis afin de bien représenter les contacts entre particules et ainsi assurer la stabilité de la méthode. De plus, les quantités associées aux interactions collisionnelles telles que la fréquence de collision ou la vitesse d'impact entre particules dépendent fortement des paramètres du modèle de contact utilisés dans la DEM. Puisque ces paramètres sont difficiles à mesurer pour une particule et que ceux-ci peuvent varier considérablement à l'intérieur du même système, les mécanismes de granulation ne peuvent pas encore être représentés avec robustesse (B. Freireich, Litster, & Wassgren, 2009). Pour cette raison, une approche combinée entre la DEM et la PBM semble être le meilleur moyen actuellement de pouvoir considérer le déplacement particulaire avec la première méthode, et les mécanismes de granulation avec la deuxième afin d'obtenir un modèle multi-échelle du procédé (Cameron, Wang, Immanuel, & Stepanek, 2005; Ingram & Cameron, 2004; J. Li, Freireich, Wassgren, & Litster, 2011). La prochaine section présente la méthode des bilans de population.

2.3.2 Bilans de population

Un bilan de population prend en compte les changements dans le temps que subissent un groupe de particules au niveau de leur nombre en fonction de leurs propriétés intrinsèques. Le bilan de population a l'avantage de pouvoir intégrer les mécanismes de granulation assez aisément dans la relation qui lui est associée. La forme générale de cette relation peut être exprimée de la manière suivante (A. D. Salman, Hounslow, & Seville, 2007; Zhao & Zheng, 2009):

(2-20)

où (m^{-6}) correspond à la distribution de taille des particules de telle manière à ce que (m^{-3}) soit le nombre de concentration particulaire dans l'intervalle de taille à au temps , ($m^3 \cdot s^{-1}$) est le noyau de coalescence pour les particules de taille et , est la probabilité de créer une particule fille de taille à partir d'une particule ayant originellement une taille , (m^{-3}) est le nombre de particules résultant du bris d'une particule de taille , (s^{-1}) est le noyau de bris, (m^{-6} s^{-1}) est le noyau de nucléation, est le volume du nucleus généré, et (s^{-1}) et (s^{-1}) sont les taux d'entrée et de sortie des particules du domaine de simulation considéré respectivement.

L'expression (2-20) est une équation intégro-différentielle partielle (Goodson & Kraft, 2004). Des solutions analytiques peuvent seulement exister lorsque des kernels de coalescence ou de bris simples sont utilisés. Cependant, ceux-ci ne représentent pas des cas physiquement observés et sont plutôt utilisés afin de valider des algorithmes associés aux bilans de population. Pour cette raison, des méthodes numériques sont requises afin de résoudre les bilans de population comportant des mécanismes complexes. Les solutions numériques sont habituellement obtenus par une discrétisation de l'équation continue (2-20) de telle sorte à représenter les termes intégraux par des sommations, ce qui facilite la résolution par des approches telles que la méthode des moments ou la famille des approches discrètes (Immanuel & Doyle Iii, 2005; Ramkrishna, 2000; Zhao & Zheng, 2009).

Lorsque le bilan de population fait intervenir seulement la taille des particules comme c'est le cas pour l'équation (2-20), le bilan est considéré comme unidimensionnel. Les bilans de population multi-dimensionnels sont utilisés lorsque les mécanismes de granulation dépendent de deux ou plusieurs autre propriétés particulaires. La granulation dépend, dans la majorité des cas, de plusieurs caractéristiques incluant la forme, la composition, la porosité et le niveau de saturation des granules. Les bilans multi-dimensionnels sont de plus en plus employés afin de simuler les procédés de granulation (Gantt & Gatzke, 2006; Immanuel & Doyle Iii, 2005; Oullion, Reynolds, & Hounslow, 2009; Ramachandran, Immanuel, Stepanek, Litster, & Doyle Iii, 2009). Par contre, il est recommandé de considérer la modélisation des mécanismes granulaires principaux

(coalescence, bris et nucléation) car, autrement, la solution du modèle peut devenir très complexe et rendre les prédictions imprécises (Rynhart, 2004). Les méthodes numériques précédemment mentionnées peuvent être employées pour résoudre les bilans multi-dimensionnels mais il est préférable d'utiliser d'autres approches comme la méthode des éléments finis ou la méthode de Monte-Carlo par exemple. Il a été démontré que ces méthodes sont beaucoup plus efficaces et peuvent donner de meilleurs résultats lorsqu'une multiplicité de paramètres est considérée (Cameron, Wang, Immanuel, & Stepanek, 2005; Y. Liu & Cameron, 2003; Ramkrishna, 2000).

Dans les bilans de population, l'écoulement particulaire n'est souvent pas pris en compte ou est seulement considéré indirectement par l'ajustement des mécanismes de granulation en fonction de certaines propriétés rhéologiques du milieu granulaire (la fréquence de collision entre les particules, leur vitesse moyenne ou les forces de déformation impliquées). Aucune étude n'a encore approfondi ou quantifié la manière dont les écoulements particulaires peuvent influencer les procédés de granulation.

CHAPITRE 3 ORGANISATION DE LA THÈSE

La granulation humide peut être représentée comme un ensemble de mécanismes granulaires qui affectent la taille moyenne ainsi que la distribution de taille des particules. Comme on a pu le voir au Chapitre 2, les trois mécanismes principaux, soit la nucléation/mouillage, la coalescence ainsi que le bris des granules, peuvent être intégrés à l'intérieur de modèles comme le bilan de population par exemple. Celui-ci peut être résolus numériquement afin de pouvoir simuler les procédés de granulation. Toutefois, l'utilisation de ces modèles se fait dans un contexte où le granulateur est considéré comme étant parfaitement mélangé.

Ainsi les objectifs spécifiques de cette thèse sont :

1. Quantifier la ségrégation et les propriétés d'écoulement de particules dans un sphéroniseur modifié;

2. Établir les frontières des types d'écoulement de particules en fonction des forces interparticulaires et des forces de cisaillement dans un sphéroniseur modifié;

3. Développer une méthode de modélisation multi-échelle (mécanismes de granulation et écoulement de particules) permettant de prédire la distribution de taille de granules en fonction du temps.

Dans le but de répondre aux objectifs spécifiques fixés, la première étape des travaux, présentée dans le premier article, consiste à s'intéresser à la manière dont le mélange et la ségrégation se comportent avec un granulateur caractérisé par un cisaillement important. Cette partie du travail permet aussi d'obtenir les patrons d'écoulement des particules dans l'équipement sélectionné pour cette étude, soit le granulateur à rotor. Les patrons d'écoulement sont utilisés dans le cadre

de la dernière étape du travail (article 4) afin d'être considérés dans les simulations du procédé de granulation humide.

Le deuxième article présente le développement d'une méthode permettant d'étudier les écoulements particulaires cohésifs qui sont retrouvés durant l'opération des équipements de granulation. Cette méthode utilise des particules enrobées d'un polymère dont la température de transition vitreuse est plus faible que la température ambiante. L'approche développée permet de contrôler les forces de cohésion dans un écoulement utilisant ces particules. Ces forces augmentent avec l'incrémentation de température ou en augmentant l'épaisseur de l'enrobage. Cette approche permet d'introduire les forces interparticulaires de manière homogène dans le lit de particules tout en utilisant les paramètres précédemment mentionnés afin d'ajuster la force de cohésion à la valeur désirée. La méthode cohésive est testée pour deux applications différentes. La première application permet de représenter des écoulements cohésifs propres à la granulation humide et l'autre application permet d'utiliser l'approche afin de reproduire l'écoulement de particules dans des lits fluidisés à haute température.

Le troisième article consiste à employer la méthode développée dans le cadre du deuxième article afin de révéler différents états d'écoulement observés dans un granulateur à rotor. La construction d'un diagramme d'écoulement présentant ces états permet de faire un parallèle avec la granulation humide qui est caractérisée par des forces capillaires dont le comportement peut être reproduit par la méthode cohésive employée. Cette partie discute aussi dans quel état d'écoulement un procédé de granulation humide devrait être idéalement opéré afin de pouvoir obtenir un produit uniforme dont les propriétés peuvent être ajustées adéquatement.

Le dernier article développe un modèle multi-échelle qui utilise les mécanismes de granulation se produisant à l'échelle particulaire tout en considérant la dynamique d'écoulement des particules à l'échelle du granulateur à rotor pour modéliser le procédé de granulation. Ce modèle utilise une approche stochastique qui résout un bilan de population avec l'aide d'une méthode de Monte-Carlo commandée par événement. L'inclusion des propriétés d'écoulement est effectuée de manière directe en employant une chaine de Markov à temps continu dont les propriétés sont

construites à partir des patrons d'écoulement obtenus des simulations DEM décrites dan le premier article.

Avant de passer à travers les quatre étapes de cette thèse, la méthodologie utilisée dans le cadre de ce travail est présentée dans le Chapitre 4 qui suit.

CHAPITRE 4 MÉTHODOLOGIE

Ce chapitre présente les différentes méthodes numériques et expérimentales utilisées dans le cadre de cette thèse afin d'atteindre l'objectif général et les objectifs spécifiques s'y rattachant. Davantage de détails sur la méthodologie ainsi que les méthodes de simulation employées seront donnés dans les articles correspondants.

4.1 Le sphéroniseur modifié en granulateur à rotor

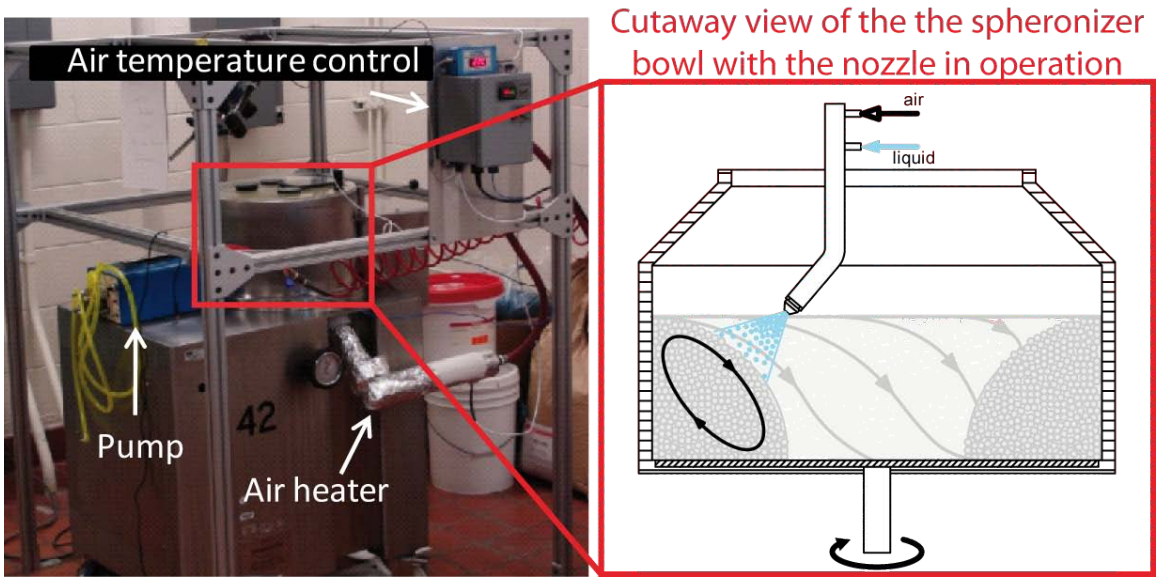

Figure 4-1: Sphéroniseur Caleva 380 utilisé pour enrober les particules et effectuer les expériences de granulation. Un atomiseur a été inséré au travers du couvercle du sphéroniseur afin d'ajouter la solution d'enrobage ou l'eau, utilisé comme liant pour les granulations, à la surface du lit de particules.

Le sphéroniseur (Caleva 380) présenté à la Figure 4-1 a été modifié afin d'inclure une entrée d'air sous le disque de l'équipement pouvant être chauffé à l'aide d'un échangeur. La température est ajustée à l'aide d'un contrôleur couplé à un thermocouple qui mesure la température à l'entrée

du tuyau d'air. Le débit d'air est ajusté avec une vanne située aussi à l'entrée du tuyau et d'un rotamètre à gaz. Une solution d'enrobage ou un liant pour la granulation peut être ajouté avec l'aide d'un atomiseur à deux fluides (BETE XA-SR 050). Dans ce cas, l'atomiseur est alimenté avec une pompe péristaltique au débit de liquide désiré tout en utilisant de l'air comprimé pour permettre la formation de gouttelettes. La vitesse de rotation du disque au bas du bol de l'équipement peut être ajusté manuellement à l'aide d'un positionneur mécanique. Le bol du sphroniseur a un diamètre de 42 cm interne avec une hauteur de 25 cm.

4.2 Modélisation de l'écoulement granulaire dans le sphéroniseur

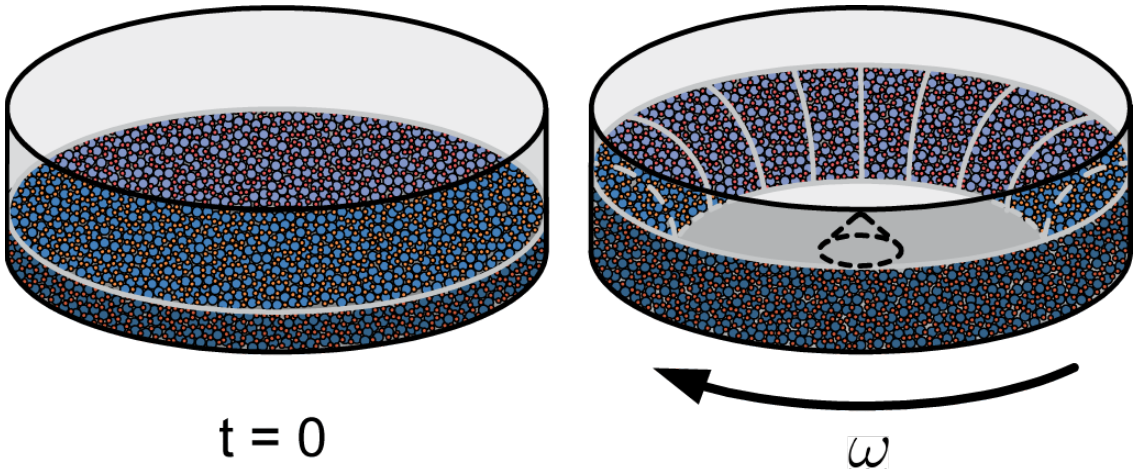

Figure 4-2: Schéma du sphéroniseur utilisé pour les simulations

Le sphéroniseur simulé avec la DEM est un cylindre de 0,3 m de diamètre et 0,2 m de hauteur au bas duquel un disque rotatif est ajouté. La vitesse de rotation a été variée entre 10 et 100 rad/s. Dans les simulations DEM, la vitesse du disque est augmentée de telle manière à atteindre sa vitesse finale en moins d'une seconde, ce qui est négligeable par rapport au temps de simulation du procédé et des comportements d'écoulement et de mélange. Un mélange avec une distribution 50/50 %m de particules sphériques de 2 mm et 4 mm a été considéré. Comme l'objectif de cette partie du travail était de quantifier la dynamique de ségrégation pour le système particulaire bidisperse, les particules ont été distribuées aléatoirement dans la géométrie. L'ajout de ces

particules a été réalisé en les positionnant dans un arrangement cubique initialement localisé au dessus du disque du sphéroniseur et qu'on a laissé sédimenter avant de lancer les simulations. Le type de particules localisé dans l'arrangement cubique a été sélectionné aléatoirement avec une fonction de densité représentant la distribution de taille des particules. Par la suite, la vitesse du disque a été ajustée de telle manière à obtenir la forme toroïdale présentée à la Figure 4-2.

Table 4-1: Paramètres de simulation

Cas		**Nombre de particules**
Remplissage élevé	Particules de 2-mm	131555
	Particules de 4-mm	16445
Remplissage faible	Particules de 2-mm	71111
	Particules de 4-mm	8999
Propriétés		**Valeur**
Module de Young		4,87 MPa
Ratio de Poisson		0,2
Masse volumique		1500 kg/m^3
Coefficient de friction (particule/particule)		0,5
Coefficient de friction normal (mur/particule)		0,5
Coefficient de friction tangentiel (mur/particule)		0,5
Coefficient de friction de roulement (mur/particule)		0,0005 m

Les simulations ont été exécutées jusqu'au moment où la ségrégation devenait stable sur la base des courbes de mélange employées. Suite à un ajustement des paramètres du modèle de la DEM (voir Table 4-1), les deux niveaux de remplissage ainsi que les vitesses de rotation du disque ont pu être étudiés. La hauteur du lit initial était de 11,1 mm et 20,5 mm pour le bas et le haut niveau de remplissage respectivement. Les simulations ont été exécutées sur une grappe IBM avec 8 processeurs Opteron d'ADM 246 (2GHz) pour le bas niveau de remplissage alors qu'une grappe Dell SC1425 avec 16 processeurs Intel Xeon (3,6 GHz) a été utilisée pour le haut niveau de remplissage.

4.3 Écoulement cohésif avec l'approche polymérique

4.3.1 Fabrication des particules

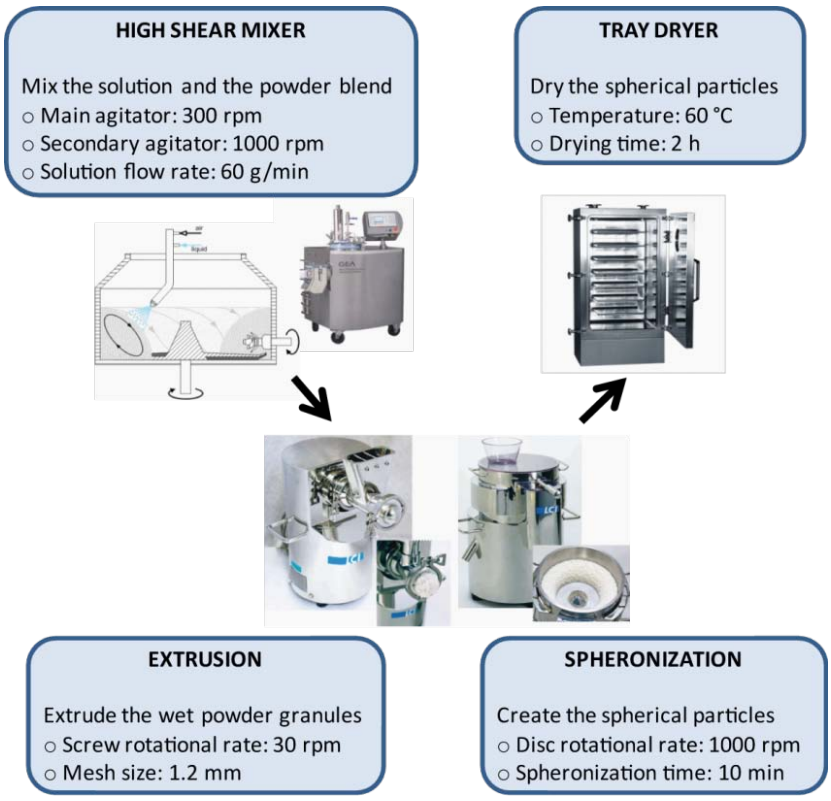

Figure 4-3: Procédé d'extrusion-sphéronisation pour produire les particules utilisées dans les expériences

La Figure 4-3 montre les équipements utilisés pour produire les particules sur lesquelles le polymère est déposé. Une étape préliminaire de mélange a été effectuée dans un mélangeur à cisaillement élevé. Lorsque le mélange de poudre présenté au Tableau 4-2 devenait homogène, une solution liante, dont la composition est présentée dans le même tableau, était ajoutée afin de granuler le matériel. Ces granules étaient par la suite alimentés à une extrudeuse et le produit résultant était transféré dans un sphéroniseur afin de créer des billes sphériques. Ces particules ont été séchées dans un séchoir à plateaux.

Tableau 4-2: Poudre et solution utilisées pour la production des particules

Éléments	**Matériel**	**Quantité (kg)**
Mélange de poudre	MCC PH-101	0,200
	Lactose monohydrate	0,200
	NaCl	0,100
Solution liante	Eau	0,315
	NaCl	0,095
	Quinoline jaune	0,002

4.3.2 Enrobage des particules avec la dispersion polymérique

L'enrobage des particules a été effectuée à l'aide du sphéroniseur modifié présenté à la Figure 4-1. Le Tableau 4-3 présente les paramètres associés au procédé d'enrobage. Durant l'opération,

la vitesse du disque était ajustée à 230 rpm de telle manière à obtenir un mélange adéquat des particules tout en prévenant leur bris pouvant survenir avec un cisaillement trop important. Le débit d'air et sa température étaient ajustés pour obtenir un séchage adéquat et ainsi prévenir l'agglomération des particules. La suspension d'enrobage est présentée dans le Tableau 4-4. Celle-ci était ajoutée avec l'aide d'un atomiseur à deux fluides (BETE XA-SR 050). L'atomiseur était alimenté avec une pompe péristaltique à un débit équivalent à environ 1 g/min en utilisant de l'air comprimé pour permettre la formation de gouttelettes. L'atomiseur était positionné à 4 cm de la surface du lit de particules, ceci permettant de minimiser les pertes de polymère le long des parties mécaniques du sphéroniseur modifié.

Tableau 4-3: Paramètres d'enrobage du polymère

Paramètres	**Valeurs**
Vitesse du disque	230 rpm
Débit d'air	42,5 m^3/h
Température d'air	30 ° C
Débit de solution	1 g/min
Pression d'atomisation	200 kPa

Tableau 4-4: Suspension d'enrobage Eudragit® NE30D

Matériel	**Masse %**
Eau	68,5
PEA/PMMA 2:1	30,0
Nonoxynol 100	1,5

4.3.3 Mesures de la morphologie de surface et de la masse volumique dynamique

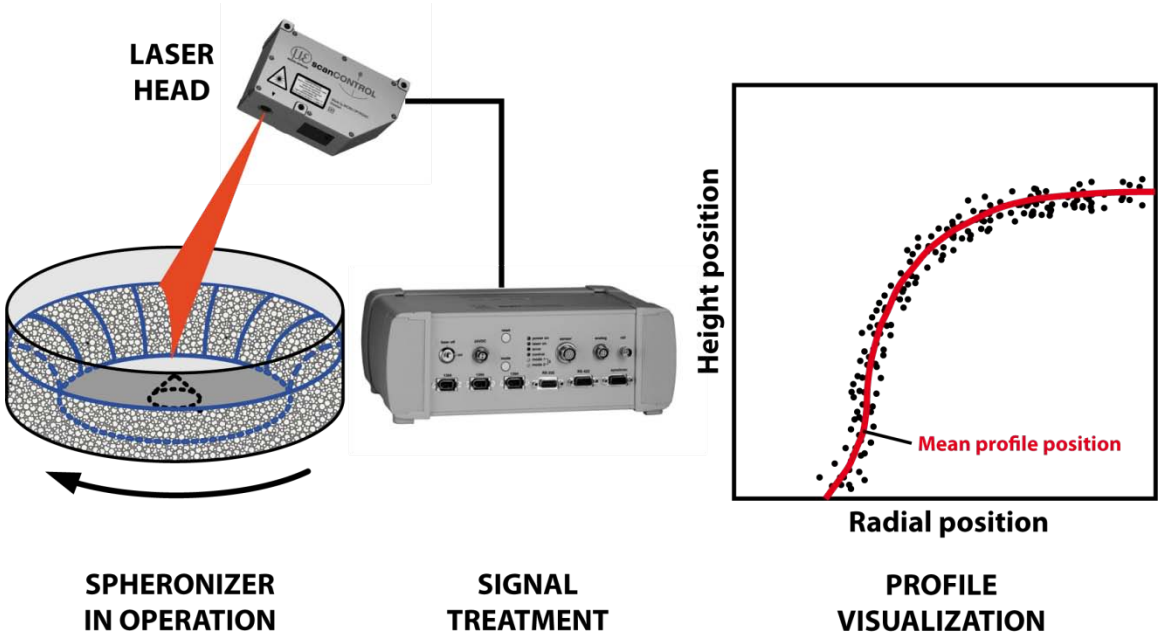

Figure 4-4: Mesure de surface avec le profileur laser. La tête de mesure crée un plan laser à la surface du lit de particules et la lumière réfléchie est enregistrée avec une caméra CCD située dans le même appareil. Le signal est alors tranféré au boitier de contrôle afin d'évaluer la position du profil de surface en deux dimensions par triangulation.

La surface du tore dans le sphéroniseur (Caleva 380) a été caractérisée en prenant des photos avec une caméra numérique et à l'aide d'un profileur laser. La Figure 4-4 présente l'équipement utilisé pour mesurer avec précision la position de la surface du tore pendant que le sphéroniseur était en opération. Un profileur laser 2800 LLT Scancontrol (Micro-Epsilon) mesurait la position de surface moyenne ainsi que la variance associée afin de calculer le volume du tore. La masse volumique dynamique était obtenue en divisant la masse totale de particules par rapport au volume calculé avec l'appareil laser. L'étendue de température considérée était supérieure à la température de transition vitreuse du polymère PEA/PMMA afin d'observer un comportement

cohésif pour les particules en écoulement. Le débit d'air était ajusté entre 20,4 et 25,5 m^3/h afin d'empêcher des changements significatifs de l'écoulement par rapport au cas où le débit d'air est nul. L'entrée d'air permettait de contrôler la température du lit de particule.

4.3.4 Mesure des propriétés des enrobages de polymère

La température de transition vitreuse a été mesurée avec un DSC Q1000 (TA Instruments, USA). Les échantillons de polymère ont été traités sous une atmosphère d'azote et chauffés et refroidis à des taux de 10 °C/min entre 20 °C et 170 °C. La force de séparation entre deux surfaces enrobées de polymère a été quantifiée avec un appareil de mesure de force de surface (SFA) pour différentes températures. Le SFA est un équipement qui permet de déterminer les forces d'interactions normales en fonction de la distance de séparation tout en mesurant la déflection d'un ressort qui supporte la surface inférieure au fur et à mesure que la distance de séparation est changée. La distance entre les deux interfaces est déterminée avec une résolution de ca. 0,2 nm en utilisant une technique d'interférométrie standard qui utilise de franges d'un ordre chromatique équivalent. Pour chaque mesure effectuée, la charge en compression était constante à 1 mN, le temps de contact était de 1 minute et le taux de décompression était gardé constant à 12,5 nm/s.

4.4 Granulation des poudres avec le sphéroniseur modifié

4.4.1 Matériel

Lactose (Lactose monohydrate 100M) fourni par Lactose (India) Ltd. (Mumbai, India) et cellulose microcrystalline (Avicel PH-101) fourni par FMC BioPolymer (Philadelphia, USA) ont été employés comme constituant du mélange de poudre utilisé pour la granulation. Le liant liquide était de l'eau.

4.4.2 Procédé de granulation et équipement

Le même sphéroniseur modifié que pour les expériences avec l'approche cohésive par enrobage de polymère a été utilisé pour effectuer les granulations. Le Tableau 4-5 présente les paramètres de procédé pour les trois expériences effectuées.

Tableau 4-5: Paramètres de procédé pour la granulation avec le sphéroniseur modifié

No.	Disque (rpm)	Débit liquide (g/s)	Temp. air entrée (°C)	Débit air (m^3/h)	Nombre d'échantillons
1	750	0,3333	35	10,2	5
2	1000	0,3333	35	10,2	5
3	1000	0,5000	35	10,2	5

4.4.3 Caractérisation des particules et gouttelettes

Durant une granulation, cinq échantillons d'environ 50 g étaient prélevés du lit de particules, ce qui demandait de cesser l'opération du sphéroniseur modifié. Une fois l'échantillon obtenu, le procédé était redémarré et le matériel échantillonné était placé dans un four à plateau. Une fois l'échantillon sec, celui-ci était pesé afin d'obtenir le contenu en eau des granules au moment de l'échantillonnage. L'échantillon sec était par la suite analysé par tamisage avec un Ro-Tap® RX-29 (W.S. Tyler, Mentor, USA) afin d'évaluer la distribution de taille particulaire. La distribution de taille des gouttelettes a été mesurée avec un Malvern Particle/Droplet sizer (Malvern Instruments Ltd., Worcestershire, UK) avec le protocole présenté par (Bouffard, Kaster, &

Dumont, 2005). La composition du lit de particules pour toutes les expériences est présentée au Tableau 4-6.

Tableau 4-6: Poudre et liant utilisés pour la granulation

Éléments	**Matériel**	**Quantité (kg)**
Mélange de poudre	MCC PH-101	0,75
	Lactose monohydrate	1,50
Liant	Eau	2,00

CHAPITRE 5 CARACTÉRISATION DES PATRONS D'ÉCOULEMENT ET DE LA SÉGRÉGATION DANS UN SPHÉRONISEUR AVEC UNE MÉTHODE PAR ÉLÉMENTS DISCRETS

5.1 Présentation du premier article

Soumis à *Computer and Chemical Engineering* le 04 Février 2011

Auteurs: Jonathan Bouffard, François Bertrand, Jamal Chaouki et Hubert Dumont

Cet article a pour objectif d'étudier l'impact des paramètres d'opération d'un sphéroniseur sur les propriétés d'écoulement de particules ayant une distribution de taille bidisperse. Une méthode par éléments discrets (DEM) a permis de simuler le mouvement toroïdal adopté par les particules afin de quantifier l'effet de la vitesse du disque et du niveau de remplissage sur les patrons de ségrégation et la dynamique d'écoulement. En utilisant des indices de mélange, il a été possible de quantifier la ségrégation dans le domaine de particules et ainsi montrer l'effet significatif des paramètres de procédé sur l'intensité de cette ségrégation.

Pour des vitesses de disque entre 20 et 100 rad/s, deux zones de ségrégation ont été observées. Lors d'une augmentation de la vitesse du disque, les petites particules ont tendance à migrer d'une zone située au centre local de rotation du tore vers une zone située près de la paroi du sphéroniseur. Pour une vitesse de disque de 10 rad/s, il a été mis en évidence que la dynamique d'écoulement induit des patrons de ségrégation qui sont très différents de ceux observés pour des vitesses plus grandes.

Une corrélation représentant la vitesse azimutale des particules dans le tore est présentée de telle manière à pouvoir considérer l'effet du cisaillement. Cette modification constitue une amélioration d'une expression similaire ayant été présentée par (Corwin, 2008).

5.2 Discrete element investigation of flow patterns and segregation in a spheronizer

5.2.1 Abstract

Powder flow in a spheronizer is characterized by a toroidal motion and the flow patterns depend on the disc velocity and the fill level, but also on the particle properties. This work investigates numerically, with a discrete element method (DEM), the impact of these parameters on segregation patterns and the flow dynamics for bidisperse particle size distributions. Characterization of the segregation, by means of a mixing index and the relation with the shear stress in the toroidal domain, is presented. Characteristics, such as mixing curves, concentration profiles and azimuthal velocity correlations, are discussed. A logarithmic expression has been developed to account for the shear stress on the evolution of the azimuthal velocity inside the particulate bed. The combination of the mixing indexes and the concentration profiles is used to quantify the changes observed on the segregation when the fill level and the rotational rate of the spheronizer disk are varied.

5.2.2 Introduction

Granular mixing is a physical phenomenon involved in a variety of industrial applications. An interesting aspect associated with particle mixing is its inherent limitation due to segregation. This phenomenon is a crucial aspect to take into account in powder mixing applications because it can lead to various problems, such as a lack of uniformity in the final product, or cause several difficulties in the subsequent operations of a multiple-step process. Most of the reported work on powder segregation has been done in the case of low speed and low shear systems such as V-blenders or other tumbling equipment, fluidized beds and silos [1, 8, 13, 14, 15, 16, 17, 20].

Such blenders, for instance, facilitate the occurrence of segregation patterns because of the predominance of the sifting and surface flow mechanisms associated with the particle dynamics [2]. Knowing how the segregation will occur and which particle patterns are created can help to predict the process behavior and alleviate potential product quality problems. For example, in a

pan coater, the large particles tend to segregate toward the outer region of the powder bed. The atomization of a liquid on the top layer of particles favors the coating of these large particles, which will cause non-uniformity in the product. Using equipment that provides high shear in

the bed of particles is known to attenuate the segregation occurrence [2, 3]. Such equipment is often used with an impeller that enhances the convective movement of the particles. The impeller can be an agitator as in high shear mixer applications or a disc located at the bottom of the equipment. The use of a disc can be found in the spheronization process.

The spheronizer is often used in the pharmaceutical industry to obtain spherical pellets from powder extrudates. This equipment comprises a cylindrical shell and a rotor located at the bottom of the processing chamber. With a large enough rotational rate of the disc, a powder toroid is created and the particles flow with a characteristic spiral motion in the direction of the global azimuthal axis. The motion of the particles in the toroid can also be described as a function of two other axes along a sectional cut, as presented in Figure 5-1. These axes are the local azimuthal axis, referring to the rotational motion of the particles around the center of the sectional cut, and the local radial axis in this same cross-section. A few papers have investigated powder flow in this relatively simple geometry. The most recent one, by Corwin [3], studied the impact of the fill level and the rotational rate of dry monodisperse particles on the shear profiles and the surface velocities in the toroid. Muguruma et al. [18] evaluated the impact of cohesive forces due to liquid bridges on the velocity profiles at the surface of the powder toroid and inside via discrete element simulations. Other studies have employed a modified Couette cell that is similar to a spheronizer except for the fact that the disc radius is equal to a fraction of the cylinder radius, which implies that this disc occupies a portion of the bottom section [12, 9]. These two studies investigate the hydrodynamics and shear at low disc rotational rates (less than 2 rad/s). The flow regime is characterized by the quasistatic behavior of the particles and the fact that only a part of the material has the ability to move while the remaining particles stay at rest. The shear stress remains low enough so that the dense granular flow regime is never reached. On the other hand, the work by Corwin [3] also covers the dense granular flow regime, which is characterized by a uniform stress distribution throughout the particle bed.

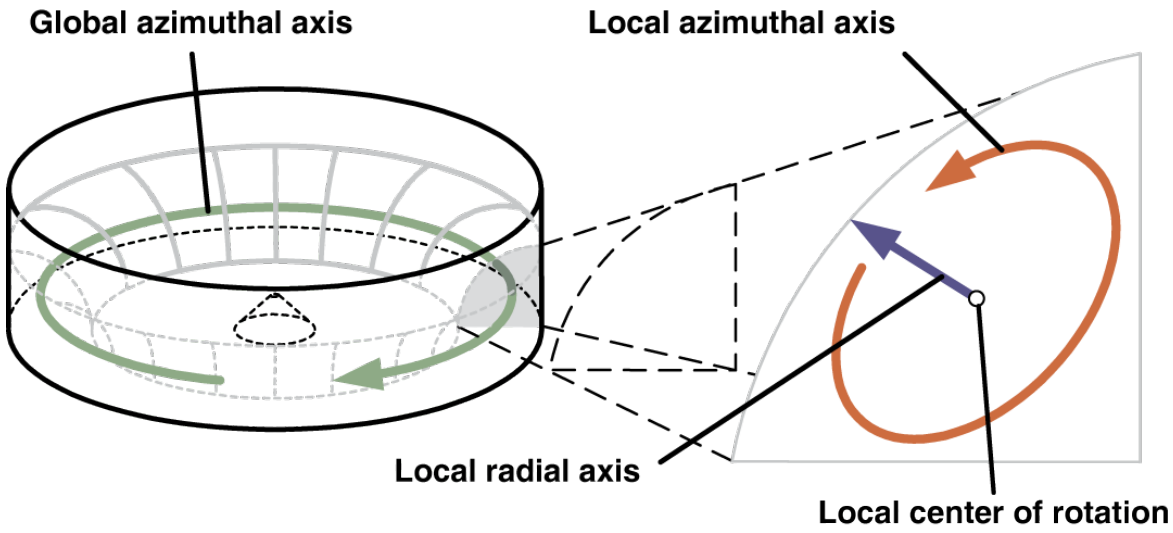

Figure 5-1: Spheronizer and its principal axes

Particle flow in a spheronizer or other rotor-based granulator equipment (with for instance a flat standard rotor such as the rotor granulators from Glatt or the Roto-Processor™ from Niro-Aeromatic, a curved rotor such as the Spir-a-flow® from Freund Vector or a conical rotor such as the Granurex® also from Freund Vector), which is often described in terms of “rope-like tumbling motion”, is still poorly understood. In this context, owing to its simple design, the spheronizer can be advantageously used to study the particle dynamics prevailing in this type of process. In fact, the investigations described above have only considered monodisperse particle size distributions, which means the effect of particle size on flow dynamics is still unknown. The objective of this work is then to gain insight into the effect of particle size on the flow behavior in a spheronizer. More precisely, emphasis is put on the impact of operating conditions on the segregation of a dry bidisperse particle size distribution. Simulation results obtained with the discrete element method (DEM), for two fill levels and different rotational rates are presented and analyzed on the basis of the azimuthal velocities. A model is also derived to shed light on the mechanisms prevailing in the spheronizer and the importance of the shear rate. To evaluate the segregation, a mixing index developed by Doucet et al. [7] is used, which leads to segregation maps. We would like to stress the importance of assessing the intensity of segregation in dry conditions first so as to better grasp how cohesive forces may impact it. If it is true that cohesion

often mitigates segregation, some authors have observed that cohesion can also enhance it (e.g. Li and McCarthy [16]).

5.2.3 Methodology

5.2.3.1 Discrete element method

The DEM is a particulate model that simulates particle motion and explicitly takes into account the collisions occurring between neighbouring particles or other solid objects like the walls of the computational domain. The particles are allowed to interpenetrate and the amount of overlap depends on a contact force model, such as the one described below and used in this work. The method calculates the motion of each particle by integrating numerically Newton's second law of motion that brings into play the force acting on it:

—— (5-1)

—— (5-2)

where , , , , and are the mass, radius, moment of inertia, position, angular velocity and rolling resistance torque of particle following the collision with particle , and where represents gravity. At each time step, the method gives the current position of each particle as well as its velocity. In this work, the collisions between two particles or a particle and a rigid surface are considered as inelastic and are modeled by means of a spring-dashpot type model with normal and tangential contributions. and represent the normal and tangential components of the total force exerted by all particles j in the vicinity of particle i. This model, which is fully described in [15], is based on the work of Cundall and Strack [4] and Zhou et al. [23]. Other hydrodynamic (e.g., drag) or non-hydrodynamic (e.g., colloidal) forces could be added to the force balance in (5-1) and (5-2). Such terms were not considered in this work.

Equations (5-1) and (5-2) were integrated using the half-step leapfrog verlet scheme. A parallel version of this DEM-based model relying on an efficient domain decomposition technique was used to reduce the computational cost of the method. To ensure that the simulations proceed without numerical instabilities, a time step of 5 10^{-7} s was used for all cases. The reader is referred to [15] for more details on the DEM-based model used in this work.

5.2.3.2 Simulation setup

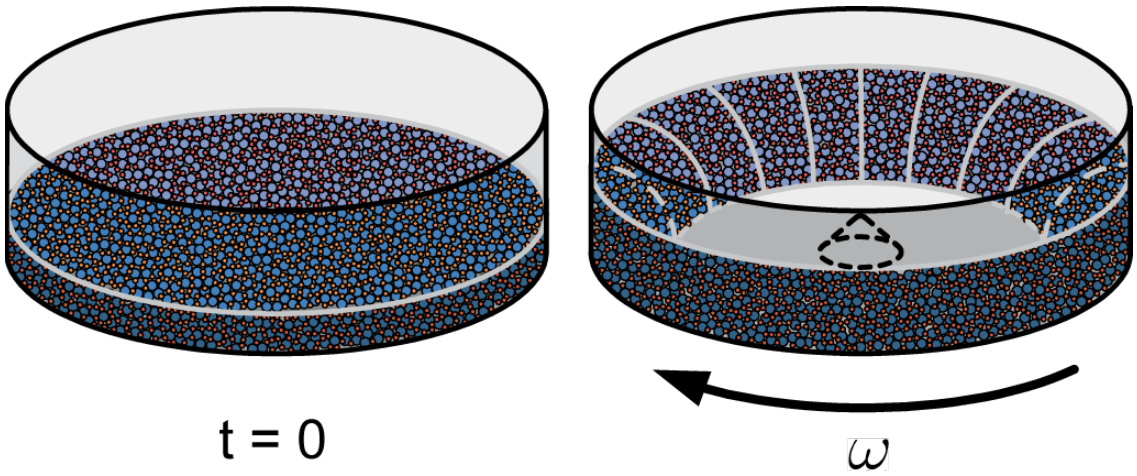

Figure 5-2: Spheronizer setup for the simulations

The spheronizer consists of a cylinder of 0.3 m in diameter and 0.2 m in height, at the bottom of which a rotating disc plate is located. The rotational rate was varied from 10 to 100 rad/s. In the DEM simulations, the disc speed was ramped up quickly initially so that its final value was reached within less than one second, which is negligible with respect to the process time, as regards flow and mixing behavior. This has been confirmed by varying the slope of the ramp in simulations. A 50/50 wt% distribution of 2 mm and 4 mm spherical particles was considered. Since the main objective of this work was to analyze the dynamics of segregation of such a bidisperse particle size distribution, the particles were initially randomly located at the bottom of the spheronizer. More precisely, the particles were positioned in a cubic arrangement located just above the spheronizer disc. The particle type, small or large, at any given position within this

structure, was selected randomly using a probability density function representing the desired particle size distribution. The particles were then dropped on the non rotating spheronizer disc, following which the simulation could be started. The required rotational rate for the disc was then applied to obtain the characteristic toroidal shape of the particle assembly shown in Figure 5-2. Simulations were executed until particle segregation became stable on the basis of mixing curves. Two types of simulations were run. First, values for the various friction coefficients in the DEM model were determined by simulating the flow of 1-mm particles and comparing the results to experimental data obtained by Corwin in the case of 1-mm spherical glass beads [3]. Note that the value of the Young's modulus used in this work, 4.87 MPa, is smaller than that of glass beads. The main reason for this is that the time step required to ensure stability in a DEM simulation is known to be inversely proportional to the Young's modulus. Using the actual value of this parameter would have resulted in very small time step and computational times of the order of one year. Our strategy here, which has been observed to work in practice (e.g. [15] and [23]), was to use a smaller value of this parameter and to calibrate the DEM model by adjusting friction coefficients so as to reproduce the experimental results obtained by Corwin [3]. More precisely, the sliding friction coefficients that we used were all equal to 0.5 and identical to those used by Corwin [3], while a rolling friction coefficient of 0.0005 was determined to yield adequate results. The rationale for adjusting only the latter friction coefficient is that Corwin [3] showed that varying the sliding friction coefficient from 0.2 to 0.75 only had a slight impact on the simulation results, which can be explained by the fact that Coulomb friction hardly affects the mean velocity of particles when these particles are allowed to roll (Dippel et al. [6]). This has been confirmed by our own simulations. To obtain the same fill level in these simulations as in the experiments, 45 mm, 1 500 000 particles were added to the computational domain.

Second, the DEM model was used to investigate the flow dynamics of distributions of 2-mm and 4-mm particles for low and high fill levels as well as various disc speeds, as described above. Details regarding these bidisperse particle flow simulations and the values of relevant physical parameters, including the friction factors, are given in Table 5-1. These two fill levels make it possible to investigate the impact of the number of particles on flow behavior. The initial bed heights for the low and high fill level cases were 11.1 mm and 20.5 mm, respectively. The simulations were performed on an IBM cluster with 8 AMD Opteron 246 (2GHz) processors for

the low fill level case while a Dell SC1425 cluster with 16 Intel Xeon (3.6 GHz) processors was used for the high fill level case. Approximately 375 hours of computational time were needed to simulate a time span of 10 s.

Table 5-1: Simulation parameters

Case		**Number of particles**
High fill	2-mm particles	131555
	4-mm particles	16445
Low fill	2-mm particles	71111
	4-mm particles	8999
Properties		**Values**
Young's modulus		4.87 MPa
Poisson ratio		0.2
Density		1500 kg/m^3
Friction coefficient (particle/particle)		0.5
Normal friction coefficient (wall/particle)		0.5
Tangential friction coefficient (wall/particle)		0.5
Rolling friction coefficient (wall/particle)		0.0005 m

5.2.3.3 Mixing index

Different methodologies can be employed to evaluate the level of mixing of powder materials. One of the most popular is to take samples from the bulk powder at different locations in the system [15]. Different measures of mixing can be used in conjunction with this intrusive experimental method. The intensity of segregation developed by Danckwerts [5] and its known variant for granular systems, the RSD (relative standard deviation), are commonly used. The reader is referred to Poux et al. [21] for a review of mixing measures for particulate systems. Some issues are related to this intrusive technique, such as the perturbation of the bulk powder with the sample thieves [19]. Numerical simulations with DEM can help understand the experimental results obtained from a sampling method since the position of all the particles can be predicted as a function of time. Two mixing indices that were developed recently in our group [7] can then be used to identify the main directions along which mixing takes place both spatially and with respect to specific properties, such as the size or the color of the particles. Such a mixing criterion, in fact, gives more information than RSD alone. These mixing criteria are described in detail in [7]. They bring into play the concepts of weak sense of mixing and strong sense of mixing, both of which are based on the trajectories of the particles and the assumption of stochastic independence.

Given a probability measure with the position of particle at time , a system is said to be mixed in the weak sense if for

(5-3)

This condition entails the independence of current position with respect to initial position . It means that the positions of the particles at time are not correlated with their initial positions, which indicates that they are spatially mixed. However, this mixing criterion does not take into account the particle organization with respect to size or any other relevant properties. Ultimately,

such organization may lead to a segregation phenomenon, as is often the case in industrial applications involving particulate materials with varying properties. Figure 5-3 shows an example of segregation taking place in a tumbler process with two powders of different colors but identical particle size distributions. Both powders are stratified in the tumbler initially and then mixed to lead to a blend that is uniform relative to color, but completely segregated relative to size. This system is mixed in the weak sense, but it is clear that this condition fails to capture the segregation state. To get a better picture of this situation, the concept of mixing in the strong sense is needed.

Given a probability measure and a set of particle properties, a system is said to be mixed in the strong sense if for :

(5-4)

This condition entails the independence of current position with respect to both initial position and properties such as the particle size or type. Obviously, any system that is mixed in the strong sense is also mixed in the weak sense. In Figure 5-3, two properties can be identified. They are the particle size and color . The particles in the tumbler are mixed in the weak sense, but not in the strong sense since a correlation between size and position exists.

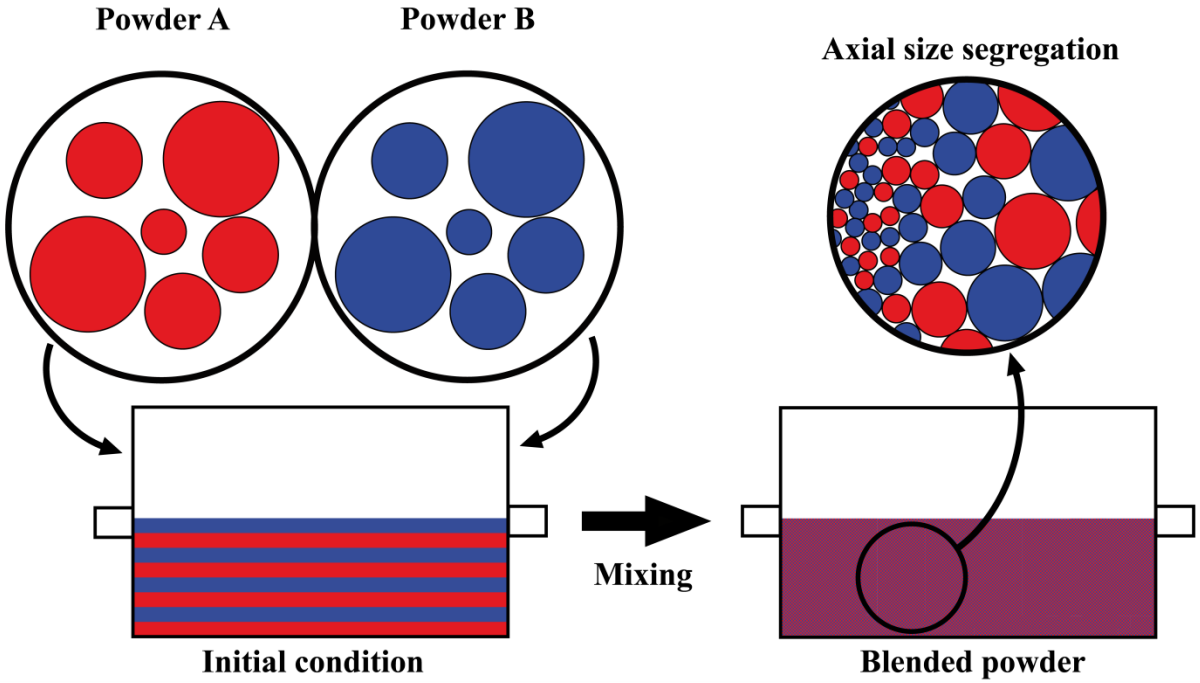

Figure 5-3: Illustration of a tumbler application for the mixing of two powders of different colors. Both powders are mixed with respect to color but segregated with respect to size. The system is mixed in the weak sense only (modified from Doucet et al. [7]).

5.2.4 Results and Discussion

The accuracy of the DEM simulations are first assessed by a comparison with experimental results obtained by Corwin [3] for the flow of monodisperse particles in a spheronizer. The mean global azimuthal velocities are compared with a correlation developed by Corwin [3]. In particular, the impact of the shear stress on this correlation is discussed. Simulation results of the flow of bidisperse particles for different rotational rates and fill levels are considered next. The segregation results are analyzed with respect to the flow dynamics and the shear stress in the spheronizer. The extent of the segregation is evaluated by means of the mixing index presented in the previous section.

5.2.4.1 Assessment of model accuracy

Simulation results obtained with the DEM-based model are compared to the experimental results of Corwin [3] in the case of monodisperse 1-mm glass beads. The particle bed surface profiles were measured with a laser profilometer with respect to the global radial axis of the spheronizer. A high speed camera was used with a velocimetry calculation method to measure the surface velocity of the particle bed. In Corwin [3], the quantity of particles was given as a function of the total mass and the fill level in the spheronizer. In our simulations, we recall that 1500000 particles were used, which corresponds to a fill level of 45 mm. Figure 5-4 compares the experimental and numerical values of the surface position and azimuthal velocity for different rotational rates. At first sight, the surface positions obtained experimentally are well represented by the surface positions predicted by the simulations. We believe that the deviations observed may still come from the values of the physical parameters used in the simulations even though our DEM model was calibrated using the simulation results of Corwin [3]. Overall, it can be readily noticed that the numerical results agree fairly well with the experimental data. More specifically, except for the 1 Hz rotational rate, the numerical global azimuthal velocities at the surface of the torus deviate from the experimental data at low values of the radial position. In these areas, larger values of the velocity are predicted. The experimental curves show that a nearly constant value of 0.5 m/s for the azimuthal velocity is reached near the center of the torus, at r = 0.05 m. A different behavior is noticed in the case of the numerical results, where the azimuthal velocity decreases monotically with respect to the radial position. In fact, a similar behavior was observed experimentally by Muguruma et al. [18], that is an almost linear decrease of the azimuthal velocities at the surface when approaching the wall of the equipment. In summary, despite discrepancies between the numerical and experimental velocities, the rather good quality of the simulation results indicates that our DEM-based model is a valuable tool for the investigation of the dynamics of particles in the spheronizer.

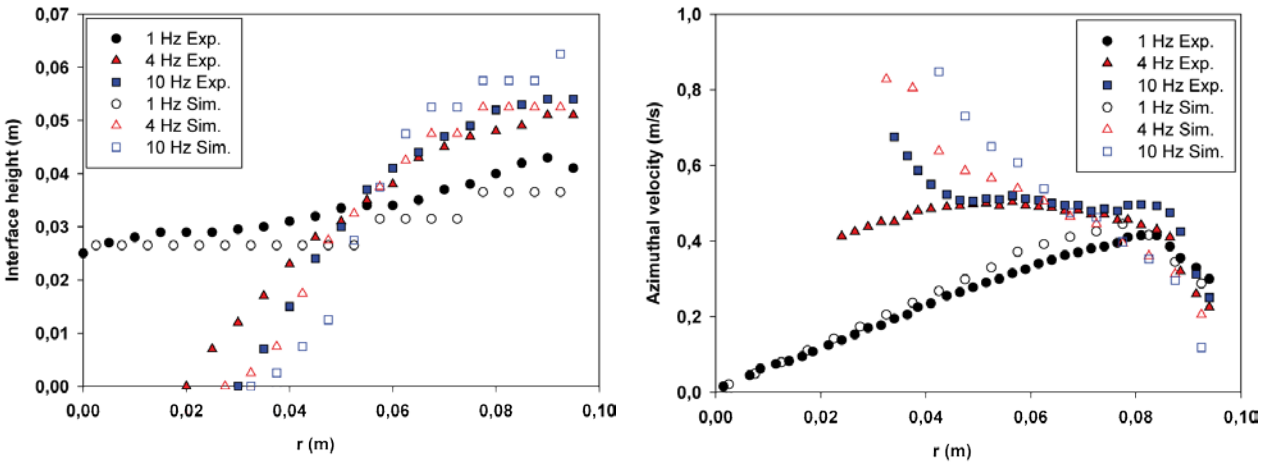

(a) Interface height

(b) Azimuthal velocity

Figure 5-4: Comparison of the DEM simulation results with experimental data obtained by Corwin [3] for a 1-mm monodisperse particle system.

5.2.4.2 Bidisperse system

The results are presented in two parts. The first part is concerned with the flow dynamics and, more particularly, the azimuthal velocity and the shear rate of the particles when the steady state has been reached. Note that the particle velocity and shear rate change mainly from the beginning of a simulation until the bed of particles has reached its final toroidal shape. After that, the changes were observed to be much less important. The second part analyzes the segregation patterns observed for the different cases that were simulated. The segregation is measured with the mixing index described in the previous section.

5.2.4.2.1 Azimuthal velocity and shear rate

The steady-state azimuthal velocity and the shear rate were computed for all cases. A modified correlation following the work of Corwin [3] and relating the azimuthal velocity and the position of the particles inside the toroidal shape is introduced and used for the analysis of the DEM results.

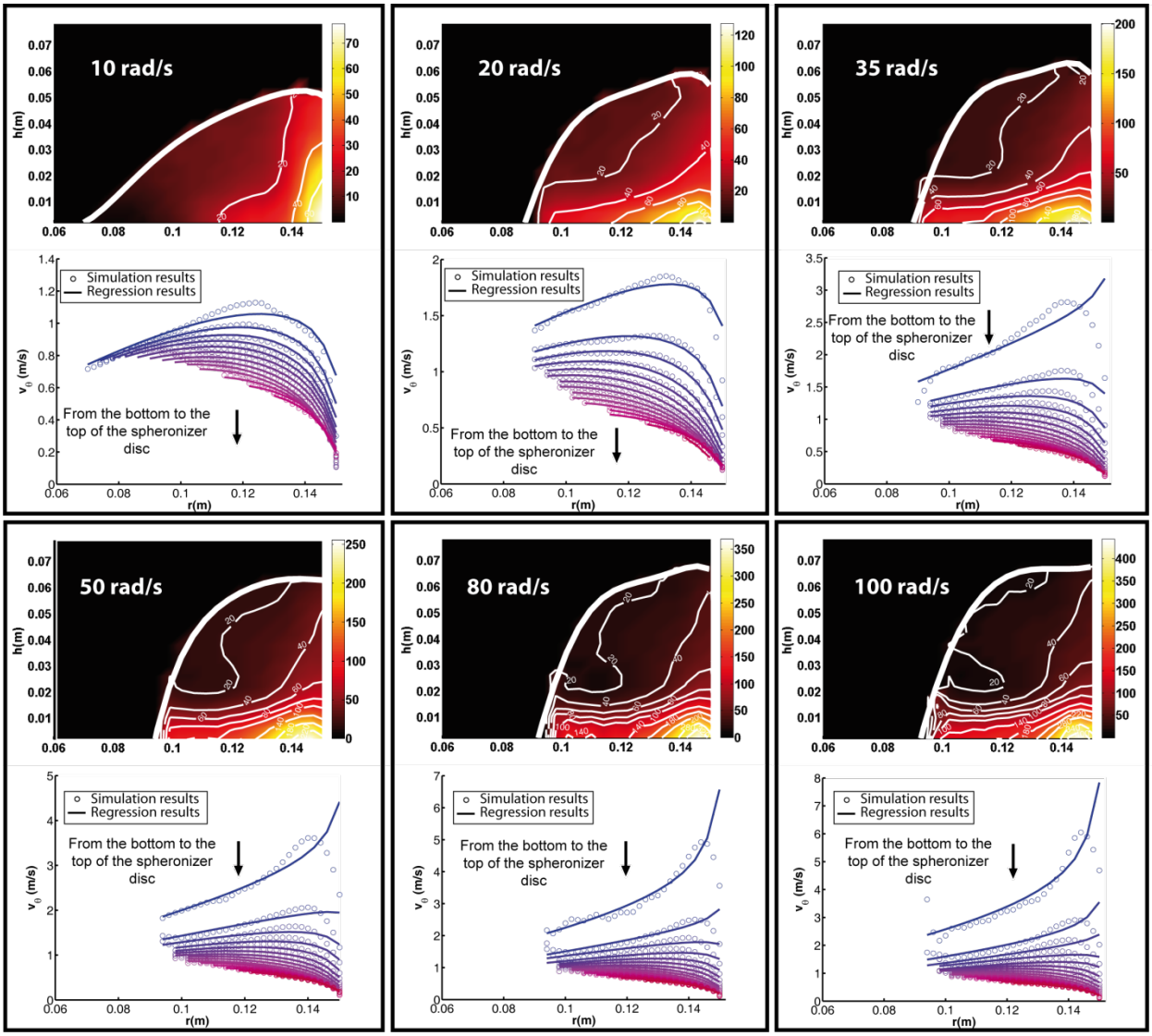

Figure 5-5: Final azimuthal velocity profiles for the low fill case and the corresponding shear rate (color map, in s^{-1})).

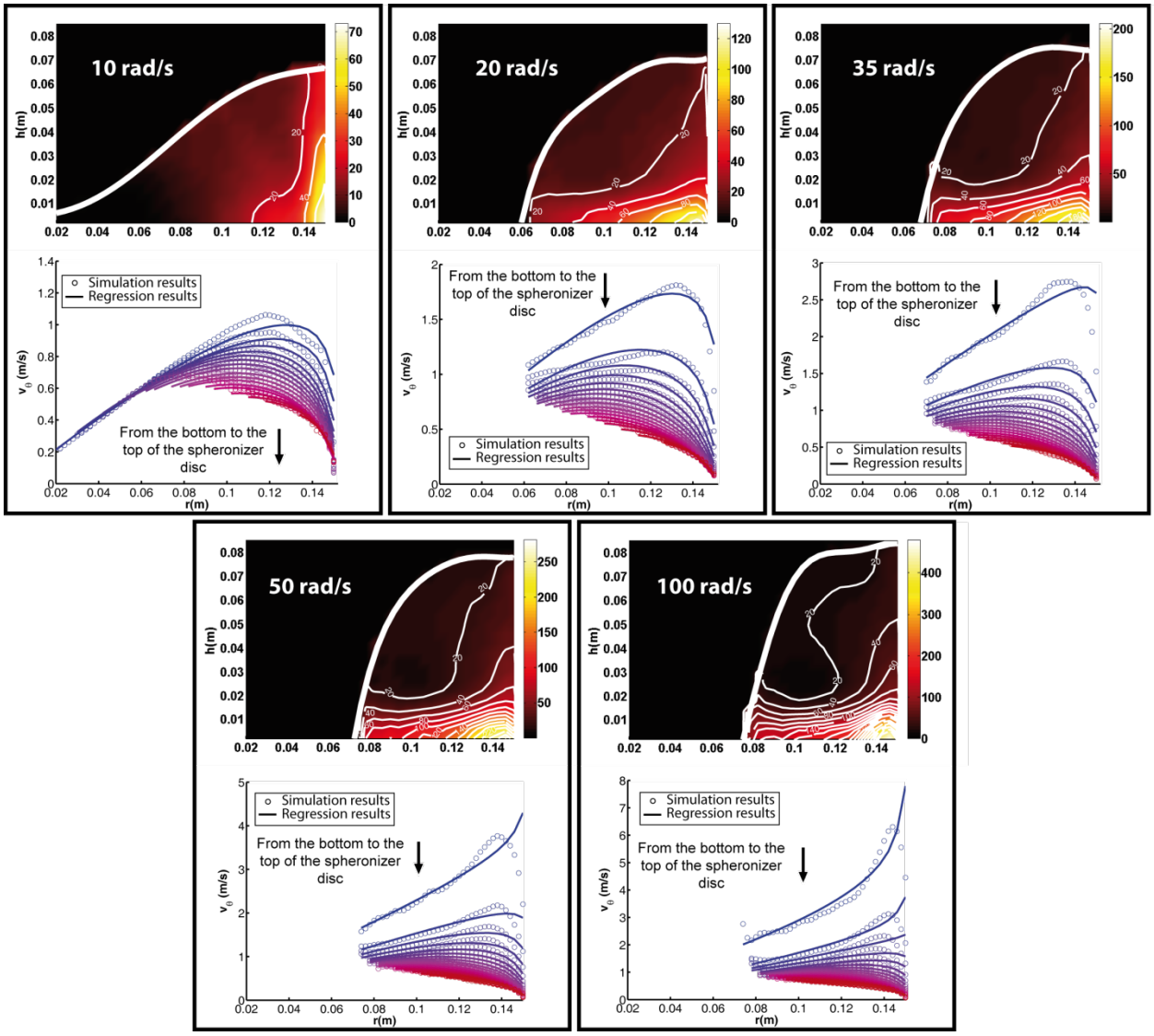

Figure 5-6: Final azimuthal velocity profiles for the high fill case and the corresponding shear rate (color map, in s^{-1})).

As described by Corwin [3], the azimuthal mean velocity can be studied by means of dimensional analysis. To this end, the following dimensionless variables are introduced:

; and , where is the radius of the spheronizer, the radial distance of the torus interface from the center of the spheronizer, evaluated from the simulation results, the rotational rate of the disc, while , and = (,) are the radial position, the height position and the azimuthal velocity inside the torus, respectively. Figure 5-5 and Figure 5-6 present the steady-state azimuthal velocity profiles obtained numerically at different

rotational rates, for the low and high fill cases respectively, along with curves obtained from the following linear regression model [3]:

$$-\qquad (5\text{-}5)$$

where, and are regression coefficients. Simulation data points and the corresponding regression curves are presented at different heights in the torus. The data at the top represents the bottom of the spheronizer, the one at the bottom the top of the spheronizer, and each curve and set of data points in between denote an increment of 0.004 m in height. The shear rate is given by:

$$\qquad (5\text{-}6)$$

where is the shear rate tensor. The color maps in Figure 5-5 and Figure 5-6 are associated with the intensity of the shear rate. The addition of contour lines highlights the low value of the shear rate in the high section of the torus. The shear rate is more important near the disk of the spheronizer and decreases rapidly until we reach 0.02 m in height for the 20 to 100 rad/s rotational rates. A different behavior can be noticed for the 10 rad/s case, with a shear rate that rather changes along the radial axis of the spheronizer. Equation (5-5) represents well the azimuthal velocity for the 10 and 20 rad/s rotational rates. As the rotational rate is further increased, the quality of the regression fit deteriorates near the wall of the spheronizer and, more particularly, near the disk. In fact, the discrepancy between the numerical data and the regression points is larger in the high shear rate regions. Since the numerical azimuthal velocity profiles appear to be strongly affected by the shear rate, we suggest modifying equation (5-5) so that it takes this dependence into account:

— (5-7)

Figure 5-7 compares the regression curves obtained with equations (5-5) (original model) and (5-7) (new model) for the 20 rad/s (graph on the left) and 100 rad/s (graph on the right), respectively. It can be noticed that the addition of the shear rate provides a very good fit near the wall, because it takes into consideration the decrease in velocity, which is important in this region. However, the modified regression model is outperformed by the original model at low rotational speed (less than 20 rad/s). At high shear rate, the azimuthal velocity exhibits a more complex behavior, which can be induced by a variation in the rheological properties with respect to the position inside the torus [11]. As the shear rate increases with the rotational speed, a good strategy would be to use the modified regression model only when this speed is above a critical value. In this work, it appears that this critical speed is around 35 rad/s. We will come back to this point below.

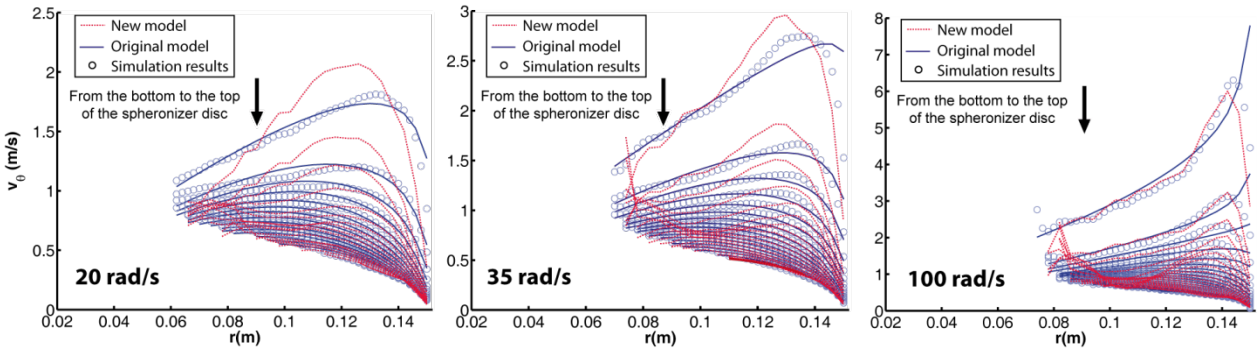

Figure 5-7: Final azimuthal velocity profiles for the high fill case obtained with equation (5-5) (Original model) and equation (5-7) (New model).

As can be seen in Figure 5-5 and Figure 5-6, the interface position is sensitive to the rotational speed. In particular, the shape of the torus for the 10 rad/s case is quite different from that at higher rotational rates. At this low disk speed, the centrifugal force is not strong enough to create the hole at the center of the spheronizer that characterizes the torus observed at higher rotational speeds. In such a case, near the center of the spheronizer, the azimuthal velocity decreases linearly with a slope that is equal to the angular velocity of the disk, at all heights, which

indicates a very low shear rate and a quasistatic regime. The flow dynamics is different for the higher rotational speeds with a rather well distributed shear rate that varies in intensity across the torus. In fact, as the disc velocity increases, the centrifugal force becomes more and more predominant over the gravity, which implies that the particles tend to get closer to the wall of the spheronizer thereby modifying the position of the interface.

Comparison of the impact of the fill level on the shear rate and azimuthal velocity can be assessed with Figure 5-5 and Figure 5-6. At a given rotational speed, the intensity and the profile of the shear rate are rather similar in the high shear zone of the torus for the low fill and high fill cases. Differences however appear over the high shear zone near the disk. In this region, the shear rate profiles, which depend on the height in the torus, are different. More precisely, the particles located at the surface near the spheronizer wall are further from the disk in the case of the high fill level case. The mean shear rate in this region is thus lower for the high fill level, as shown in Figure 5-8. As can be noticed, the variation of the mean shear rate is not linearly proportional to the rotational rate. The drastic increase of shear rate between 0 and critical speed 35 rad/s is associated with the disappearance of the no-shear quasistatic zone observed at 10 rad/s in Figure 5-5 and Figure 5-6. An almost linear increase appears when a uniform shear rate profile is present everywhere inside the torus at speeds greater than 35 rad/s. Moreover, the mean shear rate appears to be inversely proportional to the fill level, although doubling the number of particles does not reduce the mean shear rate by a factor of two. In the linear portion of the curves, the difference between the values of the shear rate for the low and high fill levels remains approximately constant with respect to the rotational rate. For the high fill level, the proportion of particles that are located in the high shear zone is less important than that for the low fill level since the size of this zone remains almost constant for both fill levels, as already discussed.

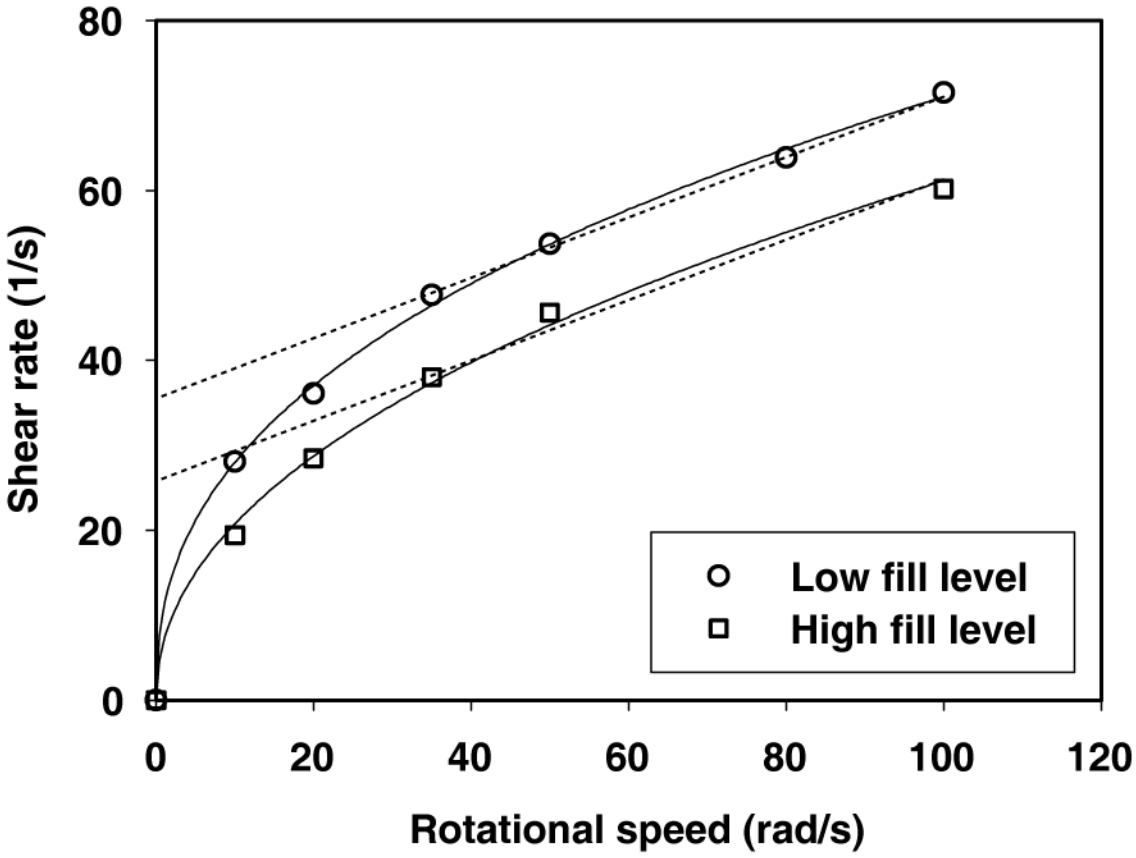

Figure 5-8: Mean shear rate with respect to rotational speed for both fill levels.

5.2.4.3 Mixing indexes and segregation maps

5.2.4.3.1 Mixing in the weak sense

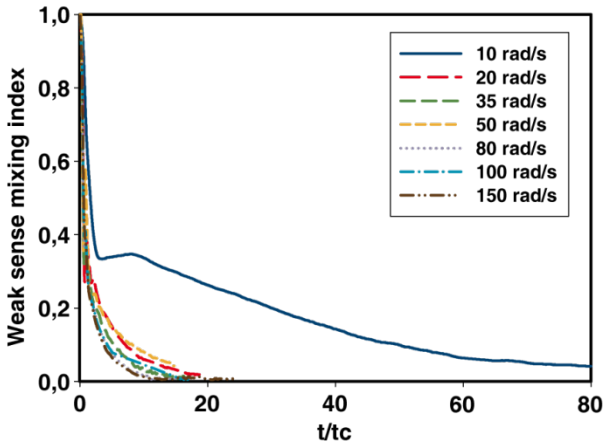

(a) Low fill level

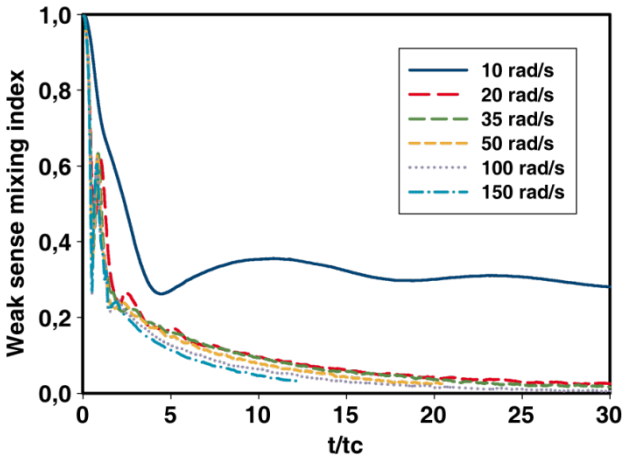

(b) High fill level

Figure 5-9: Weak sense mixing index for the low and high fill levels and different rotational speeds.

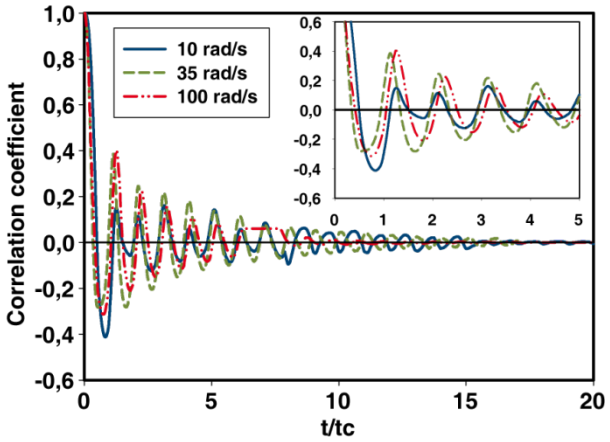

(a) Low fill level

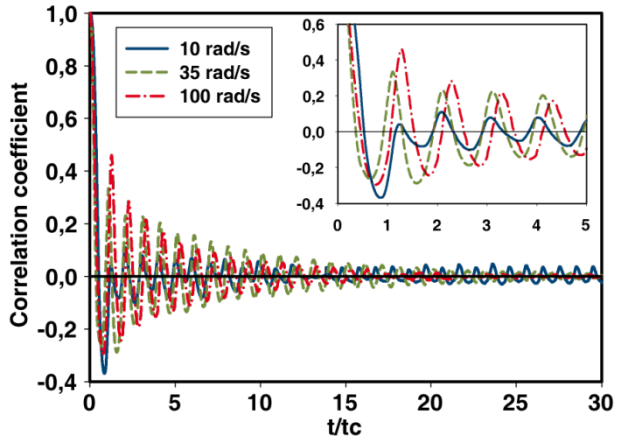

(b) High fill level

Figure 5-10: Weak sense mixing correlation coefficient relative to the global azimuthal axis.

Figure 5-9 presents the evolution of the weak sense mixing index for the low and high fill cases with respect to dimensionless time (t/tc). Variable tc represents the average time taken by the particles to make one revolution around the spheronizer in the global azimuthal direction. For all simulations, the index tends towards zero, which indicates that the particulate systems evolve

towards a completely mixed state. As expected, the mixing index for the high fill cases levels off towards zero in approximately twice the time required for the low fill cases (the high fill level contains twice as many particles as the low fill level). The index for the lowest rotational rate decreases in a different manner. Indeed, after a steep decay, the index obtained in such a case slows down its descent and stabilizes asymptotically towards a constant value. If this value is close to zero for the low fill case, it can be observed in Figure 5-9b that the index seems to stabilize towards 0.3 for the high fill case. This phenomenon points out the different particle flow behavior when the rotational speed is below 20 rad/s, as already discussed and illustrated in Figure 5-5 and Figure 5-6. It can be inferred from visual observation of the results that mixing does take place in both cases, although at a very slow pace, and that the index for the high fill case would have eventually leveled off towards zero if the simulation had not been stopped.

Mixing efficiency along a specific axis can also be investigated by plotting the evolution of the correlation coefficient used to evaluate the weak sense mixing index, as explained in detail in [7]. This correlation quantifies the dependency between the distribution (or position) of the particles at a given time and the initial distribution. Figure 5-10 displays the evolution of this correlation coefficient with respect to the global azimuthal axis. The oscillations across the abscissa of the graph are in phase with the motion of the disk in the spheronizer. Indeed, the oscillation period corresponds to the time it takes for the particles to complete one revolution along the global azimuthal axis. For the sake of clarity, only three rotational rates are considered in Figure 5-10. As can be noticed, the correlation coefficient decreases towards zero for all three cases as the particles diffuse within the toroidal shape along this axis. In a system that does not mix, such a coefficient would keep oscillating between -1 and +1. The insets included in the figure show that this diminution first occurs more rapidly at 10 rad/s for both the low and high fill cases. As time progresses, it then evolves more slowly than for the 35 and 100 rad/s cases. This behavior, which may seem counterintuitive, can be explained by the differences in the flow dynamics at low and high rotational speeds. As already mentioned and demonstrated in Figure 5-5, a quasistatic regime is observed at low speed for the particles located near the center of the spheronizer, which is not the case when this speed exceeds 20 rad/s. In such a situation, there then exist two zones within the spheronizer, which are characterized by different flow behaviors and velocity profiles. The relative motion of these two adjacent layers of particles and the fact that little or no mixing

takes place within the centermost layer explains the curve obtained at 10 rad/s. The fast decay is due to efficient azimuthal mixing occuring within the external layer characterized by its higher shear rate, whereas the subsequent residual oscillations with a rather significant amplitude can be attributed to poor mixing near the center of the spheronizer. Since the quasistatic regime is not observed above 20 rad/s, the curves obtained at such higher speeds are different and keep decreasing with time owing to good mixing (in the weak sense) throughout the spheronizer. Note also that the amplitude of the residual oscillations is larger in the high fill case, which is due to the larger size of the quasistatic zone (Figure 5-6) as compared to the one in the low fill case (Figure 5-5). Figure 5-11 displays instantaneous snapshots of the particles in the spheronizer at 10 rad/s. The particles are colored in red or blue depending on their initial position in the left or right part of the spheronizer, respectively. The quasistatic regime is clearly observed for the high fill case, as evidenced by the blue and red particles that remain unmixed near the center of the spheronizer.

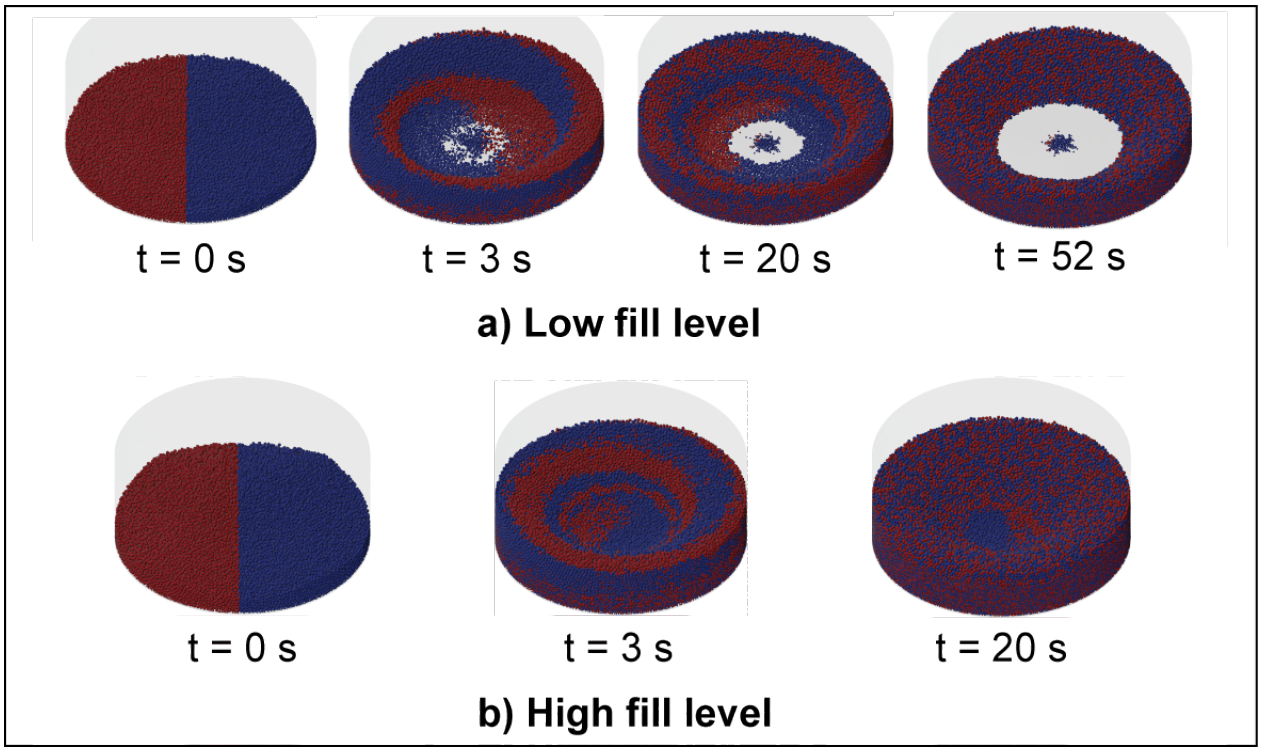

Figure 5-11: Instantaneous snapshots of the particles in the spheronizer rotating at 10 rpm for the a) low fill case and b) high fill case. Two different colors are used, depending on the initial position of the particles in the spheronizer.

5.2.4.3.2 Mixing in the strong sense

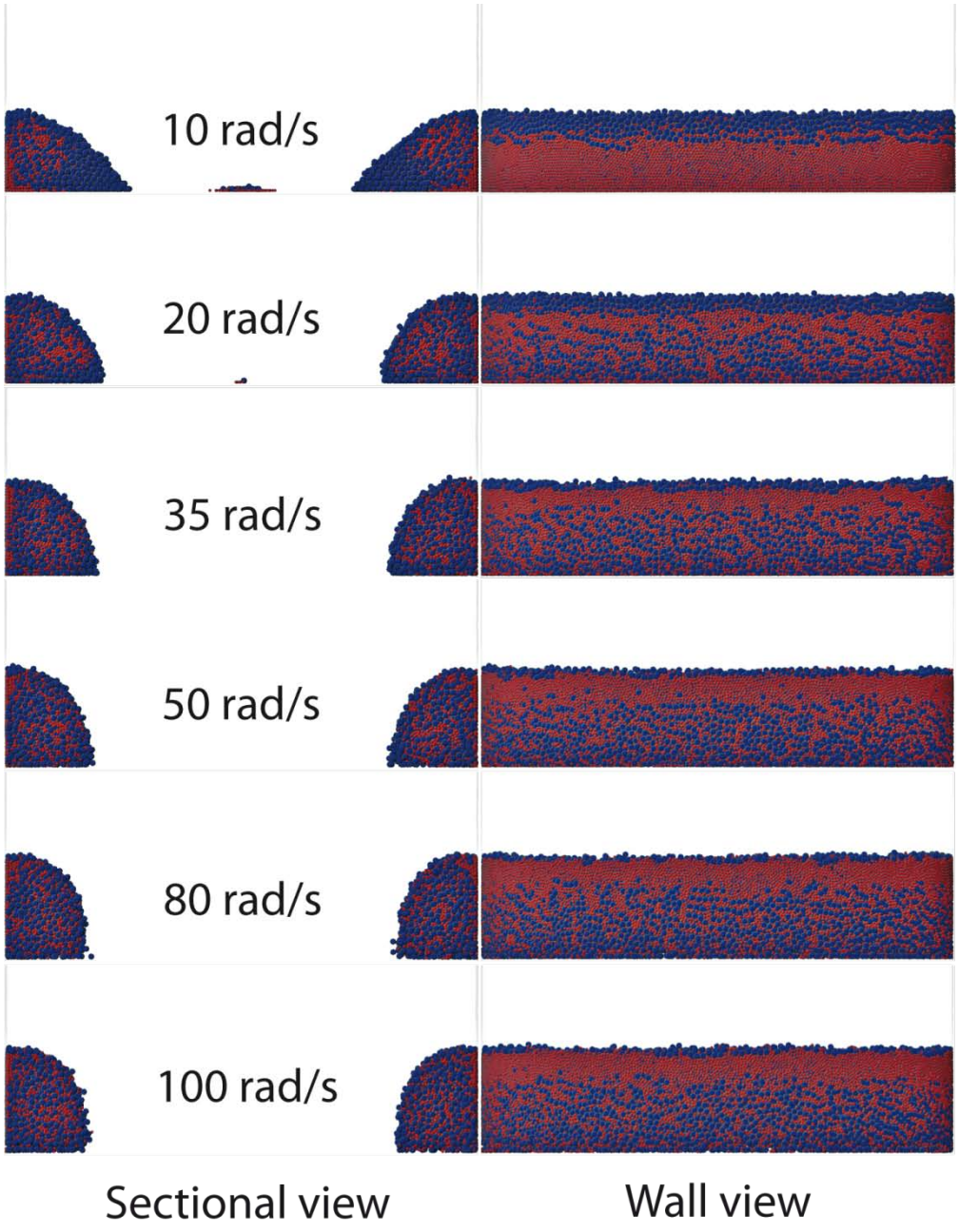

Figure 5-12: Segregation for different rotational speeds for the low fill case.

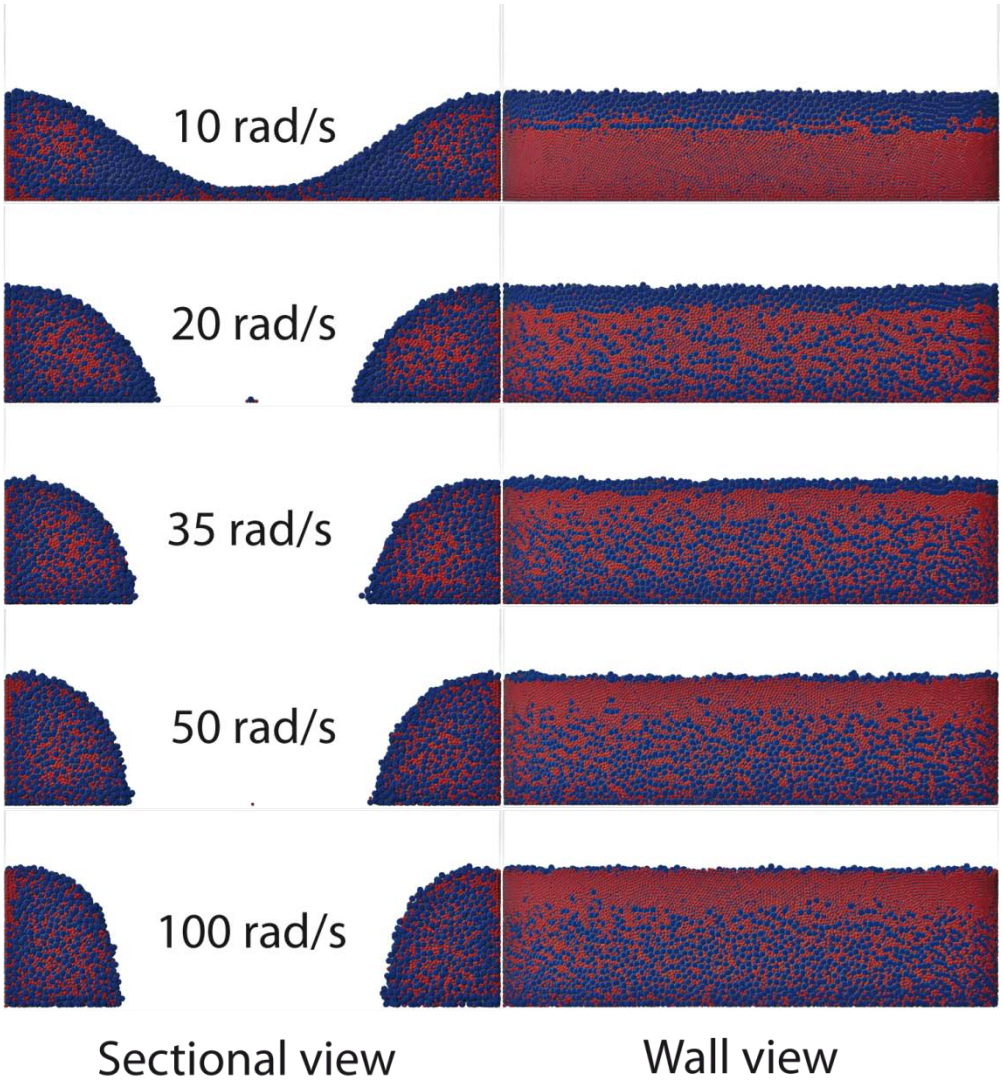

Figure 5-13: Segregation for different rotational speeds for the high fill case.

Figure 5-12 and Figure 5-13 show snapshots of the particles on a cross-section plane of the torus perpendicular to the global azimuthal direction and of the particles that are located at the spheronizer wall for the low and high fill cases, respectively. Different rotational rates and the low and high fill levels are considered, where the red and blue colors represent the small and large particles, respectively. These snapshots were taken when the particles were assumed to be mixed in the weak sense, which corresponds to the time at which the curve of the weak sense mixing index (Figure 5-9) levels off to a fixed value. While the occurence of particle segregation is obvious for all rotational rates, its extent is observed to depend on the rotational speed. The

mean concentration of the small and large particles on a cross-section of the torus with respect to the global azimuthal axis can be plotted on a graph. The procedure consists of mapping onto such a plane the position of all the particles at the same time as that used for Figure 5-12 and Figure 5-13. After this, the section of the toroid is discretized by means of a rectangular grid to calculate the concentration of both types of particles. The concentration maps of the 2-mm and 4-mm particles are given in Figure 5-14 and Figure 5-15 for the low and high fill levels, respectively. In both cases, it can be observed that the large particles are rather well distributed throughout the toroidal domain with higher concentrations near the disk of the spheronizer, particularly at low speed. On the other hand, the small particles are concentrated in two zones of the torus. The first one is located near the middle of the torus and the second one corresponds to an area in the vicinity of the spheronizer wall. This indicates the occurrence of particle segregation induced by the shear rate in the system. More precisely, as observed in previous work [22, 10], small particles tend to migrate to low shear areas. As can be noticed in the right section of Figure 5-14 and Figure 5-15, the small particle segregation zones can be directly associated with the low shear areas in the powder bed. The characteristics of the segregation zone at the center of the torus appear to be affected by the fill level, contrary to the one near the wall of the spheronizer. More specifically, the size of the low shear zone at the center of the torus increases with the fill level, which enhances the migration of small particles towards this area. This is due to the fact that the local center of rotation of the torus (ref. to Figure 5-1) moves away from the spheronizer disk where the shear rate is high. As a direct consequence, the size of the low shear rate regions increases, which favors the migration of small particles towards this zone. It can also be noticed that the relative importance of the two segregation zones for the small particles is influenced by the disk speed regardless of the fill level. Low rotational speed favors the central zone whereas 2-mm particles are found near the spheronizer wall at high speed, more importantly at the top of the torus.

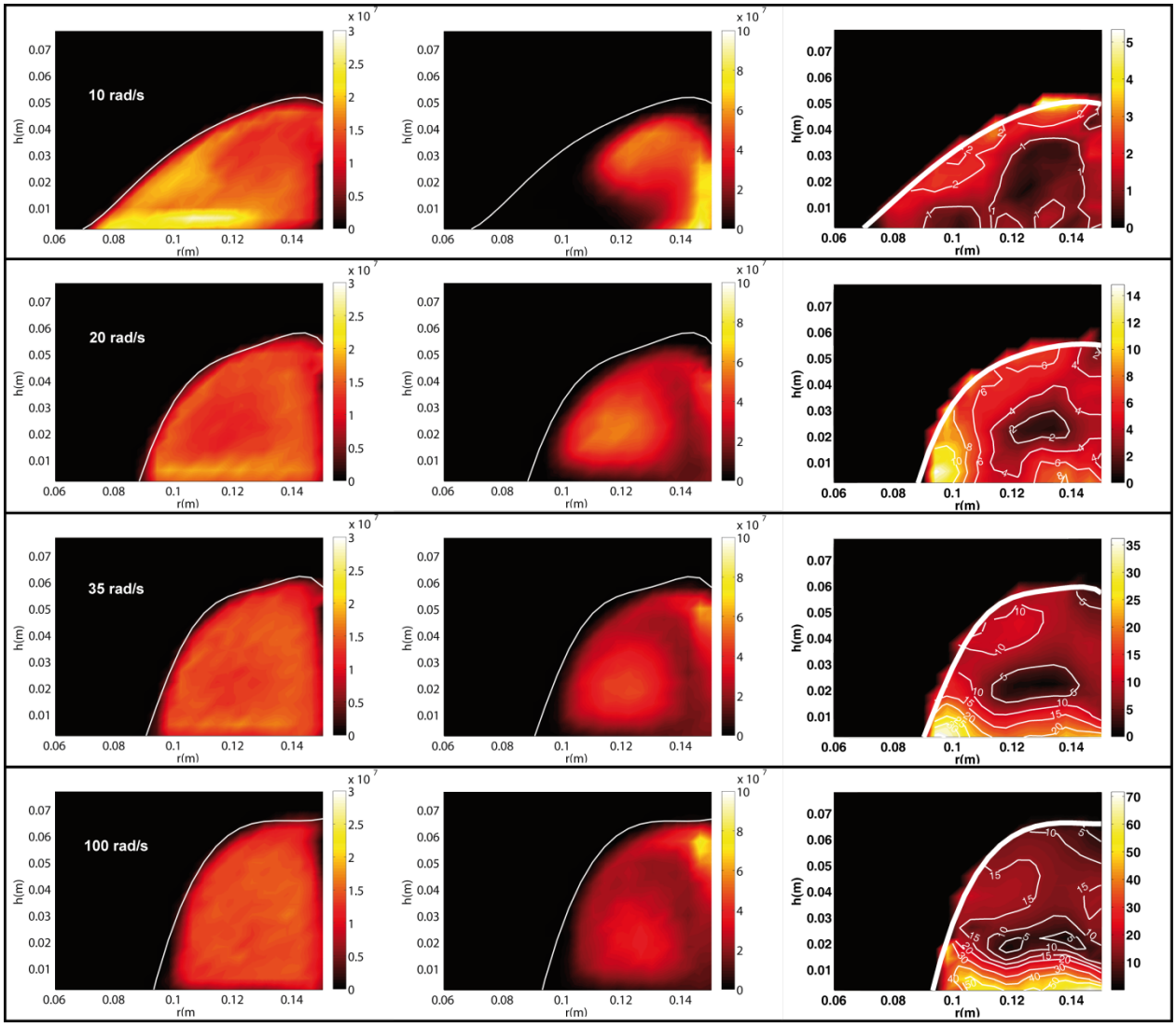

Figure 5-14: Final concentration of the small and large particles for the low fill level in number of particles per cubic meter. The left and middle sections correspond to the 4-mm and 2-mm particles, respectively. The right section shows the shear rate (s^{-1}) on a cross-section of the torus.

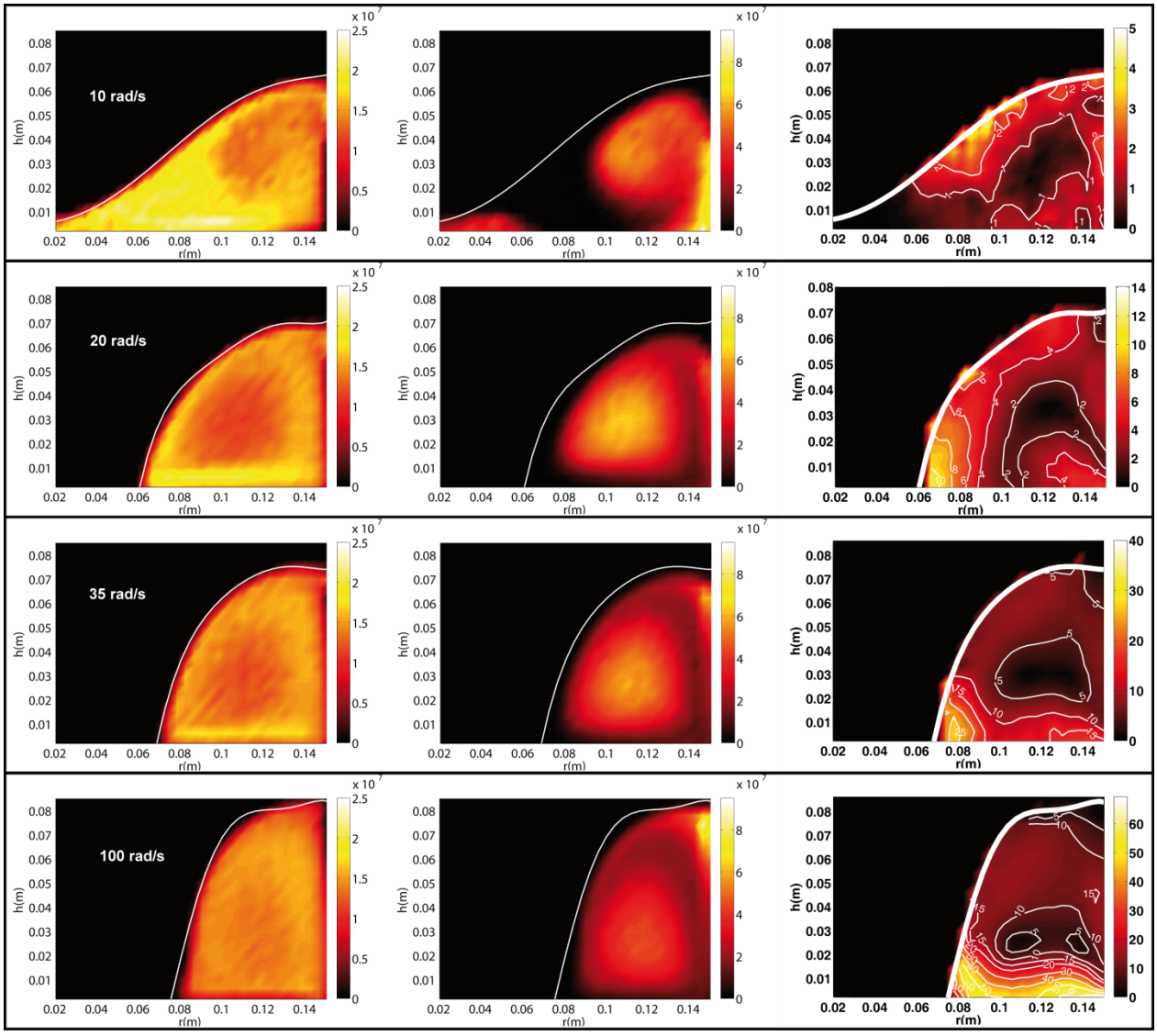

Figure 5-15: Final concentration of the small and large particles for the high fill level in number of particles per cubic meter. The left and middle sections correspond to the 4-mm and 2-mm particles, respectively. The right section shows the shear rate (s^{-1}) on a cross-section of the torus.

To evaluate more systematically the importance of segregation with respect to the rotational speed and the fill level, the strong sense mixing index with respect to particle size can be used. Figure 5-16 shows the evolution of this index. The oscillations observed at the beginning are

related to the rather intense reorganization of the particles occurring until the bed has reached its final doughnut shape. The asymptotic value reached by the different curves indicates the extent of the segregation intensity at steady state. A gradual decrease of this asymptotic value is expected when the speed is increased. It means that the state of mixedness of the particulate system improves, which is due to an increase of the mean shear rate. As can be seen in the figure, the asymptotic value does indeed decrease at first, at low rotational speed, then it reaches a minimum and increases again. This happens for both fill levels, although the critical rotational speed at which the minimum asymptotic value is reached differs in each case: 35 rad/s for the low fill level and 100 rad/s for the high fill level. This means that there exists a rotational speed at which the particulate system is mixed optimally and does not exhibit a predominant segregated zone. As can be seen in Figure 5-12 to Figure 5-15, the DEM simulations predict the formation of a cluster of 2-mm particles in the vicinity of the spheronizer wall. As the rotational speed is increased, it migrates towards the top of the torus and, when a sufficiently high speed is reached, the concentration of 2-mm particles in this cluster becomes almost identical to what it was at the bottom at low speed. The optimal rotational speed is reached when the cluster is located at the top of the torus and, beyond this value, its position does not seem to be altered significantly by a further increase of the rotational speed. As a matter of fact, an increase of the rotational speed above the optimal value causes an increase of the 2-mm particle concentration inside the cluster, which leads to a deterioration of the state of mixedness.

It is difficult to rely only on the strong sense mixing index alone to explain the change in mixing behavior as the rotational speed is varied. As a complement, plots of the strong sense mixing correlation coefficients relative to the local radial axis and the local azimuthal axis, as defined in Figure 5-1, can be used. Figure 5-17 shows these correlation coefficients for different rotational speeds. With respect to the radial axis, a positive value indicates that the small particle segregation zone at the center of the torus dominates the one near the spheronizer wall. When the value of the radial coefficient is less than zero, the opposite situation occurs. The results of Figure 5-17 can thus be observed to comply with the concentration maps and segregation zones displayed in Figure 5-14 and Figure 5-15. The azimuthal coefficients level off to near zero values in all cases except the 10 rad/s one. This latter case exhibits different flow behavior, as explained in the previous section. The large value of the azimuthal coefficient at such flow disk speed is

explained by the fact that the small particles are mainly located near the wall of the spheronizer whereas the large particles are concentrated in an area near its center. Moreover, the radial coefficient for the 10 rad/s case with a low fill level evolves differently and takes much longer to stabilize to a fixed value. This phenomenon is due to a slower migration of the small and large particles. At first, a toroid of particles is slowly created and segregation mainly takes place at the wall. This is confirmed in Figure 5-17a by a decrease of the corresponding radial coefficient towards negative values. After approximately 10 seconds, small particles start migrating towards the center of the torus and, after approximately 40 seconds, this coefficient becomes more important at this location. This behavior is not observed when the fill level is high (Figure 5-17c). The absence of a hole at the center of the particulate domain and the presence of small particles there explain why the change of sign does not occur in this particular case.

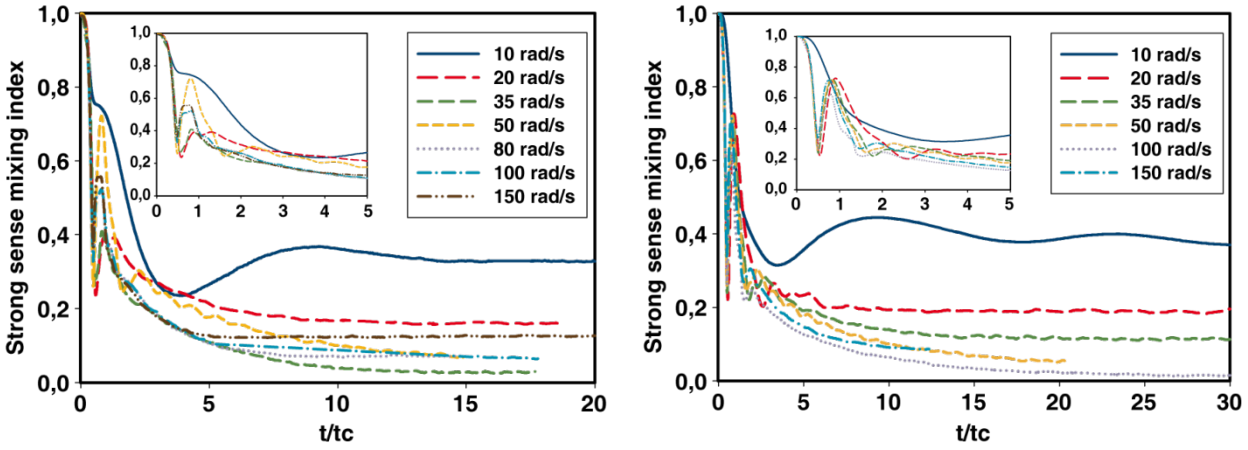

(a) Low fill level (b) High fill level

Figure 5-16: Strong sense mixing index for the low fill and high fill levels and different rotational speeds.

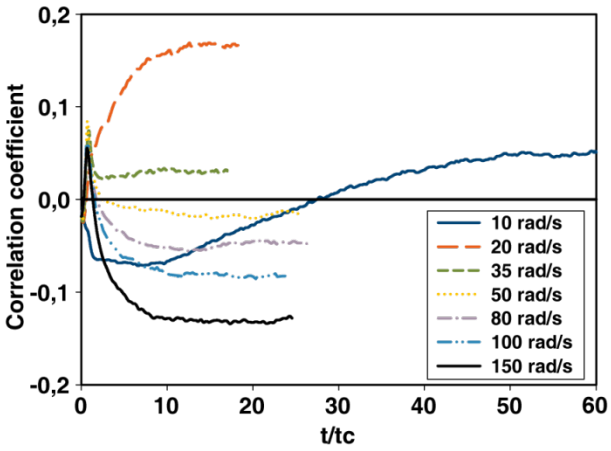

(a) Low fill level and coefficient relative to the radial axis

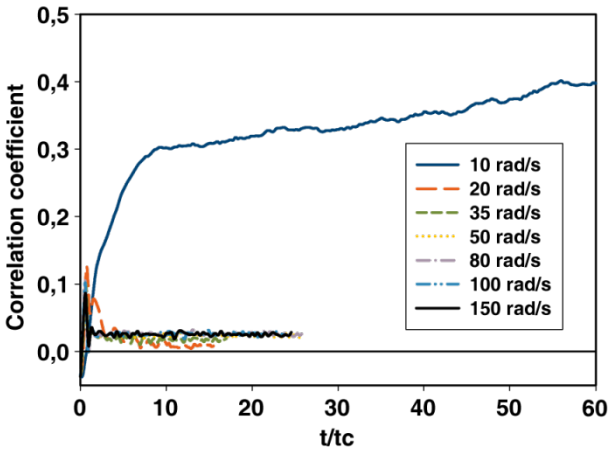

(b) Low fill level and coefficient relative to the azimuthal axis

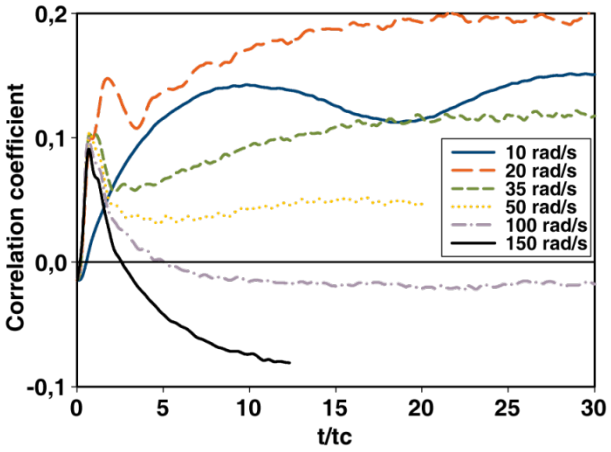

(c) High fill level and coefficient relative to the radial axis

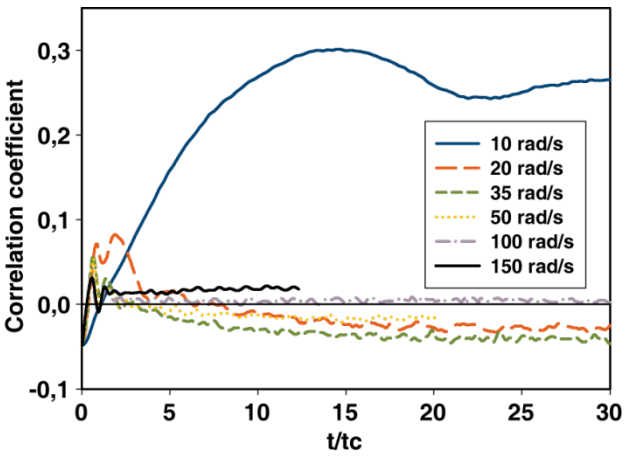

(d) High fill level and coefficient relative to the azimuthal axis

Figure 5-17: Strong sense mixing correlation coefficient relative to the local radial and azimuthal axes.

5.2.5 Conclusion

The flow of a bidisperse system of particles in a spheronizer was investigated numerically with the help of a DEM-based model for different disk speeds and particle fill levels. The validity of this model was first assessed by means of experimental data obtained by Corwin [3] for

monodisperse particles size. Despite the fact that the value of the physical parameters of the particles used in those experiments are unknown, similar trends could be predicted as regards the height of the torus and the particle velocity. The mixing of the bidisperse particles was then analyzed on the basis of mixing indices that make it possible to characterize the segregation occuring in the particle domain. It was shown that the disk rotational speed and the fill level have a significant impact on the magnitude of the segregation phenomenon. For rotational speeds from 20 to 100 rad/s, two segregation zones can be observed and, as the speed is increased, the small particles tend to migrate from a zone located at the local center of rotation of the torus towards a zone located near the wall of the spheronizer. It was also shown that, for a speed of 10 rad/s, the flow dynamics induces a pattern of segregation that is largely different from the one exhibited at larger speeds. Finally, a correlation for the azimuthal velocity was presented following the work of Corwin [3], which brings into play the shear rate. In summary, this study has shown that segregation may occur when dry free flowing particles of different sizes are mixed in a spheronizer, which indicates that similar behavior may happen in other rotor granulator equipment. These results are currently being used by our group for the development of a multiscale model that resorts to the DEM to describe locally the flow of polydisperse particles in characteristic regions of the spheronizer, and passes along this information to a population balance model at the scale of the whole domain for the simulation of the granulation process. Future work will also extend the current work to wet conditions through the addition of cohesive forces in the DEM model so as to assess the effect of cohesion on the particle flow and mixing dynamics. These models will altogether lead to a better understanding of the key mechanisms governing granulation and to the development of more efficient and controllable processes in the industry.

5.2.6 Acknowledgements

The financial support of the Natural Science and Engineering Research Council of Canada (NSERC) and Merck Frosst of Canada is gratefully acknowledged.

5.2.7 References

[1] Alexander, A., Muzzio, F., Shinbrot, T., 2003. Segregation patterns in v-blenders. Chemical Engineering Science 58, 487–496.

[2] Conway, S. L., Lekhal, A., Khinast, J. G., Glasser, B. J., 2005. Granular flow and segregation in a four-bladed mixer. Chemical Engineering Science 60, 7091–7107.

[3] Corwin, E. I., 2008. Granular flow in a rapidly rotated system with fixed walls. Physical Review E 77, 031308.

[4] Cundall, P., Strack, O., 1979. Discrete numerical model for granular assemblies. Geotechnique 29, 47–65.

[5] Danckwerts, P. V., 1952. Definition and measurement of some characteristics of mixtures. Applied Scientific Research A3 (4), 279–296.

[6] Dippel, S., Batrouni, G. G., Wolf, D. E., 1996. Collision-induced friction in the motion of a single particle on a bumpy inclined line. Physical Review E 54 (6), 6845.

[7] Doucet, J., Bertrand, F., Chaouki, J., 2008. A measure of mixing from lagrangian tracking and its application to granular and fluid flow systems. Chemical Engineering Research and Design 86 (12), 1313–1321.

[8] Fan, R., Fox, R. O., 2008. Segregation in polydisperse fluidized beds: Validation of a multi-fluid model. Chemical Engineering Science 63, 272–285.

[9] Fenistein, D., Van De Meent, J. W., Van Hecke, M., 2004. Universal and wide shear zones in granular bulk flow. Physical Review Letters 92 (9), 094301.

[10] Foo, W. S., Bridgwater, J., 1983. Particle migration. Powder Technology 36 (2), 271–273.

[11] Forterre, Y., Pouliquen, O., 2008. Flows of dense granular media. Annual Review of Fluid Mechanics 40 (1), 1–24.

[12] Jop, P., 2008. Hydrodynamic modeling of granular flows in a modified couette cell. Physical Review E - Statistical, Nonlinear, and Soft Matter Physics 77 (3).

[13] Ketterhagen, W. R., Curtis, J. S., Wassgren, C. R., Hancock, B. C., 2008. Modeling granular segregation in flow from quasi-three-dimensional, wedge-shaped hoppers. Powder Technology 179, 126–143.

[14] Laurent, B., Bridgwater, J., Parker, D., 2002. Convection and segregation in a horizontal mixer. Powder Technology 123, 9–18.

[15] Lemieux, M., Léonard, G., Doucet, J., Leclaire, L.-A., Viens, F., Chaouki, J., Bertrand, F., 2007. Large-scale numerical investigation of solids mixing in a v-blender using the discrete element method. Powder Technology 181, 205–216.

[16] Li, H., McCarthy, J., 2003. Controlling cohesive particle mixing and segregation. Physical review letters 90 (18), 184301.

[17] Meier, S. W., Lueptow, R. M., Ottino, J. M., 2007. A dynamical systems approach to mixing and segregation of granular materials in tumblers. Advances in Physics 56 (5), 757–827.

[18] Muguruma, Y., Tanaka, T., Tsuji, Y., 2000. Numerical simulation of particulate flow with liquid bridge between particles (simulation of centrifugal tumbling granulator). Powder Technology 109, 49–57.

[19] Muzzio, F. J., Goodridge, C. L., Alexander, A., Arratia, P., Yang, H., Sudah, O., Mergen, G., 2003. Sampling and characterization of pharmaceutical powders and granular blends. International Journal of Pharmaceutics 250 (1), 51–64.

[20] Ottino, J., Khakhar, D., 2000. Mixing and segregation of granular materials. Annual Review of Fluid Mechanics 32, 55–91.

[21] Poux, M., Fayolle, P., Bertrand, J., Bridoux, D., Bousquet, J., 1991. Powder mixing. some practical rules applied to agitated systems. Powder Technology 68 (3), 213–234.

[22] Stephens, D. J., Bridgwater, J., 1978. The mixing and segregation of cohesionless particulate materials part i. failure zone formation. Powder Technology 21 (1), 17–28.

[23] Zhou, Y., Wright, B., Yang, R., Xu, B., Yu, A., 1999. Rolling friction in the dynamic simulation of sandpile formation. Physica A 269, 536–553.

CHAPITRE 6 CONTRÔLE DE LA COHÉSION PARTICULAIRE PAR DES CHANGEMENTS DE TEMPÉRATURE ET ENROBAGE DE POLYMÈRE

6.1 Présentation du deuxième article

Soumis à *AIChE Journal* le 10 Novembre 2011

Auteurs: Jonathan Bouffard, François Bertrand, Jamal Chaouki et Suzanne Giasson

Le but de cet article est de développer une nouvelle approche afin d'introduire des forces interparticulaires de manière homogène et facile à contrôler pour des applications impliquant des écoulements de particules. Cette approche utilise un enrobage de copolymère PEA/PMMA qui est déposé par atomisation sur des particules dont l'écoulement doit être caractérisé. En augmentant la température des particules ou en augmentant l'épaisseur de l'enrobage de polymère, les forces interparticulaires peuvent être augmentées pour produire un écoulement particulaire davantage cohésif.

Deux applications différentes sont utilisées afin de montrer l'emploi de cette nouvelle approche. La première application considère un écoulement dense de particules qui est typiquement observé durant la granulation humide pour un granulateur à rotor. L'augmentation de température des particules produit un changement de morphologie de la surface du lit de particules ainsi qu'une diminution de la densité dynamique mesurée pendant l'opération. La deuxième application permet de démontrer la capacité de la méthode pour reproduire le comportement des écoulements particulaires observés à l'intérieur des lits fluidisés à haute température tout en ayant l'avantage d'être opérés à la température ambiante. Des mesures de pertes de charge permettent de révéler que les particules passent d'un comportement du groupe B au groupe A de Geldart et même jusqu'au groupe C lorsque la température est élevée.

6.2 Control of Particle Cohesion with a Polymer Coating and Temperature Adjustment

6.2.1 Abstract

This work presents a new approach that introduces interparticle forces induced by a change of temperature at which polymer coated particles are exposed. The particle cohesive flow behaviour is shown for two different applications. The first one considers a dense granular flow that is typically observed for wet powder granulation using a modified spheronizer. The other application shows the possibility of mimicking the particle flow behaviour observed in high temperature fluidized beds with the advantage of being operated at ambient conditions. For the first application, as the temperature increases, significant changes in the particle bed surface morphology were observed and an important reduction of the dynamic density was noticed. For the gas-solid fluidized bed application, pressure drop measurements revealed that the behaviour of the particles transited from Geldart group B to Geldart group A and even Geldart group C as the temperature increased.

6.2.2 Introduction

Granular flow dynamics has been already studied with non-cohesive and cohesive particles induced by different force types in dense granular systems, as encountered in blenders [1-3] or fluidized bed applications [4-7]. The presence of cohesive particulate material can induce a change in the flow pattern observed in process equipment when compared to a free flowing material [8]. It can also lead to the appearance or modification of segregation patterns that are different from the ones in non-cohesive cases [9-11]. In order to study and characterize the interparticle force effects on granular flow dynamics, different approaches have been used to introduce cohesive forces into the particulate material.The interparticle force can be chosen to reproduce the conditions found in a real process (e.g., the use of capillary force to study its impact on a wet granulation process), but also to mimick, in a more friendly environment, the cohesive behaviour present in a granular application difficult to characterize with experimental measurements because of extreme operating conditions. Fluid beds that operate at high

temperature are an example of one such application for which the characterization is limited to optical observations of the process [12].

The van der Waals forces have a significant impact on the interactions between particles. The cohesive forces that bind two particles are directly proportional to the particle size according to the following equation [13-14]:

$$F_{VdW} = \frac{A_H a}{12h^2} \tag{6-1}$$

where A_H is the Hamaker constant, a is the spherical particle radius and h is the separation distance between the two particle surfaces, which corresponds to the nearest distance for particles in close contact. When the particles become larger than 100 μm [15], the van der Waals forces become less significant because of the predominance of the inertial and gravity forces. This leads to a higher mobility of the particles, which is characteristic of the free flowing behavior [1]. The use of van der Waals forces to study the cohesive behavior is then difficult when large flowing particles are considered. For these particles, the cohesion must be induced by adding a cohesive agent that creates the interparticle forces. One of the most popular methods to induce a cohesive effect inside a particulate material is to introduce wet capillary bonds coming from an interstitial liquid between the particles, as shown in Figure 6-1.

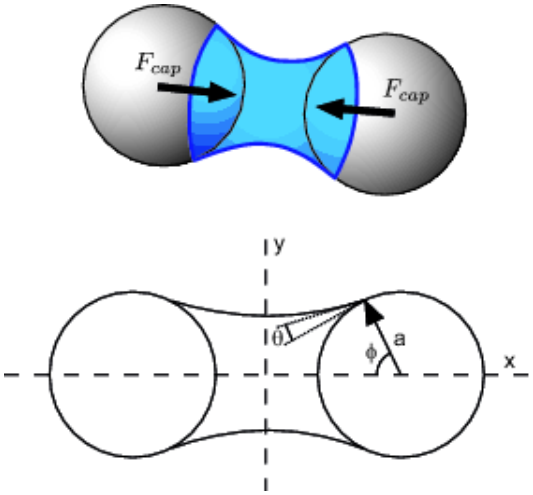

Figure 6-1: Capillary forces induced by moisture content [16].

The capillary force depends on the surface tension and the pressure differential across the air-liquid interface, according to the following expression [17]:

$$F_{cap} = 2\pi\gamma a \sin\phi \sin(\phi+\theta) + \pi a^2 \Delta p \sin^2\phi \tag{6-2}$$

where ϕ is the polar position of the liquid bridge edge relative to the particle center and the horizontal reference axis θ is the contact angle and is the particle radius, as defined in Figure 6-1 and is the surface tension. The Laplace pressure depends on the volume of liquid between the particles, which is expressed via the interface profile of the liquid bridge, :

$$\frac{\Delta p a}{\gamma} = \frac{\ddot{Y}}{(1+\dot{Y}^2)^{3/2}} - \frac{1}{Y(1+\dot{Y}^2)^{1/2}} \tag{6-3}$$

As the moisture content increases, different saturation states are reached, which induce significative change in the interparticle force [18]. The pendular state is characterized by the presence of capillary bonds linking only two particles at a time and by the fact that the cohesion is proportional to the quantity of moisture content [19]. The pendular state exists within a low moisture concentration range (1-3 vol.%) for which the control of the liquid distribution throughout the particulate bed can be difficult [18] and can introduce non-homogeneous interparticle forces throughout the particulate bed [20].

An alternative way to induce cohesive forces between the particles is by increasing magnetic interactions using the presence of a ferromagnetic component. With this approach, a magnetic field is generated to polarize the particulate material in a specific direction. The poles created inside the particles interact with each other and then induce a cohesive/repulsive behavior. One advantage of using this type of cohesion is the absence of a liquid phase that must be uniformly distributed. Also, since the magnetic force varies with the square of the magnetic field intensity for a constant particle material and size distribution [21-22], it is relatively easy to introduce and control cohesive interactions within the granular material. The flow behavior of such cohesive material is different from the flow dynamics generally encountered in industrial applications since the cohesive forces are aligned with the magnetic field following a specific direction. Due to the polar interactions, as seen in Figure 6-2, the cohesive forces are not distributed uniformly around the particles, which induces anisotropic attraction/repulsion forces into the bulk material [23]. Some work has been done to reduce the presence of the force anisotropies by employing a rotating magnetic field [22], but it does not solve the problem completely since the poles rotate around the particles by following the magnetic field. The magnetic force between two ferromagnetic particles is given in [23]:

$$F_{mag} = 12\pi\mu_0\mu_f a^2 \vec{B}^2 \left(\frac{\mu_p - 1}{\mu_p + 2} \right)^2 \vec{f}(r,\alpha) \tag{6-4}$$

where μ_0 is the magnetic constant, μ_f and μ_p are the fluid and particle relative magnetic permeabilities, respectively, $\vec{B}$ is the magnetic field, r and α are the distance and the angle between the two particles, respectively, $\vec{f}$ is the secondary field created by the magnetization of one particle and is the particle radius. Note that this secondary field due to neighboring material affects the cohesive force induced by the principal magnetic field on a specific particle.

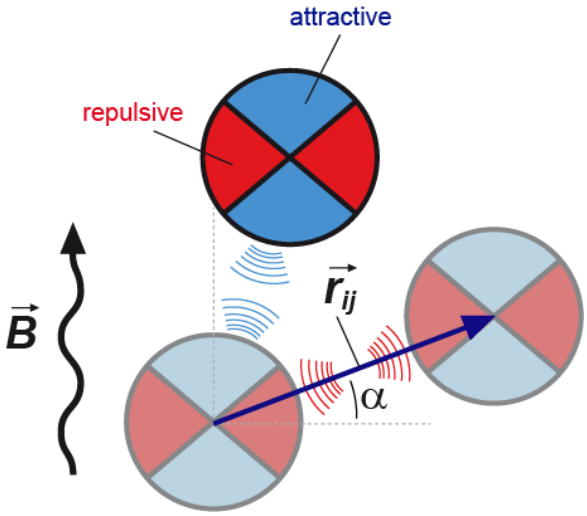

Figure 6-2: Magnetic field interaction with ferromagnetic particles (modified from [23]).

It has been shown that the aforementioned approaches have inherent limitations with respect to the control of interparticle forces, independent of the particle size, and/or the cohesive force uniformity throughout the particulate bed, which come from inherent physical limitations (distribution or evaporation of a liquid or magnetic force anisotropy). Modification of the particle surface properties is another way to induce cohesive effects throughout the particle bed. Different approaches can be used to modify the cohesive forces, such as a change of roughness [24] or the addition of nanoparticles by dry coating [25-26]. In such cases, a reduction of the cohesion is normally desired and cohesion adjustment is not necessarily the objective. The control of surface cohesion can also be achieved by coating the surface with a polymer. This approach, relatively well understood in the case of binary surface contacts, allow adhesion and friction to be controlled [27-30].

In this paper, we propose to use a polymer coating and temperature adjustment to control interparticle forces within a granular material and ensure their homogenous distribution throughout the particulate bed. To do so, we have applied this new technique to two different cases: in a spheronizer, which is characterized by a dense particle flow regime, and in a fluidized bed where the flow is fluid-like or gaseous. Description of the mechanisms involved during the polymer adhesion are first explained. The interparticle forces between coated particles with

respect to their size and the process temperature were measured using a surface forces apparatus (SFA). Common interparticle forces generally encountered in particle applications are compared to the estimated polymer forces. The cohesive flow behaviour in the spheronizer with the coated particles is qualitatively and quantitatively assessed for different temperatures through bed surface vizualization and particle bed density measurements. Finally, the behavior of coated particles in a fluidized bed is characterized through pressure drop and bed height measurements, and the results are compared with data from the literature obtained with other particle systems.

6.2.3 Polymer coating approach

The adhesion force between two polymer layers in contact strongly depends on the interdiffusion rate of the polymer chains, the area of contact, the contacting time, the compression between the layers and the decompression rate. Above the glass transition temperature, the polymer chains are able to move following a process of reptation and they can cross the interface created [31]. Figure 6-3 presents the cohesion mechanism when two coated particles collide at a temperature that is over the glass transition state. Upon colliding, the two polymer layers are deformed and create a “meniscus” across the interface. During this step, a molecular interdiffusion of the polymer chains takes place. The interdiffusion rate between these chains depends mainly on the polymer chain molecular weight, the level of entanglement and the process temperature [32-33]. As the molecular chains diffuse, the polymer relaxes and the interface disappears for a contact duration that equals the reptation time (τ_D), which depends on the diffusion of these polymer chains [33-34]:

(6-5)

where is the radius of gyration of the polymer chain and is the reptation diffusion coefficient. The reptation time at temperature *T* can be estimated by the William-Landel-Ferry empirical model:

(6-6)

where is the reference reptation time at temperature , and and are regression constants that depend on the polymer species. The reptation time then depends on the polymer properties and decreases significantly above the glass transition state. For example, for PEA with a molecular chain weight in the order of 10^5 kg/mol, the reptation time is around five hours when the temperature is 270 K, while it is around ten seconds for a temperature of 340 K [35]. As the polymer chains diffuse through the interface, the resultant adhesion force increases. The adhesion energy per unit area necessary to separate two layers of polymer completely is defined by [36]:

(6-7)

where is the initial polymer layer thickness and and are the stress and maximum strain, respectively. The stress depends on the strain but also on the debonding rate and the polymer chain weight. The adhesion energy can also be estimated from force/distance curves on approaching and separating of contacting elastic materials using the JKR theory [37]. In practice, the adhesion energy and the elastic modulus of the material are usually obtained through the JKR equation by measuring and plotting the contact area against the applied load. When the surfaces or particles are pulled apart by a constant force , they will detach from each other when reaches the adhesion force, which is also called pull-off force given by:

(6-8)

where is the radius of particles i or j [38-40]. This equation can be used in conjunction with the SFA measurements to estimate the adhesion energy. We will come back to this point in the results section.

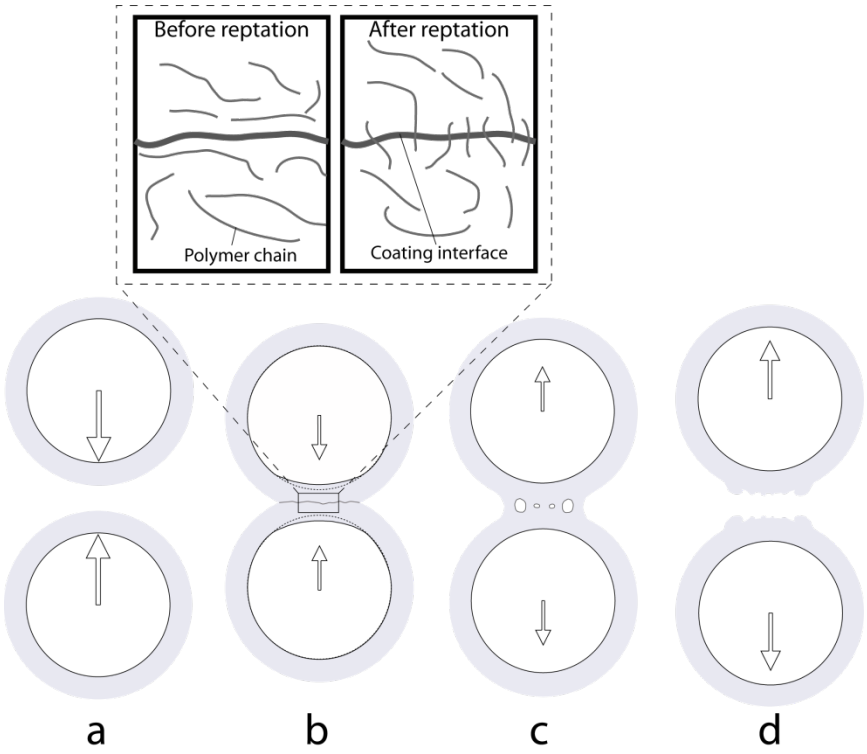

Figure 6-3: Collision of two coated particles: a) Particles before collision; b) Molecular interdiffusion of the polymer layers occurring during contact and deformation. The polymer chain ends cross the interface following a reptation mechanism; c) Separation of the particles with cavity formation. Entanglement of the polymer chains induces adhesive forces when the particles are separated; d) Formation of craters following the complete separation of the particles.

When two polymer layers are separated with a high debonding velocity ( ), the adhesion energy increases with the contact time ( ) until it reaches a maximum value , which happens in the vicinity of the reptation time (τ_D) [41-42]. When the polymer layers are separated slowly or when the contact time is larger than the reptation time, the adhesion energy can be considered constant at the maximum value . Dimensional analysis can be used to describe the failure

regime in which the contacting polymer layers are debonded. The first dimensionless number is the ratio between the contact time and the reptation time ( ), named the normalized contact time. The second is the Deborah number, which is defined by:

—— (6-9)

where is the average initial strain rate. The Deborah number represents the ratio between the material relaxation time following a deformation and the characteristic time scale of the process. Figure 6-4 shows the three different failure mechanisms encountered, depending on these two dimensionless numbers. The liquid-like and the bulk failure mechanisms occur when is large and are then associated with the maximum value of the adhesion energy, , while the presence of interfacial cracks indicates that the adhesion energy is not at equilibrium and increases with the contact time [36, 41]. The liquid-like failure is observed when the debonding rate is low enough (low De) and has no effect on the adhesive energy observed. This separation regime should not be expected in spheronizer or fluidized bed applications. At high debonding rate (high De), if the bulk failure is observed, it means that the polymer layers are strongly deformed. Because it may results in a layer breakage, this separation regime is not desired and must be avoided to ensure the coated particle integrity.

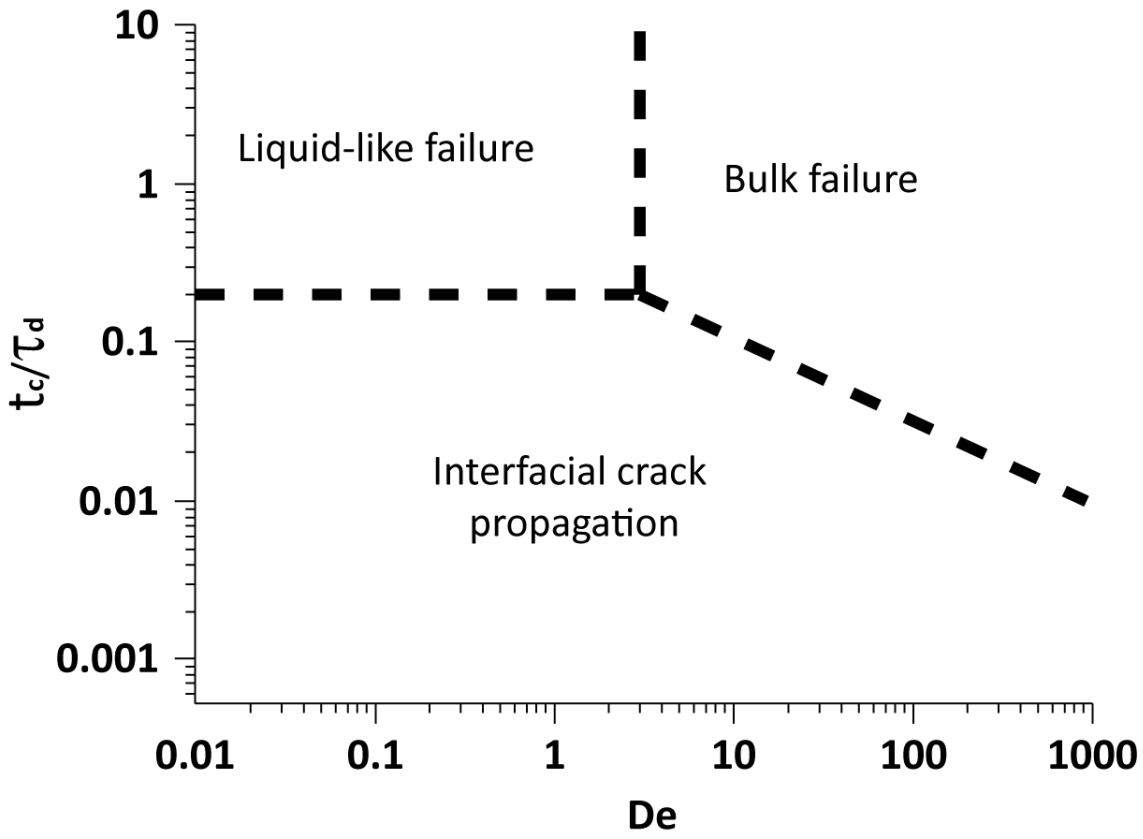

Figure 6-4. Failure mechanism map as a function of the normalized contact time and the Deborah number [36].

The particle contact time ( ) between particles is not easy to evaluate for a dense particle flow regime. The Hookean relation used for elastic particles can give an estimate of in such a situation, but it requires simulations of particulate flow to set key parameters such as the stiffness and the damping coefficients on the basis of experimental results [43]. Timoshenko and Goodier [44] developed an empirical relation that can approximate the contact time for elastic spheres:

(6-10)

where is the particle density, is the Poisson ratio, is the Young's modulus, is the particle radius and is the normal collision velocity, which is estimated by the product of the particle size and the shear rate ( ) [45]. Due to the absence of a viscous relaxation term, the

contact time calculated by this relation represents a low limit value. Nevertheless, it can be used to estimate an effective adhesion energy from [46]:

(6-11)

where the regression constants *a* and *b* vary with the polymer properties such as the molecular weight, the reptation time and the polymer structure.

As previously mentioned, the measured adhesion force strongly depends on the contact area and the contacting time between two polymer layers. Therefore it is dependent on the viscoelastic behavior of the polymer. When the polymer is in the rubbery regime over its glass transition value, the elastic modulus decreases with an increase of the temperature, which allows the polymer layer to deform more easily. The thickness of the layer has an impact on the maximum deformation that can be reached and the resulting contact area created. In fact, it has been shown that a decrease in coating thickness reduces the adhesion between the contacting layers [42].

6.2.4 Methodology

The experimental work first required the production of particles from fine pharmaceutical excipients. These particles were then coated with a polymer film using an atomization process to obtain a uniform coating layer on their surface. After these preparation steps, the particulate material was used inside a spheronizer equipment and submitted to different temperatures that altered the polymer properties and the cohesive forces.

6.2.4.1 Particle production process

Table 6-1: Process parameters for the equipment used for the production of particles

Equipment	Parameters
High shear mixer Fukae Powtec LFD-GS2J	Main agitator: 300 rpm Secondary agitator: 1000 rpm Solution flow rate: 60 g/min
Extruder LCI Multi Granulator MG-55	Screw rotational rate: 30 rpm Mesh size: 1.2 mm
Spheronizer LCI Marumerizer Model QJ-230T	Disk rotational rate: 1000 rpm Spheronization time: 10 min
Tray dryer	Temperature: 60 ° C Drying time: 2 h

Table 6-1 shows the process equipment used to produce the particles for the experimental work. A preliminary mixing step with a high shear mixer served to blend the powder materials (Table 6-2). When the powder was homogeneously mixed, a binder solution (Table 6-2) was added into the high shear mixer to granulate and color the material. The newly formed granules were then fed to an extruder and the resulting product was transferred to a spheronizer to create spherical beads. These beads were dried in a tray dryer. After the production process, the particles were spherical, as evidenced in the SEM picture of Figure 6-5, and characterized by a narrow particle size distribution with a mean size of 1.2 mm (Figure 6-6).

Table 6-2: Powder and solution used for the production of the particles

Elements	Materials	Quantity (kg)
Powder blend	MCC PH-101	0.200
	Lactose monohydrate	0.200
	NaCl	0.100
Binder solution	Water	0.315
	NaCl	0.095
	Yellow quinoline	0.002

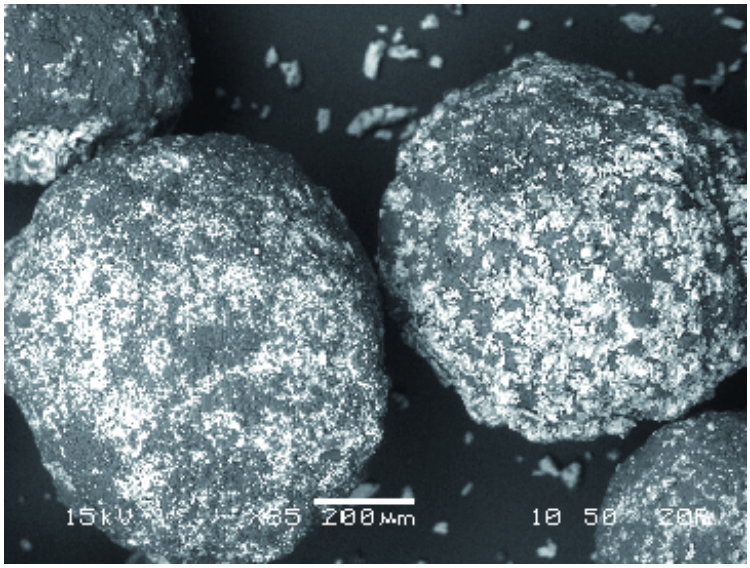

Figure 6-5: SEM picture of the uncoated spherical beads.

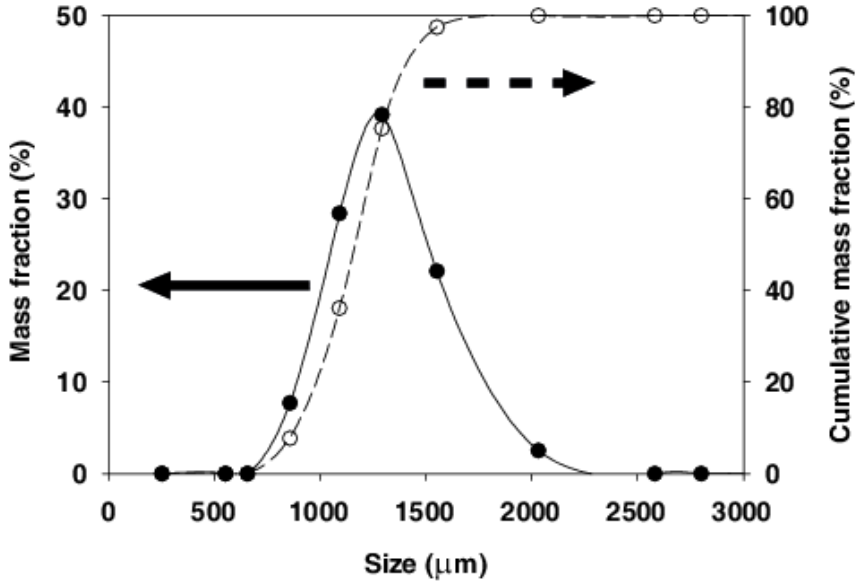

Figure 6-6: Particle size distribution of the particles used in this work.

6.2.4.2 Particle coating process

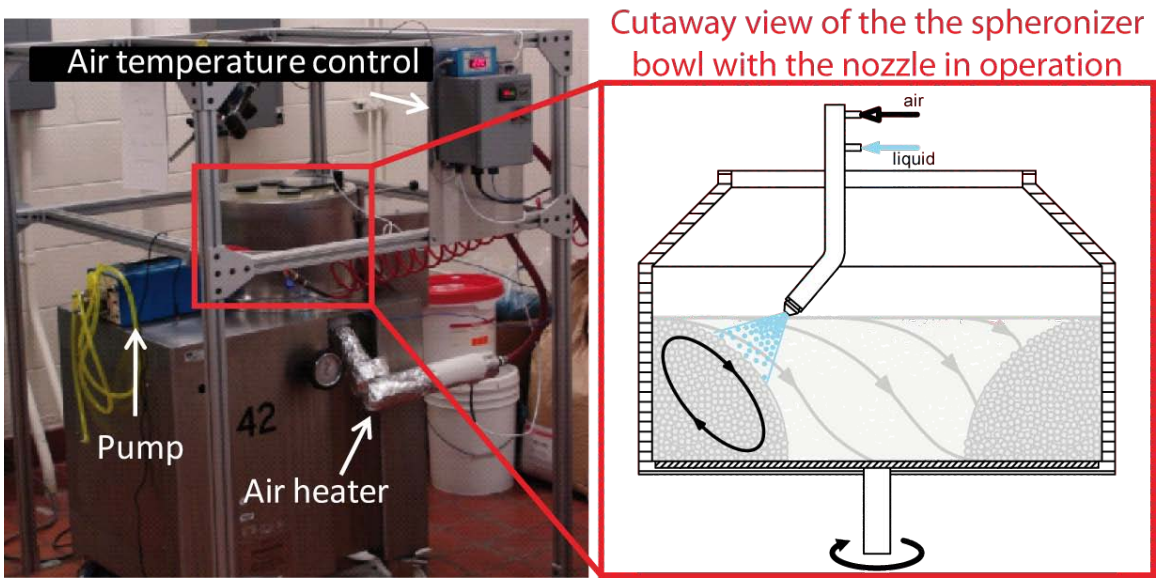

Figure 6-7: Process used to coat the particles with the polymer. An atomizing nozzle has been inserted at the top of the spheronizer bowl to spray the coating solution at the surface of the particle bed.

The next step consisted of adding a polymer layer onto the surface of the particles. To achieve this task, a spheronizer (Caleva 380), different from the one used for the particle production process, was modified to incorporate an air line located below the rotating disc. The introduction of air helps to prevent infiltration of particulate material from the bed through the spheronizer gap located between the rotating disc and the wall. Before entering the spheronizer bowl, the air passes through an electrical heater to adjust its temperature to the desired process setpoint. The temperature is set using a controller coupled with a thermocouple that measures the temperature at the entrance. To ensure that the temperature of the particles reaches steady state, an infrared cell is located at the top of the spheronizer to measure the temperature at the surface of the particulate material. The air flow rate is adjusted with a valve at the entrance of the equipment to the desired value with the help of a gas rotameter. Table 6-3 presents the parameters associated with the coating process (Figure 6-7). During the experiment, the disc rotational speed was set to provide adequate particle mixing but also to prevent the breakage of the particles due to a large shear rate. The air flow rate and the temperature were adjusted to ensure a sufficient drying rate during the coating process and to avoid particle adhesion, respectively. The particles were coated with the polymer suspension, whose composition is indicated in Table 6-4. It consists of a solution of a PEA/PMMA copolymer in a 2 to 1 ratio, which induces the cohesive effect, and nonoxynol, a surfactant employed to synthesize the polymer by emulsion polymerization. Two different quantities of this polymer suspension (commercial name Eudragit® NE30D) were added to the batches in the proportions indicated in Table 6-5. The coating layer thicknesses indicated in this table were estimated by assuming an equal distribution of the polymer dry mass on all the particles while taking into account the particle size distribution presented in Figure 6-6. The coating suspension was coated onto the particles by atomization with a two-fluid atomizer (BETE XA-SR 050). It was fed by a peristaltic pump at a flow rate equal to approximatively 1 g/min using compressed air to allow for the formation of fine droplets. The atomizer was positioned so that the tip of the nozzle was at a distance of 4 cm from the bed surface to avoid coating losses to the mechanical parts of the spheronizer. Figure 6-8 shows the appearance of the coated particles at the end of the coating process.

Table 6-3: Coating process parameters

Parameters	**Values**
Disc rotational rate	230 rpm
Air flow rate	42.5 m^3/h
Air temperature	30 ° C
Solution flow rate	1 g/min
Atomization pressure	200 kPa

Table 6-4: Coating suspension of Eudragit® NE30D

Materials	**Mass %**
Water	68.5
PEA/PMMA 2:1	30.0
Nonoxynol 100	1.5

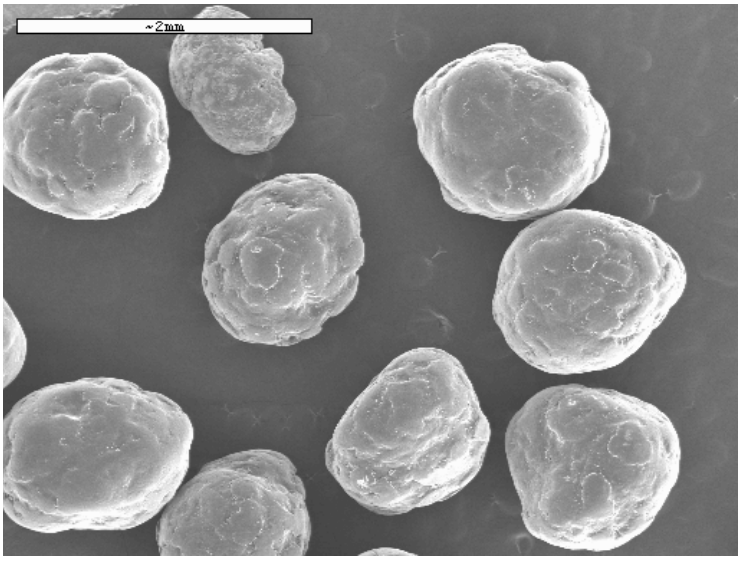

Figure 6-8: SEM picture of the Eudragit® coated particles.

Table 6-5: Final particle coating characteristics

Materials	**Thin**	**Thick**
Spherical particles (kg)	3	3
Eudragit® coating (kg)	0.045	0.090
Percentage of coating (%wt)	1.5	3.0
Coating layer thickness (μ m)	≈ 3.5	≈ 7

6.2.4.3 Measurement of the surface morphology and dynamic density

The surface of the torus of particles inside the spheronizer (Caleva 380) was characterized by pictures taken with a digital camera. The change of surface morphology was linked to the modification of cohesion forces as the temperature increased. The pictures were acquired under the process conditions presented in Table 6-6. These parameters were kept constant for all the

tests, except for the temperature of the particulate bed, which was increased by 1°C increments during each experiment. The range of temperatures selected was above the glass transition temperature (see section 3.4) of the polymer and was set to obtain a variation of the cohesive behavior. The air flow rate was set to a low value to modify the temperature of the particles and to avoid infiltration of material below the processing chamber of the spheronizer. Between 12 to 15 cfm, the air flow rate induced no significant changes on the particulate flow behavior when compared to the process operated with the absence of incoming air. Figure 6-9 shows the equipment used to measure accurately the surface position while the spheronizer was in operation. A 2800 LLT Scancontrol laser sheet profiler (Micro-Epsilon) measured the mean surface position that was used to calculate the volume of the torus. The dynamic density was obtained by dividing the total particle mass by the calculated volume.

Table 6-6: Operating parameters for the spheronizer

Parameters	**Values**
Disc rotational rate	230 rpm
Air flow rate	12-15 cfm
Temperature range	20-50 ° C
Particle bed mass	3 kg

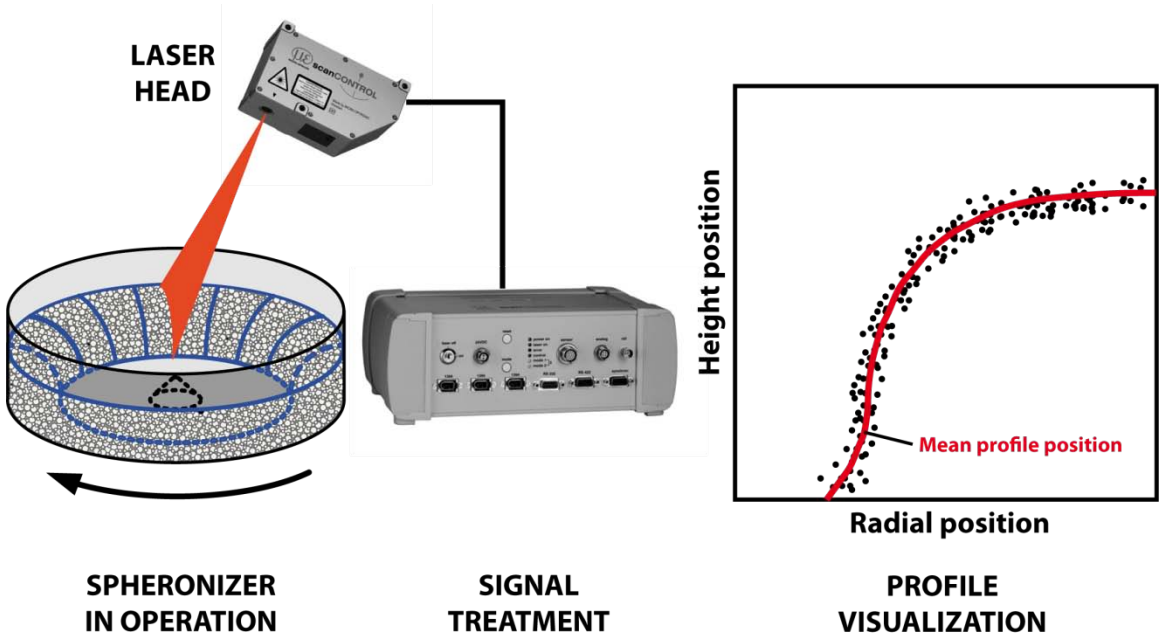

Figure 6-9: Surface measurement setup with the laser sheet profiler. The laser head projects a laser line on the particle bed and the light reflected is recorded by a CCD camera located in the same device. The signal is then transfered to the controller box, which evaluates the profile position, in two dimensions, using the triangulation principle.

6.2.4.4 Measurement of the polymer film properties

The glass transition temperature ( ) was measured with a DSC Q1000 (TA Instruments, USA). The samples of the free polymer film were processed under nitrogen atmosphere at heating and cooling rates of 10 °C/min between 20 °C and 170 °C. The glass transition temperature obtained was around -6 °C. The pull-off force between two surfaces coated with the polymer was measured using a surface forces apparatus (SFA) for different temperatures. Briefly, a basic SFA allows the normal interaction forces between two surfaces to be determined as a function of the surface separation distance by measuring the deflection of a spring that supports the lower surface as this separation distance is changed. The distance between the two surfaces is determined with a resolution of ca. 0.2 nm using the standard interferometry technique that uses fringes of equal chromatic order. More details related to this measurement technique can be

found in [47]. For each measurement, the compression load was constant (1 mN), the contacting time was 1 minute and the decompression rate was kept constant to (12.5 nm/s).

6.2.4.5 Gas-solid fluidized bed study and analysis method

This part of the experimental work involved a 400-800 μm distribution of spherical sugar beads (d_p=600.5μm, =1563 kg/m^3), which belong to the Geldart Group B. These sugar beads were coated with the same PEA/PMMA suspension and procedure as in the case of the spheronizer. The characteristics of the final product are summarized in Table 6-7.

Table 6-7: Final particle coating characteristics for the fluidized bed experiments

Materials	**Quantity**
Spherical sugar beads	3.0 (kg)
PMMA/PEA	0.10 (kg)
Mass percentage of coating	3.4 %
Coating layer thickness	5

The experimental set-up consists of a fluidization column, which was constructed with a transparent Plexiglas tube, 0.152 m I.D. and 1.5 m in height. Dried and filtered air was distributed into the bed using a perforated plate. It contains holes of 1 mm in diameter and arranged in a triangular pitch.

Air was heated with the help of an electrical heater before entering the fluidization column. It was used to adjust the temperature of the bed to the desired value. Temperature was controlled by

means of a PI controller driven by a thermocouple immersed in the bed. A thermocouple located at the windbox allowed measuring the air entrance temperature. The air flow rate was controlled with a rotameter, which confirmed a maximum superficial gas velocity of 0.75 m/s in the bed. Note that different superficial gas velocities were used for covering both the fixed bed state and the bubbling regime.

To investigate the effect of the cohesive forces on the fluidization behaviour, two systems were studied, one with uncoated sugar beads and another with coated sugar beads. Experiments with uncoated sugar beads were carried out at 20^{o}C while the ones with coated sugar beads were conducted at 20^{o}C, 30^{o}C, and 40^{o}C. Hereafter, for simplicity, we name these systems after their different operating conditions in abbreviated form: SB, CSB20, CSB30 and CSB40, which stand for uncoated sugar beads at 20^{o}C and coated sugar beads at 20^{o}C, 30^{o}C and 40^{o}C, respectively. All experiments were performed at atmospheric pressure. It is worth noting that measured variations in the air density and viscosity in the 20^{o}C to 40^{o}C temperature range were 6% and 5%, respectively, which are fairly negligible compared to the cohesion differences obtained with the proposed technique for the same temperature range. Moreover, the same amount of material was poured into the bed in all cases, which resulted in an initial bed height of approximately 20 cm at ambient conditions. For each temperature considered, the height of the bed was measured while the air flow rate was slowly decreased to zero, causing the particle flow behaviour to change from the fluidized bed state toward the fixed bed state.

The pressure drop across the bed was measured using a differential pressure transducer. It was mounted flush with the wall of the column through 15-micron inline filters and measuring ports. In particular, the ratio between the measured and calculated pressure drops across the bed, , was used to highlight changes in the fluidization behavior of the coated sugar beads with increasing temperature. Note that was calculated by dividing the bed weight by the cross-section area of the fluidized bed column.

6.2.5 Results and Discussion

In the first place, a relationship between the interparticle forces and the macroscopic flow observed in both the spheronizer and the fluidized bed is established with the help of the SFA measurements. The effects of the temperature and the coating thickness on the interparticle forces for the spheronizer application are then discussed on the basis of surface morphology measurements. The flowability of the particles with respect to the temperature is next analyzed using observed variations of the dynamic density measured with the laser sheet profiler. The last part of this section deals with the fluidized bed application and focuses on a comparison between the results obtained in this work and those reported elsewhere [48] in the case of other types of cohesive particles in fluidization columns operated at high temperature.

6.2.5.1 Relation between the cohesive forces and the macroscopic flow of the particles in the spheronizer

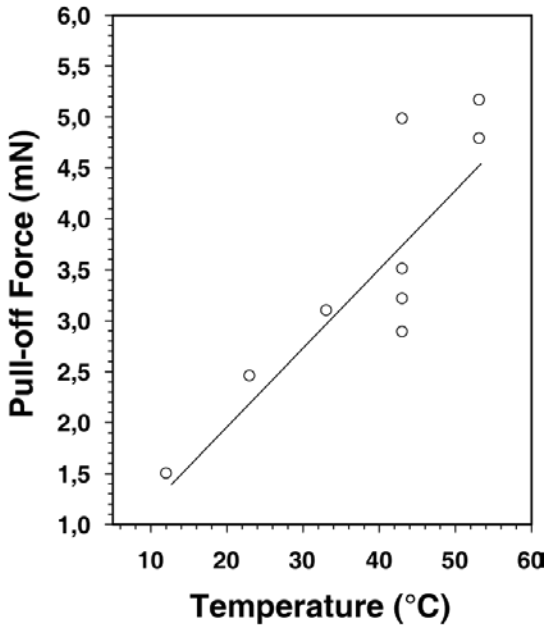

(a)

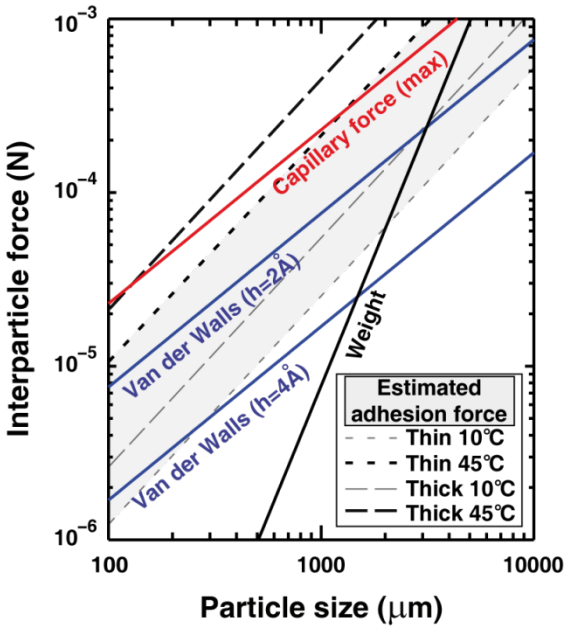

(b)

Figure 6-10: Variation of the interparticle force as a function of the temperature for a 120-nm coating thickness of Eudragit® polymer: a) Pull-off force measured with the SFA using a maximum compression force of 1 mN, a measurement speed of 0.75 μm/min and a contact time of 1 min; b) Comparison of the estimated maximum force obtained for different polymer thicknesses and temperatures with other type of forces [49]. The van der Waals force was obtained with $A_H = 6.5 \times 10^{-20}$ J while the capillary force is based on a surface tension of $\gamma = 72.8 \times 10^{-3}$ N.m^{-1} and perfect wetting. The weight is for a particle density of 1.5×10^{3} kg.m^{-3}.

Equation (6-8) can be used to estimate an adhesion energy from the measured pull-off force. As can be seen in Figure 6-10a, the pull-off force and, as a result, the adhesion energy vary linearly with the temperature. Of course, the polymer thickness also has an impact and must be taken into account. The particles used in this work have a polymer coating thickness varying between 3.5 to 7 μm. Luengo et al. [42] observed that increasing the coating thickness by 1000 times, from around 2 nm to typically 2 μm, results in an increment of the adhesion energy by approximately the same factor. They suggested that the adhesion energy is proportionnal to the coating thickness. Recent SFA measurements on our system (Eudragit polymer) have also indicated a considerable increase in the pull-off force when increasing the polymer thickness (not shown here). Based on this observation, an effective adhesion energy was evaluated for our particles using equation (6-11), where is the adhesion energy that we measured with the SFA and adjusted with respect to the coating thickness. Note that the adhesion energy obtained is because of the long contact time (1 min) considered for the SFA measurements. The contact time was estimated from equation (6-10) using a shear rate of =1 s^{-1}. In this equation, we chose a = 0.9 and b = 0.4, which come from the work of Chau et al. [46]. This choice was made because these constants are not available for Eudragit®. The values selected correpond to polyisobutylene with a comparable maximum adhesive energy and molecular chain weight (~ 10^{5} g/mol).

The interparticle forces, for thin (3.5 μm) and thick (7 μm) polymer coatings and different temperatures were calculated from the corresponding effective adhesion energy values using equation (6-8), are compared to other common forces. Figure 6-10b reveals that large variations

of interparticle forces can be obtained with the polymer coating approach. It can be noticed that the forces resulting from the thin and thick polymer coatings overlap both the capillary and the van der Waals force ranges. For the thick polymer coating at 45 °C, the polymer-induced adhesion force overcomes the other forces. As discussed later, the presence of these strong forces create cohesive phenomena that have not been observed with the other approaches used to generate particle cohesion in granular systems.

6.2.5.2 Torus surface morphology with respect to temperature

Figure 6-11 and Figure 6-12 show the particles in the spheronizer when they are submitted to different operating temperatures. When the spheronizer was operated near the laboratory conditions (20°C), the particles were able to flow freely throughout the torus. The surface is characterized by a smooth profile that subsists until the temperature reaches 44°C (resp. 40°C) for the thin (resp. thick) coatings. As the temperature was increased to 45°C (resp. 41°C), the particles remained in a free-flowing state yet they began to create weak clusters that produced a bumpy torus surface. These clusters became sturdier and larger when the temperature reached 46°C (resp. 42°C). For the thinly coated particles, the growth and consolidation of these agglomerates continued until the maximum temperature investigated, 48°C, was attained.

For the thickly coated particles, a sudden modification of the torus shape occurred when the temperature approached 43°C. At this point, the appearance of a secondary flow layer on top of the first one and near the spheronizer wall revealed a modification of the particle flow pattern. A small fraction of the material located in this new layer was then observed to disaggregate continuously and thus create agglomerates at the surface of the underneath free flowing layer. Some material located in either of the two layers remained unsegregated as it was able to move from one zone to the other by the breaking phenomenon described. When the temperature continued to rise toward 44°C, the secondary layer consolidated itself. The generation of agglomerates from the detachment of fragments of this layer also ceased. At this point, the flow of particles occurred in an apparent periodic fashion characterized by the growth of the secondary

layer until it reached the spheronizer disk where it collapsed and merged with the vanishing free flowing layer. Once the secondary layer was completely broken, it reappeared in the vicinity of the spheronizer wall at the top of the flowing layer, which initiated a new cycle. When the temperature was increased above 44°C, this periodic flow behaviour was replaced by a solid mass motion of the particle bed.

The threshold temperature at which the change in torus morphology occurred also was observed to depend on the quantity of polymer coated on the particles. More precisely, the decrease of coating thickness increased this threshold temperature as well as the temperature range within which the changes of cohesive flow behaviour were observed. Contrary to the thickly coated particles, the periodic flow behaviour was not observed for the temperature range investigated with the thinly coated particles. The observation of the torus morphologies led to the conclusion that, at a given temperature, a thinner polymer layer results in lower cohesion forces between the particles. Therefore, the appearance of a secondary flow layer for the thin coating would require a temperature that surpasses the range investigated. The results presented here show that cohesive forces generated with the proposed approach can be adjusted with two key parameters that are the temperature and the thickness of the polymer layer. Also, different flow behaviours can be induced depending on the intensity of the cohesive forces during the spheronizer operation.

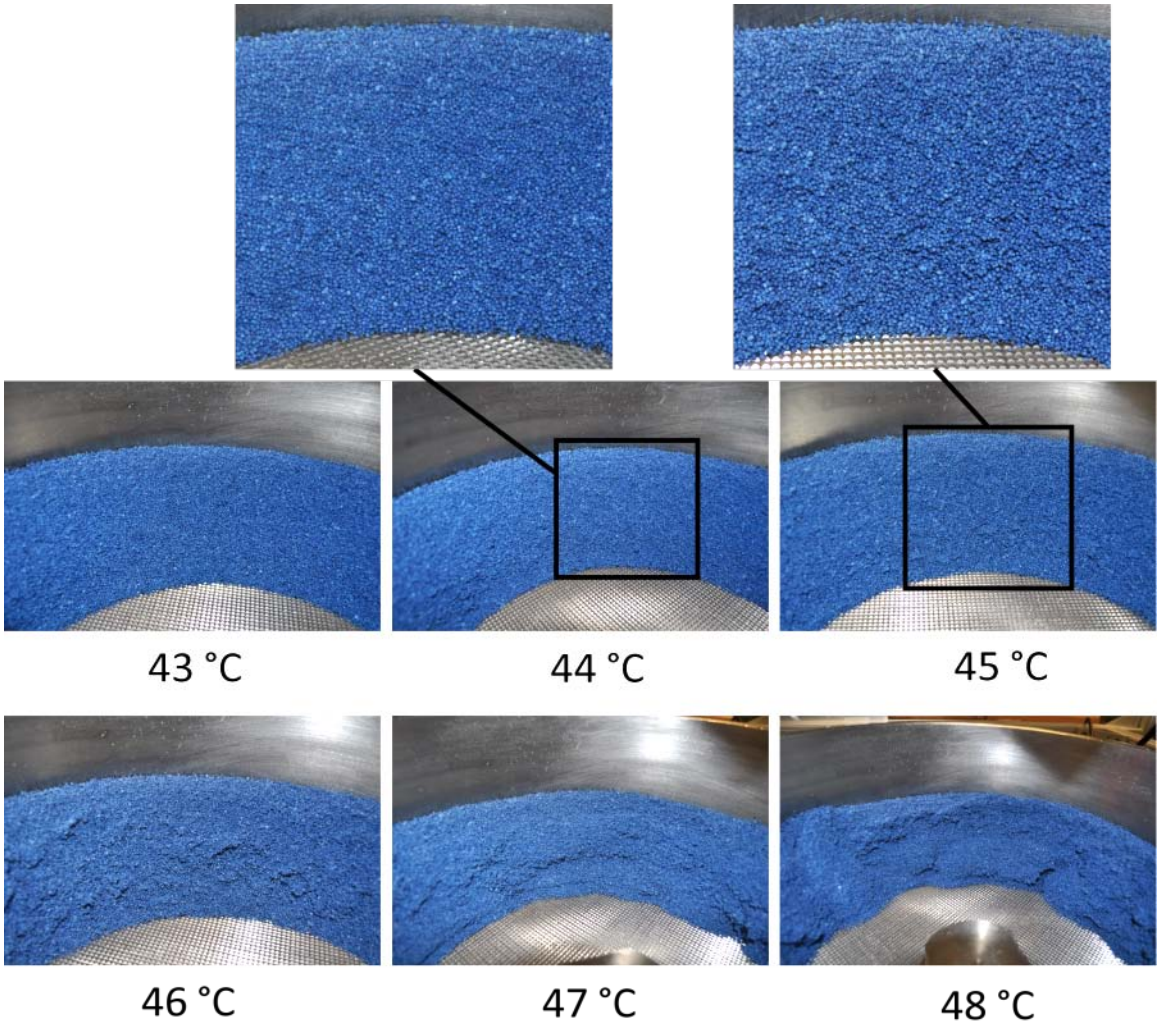

Figure 6-11: Evolution of the thinly coated particles with respect to the temperature. The figure insets corresponding to 44 °C and 45 °C show the presence of agglomerates at the surface of the torus.

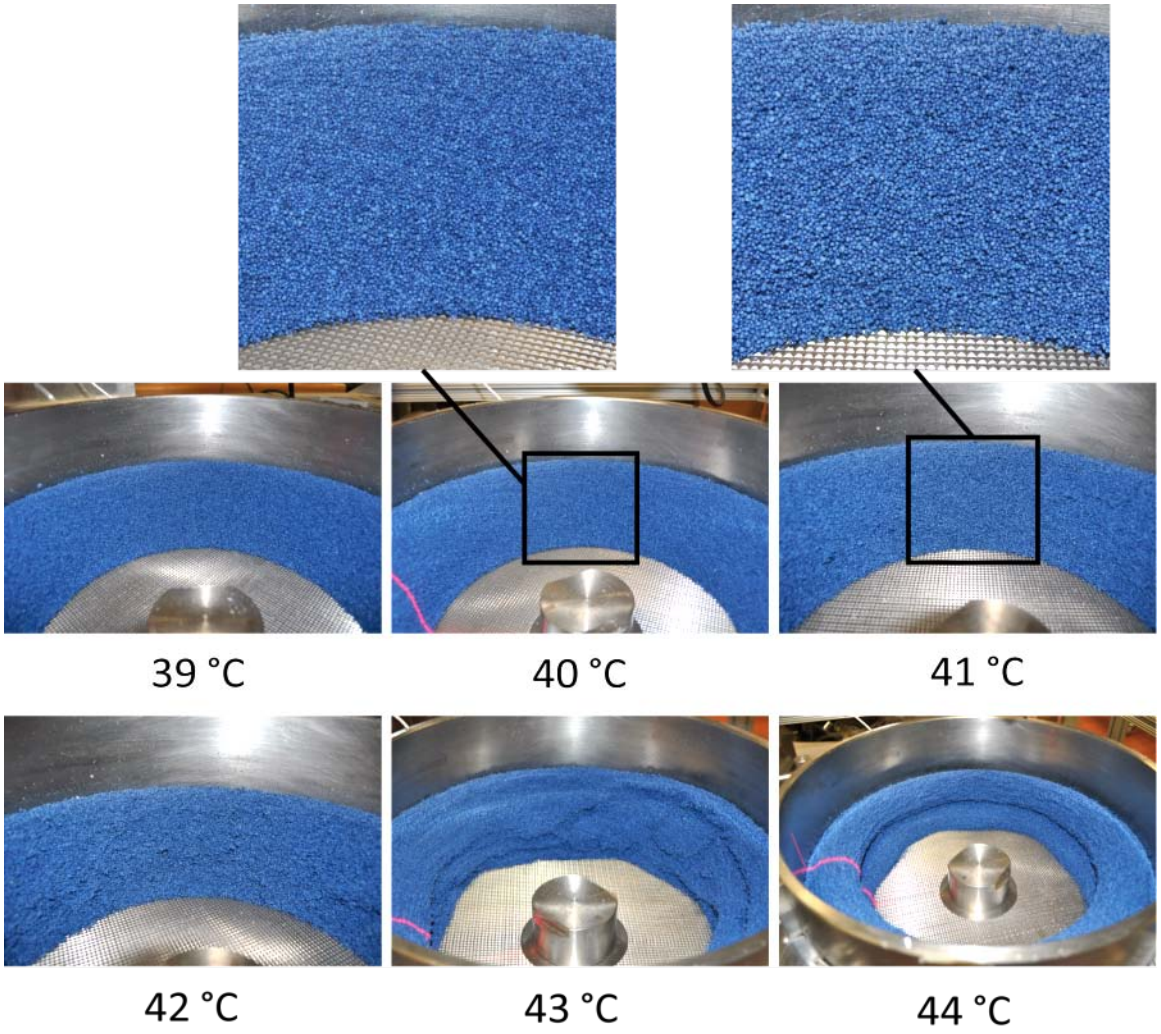

Figure 6-12: Evolution of the thickly coated particles with respect to the temperature. The figure insets corresponding to 40 °C and 41 °C show the presence of agglomerates at the surface of the torus. The red beam generated by the laser sheet profiler is apparent at 40°C, 43°C and 44°C.

The flowability of particles can be assessed by different indicators, such as the dilatational effect encountered for a particle bed in motion [50] or by bulk density measurements using the Hausner ratio [51]. A volume dilatation of a particle bed or a reduction of its bulk density is observed when particles at rest enter into a flowing state [50]. When free flowing material is considered, which means that the interparticle forces are negligible, the volume expansion comes from the collisional forces between the particles as the material moves in a dense flow regime. In the case of cohesive material, for a given shear stress, the dilatation of the particle bed depends on the

interparticle forces, which depend themselves on particle properties such as the size, the density, the moisture content and the surface roughness [51-52].

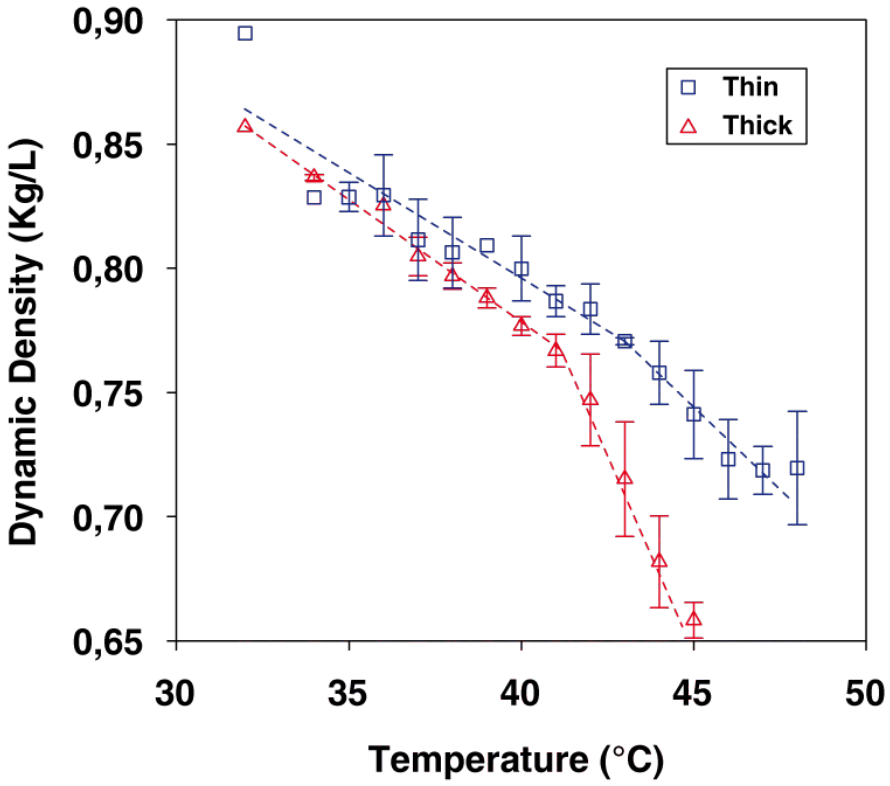

Figure 6-13: Graph of the particle dynamic density with respect to the temperature for thinly and thickly coated particles.

Figure 6-13 shows the particle bed dynamic density measured (mass of the particle bed divided by the volume of the torus calculated from the surface profile) for the thinly and thickly coated particles as a function of the temperature. The dynamic density decreases slowly in a linear fashion with the temperature as long as agglomerates are absent. As the cohesion forces increase to cause the agglomeration of particles, the linear decrease of the dynamic density is accentuated by the expansion of the volume of the torus due to the presence of larger particle clusters. It can also be noticed that the mean value of the dynamic density is lowered by the increase in coating thickness. For the thick coating case, the sudden change in the slope of the dynamic density curve is more important because the occurrence of agglomerates was more significant than for the thin

coating case. The larger cohesive forces created agglomerates that were more resistant to the spheronizer shear stress. This led to the creation of larger clusters that enhanced the expansion of the torus volume.

6.2.5.3 Fluidized bed behavior with coated particles

The most common approach to determine the fluidization state of a system consists of analyzing the bed pressure drop as a function of the superficial gas velocity U_g. The ratio (see section 6.2.4.5) can be used as a first indication of the effect of the interparticle forces on the fluidization behaviour [53]. Figure 6-14 shows, by comparing the pressure drop curves for the uncoated (SB) and coated (CSB20, CSB30, CSB40) sugar beads, that the overshoot generally observed at (minimum fluidization velocity) is enhanced by the interparticle forces. In particular, for the CSB40 case, it was observed that the relatively strong cohesive forces influenced the bed behaviour considerably, with the presence of a large mass of agglomerated particles that got lifted in the column. This phenomenon results in an increase of the pressure drop when U_g is larger than around 0.4 m/s.

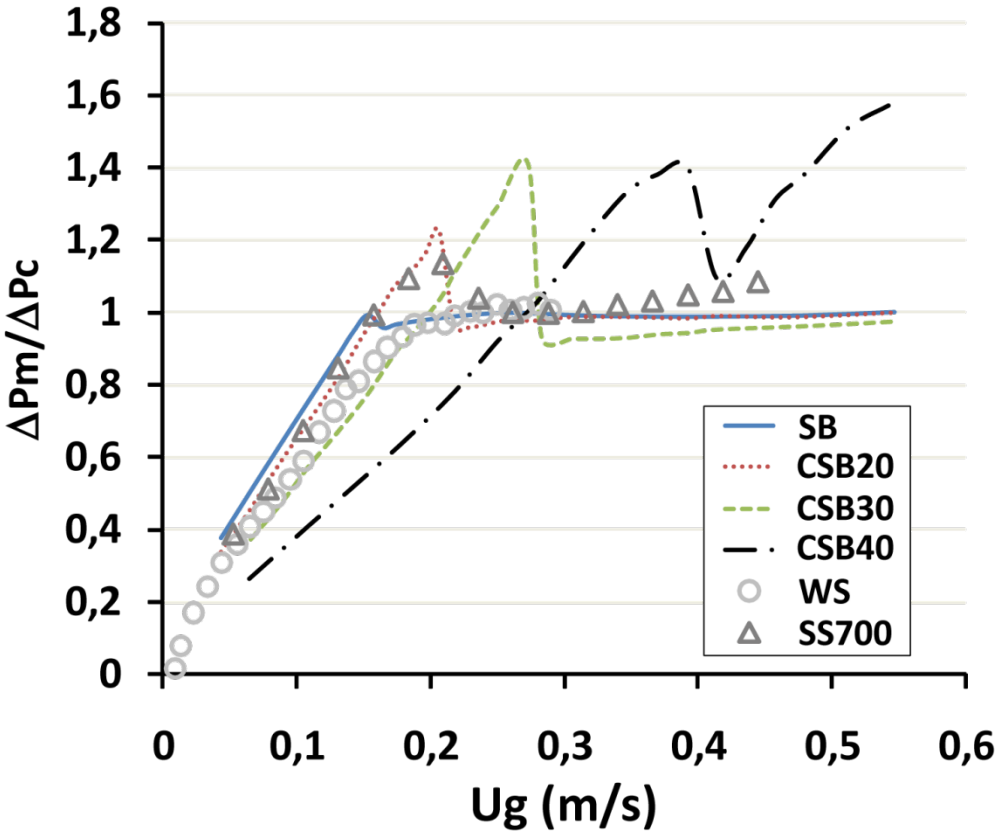

Figure 6-14: The effect of temperature on a normalized pressure drop profile for the fluidization of coated sugar beads (CSB) at 20, 30 and 40 °C and uncoated sugar beads (SB) at 20 °C. Other particles appear in the graph: free-flowing walnut shells (WS) [54] and cohesive silica sand particles (SS) at 700°C [48].

Furthermore, a decrease of the pressure drop ratio below unity when a bed is fluidized is known to indicate the degree of cohesiveness in the system [4, 53]. As can be seen in Figure 6-14, the ratios below one are similar for the SB and CSB20 cases whereas the ratio is significantly smaller than one for the CSB30 case. For the CSB40 case, the ratio remains above one because fluidization is flawed, as explained above. These results show that the enhancement of cohesive forces can cause the behaviour of the particles to change from Group B to Group A and even to Group C. Formisani et al. [12] noted that the voidage of a loosely settled bed of Groups A and B particles increases with the temperature. They attributed this phenomenon to the increase of cohesive forces with temperature. Table 6-8 reports the variation of the fixed bed

height for the uncoated and coated particles. It reveals that the fixed bed height and, equivalently, the fixed bed voidage increase with the magnitude of the cohesive forces. This result confirms the findings of Formisani et al. [12] and indicates that a bed with higher cohesive forces can hold more gas in the fixed state.

Table 6-8: Variation of the fixed bed height for the uncoated and coated sugar beads

	Fixed bed height (cm)
SB	20.3
CSB20	20.5
CSB30	21.4
CSB40	23.0

Comparison of the polymer coated particles (CSB20, CSB30, CSB40) with the free flowing (SB and WS) and the cohesive (SS) particles reveals that one can control the flowing behaviour by setting an approximate temperature. In particular, one can see in Figure 6-14 that the CSB20 particles mimic the behaviour observed for the silica sand particles heated at 700°C. It indicates that it would be possible to study the effect of interparticle forces on the particle flow behaviour encountered in a fluidized bed operated at high temperature by investigating the behaviour of coated particles in the same bed but at much small temperature. In this context, the difficulty of assessing such high-temperature processes can be significantly reduced because resorting to a phenomenologically similar low-temperature process makes it possible to use characterization methods based on immersed probes [55-56].

6.2.6 Conclusion

This work shows that by coating inert particles with a layer of a PEA/PMMA copolymer, the cohesive forces can be modified by a change of process temperature. The interaction forces between the particles were observed to strengthen with the temperature. This polymer coating approach constitutes a new and different technique to study cohesive particle flow behavior. The introduction of cohesion by heating polymer coated particles can be employed in different types of equipment, such as blenders or fluidized beds. Since it is possible to adjust the magnitude of the cohesive forces with this approach, it can be used to provide valuable information on the flow patterns at various times, in granulators for example, in which particle cohesion changes considerably during the process. A thorough SFA characterization of the force between PEA/PMMA layers with respect to the strain and stress applied as well as the time of contact between these layers will be done in a near future to measure their impacts on the interdiffusion rate. These measurements will also help to implement an appropriate cohesive force model for the discrete element simulation of the particle flow dynamics in the spheronizer as well as in other processes.

6.2.7 Acknowledgements

The financial support of the Natural Science and Engineering Research Council of Canada (NSERC), Merck Frosst of Canada, and Ratiopharm is gratefully acknowledged. We would also like to acknowledge Dr. Eric Charreault for measuring the cohesive forces with the SFA. Finally, we thank Jaber Shabanian for his help with the fluidized bed.

6.2.8 References

[1] Forsyth, A.J., Hutton, S., and Rhodes, M.J., Effect of cohesive interparticle force on the flow characteristics of granular material. Powder Technology, 2002. **126**(2): p. 150-154.

[2] Herminghaus, S., *Dynamics of wet granular matter.* Advances in Physics, 2005. **54**(3): p. 221-261.

[3] Rognon, P.G., et al., *Dense flows of cohesive granular materials.* Journal of Fluid Mechanics, 2008. **596**: p. 21-47.

[4] Geldart, D., N. Harnby, and A.C. Wong, *Fluidization of cohesive powders.* Powder Technology, 1984. **37**(1): p. 25-37.

[5] Rhodes, M.J., Wang, X.S., Forsyth, A.J., Gan, K.S., and Phadtajaphan, S., Use of a magnetic fluidized bed in studying Geldart Group B to A transition. Chemical Engineering Science, 2001. **56**(18): p. 5429-5436.

[6] Seville, J.P.K. and R. Clift, *The effect of thin liquid layers on fluidisation characteristics.* Powder Technology, 1984. **37**(1): p. 117-129.

[7] Yates, J.G., P. Lettieri, and D. Newton, *The influence of interparticle forces on the fluidization behaviour of some industrial materials at high temperature.* Powder Technology, 2000. **110**(1-2): p. 117-127.

[8] Lekhal, A., Conway, S.L., Glasser, B.J., and Khinast, J.G., *Characterization of granular flow of wet solids in a bladed mixer.* AIChE Journal, 2006. **52**(8): p. 2757-2766.

[9] Figueroa, I., H.M. Li, and J. Mccarthy, *Predicting the impact of adhesive forces on particle mixing and segregation.* Powder Technology, 2009. **195**(3): p. 203-212.

[10] Li, H.M. and J.J. McCarthy, *Phase diagrams for cohesive particle mixing and segregation.* Physical Review E, 2005. **71**(2): p. 021305.

[11] Li, H.M. and J.J. McCarthy, *Cohesive particle mixing and segregation under shear.* Powder Technology, 2006. **164**(1): p. 58-64.

[12] Formisani, B., R. Girimonte, and L. Mancuso, *Analysis of the fluidization process of particle beds at high temperature.* Chemical Engineering Science, 1998. **53**(5): p. 951-961.

[13] Hamaker, H.C., *The London-van der Waals Attraction Between Spherical Particles.* Physica IV, 1937. **10**: p. 1058.

[14] Butt, H.-J. and Michael, K., *Surface and interfacial forces*. 2010, Weinheim: Wiley-VCH Verlag GmbH & Co. KGaA.

[15] Forsyth, A.J., Hutton, S.R., Osborne, C.F., and Rhodes, M.J., *Effects of Interparticle Force on the Packing of Spherical Granular Material.* Physical Review Letters, 2001. **87**(24): p. 244301.

[16] Richefeu, V., El Youssoufi, M.S., Peyroux, R., and Radjai, F., *A model of capillary cohesion for numerical simulations of 3D polydisperse granular media.* International Journal for Numerical and Analytical Methods in Geomechanics, 2008. **32**(11): p. 1365-1383.

[17] Soulie, F., El Youssoufi, M.S., Cherblanc, F., and Saix, C., *Capillary cohesion and mechanical strength of polydisperse granular materials.* European Physical Journal E, 2006. **21**(4): p. 349-357.

[18] Iveson, S.M., J.A. Beathe, and N.W. Page, *The dynamic strength of partially saturated powder compacts: the effect of liquid properties.* Powder Technology, 2002. **127**(2): p. 149-161.

[19] Weigert, T. and S. Ripperger, *Calculation of the Liquid Bridge Volume and Bulk Saturation from the Half-filling Angle.* Particle \& Particle Systems Characterization, 1999. **16**(5): p. 238-242.

[20] Radjai, F. and V. Richefeu, *Bond anisotropy and cohesion of wet granular materials.* Philosophical Transactions of the Royal Society a-Mathematical Physical and Engineering Sciences, 2009. **367**(1909): p. 5123-5138.

[21] Lumay, G. and N. Vandewalle, *Flow of magnetized grains in a rotating drum.* Physical Review E, 2010. **82**(4): p. 040301.

[22] Peters, F. and E. Lemaire, *Cohesion induced by a rotating magnetic field in a granular material.* Physical Review E, 2004. **69**(6): p. 061302.

[23] Lumay, G. and N. Vandewalle, *Controlled flow of smart powders.* Physical Review E, 2008. **78**(6): p. 061302.

[24] Packham, D.E., *Surface energy, surface topography and adhesion.* International Journal of Adhesion and Adhesives, 2003. **23**(6): p. 437-448.

[25] Dave, R., Chen, Y.H., Jallo, L., and Quintanilla, M.A.S., *Characterization of particle and bulk level cohesion reduction of surface modified fine aluminum powders.* Colloids and Surfaces a-Physicochemical and Engineering Aspects, 2010. **361**(1-3): p. 66-80.

[26] von Rohr, P.R., A. Spillmann, and A. Sonnenfeld, *Flowability Modification of Lactose Powder by Plasma Enhanced Chemical Vapor Deposition.* Plasma Processes and Polymers, 2007. **4**: p. S16-S20.

[27] Maeda, N., Chen, N., Tirrell, M., and Israelachvili, J.N., *Adhesion and Friction Mechanisms of Polymer-on-Polymer Surfaces.* Science, 2002. **297**(5580): p. 379-382.

[28] Sinha, S.K. and B.J. Briscoe, *Polymer tribology*. 2009, London: Imperial College Press. xxvi, 697 p.

[29] Fleer, G.J., *Polymers at interfaces*. 1998, London [u.a.]: Chapman & Hall.

[30] Dillard, D.A. and A.V. Pocius, *The mechanics of adhesion*. 2002, Amsterdam [etc.]: Elsevier.

[31] Qiu, H. and M. Bousmina, *Determination of Mutual Diffusion Coefficients at Nonsymmetric Polymer/Polymer Interfaces from Rheometry.* Macromolecules, 2000. **33**(17): p. 6588-6594.

[32] Chen, N.H., Maeda, N., Tirrell, M., and Israelachvili, J., *Adhesion and friction of polymer surfaces: The effect of chain ends.* Macromolecules, 2005. **38**(8): p. 3491-3503.

[33] Gell, C.B., W.W. Graessley, and L.J. Fetters, *Viscoelasticity and self-diffusion in melts of entangled linear polymers.* Journal of Polymer Science Part B-Polymer Physics, 1997. **35**(12): p. 1933-1942.

[34] Kunz, K. and M. Stamm, *Initial Stages of Interdiffusion of PMMA across an Interface.* Macromolecules, 1996. **29**(7): p. 2548-2554.

[35] Andreozzi, L., Castelvetro, V., Faetti, M., Giordano, M., and Zulli, F., *Rheological and thermal properties of narrow distribution poly(ethyl acrylate)s.* Macromolecules, 2006. **39**(5): p. 1880-1889.

[36] Schach, R. and C. Creton, *Adhesion at interfaces between highly entangled polymer melts.* Journal of Rheology, 2008. **52**(3): p. 749-767.

[37] Johnson, K.L. *Contact mechanics*. 1985; Available from: http://www.knovel.com/knovel2/Toc.jsp?BookID=2685.

[38] Barthel, E., *Adhesive elastic contacts: JKR and more.* Journal of Physics D-Applied Physics, 2008. **41**(16).

[39] Brilliantov, N.V., Albers, N., Spahn, F., and Poschel, T., *Collision dynamics of granular particles with adhesion.* Physical Review E, 2007. **76**(5).

[40] Liechti, K.M., D.W. Xu, and K. Ravi-Chandar, *On the modified Tabor parameter for the JKR-DMT transition in the presence of a liquid meniscus.* Journal of Colloid and Interface Science, 2007. **315**(2): p. 772-785.

[41] Leger, L. and C. Creton, *Adhesion mechanisms at soft polymer interfaces.* Philosophical Transactions of the Royal Society a-Mathematical Physical and Engineering Sciences, 2008. **366**(1869): p. 1425-1442.

[42] Luengo, G., Pan, J., Heuberger, M., and Israelachvili, J.N., *Temperature and Time Effects on the "Adhesion Dynamics" of Poly(butyl methacrylate) (PBMA) Surfaces.* Langmuir, 1998. **14**(14): p. 3873-3881.

[43] Silbert, L.E., Grest, G.S., Brewster, R., and Levine, A.J., *Rheology and contact lifetimes in dense granular flows.* Physical Review Letters, 2007. **99**(6).

[44] Timoshenko, S. and J.N. Goodier, *Théorie de l'élasticité*. 1961, Paris: C.Béranger.

[45] Zhang, D.Z. and R.M. Rauenzahn, *Stress relaxation in dense and slow granular flows.* Journal of Rheology, 2000. **44**(5): p. 1019-1041.

[46] Chau, K.W. and G.S. Swei, *Contact time and interfacial fracture energy of tacky polymers.* Journal of Polymer Science Part B-Polymer Physics, 2004. **42**(16): p. 3013-3025.

[47] Heuberger, M., G. Luengo, and J. Israelachvili, *Topographic Information from Multiple Beam Interferometry in the Surface Forces Apparatus.* Langmuir, 1997. **13**(14): p. 3839-3848.

[48] Wey, M.Y., C.L. Lin, and S.D. You, *The effect of particle size distribution on minimum fluidization velocity at high temperature.* Powder Technology, 2002. **126**(3): p. 297-301.

[49] Seville, J.P.K., C.D. Willett, and P.C. Knight, *Interparticle forces in fluidisation: a review.* Powder Technology, 2000. **113**(3): p. 261-268.

[50] Faqih, A., Chaudhuri, B., Muzzio, F.J., Tomassone, M.S., Alexander, A., and Hammond, S., *Flow-induced dilation of cohesive granular materials.* AIChE Journal, 2006. **52**(12): p. 4124-4132.

[51] Abdullah, E.C. and D. Geldart, *The use of bulk density measurements as flowability indicators.* Powder Technology, 1999. **102**(2): p. 151-165.

[52] Zhu, H.P., Zhou, Z.Y., Yang, R.Y., and Yu, A.B., *Discrete particle simulation of particulate systems: Theoretical developments.* Chemical Engineering Science, 2007. **62**(13): p. 3378-3396.

[53] Lettieri, P., Bruni, G., Newton, D., and Barletta, D., *An investigation of the effect of the interparticle forces on the fluidization behaviour of fine powders linked with rheological studies.* Chemical Engineering Science, 2007. **62**(1-2): p. 387-396.

[54] Escudero, D. and T.J. Heindel, *Bed height and material density effects on fluidized bed hydrodynamics.* Chemical Engineering Science, 2011. **66**(16): p. 3648-3655.

[55] Cui, H., P. Sauriol, and J. Chaouki, *High temperature fluidized bed reactor: measurements, hydrodynamics and simulation.* Chemical Engineering Science, 2003. **58**(3-6): p. 1071-1077.

[56] Girimonte, R. and B. Formisani, *The minimum bubbling velocity of fluidized beds operating at high temperature.* Powder Technology, 2009. **189**(1): p. 74-81.

CHAPITRE 7 INVESTIGATION EXPÉRIMENTALE DE L'EFFET DE LA COHÉSION PARTICULAIRE SUR LA DYNAMIQUE D'ÉCOULEMENT DANS UN SPHÉRONISEUR

7.1 Présentation du troisième article

Soumis à *AIChE Journal* le 17 Novembre 2011

Auteurs: Jonathan Bouffard, Alexandre Cabana, François Bertrand et Jamal Chaouki

Le but de ce travail est d'étudier l'effet des forces interparticulaires pour des particules s'écoulant dans un sphéroniseur modifié. L'approche permettant d'enrober des particules avec un polymère permet d'évaluer l'effet de la cohésion des particules sur les patrons d'écoulement dans ce procédé. Quatre états d'écoulement différents sont observés selon la température du lit de particules.

Le premier état est caractérisé par un écoulement libre près de la température ambiante et pour lequel la cohésion particulaire ne présente pas un effet significatif. Le second état est associé à l'apparition d'agglomérats à la surface du lit de particules. La taille de ces agglomérats augmente au fur et à mesure que la température est incrémentée. Le troisième état concerne la formation d'un zone secondaire d'écoulement où des particules sont complètement agglomérées. Le volume de cette zone secondaire change de manière périodique avec le temps. Le quatrième état est caractérisé par un déplacement des particules suivant le mouvement d'un solide pris en masse du fait que celles-ci sont complètement agglomérées. Ces quatres états sont représentés dans un diagramme d'écoulement permettant de montrer l'usage potentiel de la technique d'enrobage afin d'étudier l'écoulement de particules dans les procédés de granulation humide.

7.2 Experimental investigation of the effect of particle cohesion on the flow dynamics in a spheronizer

7.2.1 Abstract

The flow of particles can be affected by their intrinsic physical properties (size, surface roughness or shape), but also by interparticle forces. The flow behavior can be characterized as "free flowing" when the particle motion is mainly dictated by gravity and inertia. These two forces are present in cohesive particle flows, but they are in competition with other interparticle forces. In this work, an original approach based on the polymer coating of particles is used to investigate the effect of particle cohesion on the flow dynamics inside a spheronizer. It is shown that the interparticle forces can be controlled with the temperature and the coating thickness, which is also confirmed by measurements of the dynamic density of the particle bed. Different flow states were observed as the level of interparticle forces was increased. The results are reported in a flow map that compares the forces obtained in the present approach with other interparticle forces encountered during wet granulation processes. The applicability of the polymer coating approach to study the effect of particle cohesion on the flow patterns in such processes is discussed.

7.2.2 Introduction

The cohesive particle flow behavior encountered in different applications such as granulation or particle mixing has an impact on the performance of these processes [1-3]. In the case of dry powder mixing, in tumblers for example, the interparticle forces change with respect to the particle size distribution (PSD) or from the build-up of electrical charges if the blender is not grounded appropriately [4]. The particle properties, such as size, do not change significantly during the mixing process and the interparticle forces remain almost constant. On the other hand, other processes (e.g. granulation or milling) change the PSD, which modifies the interparticle forces. In the case of granulation, the change of cohesion is also affected by an increase in the binding agent concentration [5]. The granulation processes were considered for a long time as perfectly mixed systems and were modeled accordingly before it became obvious that the particle

flow had an impact on the product obtained [6-9]. The particle flow affects the velocity gradient as well as the collisional and the residence times of the particles, which vary between the different areas of a granulator. Also, the way the shear stress propagates throughout the particle bed and the presence of dead zones are examples of the many factors affecting how the particle size distribution evolves with respect to time in such processes.

In addition, segregation is subject to occur when the particle size distribution is not monodispersed. This has been observed and characterized for various equipments used for granulation, such as rotary drums [10], rotating pans [11], vertical high-shear mixers [12], rotor-processors and fluidized beds [13]. Size segregation will cause an alteration of the frequency of collisions between granules of different sizes and their associated velocities. It can also cause a non-homogeneous distribution of the binder agent, which can favor the larger particles that pass more frequently in the spraying area than their smaller counterparts. The ability to predict the intensity of the different granulation mechanisms (e.g. nucleation, coalescence or breakage) then depends on the knowledge of the flow patterns of the segregated particles and their corresponding velocity scales within the different flowing zone of the equipment.

The characterization of the particle flow patterns within granulators is not an easy task because the flow field continuously changes over time from the modification of the particle properties. The time scale of granulation runs is typically less than half an hour for laboratory granulators (e.g. high shear mixers or fluid-bed granulators). Due to such a short time scale, it is challenging to accumulate enough data that are representative of the particle flow at specific times during the process. This time scale problem could be circumvented if one had a means to adjust the interparticle forces independently of the particle properties. It would then be possible to mimic the flow behavior observed in granulation equipments at specific operation times.

In a previous paper, we proposed a new approach to introduce cohesive forces between particles without affecting their PSD while being processed in powder equipments [14]. This approach consists of coating on the particles a uniform layer of an amorphous copolymer (PEA/PMMA) characterized by a low glass transition temperature. It was shown that, due to changes in the

polymer properties, it is possible to increase the cohesive forces between particles by increasing the temperature. The level of intensity of these forces depends on the molecular interdiffusion rate of the polymer chains and the particle contact time. The time required to reach the maximum adhesive force can be approximated by the reptation time [15], which can be estimated from the William-Landel-Ferry empirical model:

(7-1)

where is the reference reptation time known at temperature , is the temperature and and are regression constants that depend on the polymer species. When the polymer chains diffuse through the interfaces, the resultant adhesion force increases, which means that it depends on the time during which the particles are in contact. The estimation of the particle contact time, , is discussed in [14] and can be evaluated by the following relationship [16]:

(7-2)

where is the particle density, is the Poisson ratio, is the Young's modulus, is the particle radius and is the normal collision velocity, which is estimated by the product of the particle size and the shear rate ( ) [17]. Once it has been estimated, it can be used to calculate an effective adhesion energy, , from the maximum value of this adhesion energy, [18]:

(7-3)

where the regression constants *a* and *b* vary with the polymer properties. This adhesive energy can then be used to evaluate the interparticle force, , on the basis of the JKR theory for spherical polymer coated particles [14, 19-21].

Dimensional analysis can be used to describe the bonding regime that characterizes the separation of coated particles. The first dimensionless number is the Bond number (Bo) which is the ratio between the adhesive force binding the particles and the particle weight. A modified Bond number is used here to take into account not only the impact of the weight of the particle, but also the shear rate in the equipment:

(7-4)

where and are the particle radius and mass, and is the gravitational constant. The second dimensionless number is the Deborah number (De):

(7-5)

where is the average initial strain rate, which can be approximated by the shear rate .

The objective of this work was to apply the technique we introduced in [14], which is based on the polymer coating of particles, to investigate the effect of particle cohesion on the flow dynamics inside a spheronizer. The flow patterns in this device are representative of those found in rotor-based granulator equipments (e.g. the flat standard rotor used with the rotor granulators from Glatt and the conical rotor used with the Granurex® from Freund Vector). The use of a spheronizer simplifies the investigation of the flow patterns as the particles are pushed toward the wall of the equipment due to the centrifugal force. The torus shape thus created is assessed by measuring the surface profile with a laser sheet profiler [14]. The effect of particle cohesion is investigated by measuring the changes of the surface position and analyzing the surface fluctuations caused by the presence of agglomerates when the particle adhesion is strong enough.

The impacts of the process temperature and the polymer coating thickness on the particle cohesion are discussed and categorized as a function of the different flow behaviors observed. The impact of cohesion on the dynamic density of the particle bed is examined as it is related to the flowability of the particles within the equipment [3, 22]. Finally, the results obtained in this work are discussed with regard to the flow dynamics in granulation equipments.

7.2.3 Methodology

The experimental work required the production of particles from pharmaceutical excipients that can be extruded by means of a wet powder process. These particles were then coated with a polymer film using an atomization process to obtain a uniform coating layer on their surface. After these preparation steps, the particulate material was used inside the spheronizer and submitted to different temperatures that altered the polymer properties and the cohesive forces.

7.2.3.1 Production of coated particles

The particles were first produced with an extrusion-spheronization process. They are spherical and characterized by a narrow particle size distribution with a mean size of 1.2 mm, as shown in Figure 7-1.

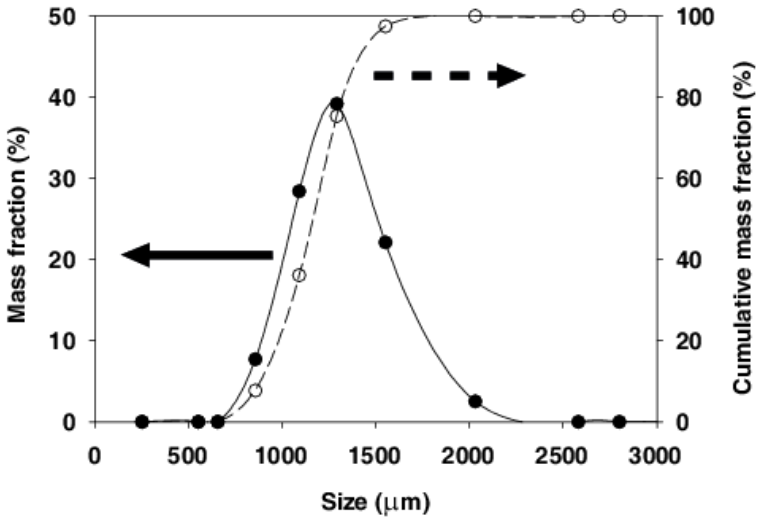

Figure 7-1: Particle size distribution [14].

The next step consisted of coating a polymer layer onto the surface of these particles. To achieve this task, a spheronizer (Caleva 380) was modified to incorporate an air line located below the rotating disc. Different batches were coated with a polymer suspension (Eudragit®) whose composition is indicated in Table 7-1. The PEA/PMMA copolymer (-6°C) in a ratio of 2 to 1 induces the cohesive effect while nonoxynol, a plasticizer, brings flexibility to the polymer. Different masses of polymer suspension, defined as high (H), medium (M) and low (L), were added to the batches without modification in the proportions indicated in Table 7-2. The coating layer thicknesses indicated were estimated by assuming an equal distribution of the polymer on all the particles while taking into account the particle size distribution of Figure 7-1. The operation protocols used to produce and then coat the particles with Eudragit® is described in detail in [14].

Table 7-1: Coating suspension of Eudragit ® NE30D

Materials	Mass %
Water	68.5
PEA/PMMA 2:1	30.0
Nonoxynol 100	1.5

Table 7-2: Final particle coating characteristics

Materials	Batch H	Batch M	Batch L
Spherical particles (kg)	3.000	3.000	3.000
Eudragit coating (kg)	0.180	0.090	0.045
Percentage of coating (%wt)	7.3	3.0	1.5
Coating layer thickness (m)	≈ 15	≈ 7	≈ 3.5

7.2.3.2 Measurement of the bed surface profile and spheronizer operation parameters

The impact of cohesion forces on the particle flow behavior inside the modified spheronizer that was used to coat the particles was assessed by measuring the surface position of the toroid shape obtained with the help of a line scanner profiler. The ScanControl 2800 LLT (Micro-Epsilon) projects a laser sheet onto the particulate shape to triangulate its position. Figure 7-2 shows a schematic that explains how profile measurements were acquired. The position of the laser head was adjusted to project the laser sheet perpendicularly to the toroid surface and the distance from the particulate bed was chosen so that the complete profile of the toroid can be scanned. The laser

scanner system operates according to the principle of optical triangulation (light intersection method). Once the laser line is projected onto the surface, the reflected light is replicated on a CMOS array by a high quality optical system and evaluated in two dimensions. This equipment was set to give the accurate position of 512 points per profile with a height resolution of 40 m at a frame rate of one profile per second. On the basis of experimental observations and the discrete element simulation of particle flow in the spheronizer [23], the time interval was chosen to ensure that the toroidal shape had the time to reorganize between two measurements and that each profile was different from the previous one.

For each batch investigated, 50 profiles of the toroid surface were acquired with the line scanner profiler. After the experiments, the profiles were analyzed simultaneously with an homemade Matlab ® code that calculated the mean position of the toroid and its variance. Figure 7-2 shows the mean position as the line that crosses the cloud of points. The domain used to calculate the variance is represented by the green rectangular box. To investigate the periodic behavior of the toroid surface profile (see section 7.2.4), the frame rate was increased to five profiles per second along with an acquisition duration higher than the characteristic period time related to the surface dynamics. The toroid surface position was acquired with the spheronizer operating parameters presented in Table 7-3. All the parameters were kept constant throughout the tests except for the temperature of the particulate bed, which was step incremented during each experiment, and the polymer coating thickness, which changed between the different batches. The range of temperatures selected was above the glass transition temperature of the polymer and was set to obtain a variation of the cohesive behavior of the flowing particles, which occurred above 25°C. The air flow rate was adjusted as indicated in Table 7-3; it was set to a low value to modify the temperature of the particles and to avoid infiltration of material below the rotating disc. In order to obtain a uniform temperature inside the spheronizer chamber, the bowl was closed with an acrylic cover on top of which a infrared captor was positioned toward the toroid surface. The measurement was taken when no temperature gradient was observed between the heated inlet air and the powder surface. An air flow rate between 12 and 15 CFM resulted in no significant changes on the particulate flow behavior when compared to an operation in absence of air flow.

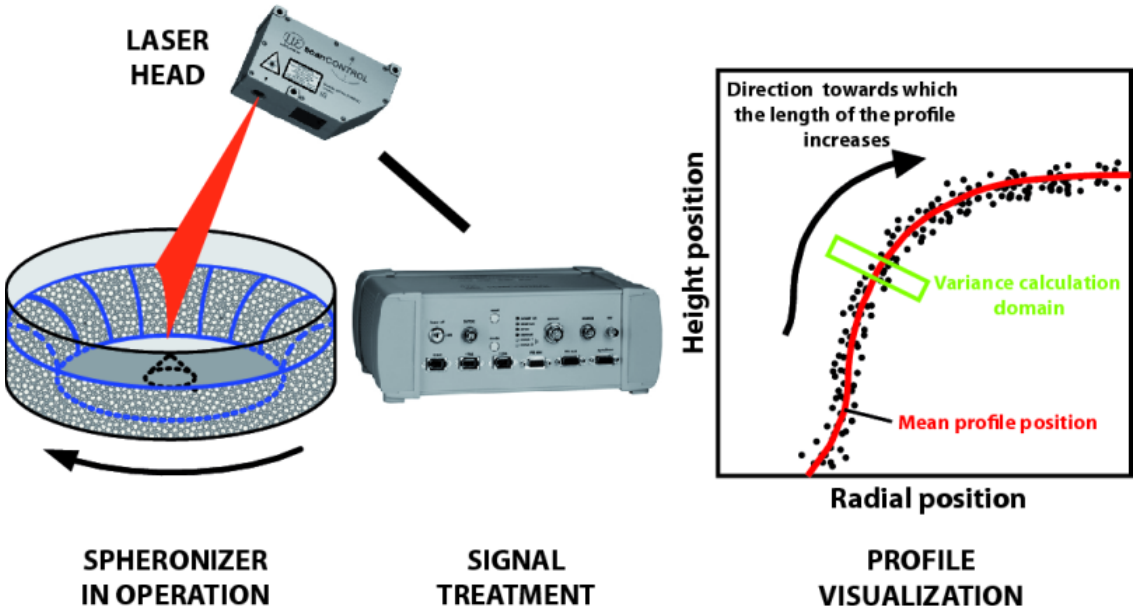

Figure 7-2: Surface measurement setup with the 2800 LLT ScanControl. The box used to calculate the variance of the profile position is oriented so that the longer edge of the green rectangle is perpendicular to the mean profile.

Table 7-3: Spheronizer operating parameters

Parameters	Values
Disc rotational rate	230 rpm
Air flow rate	12-15 cfm
Temperature range	25-45 °C
Particle bed mass	3 kg

7.2.4 Results and discussion

The effects of the temperature and the coating thickness on the interparticle forces are discussed with the help of measurements of the surface position and shape of the toroid as well as dynamic density data. Their effects on the particle bed flow behavior are next analyzed by comparing the results of batches **H**, **M** and **L** (see Table 7-2). Finally, a so-called flow state map is introduced to provide more insight into results obtained and link them to the operating conditions of other granulation processes.

7.2.4.1 Influence of the temperature on the shape of the toroid

When the toroid is created with non-cohesive material, the particles flow with a characteristic spiral motion in the azimuthal direction of the spheronizer [14]. Depending on the process temperature, the particulate bed can behave following four different states, as presented in Figure 7-3. Each state is accompanied with a representative snapshot taken during the experiments, a graph highlighting the mean and the variance associated to the profiles measured by the laser sheet profiler, and a schematic of the cut-away view of the toroid changes as the temperature was incremented. No profile is presented for the third state because periodic patterns were observed in this case, as further explained below.

The first state (FS-I) was observed at ambient conditions and for temperatures below 36°C. FS-I corresponds to a toroid shape that remains stable with respect to time and is characterized by a free-flowing behavior of the particles. The toroid profile is not affected significantly by a change of temperature.

In the second state (FS-II), the toroid shape was also stable during the experiments. The difference from FS-I comes from the presence of isolated agglomerates at the toroid surface. As shown in Figure 7-3, the presence of these agglomerates has a significant impact on the

variability of the toroid profiles measured. The schematic of FS-II also shows that the size of the agglomerates and the volume occupied by the toroid increase with the temperature. FS-II persisted until the temperature reached a threshold value (T_{per}) at which the isolated agglomerates gathered to form a secondary layer of particles.

The third state (FS-III) is a particular case as the toroid behavior is completely different from that of the other flowing states, which explains why it is treated differently in Figure 7-3. When the process temperature reaches the threshold value T_{per}, the particle flow changes significantly and the surface of the toroid becomes unstable with the occurrence of periodic fluctuations. FS-III was observed to persist over a narrow temperature range that depended strongly on the coating thickness.

The fourth state (FS-IV) presented an oscillatory but stable surface profile characterized by a solid mass motion of the toroid and occurred when the process temperature was above T_{per}.

The next three sections explain how the temperature affects the behavior of the particle flow for states FS-II to FS-IV. Since no significant changes were observed when the temperature was varied, FS-I is not further discussed.

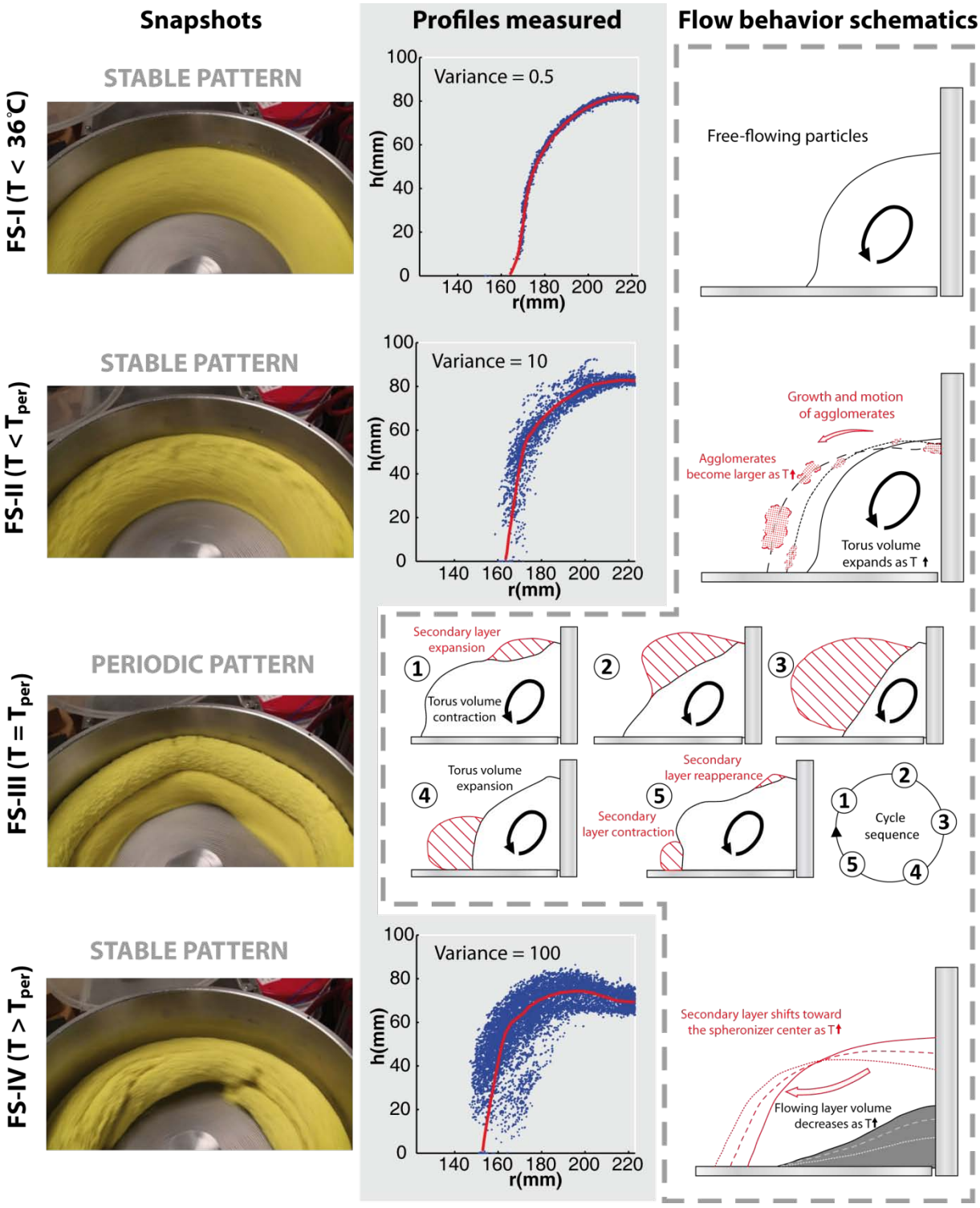

Figure 7-3 : Flow states (FS) of the toroid as the temperature increases. Snapshots taken with batch H are compared with the profiles obtained from the superposition of 50 measurements taken during each experiment. The variance indicated is related to

the mean profile represented by the line passing trough the cloud of points. The schematics of the flow states exaggerate the toroid profile variations in order to highlight how the temperature affects the particle bed shape and volume. While for FS-I only a smooth flowing layer is indicated, the other states present either agglomerates (FS-II) indicated as shaded shapes, or a consolidated secondary layer (FS-III) represented as a hatched shape. The schematic for FS-IV represents the flowing and secondary layers using different colors.

7.2.4.1.1 Toroid flow state FS-II

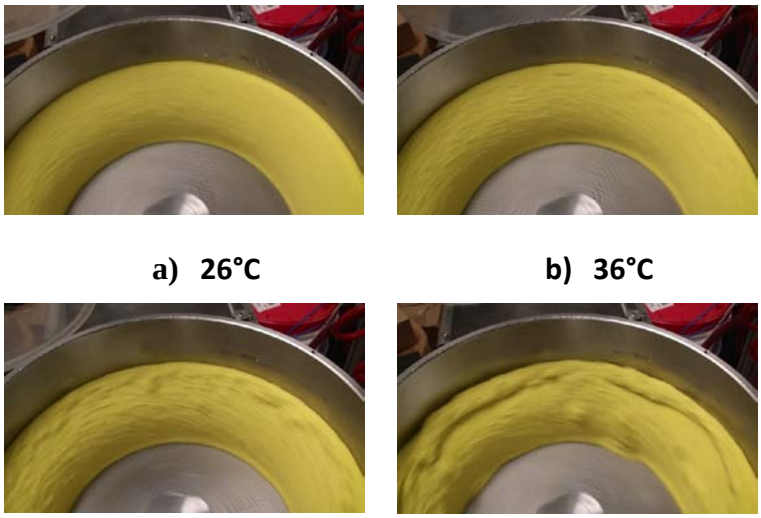

a) 26°C **b) 36°C**

c) 37°C **d) 38°C**

Figure 7-4: Snapshots of the toroid surface as the temperature was incremented in FS-II for batch **H**.

As shown in Figure 7-4a, FS-I was observed when the temperature was near the ambient conditions and the particles were able to flow freely throughout the torus domain. As the temperature was increased from 20°C to 26°C, the surface of the toroid profile was not significantly affected. For batch **H**, FS-II appeared once the temperature reached 36°C (Figure 7-4b) with the presence of agglomerates at the surface of the bed, which increased in size as the

upper temperature limit for FS-II (38°C) was approached (Figure 7-4c and Figure 7-4d). The presence of these agglomerated particles caused variations on the position and the profile of the toroid measured with the laser scanner, which resulted in an increase of the variance around its mean position (Figure 7-3).

As can be seen in Figure 7-5a, the shape of the surface profile does not change significantly between 36°C and 38°C. On the other hand, a comparison of the mean profile positions reveals small differences for this range of temperatures. In fact a slight expansion of the volume of the toroid occurred when the temperature was increased. Figure 7-5b shows that the variance of the surface position is affected by the temperature (empty symbols), which can be explained by the increase in number and size of agglomerates at the surface of the toroid (see also Figure 7-3). At this level of temperature, it was observed that these agglomerates were short-lived as they got destroyed by the spheronizer disc when they flew towards it. Beyond 38°C, the flowing state FS-III appeared and the agglomerates were replaced by a secondary consolidated layer, as discussed in the next subsection. Such behavior is due to the effect of temperature on the magnitude of the interparticle cohesive forces resulting from the polymer coating at the surface of the particles.

For the temperature range covered in FS-II, the particles were constantly convected throughout the toroid. The appearance and the growth of the agglomerates with the temperature indicate a gradual increase of the cohesion forces between the particles. Three parameters contribute to the adhesive force between colliding particles: the contact area between the polymer layers, the particle contact time and the rate of interdiffusion of the polymer chains through the interface [14]. The contact area and the contact time are affected by the elastic modulus of the polymer. Its value is known to decrease with an increase of the temperature until it reaches a stable value that depends on the polymer properties [24]. For the PEA/PMMA copolymer, the elastic modulus stabilizes at $6x10^6$ Pa around 35°C and remains around this value as the temperature is increased to 60°C [25]. The contact area and contact time are also affected by the pressure applied on the polymer layer during a collision. However the pressure plays a lesser role in this work because the disk rotational rate remained the same for the experiments. For these reasons, the adhesive

energy and the intensity of the interparticle forces are considered for FS-II to be mainly affected by the interdiffusion rate.

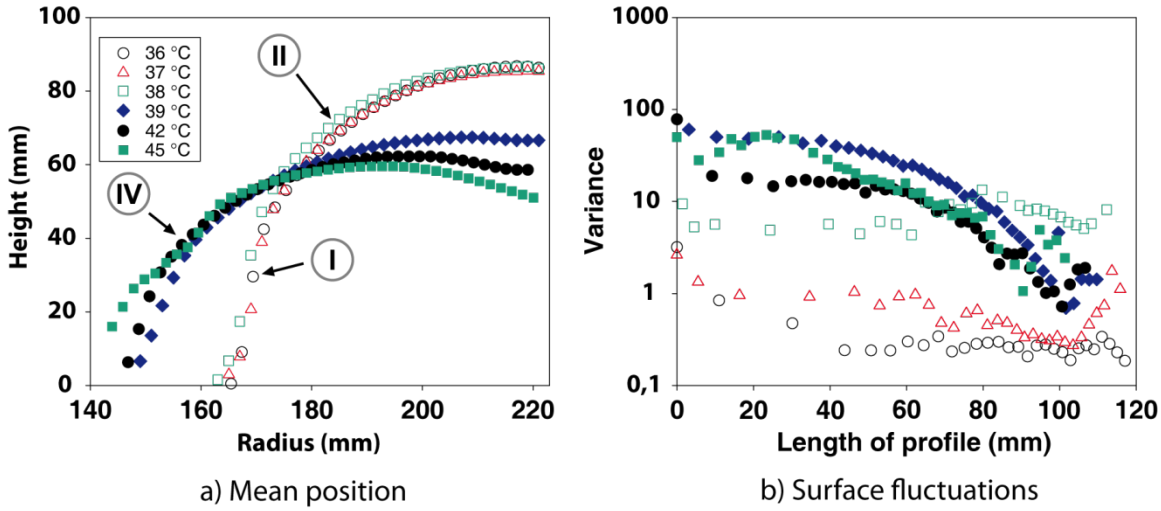

Figure 7-5: Surface position of the particle bed with respect to the temperature for batch **H**. Empty symbols are related to FS-I and FS-II flow states while the solid symbols correspond to FS-IV. The graphs highlight the effect of temperature on a) the mean position and b) the variance of the surface profile.

7.2.4.1.2 Toroid flow state FS-III

When the temperature reached a value higher than 38 °C, a change of the flow structure became apparent as the agglomeration phenomena was replaced by the creation of a second flow layer. Beyond this temperature, the agglomerates disappeared at the surface of the torus to be replaced by a consolidated layer of particles, on top of the original flowing layer, in the vicinity of the spheronizer wall, as shown in Figure 7-3. It resulted in two distinct zones with different flow behaviors. The bulk region, located at the bottom of the spheronizer, is characterized by a fast spiral-like motion of particles with no agglomerates. The second region, located on top of the first one, behaves differently, with particles that move as an apparent solid mass but at a slower pace. This zone has the properties of a dead zone, showing an absence of mixing and particles

that remain trapped with no apparent interchange with the bulk region. In fact, FS-III was observed to be unstable since the two layers continually changed of shape and volume in a cyclic manner. Once created, the top layer increased in volume as the neighboring particles from the bottom layer were swallowed into it. The enlargement of the top layer continued until it reached the disc of the spheronizer and then collapsed, which caused the toroid to return to its initial state with one single bulk layer. After a short period of time, the top secondary layer reappeared and its volume expanded, initiating the beginning of a new cycle. Typical profiles observed during one cycle are presented later in this paper for batch **M**. Note that measurements were difficult to obtain for batch **H** as the periodic behavior was somewhat blurred and appeared more sensitive to temperature. Once the temperature setpoint was reached, the behavior persisted for a short period of time before the flow state FS-III transited to FS-II or FS-IV depending on the temperature fluctuations in the spheronizer. Also note that FS-III was not observed for batch **L** (see Table 7-4).

The prolonged contact time of the particles in the secondary layer generates strong cohesion forces. This prevents a free flowing behavior and rather promotes the formation of a consolidated layer. The agglomerated particles can only be separated by the shear stress in the vicinity of the spheronizer disk. These cohesion forces surpass the shear forces at the surface of the toroid in FS-III. This explains the presence of the secondary layer and its cyclic behavior. The period of existence of this layer is related to a balance between the rate at which its volume expands and the time it takes to reach the high shear zone near the spheronizer disk where it is broken. The PEA/PMMA copolymer reptation time is not known; the measurement of this parameter could help clarify the evolution of the secondary layer by estimating the time-dependent magnitude of the cohesion forces prevailing in this layer, as discussed in Section 7.2.2.

7.2.4.1.3 Toroid flow state FS-IV

When the process temperature reached 39°C for batch **H**, the particulate bed moved as a solid mass with no apparent spiraling motion at the surface, which indicates that the cohesion forces

have become larger than the hydrodynamic forces. As can be seen in Figure 7-5, the mean surface positions above 39°C are different from those at lower temperatures, with a lower height of the toroid near the wall of the spheronizer and an expansion of this toroid toward the center of this equipment as the temperature increases. The variances of the surface measurements along the length of the profiles are also different. The material located near the spheronizer disc is submitted to high stresses, which result in the rupture of the toroid surface in this vicinity and the formation of superimposed blocks of aggregated particles, as depicted in the corresponding schematic of Figure 7-3. The presence of these blocks and the associated fracture lines create a non regular surface with peaks and valleys that explains the large values of the variance along the first half of the length of the surface profile in Figure 7-5. The snapshot for FS-IV in Figure 7-3 shows no blocks of particles in the vicinity of the spheronizer wall, hence the decrease of the variance in the second half of the surface profile length.

In FS-IV, the particles endures prolonged contact, which favors the increase of the adhesion forces. The absence of particle flow at the surface of the toroid means that, when this flow state is reached, the forces resulting from the shear rate induced by the spheronizer disc are inferior to the interparticle forces. The particle bed is then characterized by a quasistatic flow regime in which the particles flow as one single mass in the spheronizer. It is most probable that a thin layer of particles just above the spheronizer disc obeys a dense flow regime, although this phenomenon was not observed.

7.2.4.2 Influence of the coating thickness on the shape of the toroid

Table 7-4: Temperature boundaries for the four different flowing states with respect to the coating thickness

Coating thickness	FS-II (°C)	FS-III (°C)	FS-IV (°C)
H	36 – 38	38 – 39	39 <
M	40 – 43	43 – 45	45 <
L	44 – 50	50 – ?	---

As explained earlier, the coating thickness was decreased from batches **H** to **L** (see Table 7-2). As the coating layer became thinner, a higher temperature was required to induce the different flow states, as shown in Table 7-4. For batches **M** and **L**, that is for coating thicknesses of 7 μm and 3.5 μm, agglomerates were generated at process temperatures equal to 40°C and 44°C, respectively. This tendency is confirmed by the results obtained for batch **H**, let alone for a coating thickness of 15 μm, where a temperature of 36°C was necessary to produce the first agglomerates. FS-II was observed between 40°C to 43°C for batch **M** while it occurred between 44°C and 50°C for batch **L**. Hence, decreasing the coating thickness of the polymer layer allowed the expansion of the range of temperatures at which FS-II was observed. Figure 7-6 (batch **M**) and Figure 7-7 (batch **L**) show the mean positions of the toroid surface profiles and the associated variances for different temperatures and repetitions of the same experiment. All the profiles shown can be associated with FS-I or FS-II. It can be noticed that the decrease of the coating thickness led to a reduction in the variability of the results, especially as regards the variance measurements.

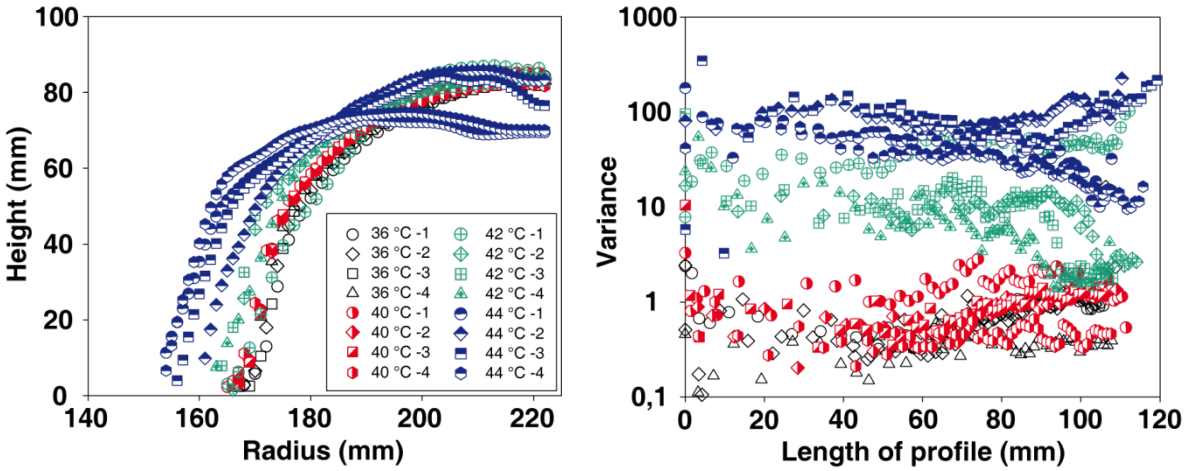

a) Mean position b) Surface fluctuations

Figure 7-6: Surface position of the particle bed with respect to the temperature for batch **M**.

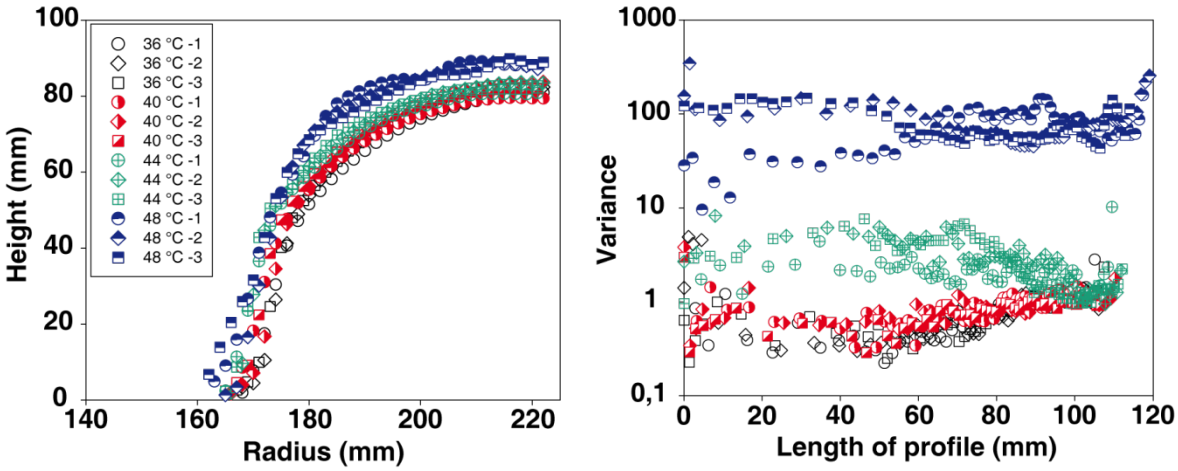

a) Mean position b) Surface fluctuations

Figure 7-7: Surface position of the particle bed with respect to the temperature for batch **L**.

The numerous measurements made during these experiments indicate that the coating layer thickness has an impact on the existence of FS-III. For the batch **H**, FS-III occurred within a temperature range of 1°C, which prevented its stabilization. Because of that, FS-III was temporarily observed as FS-II transited to the FS-IV behaviour. On the other hand, for batch **L**, the existence of the FS-III behaviour was observed, but the characteristic period was difficult to

estimate precisely as the layer at the top of the toroid was breaking at a varying rate. The cohesive forces, in this case, were outdone by the shear stresses present in the bulk layer, which prevented the creation of a coherent agglomerated structure at the top of the toroid. Contrary to the other two cases, state FS-III for batch **M** presented the periodic behavior depicted in Figure 7-8. The evolution of the top layer can be clearly observed in the insets associated with the profile curves. To ease the interpretation of the surface position profiles presented in this figure, schematics of the bulk (gray particles) and aggregated particle (red particles) layers have been added. When comparing the surface profiles measured at different times, one can see that the toroid returned to its initial shape between 14 and 16 s after the measurements started. In fact, this cycle repeated itself constantly for the temperature considered ($\approx 44^{\circ}$ C).

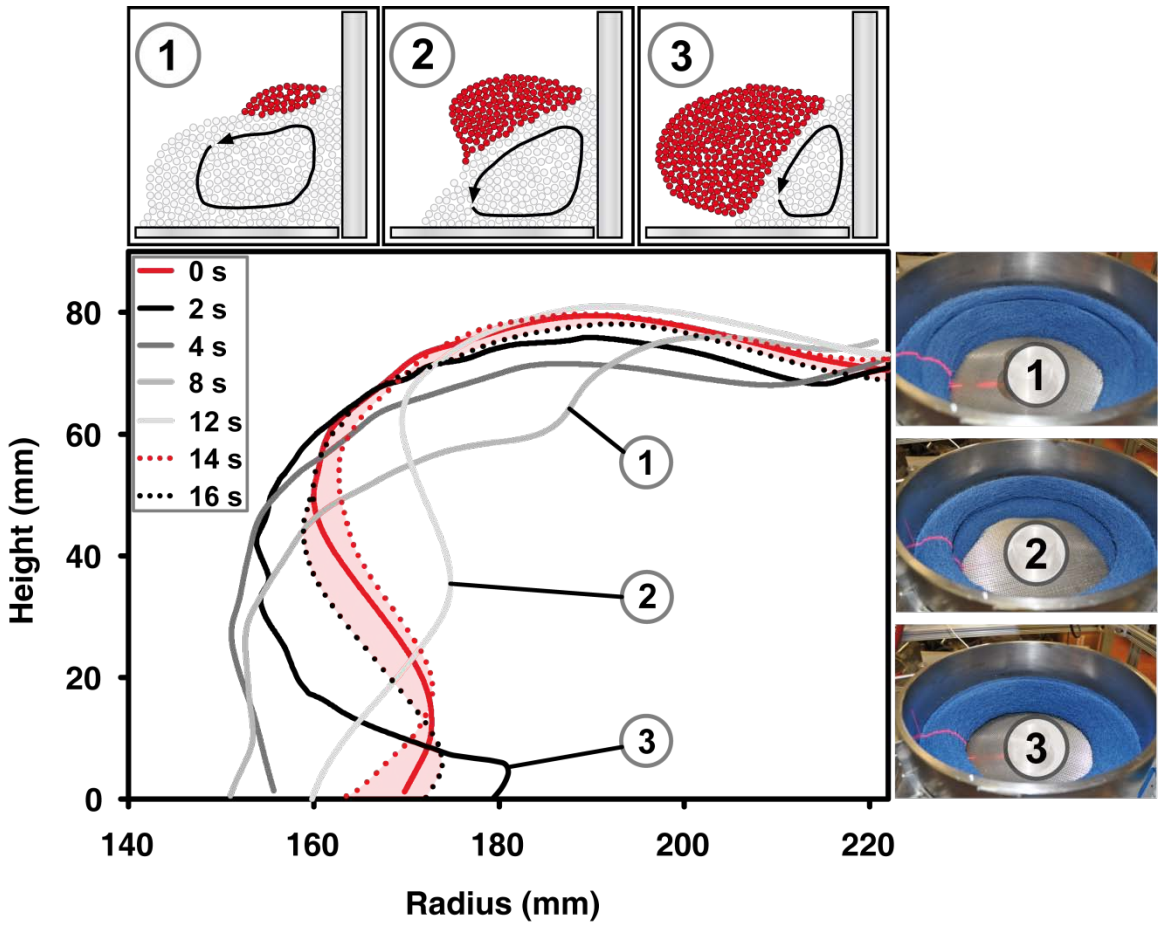

Figure 7-8: Position of the toroid surface with respect to time for batch M. The red profile corresponds to the profile (0 s) taken at the beginning of one cycle. The dotted lines

indicate the profiles measured just before and after the cycle was completed. The enclosed pink area between these two dotted lines indicates that the period of the cycle is around 15 s. One can also noticed the laser beam at the surface of the bed in the three snapshots corresponding to 2s, 8s and 12s.

7.2.4.3 Influence of the toroid flow state on the dynamic density

The volume dilatation of a particle bed or the reduction of its bulk volume can be used to assess its flowability [26-27]. Non-cohesive particles flow freely and give place to a slight expansion of the bed volume through collisional interference that increases the interparticle porosity. On the other hand, when flowing, cohesive particles generate soft agglomerates that roll over each other. As the intrinsic porosity of these agglomerates is larger than the one of a non-cohesive particle bed, the volume expansion thus becomes more important as the interparticle forces increase. With the addition of a polymer coating on the particles, the volume of the particle bed changes depending on the interparticle forces induced, which increase with the temperature [14]. Indeed, it was in that previous paper that the dynamic density decreases with an increase of the temperature. Figure 7-9 shows the variation of the measured dynamic densities (mass of the particle bed divided by the volume of the toroid calculated from the measured surface profile) and the corresponding surface profile variances with respect to temperature, for the three different batches.

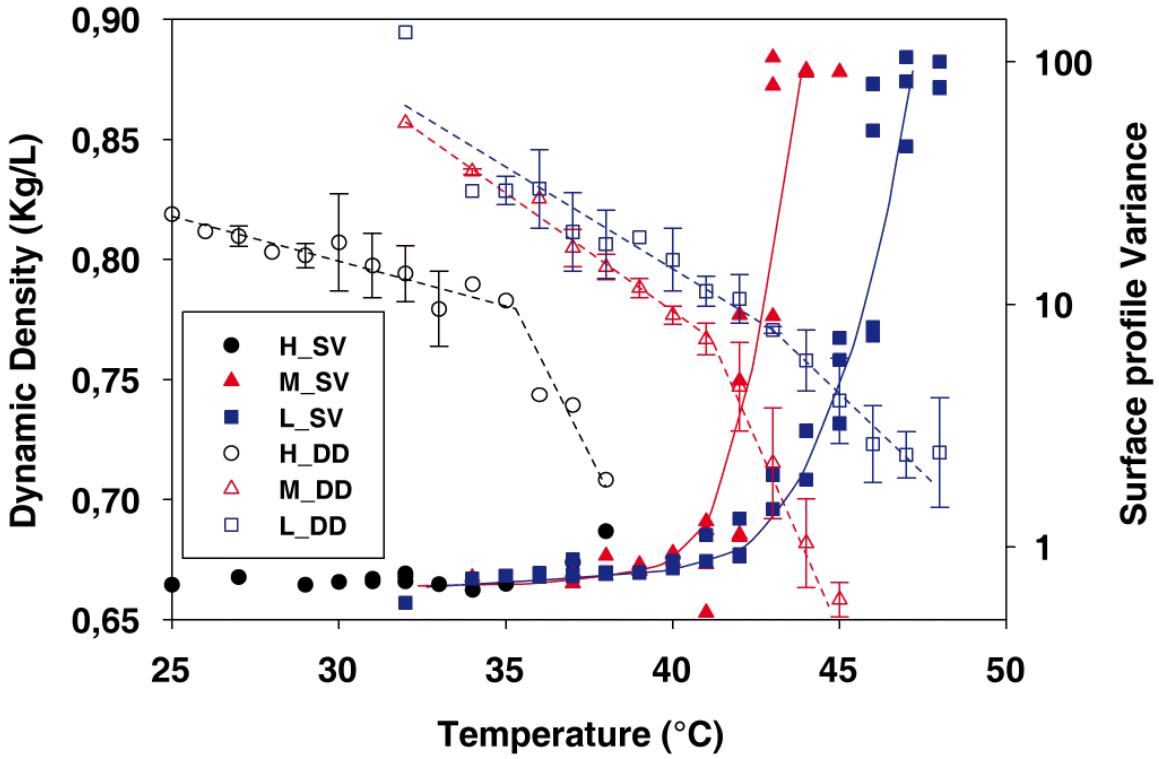

Figure 7-9: Dynamic density (DD) and surface profile variance (SV) with respect to the temperature for the three different batches.

It can be noticed that the variance remained constant when the temperature was increased from laboratory conditions (25°C) until it reached a point where it drastically increased. This threshold temperature corresponds to the appearance of agglomerates at the toroid surface, that is to a change of flow state from FS-I to FS-II. As the coating thickness was reduced, the temperature at which the variance began to increase moved toward a higher value, as explained in Section 7.2.4.2. The dynamic density decreased slowly in a linear fashion with the temperature as long as agglomerates were absent. When the cohesion forces became strong enough to cause the agglomeration of particles, the linear decrease of the dynamic density was accentuated due to a larger expansion of the toroid resulting from the large particle clusters. This is evidenced by the breaking points in the dynamic density and surface variance curves, which occur at similar temperatures.

7.2.4.4 Flow state map and potential use in granulation

The applicability of the polymer coating approach to study cohesive flow in granulators is discussed in this section. Beforehand, the inter-particle forces observed with a change of temperature or coating thickness are compared to other typical forces encountered during granulation using dimensional analysis.

Figure 7-10 displays a flow state map as a function of the dimensionless Bond number (Bo) and the modified Deborah number (De*). The latter number is obtained by dividing the value of De defined in (7-5) by its value at maximum shear rate. Such normalization facilitates the comparison of different temperature/coating cases. It can be noticed from equations (7-1) to (7-4) that Bo and De depend, in particular, on the reptation time , the interparticle adhesion force and the normal collisional velocity . The interparticle cohesion force is related to the adhesive energy, which depends on the contact time . The reptation time is unknown for the PEA/PMMA copolymer and its value was estimated as that of a PEA homopolymer of the same molecular weight, s at K, as proposed in [14]. Because the value for the PEA homopolymer (°C) is smaller than that for the PEA/PMMA copolymer (°C), this estimated value of the reptation time is smaller than the actual one. Using this value as a reference reptation time at 291 K, the reptation time was then calculated by means of the WLF empirical model in (7-1) and values , taken from [28]. The contact time was calculated while taking into account the change with temperature of the elastic modulus of the PEA/PMMA copolymer [25]. Different value of the shear rate from 0.01 s^{-1} to 200 s^{-1} were used to calculate the mean normal collision velocity, which are representative of the values considered in [23, 29]. Finally, it was shown in [14] that the adhesive energy increases linearly from 0,022 J/m^2 at 20°C to 0,09 J/m^2 at 50°C for a PEA/PMMA coating thickness of 120 nm. Therefore, these adhesive energies were scaled proportionally to the thickness of the polymer layer on the particles [30].

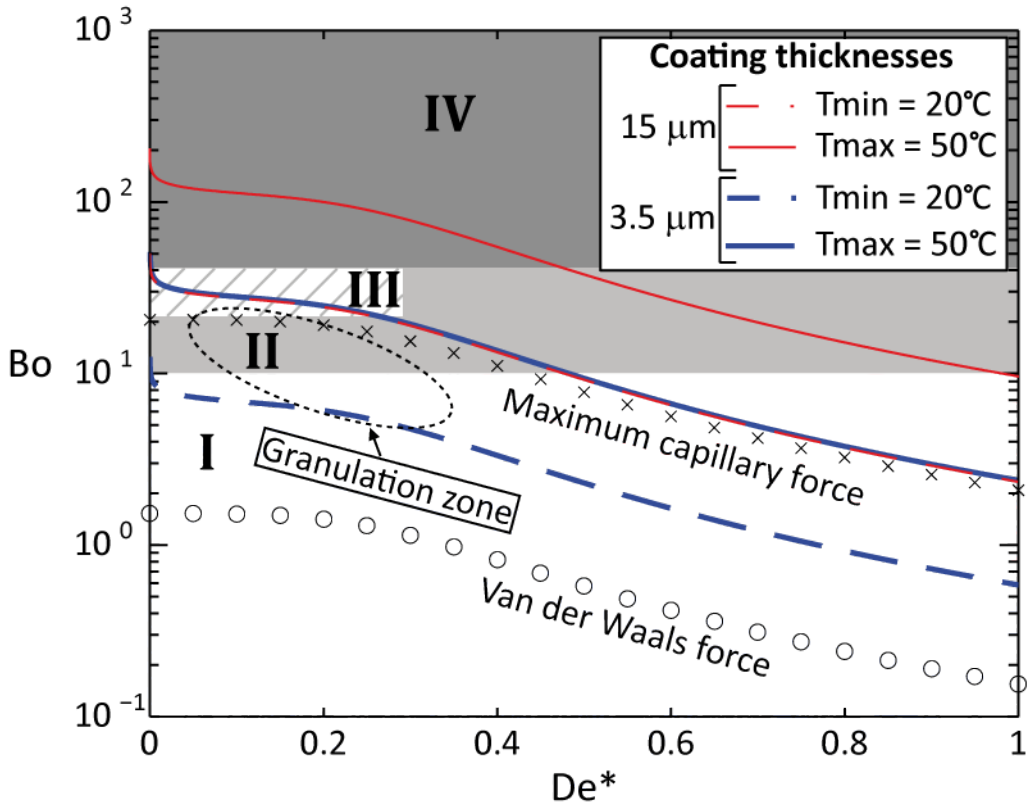

Figure 7-10: Flow state map associated with the cohesion induced by polymer coating in comparison with typical interparticle forces encountered in granulation. The converted maximum capillary (surface tension = 0.073 N/m) and Van der Waals (A_H = 6.5 × 10^{-20} J and h = 4Å) forces have been added for a mean particle size of 1.2 mm. The details concerning the calculation of these forces are presented in [14]. The regions marked by roman numbers expose qualitatively the boundary limits of the flow states (FS). The zone inside the ellipse represents the expected flow conditions during wet granulation.

For the spheronizer, the highest shear rate within the toroid is found near the rotating disc (highest De* value) and the lowest near the surface in the vicinity of the wall (lowest De* value) [23]. Each curve presented in Figure 7-10 was obtained by varying the shear rate and can then be seen as the profile of cohesion in the particle bed from the surface of the toroid toward the a position near of the spheronizer disc as De* increases. Flow state regions have been added to the graph on the basis of the results presented earlier for varying temperatures and coating

thicknesses. Note that the concept of flow state is a local one as it may and often does change from the surface of the toroid to the vicinity of the spheronizer disc. For example, the top-most curve, corresponding to a 15 m coating thickness and a temperature of 50°C, shows that, under these conditions, the surface of the toroid is in flow state FS-IV, its core region in flow state FS-II and its bottom, near the disc, in free-flowing agglomerate-free flow state FS-I. It is true, however, that these flow states were defined from observations at the surface of the bed. FS-I was observed to extend to Bo values around 10 with the absence of agglomerates in this range, which complies with the findings of McCarthy et al. [31] as regards weakly cohesive particle flow. Values of Bo between 10 and 40 led to strongly cohesive flow behavior and are represented by FS-II, which is in agreement with the work of Khinast et al. [5]. FS-III is a difficult state to position within the graph because it is characterized by two particle layers that present different shear rate intensities along with a periodic behaviour. Another difficulty comes from the fact that this state was not observed in the case of batch **L** and it did not exist for a long enough period of time for batch **H**. FS-III requires that the shear rate and the adhesion force at the surface in the vicinity of the spheronizer wall are sufficiently low to sustain a secondary layer. The FS-III zone in Figure 7-10 was set accordingly and shows that the two curves corresponding to (15 m, 20°C) and (3,5 m, 50°C) represent cases where FS-III was observed. Finally, FS-IV was placed in the graph for Bond numbers higher than 40, which corresponds to the experimental observations for batches **M** and **H**.

In order to compare the Bond number of the polymer coating layers to the forces encountered in granulation systems, two common interparticle forces found in such processes, let alone the capillary and van der Waals forces, have been added to Figure 7-10. As a general indication, a dashed ellipse representing the common operation zone of granulators and covering three flow states has also been added to the graph. As can be seen, the capillary force curve lies between Bond numbers 2 and 20. As expected, the van der Waals forces, do not have a significant impact for the mean particle size considered (1.2mm) in this work, as the related curve lies in a region where $Bo < 1$.

The use of the polymer coating approach allowed modifying significantly the flow behavior in the spheronizer as described by the different flowing states and the dynamic density values representing the bulk cohesivity of the particle bed. Because the method can be used without affecting the particle size distribution, its employment in a spheronizer that mimics particle flow in granulation equipment sheds light on the impact of cohesion on the progression of more complex granulation processes.

In Figure 7-10, the wet granulation zone indicates that the flow state FS-II should be observed under efficient operating conditions. In FS-II, the particles are mixed homogeneously during the operation and the interparticle forces are strong enough to promote their agglomeration. These two operational characteristics are not found for the other flow states. The interparticle forces are too weak in FS-I and do not promote the particle agglomeration. Moreover, the flow pattern is divided into two different zones in FS-III and the particles do not mix at all in FS-IV.

The granulation zone is bounded above by a Bond number close to the maximum capillary force curve where the particle bed becomes binder saturated. If this limit is surpassed, it means that the maximum capillary force is reached, which can potentially cause the flow state to migrate from FS-II to FS-III and lead to a fast and difficult to control particle growth. The granulation zone is bounded below by a Bond number associated with small interparticle forces that are too weak to promote particle agglomeration found in FS-II. In a granulation process, such a phenomenon is observed when the binder content is too low. The granulation zone is also limited by Deborah number values which can be directly linked to the intensity of shear rate provided by an agitator or a rotating disc, for example. The minimum Deborah number corresponds to a low shear rate (slow agitator or disc speed) and relatively poor particle mixing, which is typical of the FS-III behavior. The maximum Deborah number corresponds to high shear rate (high agitator or disc speed), which favors particle breakage and prevents particle agglomeration. Note that the granulation zone presented here is a general indication of where the process should be operated in order to obtain a homogeneous product with optimal performance. The binder content that affects the interparticle forces, and the speed of the agitator should be set to obtain the FS-II behavior.

On the other hand, their exact values should be determined according to the desired product properties, which also depend on the evolution of the particle flow during the whole operation.

Recently, the flow behavior in a high shear granulation process was evaluated in 3D with a non-intrusive PEPT method [9]. The results revealed the existence of different regions with characteristic flow patterns that change over time. In order to accumulate enough data to represent these flow patterns, a 35-minutes granulation run was divided into 7 smaller time periods. It resulted in a characterization of the particle flow during a period of 5 min and led to a rough estimation of the velocity profile and the residence time of the PEPT tracer within the particle bed. A longer data acquisition time could be considered to refine the information obtained so far, but this assumes that the flow patterns remain stable during the measurement. The use of polymer coating offers the possibility to control the interparticle forces without affecting the particle size distribution. It means that specific flow patterns representative of those in a granulation system at a specific time could be reproduced and characterized easily with this method.

7.2.5 Conclusion

This work used inert particles coated with a layer of a PEA/PMMA copolymer to investigate how temperature-dependent interparticle forces affect the flow behavior in a spheronizer. Four different flow states were observed depending on the temperature of the particle bed. The first state is associated with free-flowing behavior of the particles and was observed near the ambient laboratory conditions. The second state is characterized by agglomerates appearing at the surface of the particle bed, the size of which increases as the temperature is incremented. The third flow state concerns the formation of a secondary layer of agglomerated particles whose volume changes in a periodic fashion with time. The fourth state is characterized by a solid-like motion as the particles are completely agglomerated. A flow map presenting the flowing states was derived to show the potential use of the polymer coating approach for mimicking the flow behavior in granulation processes. A more elaborate characterization of the forces between PEA/PMMA

copolymer layers will be done in a near future so as to gain more insight into the interdiffusion rate and the increase of adhesive energy with respect to temperature and contact time. These measurements will help refine the model parameters used in this work and thus improve the predictability of the phenomena observed. These measurements will also help develop a cohesive force model for the discrete element simulation of the particle flow dynamics in the spheronizer considered in this work or other related granulation processes.

7.2.6 Acknowledgements

The financial support of the Natural Science and Engineering Research Council of Canada (NSERC), Merck Frosst of Canada and Ratiopharm is gratefully acknowledged. We would like to thank the support of Mr. David Dube for the development of the acquisition program used with the laser profiler.

7.2.7 References

[1] Lekhal, A., Conway, S.L., Glasser, B.J., and Khinast, J.G., *Characterization of granular flow of wet solids in a bladed mixer.* AIChE Journal, 2006. **52**(8): p. 2757-2766.

[2] Li, H.M. and J.J. McCarthy, *Cohesive particle mixing and segregation under shear.* Powder Technology, 2006. **164**(1): p. 58-64.

[3] Faqih, A., Chaudhuri, B., Muzzio, F.J., Tomassone, M.S., Alexander, A., and Hammond, S., *Flow-induced dilation of cohesive granular materials.* AIChE Journal, 2006. **52**(12): p. 4124-4132.

[4] Chaudhuri, B., Mehrotra, A., Muzzio, F.J., and Tomassone, M.S., *Cohesive effects in powder mixing in a tumbling blender.* Powder Technology, 2006. **165**(2): p. 105-114.

[5] Khinast, J.G., Radl, S., Kalvoda, E., and Glasser, B.J., *Mixing characteristics of wet granular matter in a bladed mixer.* Powder Technology, 2010. **200**(3): p. 171-189.

[6] Iveson, S.M., *Limitations of one-dimensional population balance models of wet granulation processes.* Powder Technology, 2002. **124**(3): p. 219-229.

[7] Fan, X.F., Yang, Z.F., Parker, D.J., Ng, B., Ding, Y.L., and Ghadiri, M., *Impact of surface tension and viscosity on solids motion in a conical high shear mixer granulator.* AIChE journal, 2009. **55**(12): p. 3088-3098.

[8] Forrest, S., Bridgwater, J., Mort, P.R., Litster, J., and Parker, D.J., *Flow patterns in granulating systems.* Powder Technology, 2003. **130**(1-3): p. 91-96.

[9] Saito, Y., Fan, X.F., Ingram, A., and Seville, J.P.K., *A new approach to high-shear mixer granulation using positron emission particle tracking.* Chemical Engineering Science, 2011. **66**(4): p. 563-569.

[10] Wang, F.Y. and Cameron, I.T., *Review and future directions in the modelling and control of continuous drum granulation.* Powder Technology, 2002. **124**(3): p. 238-253.

[11] Perry, R.H. and Green, D.W. *Perry's chemical engineers' handbook.* 2008; Available from: http://site.ebrary.com/id/10211725.

[12] Litster, J.D., Hapgood, K.P., Michaels, J.N., Sims, A., Roberts, M., and Kameneni, S.K., *Scale-up of mixer granulators for effective liquid distribution.* Powder Technology, 2002. **124**(3): p. 272-280.

[13] Rudolph, V., Rasul, M.G., and Carsky, M., *Segregation potential in binary gas fluidized beds.* Powder Technology, 1999. **103**(2): p. 175-181.

[14] Bouffard, J., Bertrand, F., Chaouki, J., and Giasson, S., *Control of particle cohesion with a polymer coating and temperature adjustments.* submitted to AIChE journal, 2011.

[15] Schach, R. and Creton, C., *Adhesion at interfaces between highly entangled polymer melts.* Journal of Rheology, 2008. **52**(3): p. 749-767.

[16] Timoshenko, S. and Goodier, J.N., *Théorie de l'élasticité.* 1961, Paris: C.Béranger.

[17] Zhang, D.Z. and Rauenzahn, R.M., *Stress relaxation in dense and slow granular flows.* Journal of Rheology, 2000. **44**(5): p. 1019-1041.

[18] Chau, K.W. and Swei, G.S., *Contact time and interfacial fracture energy of tacky polymers.* Journal of Polymer Science Part B-Polymer Physics, 2004. **42**(16): p. 3013-3025.

[19] Barthel, E., *Adhesive elastic contacts: JKR and more.* Journal of Physics D-Applied Physics, 2008. **41**(16).

[20] Brilliantov, N.V., Albers, N., Spahn, F., and Poschel, T., *Collision dynamics of granular particles with adhesion.* Physical Review E, 2007. **76**(5).

[21] Liechti, K.M., Xu, D.W., and Ravi-Chandar, K., *On the modified Tabor parameter for the JKR-DMT transition in the presence of a liquid meniscus.* Journal of Colloid and Interface Science, 2007. **315**(2): p. 772-785.

[22] Pingali, K.C., Shinbrot, T., Hammond, S.V., and Muzzio, F.J., *An observed correlation between flow and electrical properties of pharmaceutical blends.* Powder Technology, 2009. **192**(2): p. 157-165.

[23] Bouffard, J., Bertrand, F., Chaouki, J., and Dumont, H., *Discrete Element Investigation of Flow Patterns and Segregation in a Spheronizer.* submitted to Computers and Chemical Engineering, 2011.

[24] Sinha, S.K. and Briscoe, B.J., *Polymer tribology*. 2009, London: Imperial College Press. xxvi, 697 p.

[25] Lafferty, S.V., Newton, J.M., and Podczeck, F., *Kinetic examination of the mechanical transition of polymethyl methacrylate films prepared from aqueous dispersions.* International Journal of Pharmaceutics, 2002. **239**(1-2): p. 179-183.

[26] Abdullah, E.C. and Geldart, D., *The use of bulk density measurements as flowability indicators.* Powder Technology, 1999. **102**(2): p. 151-165.

[27] Zhu, H.P., Zhou, Z.Y., Yang, R.Y., and Yu, A.B., *Discrete particle simulation of particulate systems: Theoretical developments.* Chemical Engineering Science, 2007. **62**(13): p. 3378-3396.

[28] Andreozzi, L., Castelvetro, V., Faetti, M., Giordano, M., and Zulli, F., *Rheological and thermal properties of narrow distribution poly(ethyl acrylate)s.* Macromolecules, 2006. **39**(5): p. 1880-1889.

[29] Corwin, E.I., *Granular flow in a rapidly rotated system with fixed walls.* Physical Review E, 2008. **77**(3).

[30] Luengo, G., Pan, J., Heuberger, M., and Israelachvili, J.N., *Temperature and Time Effects on the "Adhesion Dynamics" of Poly(butyl methacrylate) (PBMA) Surfaces.* Langmuir, 1998. **14**(14): p. 3873-3881.

[31] McCarthy, J.J., Nase, S.T., Vargas, W.L., and Abatan, A.A., *Discrete characterization tools for cohesive granular material.* Powder Technology, 2001. **116**(2-3): p. 214-223.

CHAPITRE 8 SIMULATION À L'AIDE D'UN MODÈLE MULTI-ÉCHELLE D'UN PROCÉDÉ DE GRANULATION UTILISANT UN ÉQUIPEMENT AVEC ROTOR

8.1 Présentation du quatrième article

Soumettre à *Chemical Engineering Science* Décembre 2011

Auteurs: Jonathan Bouffard, François Bertrand et Jamal Chaouki

Cet article présente un modèle multi-échelle permettant de résoudre des bilans de population par une approche de Monte-Carlo commandée par événement. Celui-ci permet de modéliser des expériences de pellétisation avec un granulateur à rotor (sphéroniseur modifié) en considérant le déplacement particulaire à travers trois zones importantes du lit de particules à l'aide d'une approche compartimentée. Chacune des zones du lit est associée à un mécanisme de granulation, soit le mouillage, la coalescence ou le bris des granules. Le mouvement des granules a été inclus dans le bilan de population au moyen d'une chaine de Markov à temps continu, construite à partir des résultats de simulations obtenus avec la DEM et discutés dans le premier article.

Le modèle multi-échelle est comparé à un bilan de population conventionnel qui ne tient pas compte du mouvement des granules. Une fois les paramètres des simulations ajustés de telle manière à simuler les expériences de granulation, on voit que le modèle multi-échelle permet de mieux représenter l'évolution de la distribution de taille des particules dans le temps. Par contre, ceci n'est vrai que lorsque le débit de liant liquide est inférieur à 30 g/min. Lorsque le débit atteint ce seuil, les deux modèles de bilan de population prédisent des résultats similaires. Une explication possible permettant d'expliquer ce phénomène est que le taux de croissance est peut-être trop élevé pour discerner l'impact des paramètres d'écoulement dans ce cas.

8.2 A multiscale model for the simulation of granulation in rotor-based equipment

8.2.1 Abstract

Granulation processes can be modeled with the help of population balance models. Numerous studies considered mechanisms such as the coalescence or breakage to predict the evolution of granulation with respect to time. Although these mechanisms play a fundamental role in representing the real behavior of such systems, it has become apparent that the flow pattern of the particles also needs to be modeled. This work investigates granulation with a rotor processor by means of a multiscale model involving a population balance model at the process scale, a compartmental approach that takes into account specific flow behaviors in different zones of the equipment, and a discrete element based model at the particle scale. The population balance model is based on an event-driven Monte-Carlo algorithm and a time-continuous markov chain to reproduce the particle motion in each compartment. The markov chain properties are obtained from a discrete element simulation of the particle flow dynamics in the whole domain. The results show that the proposed approach improves the accuracy of the population balance model when the particle flow is considered.

8.2.2 Introduction

Until recently, granulation processes were modeled based on the perfectly mixed assumption. This hypothesis was not considered only to simplify the granulation models but also to support the generally admitted idea that the presence of interparticle forces help to mix the particles during the process. With the availability of more and more powerful computers, the difficulty to include inhomogeneous flow patterns in simulations has been significantly reduced. Moreover, since the last decade, several studies have revealed that, even with the presence of interparticle

forces, the state of particle mixedness is not perfect and in some cases, it can in fact enhance the segregation compared to the behavior of non-cohesive systems [1-2]. On the other hand, the cohesive forces involved during granulation also have a significant impact on the flow patterns of the particles [3-4]. The modifications induced can affect the preferential path followed by the particles through different zones of the granulator where breakage, coalescence or spraying of the binder has different predominances. Several authors have revealed the importance of considering the flow behavior of the particles and its impact on wet granulation processes, such as in high shear mixers, fluid bed granulators or other type of granulators [5-8]. The particle flow pattern prevailing in this equipment can be challenging to assess as it evolves with the change of particle properties (e.g., size distribution, shape), but also from the increase of capillary forces with respect to operation time. These difficulties explain the limited number of experimental research and process modeling investigations concerning this subject, which actually can be considered in its nascent stage [9].

8.2.2.1 Granulation mechanisms

Three principal mechanisms are generally present during granulation: the wetting/nucleation, the growth and the breakage of the aggregates [10-11], as presented in Figure 8-1. Nucleation occurs in the initial stage of granulation and involves the formation of the initial agglomerates from the interaction of binder droplets and dry powder [4, 12]. Following the nucleation step, the growth of the nuclei can occur by layering, which is the uptake of fine particles onto larger agglomerates [13], or by coalescence, which is associated with the successful collision between two particles resulting into their fusion [14]. Breakage is the least well understood of all the granulation mechanisms, as it can happen following different paths, such as attrition, which removes a portion of the material at the surface of particles, which results in the creation of finer material. It can also occur following the fragmentation of a whole particle in multiple daughter particles, whose number and size are difficult to predict, because they depend on the particle properties, but the past events encountered by the breaking particle [10].

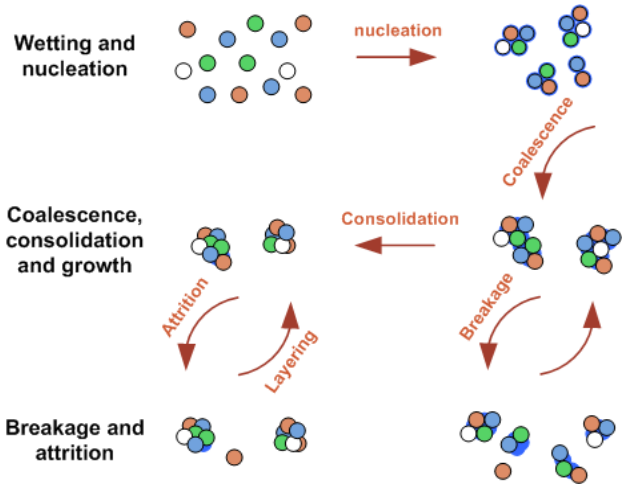

Figure 8-1: Granulation mechanisms.

8.2.2.2 Modeling approaches

Different modeling approaches have been developed to represent granulation processes, which go from empirical models fitting an arbitrary function to granulation results, to mechanistic models that incorporate more fundamental physics and chemistry to explain the behaviour observed [15]. The empirical approaches are often limited to a specific application and can hardly be extended toward other granulation processes. On the other hand, although the mechanistic models also require some data fitting, it is more physical by nature and its application can lead to a real and better understanding of the process investigated. These mechanistic models, which are theoretically or empirically based [11, 16-17] are reviewed in detail in [10-11, 15]. They are easily integrated into population balance equations (PBE), which can be numerically solved in order to predict the particle properties over the course of a simulation. The population balance can include multiple granulation mechanisms, as shown in the following general equation [11, 18]:

(8-1)

Table 8-1 gives the definition of each variable used in equation (8-1). Note that the simulation domain can consider the whole particle system or only a part of it, which means that the system can be divided into several zones that exchange particles. Analytical solutions of equation (8-1) are very difficult to obtain and this equation must generally be solved numerically. When only the particle size is considered, the solution leads to a one-dimensional population balance that can be used to predict the granulation evolution with respect to time. Although the one-dimensional model is simple to use, it may fail to represent adequately the real granulation behaviour since other parameters may affect the evolution of the particle size distribution (PSD), such as the particle porosity or the moisture content [5]. In such a case, the inclusion of supplementary parameters becomes necessary, which can be done using a multi-dimensional population balance.

Table 8-1: Variables used in the population balance equation (8-1)

Variables	Units	Comments
	[m^3]	Volume of the particle
	[m^3]	Volume of the nucleus generated
	[s]	Time
	[m^{-6}]	Size distribution of the particles such that (m^{-3}) is the number concentration of the particles in the size range to at time
	[$m^3 \cdot s^{-1}$]	Agglomeration kernel for particles of size and size at time
	[-]	Probability of producing a daughter particle of size from a parent particle of volume
	[m^{-3}]	Number of particles resulting from the breakage of particles of volume
	[s^{-1}]	Breakage kernel
	[m^{-6} s^{-1}]	Nucleation kernel
	[-]	New particle of volume generated by nucleation
	[s^{-1}]	Rate of particle inflow
	[s^{-1}]	Rate of particle outflow

Multi-dimensional population balances, which consider other properties, such as the moisture content, simultaneously with the particle size are almost impossible to solve analytically. This is why there is no other choice than solving the integro-differential equations numerically, which can be done by different approaches. The most popular class of numerical methods is based on the use of Euler coordinates and consists of solving the PBEs directly. It comprises the method of moments and the discrete family methods [18-20]. The Eulerian methods have been used for 2-D and 3-D population balances and are known to be complex to implement. Also these methods have difficulty to preserve the structure of the particle distribution represented by the higher moments [21]. The second class of methods adapts itself directly to the discrete nature of the population balance model (PBM) using Monte-Carlo (MC) schemes to solve the underlying equations [15, 20]. The MC methods can be classified depending on how they manage the time increments during the simulation, which can be time-driven or event-driven. The MC methods are also classified according to whether the number of particles is kept constant or not [22]. MC methods can keep track of the information concerning the history of the particles over the course of a simulation. This means that it is possible to track not only the main moments representing the PSD but also the fluctuations associated with the particle properties. The several advantages of the MC methods explain the fact that they are often recommended to solve multi-dimensional population balances even if the computational time is generally larger than that with the Eulerian methods [23-25].

Depending on the conditions prevailing in a granulator, the intensity of the different granulation mechanisms can vary between specific zones of the equipment [26-30]. The particle flow pattern during the granulator operation and the visit frequency of these zones have an effect on the evolution of the particle properties. The particle flow can be accounted for in a simulation by a compartmental model, which can be implemented in the PBM. Each compartment or zone, which is considered as perfectly mixed, can be associated with one or more specific granulation mechanisms. The exchange of particle between the zones can be defined through experimental observations or numerically with the use of CFD. For instance, a CFD-PBM approach was used in the case of diluted particles/droplets dispersed into a fluid [31-32]. The discrete element method (DEM) can also be combined with the PBM when a dense flow of particles is considered [26-27]. In the case of granulation processes involving high-shear mixers or rotor-based

equipment, the DEM-PBM approach is the most appropriate choice. Freireich et al. used this technique for large particles blended in a dual-axis mixer in the context of coating applications [26]. The domain was separated into two compartments to represent the spray zone and the rest of the particle bed. Only layering granulation and particle coating were investigated and no particle coalescence or breakage mechanisms were taken into account.

The objective of this work consists of developing a multiscale granulation model that brings into play a population balance model at the process scale, a compartmental approach to take into account specific flow behaviors in different zones of the equipment, and previously [33] discrete element results of the particle scale. To do so, the general algorithm of the event-driven Monte-Carlo (EDMC) based PBM is used and fully described. The different granulation mechanisms and the way they are considered in the PBM are discussed. Next, the compartmental model, which relies on a continuous-time Markov process built from DEM results, is introduced. The accuracy of the PBM alone, without the compartmental model, is then studied using an analytical test case, followed by the assessment of the full multiscale model. In the latter, mass conservation in the different zones of the computational domain is considered. Finally, the multiscale model is applied to the simulation of granulation and the results obtained are compared to experimental data.

8.2.3 Particle motion within bed zones

Figure 8-2 presents a schematic of the granulator, which is a modified spheronizer fully described in [33]. This rotor processor consists of a bowl at the bottom of which a disk is rotating. Rotation shapes the particle bed into a torus on which water droplets coming from an atomizer are sprayed at its surface. The cut-away view of Figure 8-2 shows the three zones that are used in the compartment-based multiscale model developed in this work. More details about the characteristics of this equipment are given in section 8.2.7.2. Note that DEM simulations were used in order to delimitate these three zones and obtain the particle flow patterns inside the granulator.

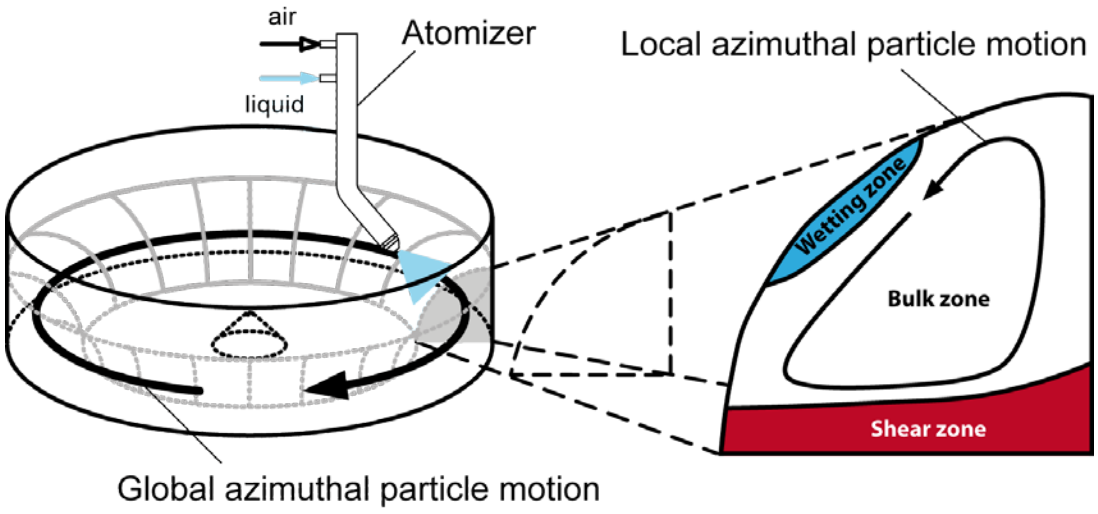

Figure 8-2: Particle motion in the spheronizer with the three zones of the torus considered for the PBM.

8.2.3.1 DEM simulation data for the rotor-processor

The DEM is a method that simulates particle motion and explicitly takes into account the collisions occurring between neighbouring particles or other solid objects like the walls of the computational domain. The particles are allowed to interpenetrate and the amount of overlap depends on a contact force model, such as the one described below and used in this work. The method calculates the motion of each particle by integrating numerically Newton's second law of motion that brings into play the forces acting on it:

(8-2)

(8-3)

where , , , , and are the mass, radius, moment of inertia, position, angular velocity and rolling resistance torque of particle *i*, and where represents gravity. At each time step, the method gives the current position of each particle as well as its velocity. In this work, the collisions between two particles or a particle and a rigid surface are considered as inelastic and are modeled by means of a spring-dashpot type model with normal and tangential contributions.

and represent the normal and tangential components of the total force exerted by all particles *j* in the vicinity of particle *i*. This model, which is fully described in [34], is based on the work of Cundall and Strack [35] and Zhou et al. [36]. Note that other hydrodynamic (e.g., drag) or non-hydrodynamic (e.g., colloidal) forces could be added to the force balance in (8-2) and (8-3). Equations (8-2) and (8-3) were integrated using the half-step leapfrog verlet scheme. A parallel version of this DEM-based model relying on an efficient domain decomposition technique was used to reduce the computational cost of the method. To ensure that the simulations proceed without numerical instabilities, a time step of s was used for all cases.

In [33], the simulation of the particle motion in the spheronizer considered in the current work was calculated for a bi-disperse particle size distribution comprising particles of 2 and 4 mm. The particle physical parameters, let alone the Young's modulus and the friction factor, were adjusted in order to mimic the flow behaviour observed for a real experiment by Corwin [37]. Even if the material used was glass beads, which are different from what was used for real granulation, the flow pattern obtained can nevertheless be used to estimate realistically the flow behaviour in the spheronizer instead of considering it as perfectly mixed. Since the objective is to use these data in order to evaluate the particle flow rate from one compartment to another one and that we are not interested here in parameters such as the collisional rate, which depends strongly on the material properties, that approach was considered appropriate.

The DEM simulations considered dry particles and did not take into account the effect of interparticle forces, which can induce a reduction of the local azimuthal speed of the particle bed (see Figure 8-2). Muguruma et al. showed that an increase of the moisture content from a dry case to a saturation ratio of 0.125, which is lower than the value for granulation [13], led to a reduction of the local azimuthal speed by approximately a factor of two [38]. An appropriate selection of the disc rotational rate used in a DEM simulation can mimicked the reduction that would be expected with the increase of moisture content. For example, it can be seen in Figure 8-3 that a DEM simulation with a disk speed of 35 rad/s leads to a 50% decrease of the local azimuthal rotational rate obtained at 100 rad/s.

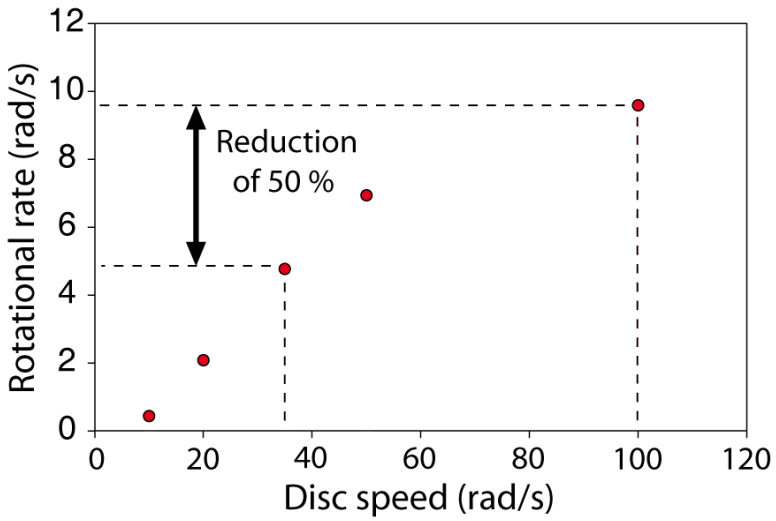

Figure 8-3: Local azimuthal rotational rate from the DEM simulations [33]. The dotted lines have been added to show the reduction of this rate with a decrease of the spheronizer disc speed.

As shown in Figure 8-2, three zones in torus were delimited with the help of DEM simulation results. A first zone near the rotating disk is characterized by high shear rates. For a rotational disc varying between 20 and 100 rad/s, the height of this high shear zone extends to 0.02 m from the equipment disc, corresponding to ten particle diameters (2 mm) [33]. A wetting zone is located at the surface of the torus in the vicinity of the atomizer, which is used to spray the binder liquid. This zone consists of a particle bed surface of 0.03 m in diameter, which is exposed to the

atomizer spray, with a penetration depth corresponding to the diameter of four particles. The remaining of the particle bed is the bulk zone.

8.2.4 General algorithm for the event-driven Monte-Carlo based PBM

As indicated earlier, different Monte-Carlo methods can be used to solve population balance equations. The present work is based on the event-driven differentially PSD-weighted Monte-Carlo based PBM (EDMC) presented by Haibo et al. [22], which has been used for different purposes in other works [39-40]. The main steps of this method, which are regrouped into an algorithm in Figure 8-4, are now discussed in detail..

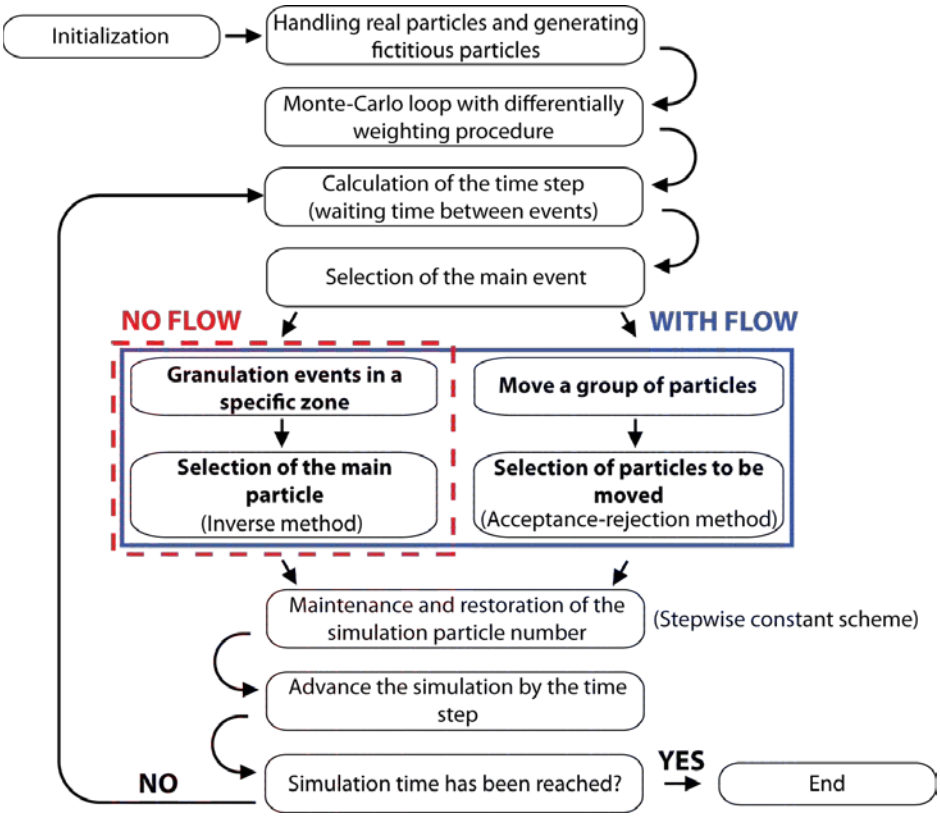

Figure 8-4: Event-driven Monte-Carlo based PBM procedures.

8.2.4.1 Initialization and weighting procedure

The first two steps in Figure 8-4 consists of generating fictitious particles for the EDMC based PBM simulations, the size distribution of which is differentially weighted according to the initial size distribution of the real particles. Each fictitious particle i is associated to a weight representing a fraction of the real number of particles with the same size and moisture content. While the number of fictitious particles remain constant during the simulation, the total number of real particles, represented by , is the one that fluctuates as a function of the granulation events. The flow of simulation droplets coming from the atomizer is also represented by a similar weighting procedure. To do so, the spray volumetric rate is distributed among a fictitious number of droplets according to their size distribution. Further details about the procedure to generate the simulation particle and droplet size distributions are given in [22]. Once the PSD and the droplet size distribution (DSD) have been generated, the next step consists of calculating the time step according to granulation events. For the EDMC based PBM, the event rates for wetting, agglomeration, and breakage must be first calculated to determine the time step between two consecutive events and to select events and the particles affected by them.

8.2.4.2 Granulation event rates

Each zone in Figure 8-2 is associated with a granulation mechanism following along the lines of Litster [41] for similar equipment. The wetting of particles occurs in the vicinity of the bed surface where the atomizer is located, while the coalescence and breakage mechanisms occur in the bulk of the bed and the shear zone located near the rotating disc, respectively. To incorporate these granulation mechanisms into the EDMC based PBM, their rate of occurrence has to be defined. Table 8-2 presents the granulation mechanisms considered for each particle bed zone along with the equations used to calculate their rate of occurrence during the simulations.

Table 8-2: Event rate equations for the granulation mechanism (G.M.) in each particle bed zone.

Zones	G M	Event rate equations [m^{-3} s^{-1}]	Specific parameters
Shear (1)	Breakage	—	: Kroenecker delta for particle located in zone number compared to zone 1 [s^{-1}]: Breakage constant [m^3] : volume of the smallest particle achievable following particle breakage [m^3]: Shear zone volume
Wetting (2)	Wetting	———————	: Kroenecker delta for particle located in zone number compared to zone 2 [kg m^{-3}] : Water density [kg] : Dry particle bed mass [s^{-1}]: Rate of change of the number of droplets [m^3]: Wetting zone volume
Bulk (3)	Agglomeration	— — — ———————	[m^2s^{-1}]: Agglomeration kernel for particles and : Kroenecker delta for particle located in zone number compared to zone 3 [m^3]: Bulk zone volume
Common parameters		: Number of fictitious particles; [m^3] : Volume of particle ; : PSD weight associated with particle	

A few comments are in order. In the wetting rate expression the spray rate is not taken into account directly but through weighting factor associated to each fictitious droplet as described in Section 8.2.4.1.

The choice of an agglomeration kernel depends on the particle properties, equipment type, operation parameters and the mechanism of granulation [14]. The following expression describes the EKE kernel and shows how it is affected by the moisture saturation [42-43]:

(8-4)

where is the kernel constant ($m^{1.5}.s^{-1}$), is the liquid binder saturation ratio and is the critical liquid binder saturation ratio. The EKE kernel which is used in this work, has been tested in the case of granulation in a high shear mixer and other high shear equipment [44]. The addition of a constraint relative to the moisture content takes into account the two-step dynamics normally encountered in granulation, which comes from the fact that a critical liquid saturation must be met before particle agglomeration starts.

The breakage mechanism is not at the same stage of development as the agglomeration mechanism. The breakage kernel and the related distribution functions are for the most part semi-empirical as the granulation mechanism is not well understood. In order to account for breakage in the present work, a simple relation has been considered, which creates two daughter particles once a parent particle is broken [22]. When a breakage event occurs, the particle daughters are chosen following a uniform PSD extending from to [45]. In this work, the smallest particle size is taken as the D10 value of the initial particle size distribution. It gives a good estimate of the size of the particles in the left-hand tail on the PSD in the real system.

Finally, note that parameters and in equation (8-4) and the breakage constant in Table 8-2 are unknown parameters that have to be adjusted in order to obtain a simulated PSD that represents as closely as possible the experimental results. We will come back to this and to the calibration of the whole model in subsequent sections.

8.2.4.3 Time step calculation

Once the rates of the different granulation mechanisms have been obtained, the next step in the algorithm of Figure 8-4 is the calculation of the time step. An important advantage of the event-driven MC approach is the simplicity of the time increment calculations. The time step is simply calculated with the following expression:

(8-5)

where is the time step at iteration k, and (s-1.m-3) are the compartment volume and the event rate associated to the zone number (as indicated in Table 8-2) at iteration . The selection of the event occurring for a given time step is based on the probabilities of occurrence of the granulation mechanisms relative to the other:

(8-6)

where is the probability of occurrence of event and is the rate at which the corresponding granulation mechanism occurs.

8.2.4.4 Selection of the main event

The main event at each time step is selected from the probabilities of occurrence of the possible events (agglomeration: , breakage: and wetting:). A random number ( ), generated from a uniform distribution in the interval [0,1], is used for this purpose such that means that agglomeration is selected, means that breakage is selected and means that a wetting event occurs.

Once the main event is selected, the main fictitious particle has to be chosen from all the simulated particles with the help of the same random number and the so-called inverse method proposed by Zhao et al. [18]. For the wetting event, the particle is chosen such that the following expression, derived from the wetting rate equation in Table 8-2, is satisfied:

(8-7)

Note that the droplet involved during the wetting event is chosen by a random selection throughout the DSD. For the agglomeration event, the particle is chosen such that the following expression, derived from the rate equation in Table 8-2, is satisfied:

(8-8)

For this event, a second particle must also be selected. The random number used previously to select the main particle is used again following the procedure suggested by Zhao et al. [18]:

— — (8-9)

For the breakage event, the particle is chosen such that the following expression, derived from the breakage rate equation in Table 8-2, is satisfied:

(8-10)

8.2.4.5 Adjustment of fictitious particle properties

The last step of the EDMC based PBM before the time is advanced consists of adjusting the properties of the fictitious particles, presented in Table 8-3. In this table, the subscript “old” and “new” denote the related quantity before and after the event, respectively. Except for the wetting event, the adjustment of the different granulation properties are detailed in [18] and are briefly described here. For the wetting event, the fictitious particle of volume ( ) and weight ( ) are not modified but the moisture weight ( ) is altered by the addition of fictitious droplets . The moisture weight added to the fictitious particle is divided by the particle weight in order to consider a uniform distribution within the real particle represented. The coalescence event requires the adjustment of the new particle volume or weight depending on the relative importance of the old weight of the two fictitious particles involved. For the breakage event, the first fragment of volume is stored in the position of the parent particle . The other fragment is merged with a particle having the most similar volume ( ). In case of multiple possibilities, the second fragment is merged with a particle randomly selected throughout the possible choices.

Table 8-3: Adjustment of fictitious particle properties for the different granulation events.

Event	Particle volume	Particle weight	Moisture weight
Wetting			
Coalescence			
Coalescence			
Breakage			

While the coalescence and the wetting events do not present any problem to respect the particle mass and moisture balances, this is also the case for the breakage moisture balance but not necessarily for the breakage event particle mass balance. Since the main particle selected in that case resulted in two daughter particles, one of them has to be merged with the most similar existing fictitious particle in order to keep the same total number of simulation particles. That inevitably induces some error relative to the mass conservation except if they are the same size.

After the selection of the event and the adjustment of the properties of the corresponding fictitious particle, the simulation time is incremented by the time step calculated in the first part of the algorithm. Another iteration is performed if the final time has not been reached. The next section presents the development of the particle motion event, which is based on a continuous-time Markov chain constructed from DEM results.

8.2.5 Addition of the particle motion event to the EDMC based PBM

As explained earlier, the motion of the particles throughout the particle domain is taken into account in this work through a compartmental model. This means that it is not necessary to know the exact particle coordinates, but only in which compartment they are. The particle flow is ruled by a residence time function associated with each compartment and the particle transfer from one zone to another is done with the help of a matrix containing the probabilities of transition. The incorporation of such a continuous-time Markov chain in the EDMC based PBM is straightforward while the residence time functions and the transition matrix can be easily built from DEM simulation results.

The motion of particles through the three zones specified in Figure 8-2 proceeds in two steps. The first one is associated with the particle residence time in each of these specific zones while the second step manages the transition of the particles from one zone to another. To do so, we introduce a vector that contains information about the residence time in each compartment and a transition matrix that contains the probabilities for the particles to move between these compartments. The construction of these data structures, as fully explained below, is done with the help of the DEM results of the flow of particles inside the spheronizer used for the granulation experiments. By tracking these particles during the simulation, the rate at which a given particle goes out of a specific zone into another one can be calculated.

In a Markov process, the rate of transition of the particles must be represented by a function that satisfies the non-aging condition. This condition refers to the fact that future and the past are mutually independent if the present is given [46]. Only the exponential or the more general gamma functions satisfy this criterion for continuous-time Markov chains [47]. In this work, an exponential function is used, which leads to the following cumulative distribution function of residence time :

(8-11)

where , the inverse of the mean residence time in the corresponding compartment, is evaluated by means of the DEM results. For each fictitious particle, the calculation of the residence time is done by replacing with a randomized number following a uniform distribution between [0, 1]. The transition matrix that describes the motion of the particles between the three zones is given by:

(8-12)

where is the probability for a particle to move from compartment i to compartment j. The terms are always equal to zero in this particular form of the Markov process since the residence time gives the time spent by a particle in a compartment before it leaves it. The entries of matrix are obtained from DEM results. In practice, a random number is generated from a uniform distribution between [0,1] to obtain the residence time for a particle in compartment j using equation (8-11):

(8-13)

The rate of particle motion can then be obtained by summing the values for all the particles. By taking into account the volume of the compartment where the particle is located, the motion rate expression used for the EDMC algorithm is simply given by:

(8-14)

where is the number of particles that move simultaneously during a motion event and is the inverse of the mean residence time for particle corresponding to compartment .

When the motion event occurs, particles are selected randomly with the help of an expression similar as the ones taken for the wetting and breakage event represented by equations (8-7) and (8-10) respectively. Once selected, the particles are moved according to the transition matrix (8-12) from their old to the new compartment.

8.2.6 Assessment of the EDMC based PBM

The EDMC based PBM is first assessed with a problem solved analytically where the motion of the particles is not considered. It is then applied to the simulation of the particle motion in the rotor processor described in section 8.2.3. The continuous-time Markov chain is constructed from a DEM simulation for a disc rotational rate of 35 rad/s.

8.2.6.1 Analytical case with no particle motion event

Table 8-4: Parameters for the different PBM simulations

Case	(s)	(s)		( )	Time (s)
1	50	200	1000	1	5000
2	10	200	1000	1	1000
3	1	200	1000	1	100

The EDMC based PBM is compared with analytical results obtained by Blatz et Tobolsky [48], which was used by Lee et al. [21] and Haibo et al. [22] to assess the accuracy of their Monte-Carlo algorithm. In this problem, primary particles (monomers) coalesce to form larger agglomerates, which are affected by the breakage mechanism presented earlier to form two daughter particles. The coalescence kernel in Table 8-4 is equal to the constant . The characteristic coalescence time is given by —— ——. Only the particles of volume that are larger than the primary particles can break up and the smallest fragment size is equal to . The breakage rate is proportional to the number of primary particles contained in an agglomerate and is given by , where is a constant and . The characteristic breakage time is given by . The change of the average size with respect to time is given by:

— — ——— (8-15)

For this analytical case, is the number of fictitious particles and is the initial number of real particles. Three different cases are considered for the assessment of the Monte-Carlo algorithm, whose parameters are given in Table 8-4. The steady-state size is obtained by setting the time derivative in equation (8-15) to zero:

(8-16)

The analytical solution with the initial condition for the approach to the steady-state is:

(8-17)

The initial distribution consists of primary particles and, because they do not fragment, the average size always increases with respect to time. The size distribution is given by:

(8-18)

where is the ratio of the number of particles containing primary particles of volume to the total number of particles at time . It can be shown that [22]. Figure 8-5 presents the mean particle size, the mass conservation and the PSD obtained with the EDMC based PBM.

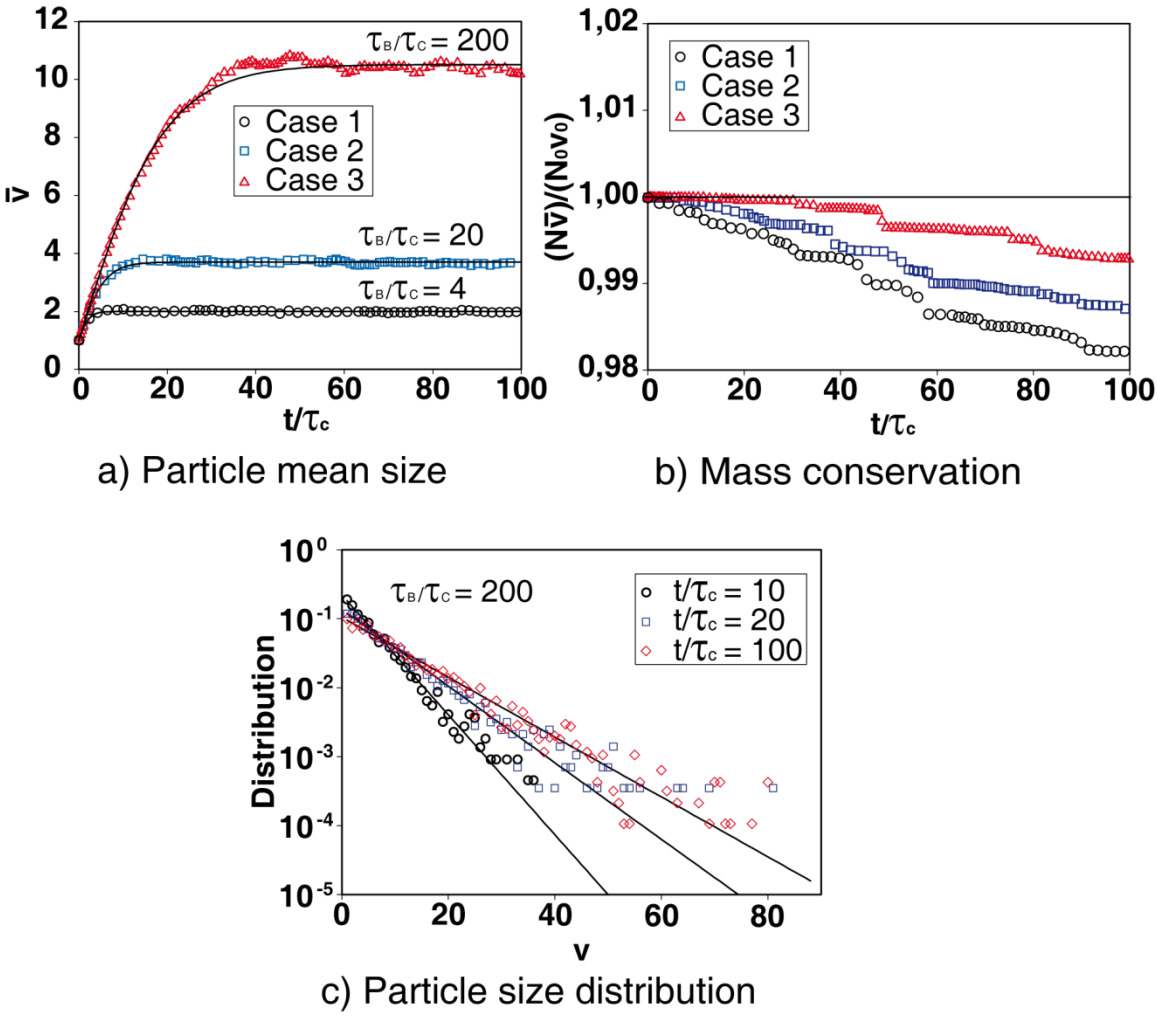

Figure 8-5: Results obtained with the EDMC based algorithm and 1000 fictitious particles: a) Mean particle size, b) mass conservation, and c) particle size distribution. The mass conservation expressed as the number of real particles ( ) multiplied by the mean particle volume ( ). The particle size distribution is presented for the ratio at different dimensionless times. The simulations are compared to the analytical cases [48] represented by the plain lines.

It can be readily noticed that the EDMC based PBM yields results that are in good agreement with the analytical results with one thousand fictitious particles. In particular, the model adequately predicts an increase of the mean particle size at steady-state when the characteristic coalescence time is decreased. The mass conservation decreases slightly for all the cases and even for the long simulation time (case 1), the error does not exceed 2%. This slight decrease of

mass conservation comes from the relocation of the daughter particle following a breakage event for which no fictitious particle of the same size exists. In such a case, it is merged with fictitious particle with the closest size, which creates mass discrepancies. As indicated by Lee et al. [21], the resolution and the accuracy of the size distribution presented in Figure 8-5 depends on the histogram bin size, which can be adjusted. It is known that larger bin sizes lead to a reduction of data scattering, but at the expense of a more jagged distribution.

8.2.6.2 Assessment of the particle motion event in the model

The motion of the particles in the three zones of the rotor processor, the spheronizer of Figure 8-2, was next investigated through a DEM simulation for a rotational rate of 35 rad/s. The residence time of the particles in each of these three compartments is depicted in the graphs of Figure 8-6. As can be seen, the residence curves are well fitted by exponential functions with different values of , the inverse of the mean residence time. The largest value of is associated with the spray zone, which has the smallest size and mean residence time. The Markov process can be used to represent the migration of the particles from one compartment to another as it respects the non-aging property. It means that the time a particle will spend in one compartment does not depend on the amount of time it has spent in a previous one (memoryless process).

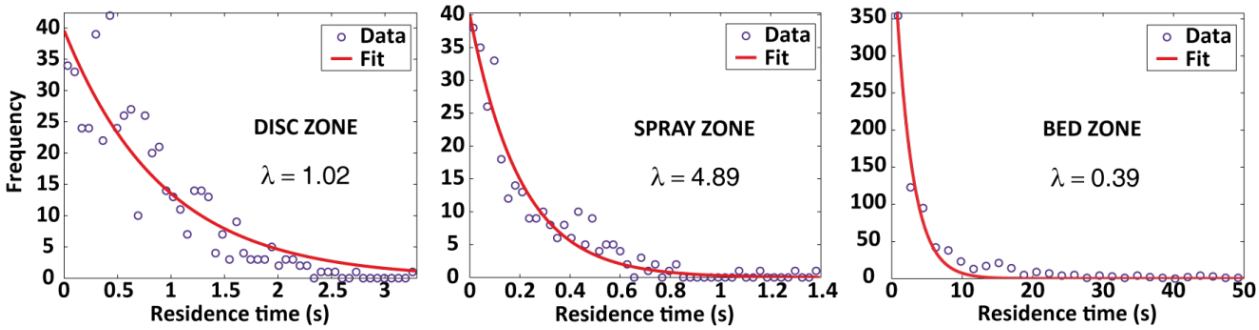

Figure 8-6: Residence time of the particles in the three zones of the bed with a disc speed of 35 rad/s. Each set of data is fitted with an exponential function represented by the continuous line.

The transition matrix that characterizes the motion of the particles between the three compartments can be built from the DEM results:

. (8-19)

Using this transition matrix and the mean residence times, along with the procedure for a particle motion event described in section 8.2.5, the impact of the number of fictitious particles on the flow dynamics was assessed on the basis of the mass conservation in the different compartments with respect to time. Since the particle motion rate in equation (8-14) is expected to be greater than the granulation mechanism rate (coalescence, breakage and wetting in Table 8-2), the fictitious particles, instead of being moved one by one, were regrouped in packets that were moved during particle motion events. That procedure permitted speeding up the population balance simulations. Figure 8-7 shows evolution of the particle mass fraction within the disc zone of the torus when only particle motion is considered at 35 rad/s, which was selected to represent the 100 rad/s disc speed with a wetted particle bed, as presented in Figure 8-3. The noisy line represents the mass fraction when the process is simulated for one particle moving per event. The 200, 1000 and 2000 particle cases were simulated with 5% of the total number of particles per motion event, represented by in equation (8-14). This ratio results in smaller computational times while being small enough to have little impact on the much slower granulation mechamisms. Except for the 200 particle case, the mass fluctuations within the disc zone are observed to be in the range predicted when only one particle is moved per event. Note that the mass fluctuations for the bulk and wetting zones have not been added to Figure 8-7 as they present a behavior similar to those for the shear zone.

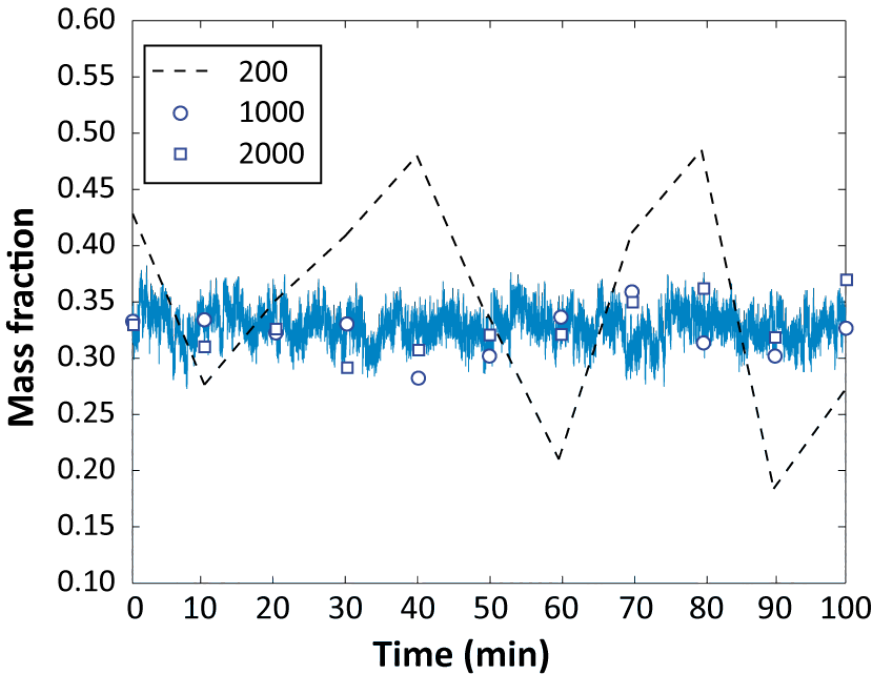

Figure 8-7: Mass fraction of particles in the disc zone. The noisy line indicates the mass fluctuations of when one single particle is moved per event. The dotted curves represent the mass fraction during the population balance simulation.

Moreover, it has been observed for other granulation applications that when the total number of fictitious particle reaches 1000, the simulation results conveniently approximate the solution of the problem [13, 16, 25, 49]. For the simulation of the granulation application of this work, the number of fictitious particles was set to 2000 for increased accuracy.

8.2.7 Wet granulation process

The wet granulation process was modeled with two variants of the EDMC based PBM, one the particle motion event and the other one without it. The numerical results are compared to experimental data obtained by granulating a blend of two pharmaceutical excipients by means of the rotor processor.

8.2.7.1 Materials and method

Lactose (Lactose monohydrate 100M) provided by Lactose (India) Ltd. (Mumbai, India) and microcrystalline cellulose (Avicel PH-101) supplied by FMC BioPolymer (Philadelphia, USA) were used as the powder blend for the granulation. The binder used was water. Table 8-5 gives the composition of the powder blend used for the granulation experiments and the total amount of binder added.

Table 8-5: Powder and binder used for granule production

Elements	Materials	Quantity (kg)
Powder blend	MCC PH-101	0.75
	Lactose monohydrate	1.50
Binder	Water	2.00

To achieve the granulation experiments, a Caleva Spheronizer 380 was modified to incorporate an air line located below the rotating disc. The introduction of air helps to avoid infiltration of particulate material from the particle bed through the gap located between the rotating disc and the wall. Before entering the processing chamber, the air passes through an electrical heater to adjust the temperature to the desired process setpoint. The temperature was set using a controller coupled to a thermocouple that measures the temperature at the entrance. The air flow rate was adjusted with a valve at the entrance of the equipment to the desired value with the help of a gas rotameter. The binder was added by atomization onto the particles with a XA-SR 050 two-fluid atomizer (BETE, Greenfield, MA, USA). It was fed by a peristaltic pump at a flow rate and air pressure that allows the formation of fine droplets. The atomizer was located such that the tip of the nozzle was at a distance of 4 cm from the torus surface. The process parameters are presented in Table 8-6. During each experiment, five samples were extracted from the particle bed by stopping temporarily the operation and scooping around 50 g of material in order to measure their

moisture content and PSD. The sampling operations were distributed evenly throughout the experiment and the total amount of powder extracted was around 6 % of the total particle bed mass. The reproducibility of the experiments was verified with three repetitions of experiment #1.

Table 8-6: Process parameters for the equipment used for the granule production

Exp.	**Disc rot. rate (rad/s)**	**Binder flow rate (g/s)**	**Inlet air temp. (°C)**	**Air flow rate (cfm)**
1	78.5	0.3333	35	6
2	104.7	0.3333	35	6
3	104.7	0.5000	35	6

Once a granular sample extracted, the material was weighed before being placed in a tray dryer. The dry sample was then weighed again to calculate the moisture content loss and was also analyzed by sieve shaking with a Ro-Tap® RX-29 (W.S. Tyler, Mentor, USA) to evaluate the particle size distribution (PSD). The droplet size distribution (DSD) was measured with the help of a Malvern Particle/Droplet sizer (Malvern Instruments Ltd., Worcestershire, UK) with the protocol presented in [50]. Table 8-7 presents the size distribution of the primary powder blend used for the granulation and the droplet size distribution generated by the two-fluid atomizer.

Table 8-7: Particle and spray droplet size distributions

Elements	D10	D50	D90
Spray droplets	5 μm	16 μm	30 μm
Primary particles	75 μm	133 μm	190 μm

8.2.7.2 Reproducibility of the experiments

It is widely known that it is difficult to obtain reproducible granulation results because of the inherent variability of the process. Granulation experiments have already been recognized as strongly user dependent [51] and even small differences in the operating conditions can have a large impact on the final granulation results [52]. Figure 8-8 presents the particle size distributions obtained for three repetitions of experiment #1 Table 8-6. It can be seen that, while the particle sizes measured for the first two assays are reasonably close, except for D90 at 100 min, the results obtained for the third assay are a little more isolated, especially for D10 at 3 min and D50 at 100 min. The first and second assays were produced the same day while the third one was obtained the day after. As the granulation is affected very easily by slight variations of the environment, the differences observed may have resulted from small changes in the ambient conditions. The longest variation observed for the three assays of experiment #1 was around 20% for the mean granule size. This variation was considered as an upper bound for the uncertainty of experiments #2 and #3 that are presented later. On the other hand, the water content absorbed by the particles with respect to time, could be reproduced very well as shown in Figure 8-8. Due to the air stream entering the equipment, some water was removed continuously from the granular bed during the experiments. This water removal was taken into account in the EDMC PBM simulations by adjusting the spray rate in order to represent adequately the experimental moisture content observed. Another possibility would be to add a drying event for the particles, which would be difficult to define in the present work since the distribution of the air stream through the particle bed was not measured.

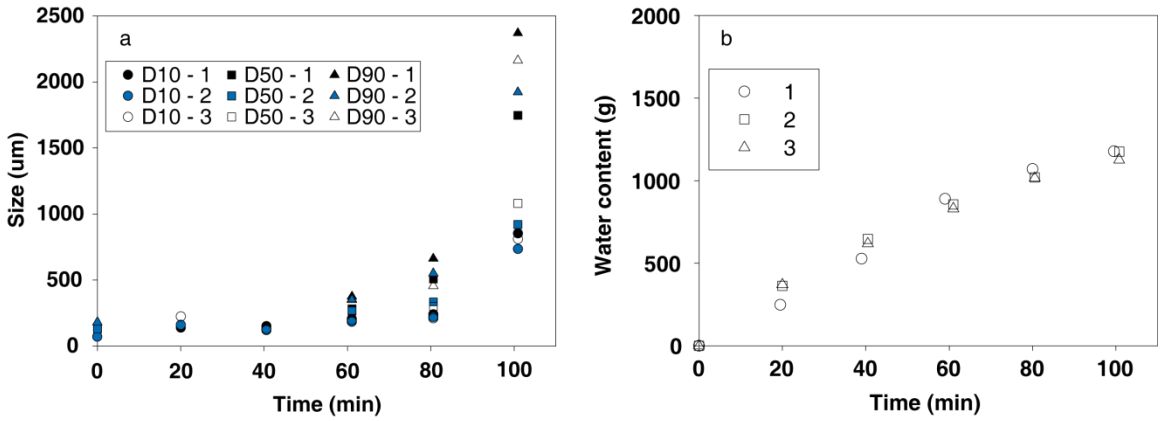

Figure 8-8: Three repetitions of experiment #1.

8.2.7.3 Comparison of simulation results and experimental data

Table 8-8: EDMC based PBM fitting parameters

Simulation	
Exp. #2 without motion	0.50
Exp. #2 with motion	0.50
Exp. #3 without motion	0.35
Exp. #3 with motion	0.35

The EDMC based PBM developed in this work was used to simulate experiments #2 and #3 (Table 8-6) with and without the particle motion event. The parameters for the two modeling approaches are given in Table 8-8. A generalized pattern search algorithm (e.g. [53]) was used to find the coalescence constant (, the breakage constant ( ) and the critical liquid binder saturation ratio ( ) that give the best match between the numerical results and experimental data.

Figure 8-9a compares the EDMC-based PBM results obtained with and without the particle motion event to experimental data for experiment #2, which corresponds to the lower spray rate investigated. For the two modeling approaches, the parameters in Table 8-8 are similar with a small difference for the coalescence constant . Yet, one can observe that these approaches yield significantly different particle sizes with respect to time. Quite clearly, adding the particle motion event improves the accuracy of the predicted results. The experimental curve evolves following an induction behaviour [4], which is also observed when the particle motion event is used. When it is not, the increase in particle size is rather related to a steady growth behaviour [4]. The differences between the two modeling approaches are more important for the 90th percentile of the particle size distribution (D90). This can be associated to the tendency for the large particles to visit the wetting zone more often than the small particles. The segregation of the large particles near the bed surface was indeed observed when analyzing the DEM results used in this work to construct the transition matrix [33].

The small value for indicates that particle breakage is not important compared to the coalescence mechanism. Parameter appears to be higher than 40 %, a value reported in the literature for a lactose/avicel ratio [54]. This lower critical saturation ratio value was obtained with a high shear granulation equipment provided with an impeller. Compared to this equipment, the spheronizer produces a lower level of particle consolidation as it uses a disc instead of an impeller. As the granule consolidates, its porosity decreases. This favours the binder availability at the granule surface and helps the granulation. The larger value for can then be explained by the higher granule porosity for the spheronizer. The effect of the particle consolidation is not taken into account explicitly in the current EDMC-based PBM. To do so, porosity measurements would be required.

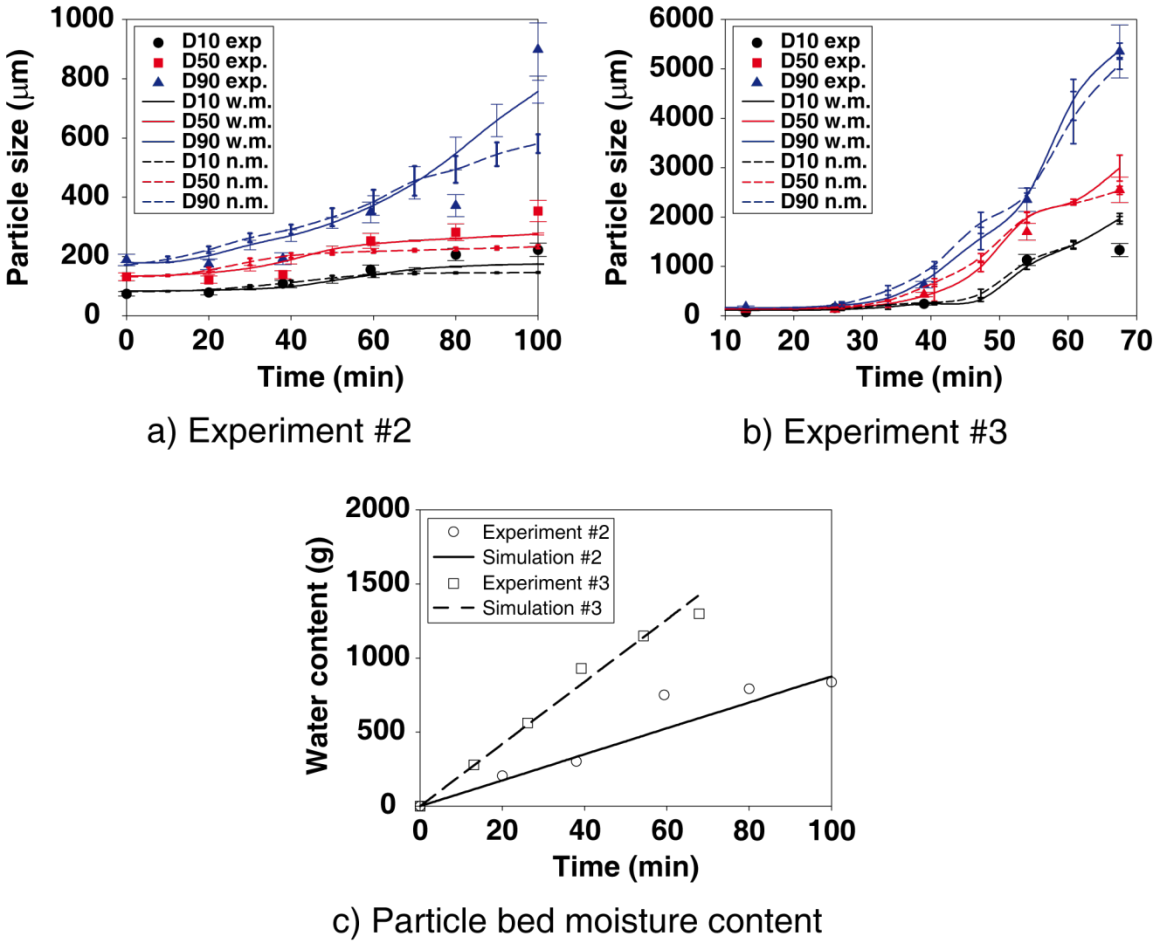

Figure 8-9: Particle size distribution and bed moisture content with respect to time for the granulation experiments #2 and #3. The EDMC based PBM simulation results with (w.m.) and without (n.m.) the particle motion event are compared to experimental data.

Figure 8-9b shows the results obtained for experiment #3, which corresponds to the higher spray rate. The two modeling approaches give similar trends although the values of the coalescence constant are significantly different and smaller than for experiment #2 (**Error! Reference source not found.**). This resulted in a larger agglomeration rate for experiment #2 and larger particle sizes at the end of the granulation. Contrary to experiment #2, it appears that the flow dynamics has a more limited impact on the PBM results as the models with and without the particle motion event yield similar particle size curves. Moreover, is close to the reported

value of 40% for the lactose/avicel blend. It can be observed in Figure 8-9c that the water content of the particle bed is for experiment #3 almost twice that for experiment #2 both numerically and experimentally. The higher water content can increase the consolidation rate of the granules by reducing their mechanical strength [11]. The enhancement of the granulation mechanisms can then limit the impact of the flow dynamics on the evolution of the particle size. While the difference between the values of the coalescence constant for the EDMC-based PBM with and without the particle motion event can be partly due to the flow dynamics, one must keep in mind that other granulation mechanisms such as consolidation and layering growth [13], which are not taken into account in the model, can play a role in the granule formation.

Although the DEM simulation results corresponded to a dry case basis and do not model the increase in size of the particles in the granulation, their use provided valuable information about the particle motion inside the granulator. They gave indication about the frequency at which a particle visits the three compartments of the rotor processor as well as the sequence it follows to migrate from zone to zone. Since the granulation mechanism intensity changes in the different compartments, this sequence has a significant impact on the evolution of the particle growth. Despite the fact that the present work has shown that the DEM-based particle dynamics has a significant impact on the PBM predictions when the spray rate was low (20 g/min), these results could be improved by including in the DEM model the interparticle forces coming from the presence of capillary bonds. These capillary forces are known to reduce the local azimuthal rotational speed of the particles in the torus. They could also lead to a better estimation of the boundaries of the three zones used in this work and to more accurate values of the occupancy time of the particles within these zones [8].

8.2.8 Conclusion

The objective of this work was to investigate granulation with a rotor processor by means of a new multiscale event-driven Monte-Carlo based population balance model. Three granulation experiments obtained with a modified spheronizer were modeled by combining the particle

dynamics through a compartmental approach with granulation mechanisms (wetting, coalescence and breakage). The motion of the particles was included in the population balance model through a continuous-time Markov chain, which was built with the help of DEM results reproducing the dense particle flow in the rotor processor. Although the DEM simulation did not consider the capillary forces, which are important in wet granulation processes, the dry case that was selected to provide particle flow data corresponds to a similar piece of equipment operating with wet material [38]. The addition of the particle motion event into the population balance model was then observed to improve the predicted particle growth when the spray rate was low (20 g/min). Despite the fact that this work has shown the potential of the proposed multiscale EDMC-based PBM, the change in the flow dynamics during granulation was not taken into account. This is presently under investigation using a new experimental technique [55] to study the impact of the interparticle force on the particle flow in the same rotor-based equipment. These experimental data will be used to implement a JKR force model in our DEM code and thus provide more accurate data for the construction of the transition matrix required in the EDMC-based PBM.

8.2.9 Acknowledgements

The financial support of the Natural Science and Engineering Research Council of Canada (NSERC), Merck Frosst of Canada and Ratiopharm is gratefully acknowledged. We would also like to acknowledge Mr. Alexandre Cabana for his help with the experimental granulations.

8.2.10 References

[1] Li, H.M. and J.J. McCarthy, Cohesive particle mixing and segregation under shear. Powder Technology, 2006. 164(1): p. 58-64.

[2] Figueroa, I., H.M. Li, and J. Mccarthy, Predicting the impact of adhesive forces on particle mixing and segregation. Powder Technology, 2009. 195(3): p. 203-212.

[3] Saito, Y., Fan, X.F., Ingram, A., and Seville, J.P.K., A new approach to high-shear mixer granulation using positron emission particle tracking. Chemical Engineering Science, 2011. 66(4): p. 563-569.

[4] Iveson, S.M., Litster, J.D., Hapgood, K., and Ennis, B.J., Nucleation, growth and breakage phenomena in agitated wet granulation processes: a review. Powder Technology, 2001. 117(1-2): p. 3-39.

[5] Iveson, S.M., Limitations of one-dimensional population balance models of wet granulation processes. Powder Technology, 2002. 124(3): p. 219-229.

[6] Forrest, S., Bridgwater, J., Mort, P.R., Litster, J., and Parker, D.J., Flow patterns in granulating systems. Powder Technology, 2003. 130(1-3): p. 91-96.

[7] Michaels, J.N., Farber, L., Wong, G.S., Hapgood, K., Heidel, S.J., Farabaugh, J., Chou, J.-H., and Tardos, G.I., Steady states in granulation of pharmaceutical powders with application to scale-up. Powder Technology, 2009. 189(2): p. 295-303.

[8] Laurent, B.F.C., Structure of powder flow in a planetary mixer during wet-mass granulation. Chemical Engineering Science, 2005. 60(14): p. 3805-3816.

[9] Paul R, M., Scale-up and control of binder agglomeration processes — Flow and stress fields. Powder Technology, 2009. 189(2): p. 313-317.

[10] Salman, A.D., M. Ghadiri, and M.J. Hounslow, Particle Breakage. Chemical, Petrochemical & Process. 2007: Elsevier Science. 1-1213.

[11] Salman, A.D., M.J. Hounslow, and J.P.K. Seville, Granulation. Chemical, Petrochemical & Process. 2007: Elsevier Science. 1-1373.

[12] Hapgood, K.P., J.D. Litster, and R. Smith, Nucleation regime map for liquid bound granules. Aiche Journal, 2003. 49(2): p. 350-361.

[13] Oullion, M., G.K. Reynolds, and M.J. Hounslow, Simulating the early stage of high-shear granulation using a two-dimensional Monte-Carlo approach. Chemical Engineering Science, 2009. 64(4): p. 673-685.

[14] Liu, L. and J. Litster, Population balance modelling of granulation with a physically based coalescence kernel. Chemical Engineering Science, 2002. 57(12): p. 2183-2191.

[15] Cameron, I.T., Wang, F.Y., Immanuel, C.D., and Stepanek, F., Process systems modelling and applications in granulation: A review. Chemical Engineering Science, 2005. 60(14): p. 3723-3750.

[16] Gantt, J.A. and E.P. Gatzke, A stochastic technique for multidimensional granulation modeling. Aiche Journal, 2006. 52(9): p. 3067-3077.

[17] Ramachandran, R., Immanuel, C.D., Stepanek, F., Litster, J.D., and Doyle Iii, F.J., A mechanistic model for breakage in population balances of granulation: Theoretical kernel development and experimental validation. Chemical Engineering Research and Design, 2009. 87(4): p. 598-614.

[18] Zhao, H.B. and C.G. Zheng, A new event-driven constant-volume method for solution of the time evolution of particle size distribution. Journal of Computational Physics, 2009. 228(5): p. 1412-1428.

[19] Immanuel, C.D. and F.J. Doyle Iii, Solution technique for a multi-dimensional population balance model describing granulation processes. Powder Technology, 2005. 156(2-3): p. 213-225.

[20] Ramkrishna, D., Population Balances. Chemical, Petrochemical & Process. 2000: Academic Press. 1-355.

[21] Lee, K. and T. Matsoukas, Simultaneous coagulation and break-up using constant-N Monte Carlo. Powder Technology, 2000. 110(1-2): p. 82-89.

[22] Haibo, Z., Z. Chuguang, and X. Minghou, Multi-Monte Carlo approach for general dynamic equation considering simultaneous particle coagulation and breakage. Powder Technology, 2005. 154(2-3): p. 164-178.

[23] Lin, Y.L., K. Lee, and T. Matsoukas, Solution of the population balance equation using constant-number Monte Carlo. Chemical Engineering Science, 2002. 57(12): p. 2241-2252.

[24] Vikhansky, A. and M. Kraft, Single-particle method for stochastic simulation of coagulation processes. Chemical Engineering Science, 2005. 60(4): p. 963-967.

[25] Braumann, A., M. Kraft, and W. Wagner, Numerical study of a stochastic particle algorithm solving a multidimensional population balance model for high shear granulation. Journal of Computational Physics, 2010. 229(20): p. 7672-7691.

[26] Freireich, B., Li, J., Litster, J., and Wassgren, C., Incorporating particle flow information from discrete element simulations in population balance models of mixer-coaters. Chemical Engineering Science, 2011. 66(16): p. 3592-3604.

[27] Li, J., Freireich, B., Wassgren, C., and Litster, J.D., A general compartment-based population balance model for particle coating and layered granulation. Aiche Journal, 2011: p. n/a-n/a.

[28] Portillo, P.M., F.J. Muzzio, and M.G. Ierapetritou, Hybrid DEM-compartment modeling approach for granular mixing. Aiche Journal, 2007. 53(1): p. 119-128.

[29] Rojas, R., J. Pina, and V. Bucala, Solids Transport Modeling in a Fluidized Drum Granulator. Industrial & Engineering Chemistry Research, 2010. 49(15): p. 6986-6997.

[30] Turchiuli, C., T. Jimenèz, and E. Dumoulin, Identification of thermal zones and population balance modelling of fluidized bed spray granulation. Powder Technology, 2011. 208(2): p. 542-552.

[31] Vikhansky, A. and M. Kraft, Modelling of a RDC using a combined CFD-population balance approach. Chemical Engineering Science, 2004. 59(13): p. 2597-2606.

[32] Srilatha, C., Morab, V., Mundada, T.P., and Patwardhan, A.W., Relation between hydrodynamics and drop size distributions in pump-mix mixer. Chemical Engineering Science, 2010. 65(11): p. 3409-3426.

[33] Bouffard, J., et al., Discrete Element Investigation of Flow Patterns and Segregation in a Spheronizer. sumitted to Computers and Chemical Engineering, 2011.

[34] Lemieux, M., Léonard, G., Doucet, J., Leclaire, L.-A., Viens, F., Chaouki, J., and Bertrand, F., Large-scale numerical investigation of solids mixing in a V-blender using the discrete element method. Powder Technology, 2007. 181: p. 205-216.

[35] Cundall, P.A. and O.D.L. Strack, Discrete numerical model for granular assemblies. Geotechnique, 1979. 29: p. 47-65.

[36] Zhou, Y.C., Wright, B.D., Yang, R.Y., Xu, B.H., and Yu, A.B., Rolling friction in the dynamic simulation of sandpile formation. Physica A, 1999. 269: p. 536-553.

[37] Corwin, E.I., Granular flow in a rapidly rotated system with fixed walls. Physical Review E, 2008. 77: p. 031308.

[38] Muguruma, Y., T. Tanaka, and Y. Tsuji, Numerical simulation of particulate flow with liquid bridge between particles (simulation of centrifugal tumbling granulator). Powder Technology, 2000. 109(1-3): p. 49-57.

[39] Zhao, H.B., F.E. Kruis, and C.G. Zheng, A differentially weighted Monte Carlo method for two-component coagulation. Journal of Computational Physics, 2010. 229(19): p. 6931-6945.

[40] Zhao, H. and C. Zheng, Two-component Brownian coagulation: Monte Carlo simulation and process characterization. Particuology, 2011. 9(4): p. 414-423.

[41] Litster, J. Using a Population Balance Framework to Develop Design Models for Granulation Processes. in Particle Technology Laboratory. 2008. ZURICH.

[42] Le, P.K., Avontuur, R., Hounslow, M.J., and Salman, A.D., The kinetics of the granulation process: Right from the early stages. Powder Technology, 2009. 189(2): p. 149-157.

[43] Biggs, C.A., Sanders, C., Scott, A.C., Willemse, A.W., Hoffman, A.C., Instone, T., Salman, A.D., and Hounslow, M.J., Coupling granule properties and granulation rates in high-shear granulation. Powder Technology, 2003. 130(1-3): p. 162-168.

[44] Hounslow, M.J., J.M.K. Pearson, and T. Instone, Tracer studies of high-shear granulation: II. Population balance modeling. Aiche Journal, 2001. 47(9): p. 1984-1999.

[45] Reynolds, G.K., Fu, J.S., Cheong, Y.S., Hounslow, M.J., and Salman, A.D., Breakage in granulation: A review. Chemical Engineering Science, 2005. 60(14): p. 3969-3992.

[46] Berthiaux, H. and V. Mizonov, Applications of markov chains in particulate process engineering: A review. Canadian Journal of Chemical Engineering, 2004. 82(Compendex): p. 1143-1168.

[47] Ross, S., Stochastic processes. 1996, New York: Wiley.

[48] Blatz, P.J. and A.V. Tobolsky, Note on the Kinetics of Systems Manifesting Simultaneous Polymerization-Depolymerization Phenomena. The Journal of Physical Chemistry, 1945. 49(2): p. 77-80.

[49] Smith, M. and T. Matsoukas, Constant-number Monte Carlo simulation of population balances. Chemical Engineering Science, 1998. 53(9): p. 1777-1786.

[50] Bouffard, J., M. Kaster, and H. Dumont, Influence of Process Variable and Physicochemical Properties on the Granulation Mechanism of Mannitol in a Fluid Bed Top Spray Granulator. Drug Development and Industrial Pharmacy, 2005. 31(9): p. 923-933.

[51] Sochon, R.P.J., Zomer, S., Cartwright, J.J., Hounslow, M.J., and Salman, A.D., The variability of pharmaceutical granulation. Chemical Engineering Journal, 2010. 164(2-3): p. 285-291.

[52] Fu, J.S., Cheong, Y.S., Reynolds, G.K., Adams, M.J., Salman, A.D., and Hounslow, M.J., An experimental study of the variability in the properties and quality of wet granules. Powder Technology, 2004. 140(3): p. 209-216.

[53] Hayes, R.E., Bertrand, F.H., Audet, C., and Kolaczkowski, S.T., Catalytic combustion kinetics: Using a direct search algorithm to evaluate kinetic parameters from light-off curves. Canadian Journal of Chemical Engineering, 2003. 81(6): p. 1192-1199.

[54] Chitu, T.-M., Granulation humide des poudres cohesives: Rheologie, mecanismes de croissance et tenue mecanique des granules, in Génie des procédés. 2009, Institut National Polytechnique de Toulouse: Toulouse. p. 228.

[55] Bouffard, J., J. Chaouki, and F. Bertrand, Control of particle cohesion with a polymer coating and temperature adjustments. submitted to AIChE journal, 2011.

CHAPITRE 9 DISCUSSION GÉNÉRALE

Les procédés de granulation humide sont très couramment rencontrés dans plusieurs domaines industriels et ce depuis plus d'une cinquantaine d'années. Même si la compréhension des différents phénomènes y étant impliqués s'est significativement améliorée, la granulation humide souffre toujours de lacunes importantes au niveau des connaissances associées à l'impact de certains d'entre eux tels que la capacité de bien représenter les mécanismes complexes qu'on y retrouve (ex :le bris particulaire) ou d'évaluer l'influence du comportement mécanique des granules (déformation et résistance mécanique). D'autre part, un autre aspect important à améliorer est la manière dont les granulateurs doivent être construits ou opérés afin d'obtenir des propriétés granulaires optimales. Ce dernier aspect est principalement relié à la problématique des écoulements granulaires autour duquel tourne l'objectif principal de cette thèse.

Dû à l'opacité des matériaux granulaires, la caractérisation des opérations où ils interviennent est complexe. Les patrons d'écoulement et de ségrégation sont généralement obtenus expérimentalement à l'aide de méthodes sophistiquées (ex : tomographie, PEPT ou RPT) permettant de mesurer ces propriétés de manière non-invasive. On peut aussi recourir à la simulation numérique des écoulements granulaires par l'emploi de la DEM ou d'une approche de dynamique moléculaire par exemple. Toutefois, les paramètres physiques associés à ces simulations doivent être comparés à des mesures expérimentales afin de vérifier leur validité. D'un autre côté, les procédés de granulation sont caractérisés par une évolution continue des propriétés granulaires, telles que leur taille moyenne et la distribution y étant associée, ce qui rend la tâche de mesurer les écoulements granulaires difficile et explique le peu d'information existante sur le sujet jusqu'à maintenant. Les différents objectifs spécifiques de cette thèse ont permis d'apporter une contribution aux efforts actuellement déployés dans ce domaine.

Il est maintenant bien établi que pour les écoulements granulaires, le mélange des granules est toujours associé à la présence de ségrégation. Il a été longtemps considéré que l'ajout d'un liant dans un lit de particules, comme c'est le cas pour la granulation humide, permettait de réduire

substantiellement et même d'éliminer la ségrégation étant donné les forces cohésives présentes. C'est tout récemment que cette perception a été infirmée par divers travaux. Certains d'entre eux indiquent que la ségrégation peut même devenir plus importante en présence des forces interparticulaires. Une autre tendance généralement admise était que l'incrémentation de l'intensité du mélange, qui peut être obtenue par l'augmentation de la vitesse d'agitation par exemple, faisait en sorte que la ségrégation des particules s'en trouvait diminuée. Dans la première partie de ce travail, la caractérisation de l'écoulement particulaire, en présence d'une population de particules bidisperses, a permis d'obtenir les patrons de ségrégation associés à l'opération d'un granulateur à rotor à l'aide de la DEM. Les résultats des simulations ont pu mettre en évidence que la ségrégation est présente dans le granulateur à rotor et ce même si l'intensité du cisaillement dans le lit toroidal est élevée. Il existe une vitesse de disque optimale, autour de 35 rad/s pour le bas niveau de remplissage et 100 rad/s pour le niveau élevé, pour laquelle la ségrégation obtenue est minimale. Ce point de transition correspond au passage d'une ségrégation principalement localisée au centre du lit toroidal vers une ségrégation qui est davantage située vers la paroi de l'équipement. En plus de l'évaluation du phénomène de ségrégation, les profils de vitesse des particules ainsi qu'une estimation du déplacement particulaire à travers différentes zones dans le lit toroidal ont pu être obtenus. Cette information a été très utile dans la dernière partie du travail. Elle a permis de construire le processus stochastique représentant le mouvement des particules fictives dans le modèle multi-échelle permettant de simuler la granulation humide.

Il est important de noter que les simulations DEM ne considèrent pas les forces capillaires dans le lit de particules, ce qui fait en sorte que l'on peut s'attendre à ce que le comportement de l'écoulement qui prendrait en compte ces forces serait différent. Par contre, il faut rappeler que le but visé n'était pas de représenter fidèlement l'écoulement cohésif mais plutôt d'obtenir une estimation du profil d'écoulement pouvant être réutilisée dans les simulations de la dernière partie du travail. La poursuite des travaux entamés dans cette partie de la thèse serait logiquement d'inclure les forces capillaires à l'intérieur de la DEM. Pour des cas où seulement deux particules en interaction sont considérées (état de saturation pendulaire), l'inclusion de cette force est directe et ne pose aucun problème. Il en va tout autrement lorsqu'un lit de particules est considéré comme c'est le cas dans les simulations DEM employées dans cette thèse. Ceci

s'explique par le fait qu'il est impératif de considérer l'état de saturation en liquide du lit de particules (pendulaire, funiculaire ou capillaire) afin de savoir de quelle manière les ponts liquides sont agencés dans l'espace. L'état pendulaire est l'état le plus simple à intégrer dans la DEM puisque les ponts liquides font encore intervenir des interactions binaires entre les particules du lit. Ainsi, en considérant une distribution uniforme du liquide à travers le lit de particules, le comportement cohésif des particules en écoulement peut être estimé. Par contre, l'état pendulaire survient lorsque le niveau de saturation ne dépasse pas 1 à 3 %vol, ce qui ne correspond pas à la concentration à laquelle la granulation est observée. Au-delà de ce niveau de saturation, la morphologie des ponts liquides devient beaucoup plus complexe et commence à faire interagir plusieurs particules simultanément. Il est alors très difficile de modéliser les forces capillaires et le recours à des outils plus complexes, tels que la méthode VOF (*volume of fluid*), est nécessaire. Cette modélisation demande alors des temps de calcul très imposants et peut seulement s'effectuer pour quelques particules en interactions simultanément.

L'étude expérimentale des écoulements cohésifs dus à la présence des forces capillaires n'est pas nécessairement plus aisée. Tout d'abord, il est en pratique très compliqué d'employer des matériaux granulaires qui sont utilisés dans le cadre des procédés de granulation. En effet, pour caractériser l'écoulement particulaire, les propriétés des granules doivent demeurer stables tout au long de l'expérience où le rester suffisamment longtemps pour obtenir des données valables. Il en va tout autrement des matériaux granulaires utilisés dans les procédés de granulation. Ceci explique pourquoi la majorité des travaux actuels se sont rabattus sur des particules respectant ce critère essentiel comme des billes de verre, par exemple. D'un autre côté, l'emploi de ces particules fait en sorte que la densité, la déformabilité et même la manière dont les forces capillaires s'établissent peuvent dévier fortement des propriétés réelles des particules utilisées dans la granulation humide.

Le développement d'une nouvelle approche pouvant intégrer des forces interparticulaires mais qui fait intervenir des particules dont les matériaux sont les mêmes que ceux utilisés dans la granulation devient alors intéressant. La deuxième partie de la thèse a présenté une méthode permettant d'introduire des forces interparticulaires à l'aide d'un enrobage de copolymère de

PEA/PMMA déposé sur des particules composées de matériaux typiquement utilisés en granulation humide. D'autre part, cette approche rend possible le contrôle des forces cohésives de manière simple en changeant la température des particules enrobées ou l'épaisseur de la couche de polymère.

Tel que présenté dans cette partie du travail, une incrémentation de température de 35 °C permet de faire augmenter la force interparticulaire d'environ un ordre de grandeur. En effet, la force obtenue varie entre le niveau d'intensité des forces de van der Waals et celui des forces capillaires maximales pour une même taille de particule. De plus, la force interparticulaire augmente proportionnellement en fonction de l'épaisseur d'enrobage, ce qui donne un autre paramètre pouvant servir à ajuster le niveau de cohésion particulaire. La force interparticulaire a été mesurée avec un SFA, appareil permettant la mesure de la force de séparation de deux interfaces de polymère en contact. Il peut mesurer cette force à une échelle de taille, donné par le rayon de courbure des ménisques de support, qui est similaire à celle des particules utilisées dans le cadre de ce travail. De plus, il permet de transposer facilement les résultats de force de séparation obtenus à des contacts de particules sphériques, étant donné la similarité géométrique.

Le potentiel d'utilisation de l'approche du contrôle de cohésion par enrobage de polymère a été démontré pour deux applications différentes, la première impliquant un écoulement particulaire dense à l'intérieur d'un sphéroniseur, et la deuxième étant associée aux lits fluidisés. Dans le premier cas, la décroissance de densité dynamique observée avec l'augmentation de température met en évidence la réduction de l'indice d'écoulement (la capacité d'écoulement) des particules. Pour les deux épaisseurs d'enrobage qui ont été considérées (3,5 et 7,0 μm), une diminution linéaire de la densité est apparue suivant deux étapes distinctes associées à des taux de décroissance différents. La première étape mesurée entre 32 et 42 °C avait le taux de décroissement le plus faible et correspondait à une augmentation de forces cohésives sans apparition d'agglomérats à la surface du tore. La deuxième étape de décroissance de densité (>42°C), cette fois plus rapide, apparaissait avec la formation d'agrégats de particules, lesquelles étaient visibles à la surface. C'est la présence de ces agglomérats qui explique la valeur plus élevée du taux de décroissance de la densité dynamique. Dans la deuxième application étudiée,

un lit de particules enrobées était fluidisé afin de pouvoir mesurer la perte de charge obtenue en fonction de la température. Les résultats ont bien exposé le dépassement de la perte de charge mesurée par rapport à la valeur théorique correspondant au poids du lit de particules utilisé ( ). Une comparaison avec des mesures similaires pour les lits fluidisés à haute température a permis de démontrer le potentiel de cette approche afin de pouvoir reproduire le comportement des particules fluidisées dans ce type d'application. De plus, l'approche du contrôle de cohésion par enrobage de polymère est associée à un mécanisme d'agglomération des particules qui est très similaire au mécanisme de frittage des particules dans les lits fluidisés à haute température. Puisqu'il est très difficile de pouvoir effectuer des mesures intrusives à l'aide de sonde dans les lits fluidisés à haute température, le fait d'avoir la possibilité d'étudier un comportement similaire, mais à des températures ambiantes, constitue un avantage marqué dans le but de faire des avancées importantes menant à l'amélioration de la compréhension des mécanismes d'écoulement pour ces procédés.

Dans la troisième partie de la thèse, une étude plus approfondie de l'écoulement dense de particules cohésives a été effectuée, ce qui a permis d'observer quatre différents états d'écoulement à l'intérieur du sphéroniseur. Trois de ces états d'écoulement (FS-I, FS-II et FS-IV) avaient un comportement stable, c'est-à-dire qu'il ne changeait pas en fonction du temps. Contrairement aux autres, FS-III présentait un comportement transitoire où deux zones d'écoulement distinctes pouvaient être observées et le volume de ces zones variait périodiquement durant l'opération du sphéroniseur. Les quatre états ont été représentés dans un diagramme en fonction de nombres adimensionnels en délimitant leur région d'influence par des frontières approximées selon les expériences effectuées. Ceci a permis de comparer ces états au comportement des écoulements dans un contexte de granulation humide. Une suite logique du travail entamé dans cette partie de la thèse serait de faire une étude exhaustive des états d'écoulement afin de pouvoir bien délimiter les frontières entre ceux-ci dans le diagramme. D'autre part, l'emploi de cette méthode pour d'autres types d'équipement ayant à traiter avec des écoulements cohésifs pourrait aussi permettre de généraliser le diagramme des écoulements pour d'autres applications telles que les lits fluidisés par exemple. Dans un autre ordre d'idée, cette partie du travail ouvre la voie vers une compréhension plus approfondie de la relation entre les écoulements granulaires et les processus de granulation. Étant donné qu'il est possible d'ajuster

l'intensité des forces interparticulaires, le comportement d'un écoulement particulaire cohésif qui serait normalement observé à différentes étapes de la granulation peut être représenté. Ainsi, l'emploi de cette approche pourrait permettre de modifier les designs de granulateur de telle manière à rendre les écoulements propices à l'obtention de caractéristiques granulaires optimales soit en favorisant la distribution des liants ou en limitant les zones mortes des patrons d'écoulement par exemple.

La dernière partie de cette thèse a permis de mettre en place un modèle multi-échelle considérant l'impact de l'écoulement particulaire pour la simulation de la granulation humide à l'aide d'un bilan de population. Utilisant une méthode de Monte-Carlo dirigée par événement, des mécanismes de granulation simples ont pu être intégrés dans le bilan de population. Le travail de la première partie a par la suite été utilisé afin de construire une chaine de Markov dont les propriétés ont été tirées directement du patron d'écoulement caractérisant le mélange de particules bidisperses et obtenu de simulations DEM. Le lit granulaire a été séparé en trois zones caractérisées chacune par un mécanisme de granulation différent, selon une approche par compartiment. La considération de l'écoulement granulaire a permis d'améliorer, par rapport à un bilan de population conventionnel, les prédictions de taille de particules obtenues expérimentalement dans le sphéroniseur modifié. Il apparaît toutefois que cette amélioration est limitée par le débit de liant ajouté. Le modèle multi-échelle ne donne pas de meilleurs résultats que l'approche conventionnelle si la quantité de liant est ajoutée trop rapidement. Dans ce cas, il est possible que l'impact du patron d'écoulement soit réduit par rapport à la croissance très rapide de la taille moyenne granulaire. Il est important de rappeler que le contrôle de la granulation dépend de manière significative de la capacité de bien distribuer le liant à travers le lit de particules. Pour des débits de liant faibles, il est possible d'observer beaucoup plus de disparités par rapport au contenu en eau des particules que lorsque ce débit est élevé. Ceci peut expliquer pourquoi le modèle multi-échelle et le bilan de population conventionnel ne donnent pas des résultats significativement différents lorsque le débit de liant est élevé. Une des limitations de cette partie du travail est reliée à l'emploi de simulations DEM de l'écoulement granulaire qui ne présentent pas de forces cohésives représentatives de la granulation humide. Pour palier en partie à ce problème, un patron d'écoulement correspondant à une vitesse de disque inférieure à celle utilisée dans les expériences de granulation a été sélectionnée afin d'approximer le comportement

de particules cohésives. Il est indéniable que les prédictions du modèle multi-échelle profiteraient de l'intégration des propriétés d'écoulement cohésif représentatives du comportement dans le granulateur. L'approche du contrôle des forces interparticulaires par l'enrobage de polymère conduit à l'implantation des forces cohésives dans la DEM plutôt qu'à celui de forces capillaires. Par l'emploi d'un modèle JKR ou DMT, lequel est choisi en fonction des propriétés des particules, il devient en effet possible d'inclure les modèles de forces cohésives intervenant dans cette approche dans la DEM.

CONCLUSION ET RECOMMANDATIONS

L'objectif principal de cette thèse était de comprendre et de quantifier la manière dont les propriétés d'un écoulement dense de particules peuvent affecter les procédés de granulation. Afin de remplir cet objectif, quatre articles ont été présentés.

Les procédés de granulation sont complexes à étudier étant donné la multitude de mécanismes impliqués qui ont la plupart du temps une interdépendance entre eux. Les paramètres intrinsèques des granules tels que leur taille, leur forme, leur porosité, leur composition ou leur niveau de saturation en liant jouent un rôle important quant à la manière dont ces mécanismes agissent pendant la granulation. La majeure partie des efforts de recherche sur les procédés de granulation est d'ailleurs concentrée, encore aujourd'hui, au niveau des impacts de ces paramètres afin de corriger ou de créer des modèles phénoménologiques. C'est plus récemment que l'impact des écoulements de particules sur la granulation a commencé à être étudié. Le travail présenté dans cette thèse a permis d'apporter une contribution à ce champ de recherche.

Dans un premier temps, il est possible d'employer la DEM afin de pouvoir obtenir des caractéristiques importantes des écoulements particulaires, soient les patrons de ségrégation et d'écoulement. On a vu que la DEM peut être utilisée de manière à non seulement caractériser les écoulements granulaires, mais aussi à déterminer les points d'opération optimaux permettant de minimiser la ségrégation ou de favoriser un type de patron d'écoulement particulier. Les résultats obtenus avec cet outil numérique peuvent alors aider à orienter les efforts de paramétrisation des procédés de granulation de manière à s'approcher d'une opération optimale des équipements employés.

D'un autre côté, la considération des forces cohésives à l'intérieur des modèles numériques, ainsi qu'au niveau des études expérimentales, est très importante pour bien caractériser les procédés de granulation. Étant fondamentalement associées à la granulation humide, l'utilisation des forces capillaires est un moyen évident de les inclure. Par contre, du point de vue numérique, le

problème associé à la difficulté d'inclure des ponts liquides et d'en assurer la distribution pendant une simulation au-delà d'un certain niveau de saturation en liant liquide a été exposé. De plus, la considération des forces capillaires avec des particules typiquement utilisées expérimentalement pendant la granulation humide pose un autre problème. En effet, étant soumises aux mécanismes de granulation, ces particules ne peuvent conserver les mêmes propriétés durant la caractérisation de l'écoulement. Les particules de verre ou de sable, malgré qu'elles puissent permettre une mesure continue de l'écoulement, possède des propriétés différentes de celles associées aux matériaux granulaires utilisés dans un contexte de granulation humide en industrie. L'emploi de la méthode d'enrobage avec polymère développée dans cette thèse vient répondre en partie à cette problématique. En effet, elle permet d'ajuster les forces interparticulaires de manière à reproduire le niveau d'intensité d'autres types de forces comme celles provenant des ponts capillaires. D'autre part, cette approche offre la possibilité d'utiliser les mêmes matériaux que dans la granulation humide tout en ayant l'avantage de conserver les propriétés inhérentes des particules.

Finalement, l'utilisation de la DEM peut permettre de considérer le mouvement de particules dans les simulations des procédés de granulation afin d'affiner les prédictions obtenues avec un modèle multi-échelle par exemple. L'inclusion des propriétés d'écoulement peut aider à mieux prédire les tendances associées à l'évolution des caractéristiques granulaires par rapport aux expériences de granulation. Toutefois, il reste du travail à effectuer du point de vue de la modélisation des écoulements en DEM afin de pouvoir tenir compte des forces cohésives.

Afin de pousser plus loin l'étude des écoulements dans les procédés de granulation, les recommandations suivantes peuvent être faites :

1. Développer des modèles de force interparticulaires associés à l'approche utilisant un enrobage de polymère de manière à les inclure dans la DEM. Ceci permettra de simuler les états d'écoulement granulaire cohésif qui sont observés dans le contexte de l'opération des granulateurs.

2. Effectuer une caractérisation plus poussée de la force interparticulaire pour le contact de deux interfaces de polymère à l'aide du SFA. Ceci pourra permettre de mieux caractériser le comportement cohésif en fonction de l'épaisseur de l'enrobage et de la température, mais aussi de la vitesse de séparation et du temps de contact. Ces deux derniers paramètres sont importants à caractériser, entre autre pour améliorer la fonction d'adhésion effective en fonction du temps de contact.
3. Étendre l'approche par enrobage de polymère à d'autres applications. Un des procédés pouvant bénéficier directement de l'emploi de cette approche est associé aux lits fluidisés à haute température pour lesquels il est difficile de caractériser les écoulements particulaires. En ramenant les opérations à température ambiante avec l'approche par enrobage de polymère, cette limitation disparaît en bonne partie.
4. Définir plus précisément les frontières des états d'écoulement décrits dans le diagramme développé dans ce travail en fonction du nombre de Bond et du nombre de Deborah. Il sera alors possible de pouvoir tester le diagramme sur d'autres systèmes granulaires et ainsi le généraliser.
5. Considérer des écoulements cohésifs dont les propriétés sont tirées soit de la DEM ou d'une méthode de mesure expérimentale non intrusive comme la RPT afin d'améliorer le modèle multi-échelle employé pour résoudre les bilans de population.

BIBLIOGRAPHIE

Alexander, A., Muzzio, F. J., & Shinbrot, T. (2003). Segregation patterns in V-blenders. *Chemical Engineering Science, 58*(2), 487-496.

Bertrand, F., Leclaire, L. A., & Levecque, G. (2005). DEM-based models for the mixing of granular materials. *Chemical Engineering Science, 60*(8-9), 2517-2531.

Bouffard, J., Kaster, M., & Dumont, H. (2005). Influence of Process Variable and Physicochemical Properties on the Granulation Mechanism of Mannitol in a Fluid Bed Top Spray Granulator. [doi: 10.1080/03639040500272124]. *Drug Development and Industrial Pharmacy, 31*(9), 923-933.

Butt, H.-J., & Michael, K. (2010). *Surface and interfacial forces*. Weinheim: Wiley-VCH Verlag GmbH & Co. KGaA.

Cameron, I. T., Wang, F. Y., Immanuel, C. D., & Stepanek, F. (2005). Process systems modelling and applications in granulation: A review. *Chemical Engineering Science, 60*(14), 3723-3750.

Campbell, C. S. (1990). Rapid Granular Flows. *Annual Review of Fluid Mechanics, 22*, 57-92.

Campbell, C. S. (2006). Granular material flows - An overview. *Powder Technology, 162*(3), 208-229.

Conway, S. L., Lekhal, A., Khinast, J. G., & Glasser, B. J. (2005). Granular flow and segregation in a four-bladed mixer. *Chemical Engineering Science, 60*(24), 7091-7107.

Corwin, E. I. (2008). Granular flow in a rapidly rotated system with fixed walls. *Physical Review E, 77*, 031308.

Cundall, P. A., & Strack, O. D. L. (1979). Discrete numerical model for granular assemblies. *Geotechnique, 29*, 47-65.

de Gennes, P. G. (1998). Reflections on the mechanics of granular matter. *Physica A, 261*(3-4), 267-293.

Ennis, B. J., Tardos, G., & Pfeffer, R. (1991). A Microlevel-Based Characterization of Granulation Phenomena. *Powder Technology, 65*(1-3), 257-272.

Figueroa, I., Li, H. M., & Mccarthy, J. (2009). Predicting the impact of adhesive forces on particle mixing and segregation. *Powder Technology, 195*(3), 203-212.

Forrest, S., Bridgwater, J., Mort, P. R., Litster, J., & Parker, D. J. (2003). Flow patterns in granulating systems. [doi: 10.1016/S0032-5910(02)00232-2]. *Powder Technology, 130*(1-3), 91-96.

Forsyth, A. J., Hutton, S., & Rhodes, M. J. (2002). Effect of cohesive interparticle force on the flow characteristics of granular material. *Powder Technology, 126*(2), 150-154.

Forsyth, A. J., Hutton, S. R., Osborne, C. F., & Rhodes, M. J. (2001). Effects of Interparticle Force on the Packing of Spherical Granular Material. *Physical Review Letters, 87*(24), 244301.

Forsyth, A. J., Hutton, S. R., Rhodes, M. J., & Osborne, C. F. (2001). Effect of applied interparticle force on the static and dynamic angles of repose of spherical granular material. *Physical Review E, 6303*(3), 031302.

Fournier, Z., Geromichalos, D., Herminghaus, S., Kohonen, M. M., Mugele, F., Scheel, M., et al. (2005). Mechanical properties of wet granular materials. *Journal of Physics-Condensed Matter, 17*(9), S477-S502.

Freireich, B., Li, J., Litster, J., & Wassgren, C. (2011). Incorporating particle flow information from discrete element simulations in population balance models of mixer-coaters. [doi: 10.1016/j.ces.2011.04.015]. *Chemical Engineering Science, 66*(16), 3592-3604.

Freireich, B., Litster, J., & Wassgren, C. (2009). Using the discrete element method to predict collision-scale behavior: A sensitivity analysis. *Chemical Engineering Science, 64*(15), 3407-3416.

Gantt, J. A., & Gatzke, E. P. (2005). High-shear granulation modeling using a discrete element simulation approach. *Powder Technology, 156*(2-3), 195-212.

Gantt, J. A., & Gatzke, E. P. (2006). A stochastic technique for multidimensional granulation modeling. *Aiche Journal, 52*(9), 3067-3077.

Goldhirsch, I. (1999). Scales and kinetics of granular flows. *Chaos, 9*(3), 659-672.

Goodson, M., & Kraft, M. (2004). Simulation of coalescence and breakage: an assessment of two stochastic methods suitable for simulating liquid-liquid extraction. *Chemical Engineering Science, 59*(18), 3865-3881.

Gu, L., Liew, C. V., & Heng, P. W. S. (2004). Wet spheronization by rotary processing - A multistage single-pot process for producing spheroids. *Drug Development and Industrial Pharmacy, 30*(2), 111-123.

Hamaker, H. C. (1937). The London-van der Waals Attraction Between Spherical Particles. *Physica IV, 10*, 1058.

Hapgood, K. P., Litster, J. D., & Smith, R. (2003). Nucleation regime map for liquid bound granules. *Aiche Journal, 49*(2), 350-361.

Immanuel, C. D., & Doyle Iii, F. J. (2005). Solution technique for a multi-dimensional population balance model describing granulation processes. [doi: 10.1016/j.powtec.2005.04.013]. *Powder Technology, 156*(2-3), 213-225.

Ingram, G. D., & Cameron, I. T. (2004). Challenges in Multiscale Modelling and its Application to Granulation Systems. *Developments in Chemical Engineering and Mineral Processing, 12*(3-4), 293-308.

Iveson, S. M. (2001). Granule coalescence modelling: including the effects of bond strengthening and distributed impact separation forces. *Chemical Engineering Science, 56*(6), 2215-2220.

Iveson, S. M. (2002). Limitations of one-dimensional population balance models of wet granulation processes. *Powder Technology, 124*(3), 219-229.

Iveson, S. M., Beathe, J. A., & Page, N. W. (2002). The dynamic strength of partially saturated powder compacts: the effect of liquid properties. *Powder Technology, 127*(2), 149-161.

Iveson, S. M., & Litster, J. D. (1998a). Fundamental studies of granule consolidation - Part 2. Quantifying the effects of particle and binder properties. *Powder Technology, 99*(3), 243-250.

Iveson, S. M., & Litster, J. D. (1998b). Growth regime map for liquid-bound granules. *Aiche Journal, 44*(7), 1510-1518.

Iveson, S. M., Litster, J. D., & Ennis, B. J. (1996). Fundamental studies of granule consolidation .1. Effects of binder content and binder viscosity. *Powder Technology, 88*(1), 15-20.

Iveson, S. M., Litster, J. D., Hapgood, K., & Ennis, B. J. (2001). Nucleation, growth and breakage phenomena in agitated wet granulation processes: a review. [doi: DOI: 10.1016/S0032-5910(01)00313-8]. *Powder Technology, 117*(1-2), 3-39.

Iveson, S. M., Wauters, P. A. L., Forrest, S., Litster, J. D., Meesters, G. M. H., & Scarlett, B. (2001). Growth regime map for liquid-bound granules: further development and experimental validation. [doi: 10.1016/S0032-5910(01)00317-5]. *Powder Technology, 117*(1-2), 83-97.

Jenkins, J. T., & Savage, S. B. (1983). A theory for the rapid flow of identical, smooth, nearly elastic, spherical particles. *Journal of Fluid Mechanics, 130*(-1), 187-202.

Jop, P., Forterre, Y., & Pouliquen, O. (2006). A constitutive law for dense granular flows. *Nature, 441*(7094), 727-730.

Knight, P. (2004). Challenges in granulation technology. *Powder Technology, 140*(3), 156-162.

Knight, P. C., Johansen, A., Kristensen, H. G., Schaefer, T., & Seville, J. P. K. (2000). An investigation of the effects on agglomeration of changing the speed of a mechanical mixer. *Powder Technology, 110*(3), 204-209.

Laurent, B. F. C. (2005). Structure of powder flow in a planetary mixer during wet-mass granulation. [doi: 10.1016/j.ces.2005.02.011]. *Chemical Engineering Science, 60*(14), 3805-3816.

Laurent, B. F. C., Bridgwater, J., & Parker, D. J. (2002). Convection and segregation in a horizontal mixer. *Powder Technology, 123*(1), 9-18.

Le, P. K., Avontuur, P., Hounslow, M. J., & Salman, A. D. (2011). A microscopic study of granulation mechanisms and their effect on granule properties. *Powder Technology, 206*(1-2), 18-24.

Lemieux, M., L\'eonard, G., Doucet, J., Leclaire, L.-A., Viens, F., Chaouki, J., et al. (2007). Large-scale numerical investigation of solids mixing in a V-blender using the discrete element method. *Powder Technology, 181*, 205-216.

Li, H. M., & McCarthy, J. J. (2003). Controlling cohesive particle mixing and segregation. *Physical Review Letters, 90*(18).

Li, H. M., & McCarthy, J. J. (2005). Phase diagrams for cohesive particle mixing and segregation. *Physical Review E, 71*(2), 021305.

Li, H. M., & McCarthy, J. J. (2006). Cohesive particle mixing and segregation under shear. *Powder Technology, 164*(1), 58-64.

Li, J., Freireich, B., Wassgren, C., & Litster, J. D. (2011). A general compartment-based population balance model for particle coating and layered granulation. *Aiche Journal*, n/a-n/a.

Litster, J., & Ennis, B. (2004). *The science and engineering of granulation processes*. Dordrecht; Boston: Kluwer Academic Publishers.

Liu, L., & Litster, J. (2002). Population balance modelling of granulation with a physically based coalescence kernel. [doi: DOI: 10.1016/S0009-2509(02)00110-0]. *Chemical Engineering Science, 57*(12), 2183-2191.

Liu, L. X., Litster, J. D., Iveson, S. M., & Ennis, B. J. (2000). Coalescence of deformable granules in wet granulation processes. *Aiche Journal, 46*(3), 529-539.

Liu, Y., & Cameron, I. T. (2003). A new wavelet-based adaptive method for solving population balance equations. *Powder Technology, 130*(1-3), 181-188.

Lumay, G., & Vandewalle, N. (2010). Flow of magnetized grains in a rotating drum. *Physical Review E, 82*(4), 040301.

McCarthy, J. J., Khakhar, D. V., & Ottino, J. M. (2000). Computational studies of granular mixing. *Powder Technology, 109*(1-3), 72-82.

MiDi, G. D. R. (2004). On dense granular flows. *European Physical Journal E, 14*(4), 341-365.

Mort, P. (2009). Scale-up and control of binder agglomeration processes — Flow and stress fields. [doi: 10.1016/j.powtec.2008.04.022]. *Powder Technology, 189*(2), 313-317.

Muguruma, Y., Tanaka, T., & Tsuji, Y. (2000). Numerical simulation of particulate flow with liquid bridge between particles (simulation of centrifugal tumbling granulator). [doi: 10.1016/S0032-5910(99)00226-0]. *Powder Technology, 109*(1-3), 49-57.

Ottino, J. M., & Khakhar, D. V. (2000). Mixing and segregation of granular materials. *Annual Review of Fluid Mechanics, 32*, 55-91.

Oullion, M., Reynolds, G. K., & Hounslow, M. J. (2009). Simulating the early stage of high-shear granulation using a two-dimensional Monte-Carlo approach. *Chemical Engineering Science, 64*(4), 673-685.

Paul R, M. (2009). Scale-up and control of binder agglomeration processes — Flow and stress fields. [doi: 10.1016/j.powtec.2008.04.022]. *Powder Technology, 189*(2), 313-317.

Pearson, J. M. K., Hounslow, M. J., & Instone, T. (2001). Tracer studies of high-shear granulation: I. Experimental results. *Aiche Journal, 47*(9), 1978-1983.

Peters, F., & Lemaire, E. (2004). Cohesion induced by a rotating magnetic field in a granular material. *Physical Review E, 69*(6), 061302.

Pietsch, W. (2002). *Agglomeration processes : phenomena, technologies, equipment*. Weinheim: Wiley-VCH.

Poon, J. M. H., Immanuel, C. D., Doyle, F. J., & Litster, J. D. (2008). A three-dimensional population balance model of granulation with a mechanistic representation of the nucleation and aggregation phenomena. *Chemical Engineering Science, 63*(5), 1315-1329.

Radjai, F., & Richefeu, V. (2009). Bond anisotropy and cohesion of wet granular materials. *Philosophical Transactions of the Royal Society a-Mathematical Physical and Engineering Sciences, 367*(1909), 5123-5138.

Ramachandran, R., Immanuel, C. D., Stepanek, F., Litster, J. D., & Doyle Iii, F. J. (2009). A mechanistic model for breakage in population balances of granulation: Theoretical kernel development and experimental validation. [doi: DOI: 10.1016/j.cherd.2008.11.007]. *Chemical Engineering Research and Design, 87*(4), 598-614.

Ramaker, J. S., Jelgersma, M. A., Vonk, P., & Kossen, N. W. F. (1998). Scale-down of a high-shear pelletisation process: Flow profile and growth kinetics. *International Journal of Pharmaceutics, 166*(1), 89-97.

Ramkrishna, D. (2000). *Population Balances*: Academic Press.

Reynolds, G. K., Fu, J. S., Cheong, Y. S., Hounslow, M. J., & Salman, A. D. (2005). Breakage in granulation: A review. [doi: DOI: 10.1016/j.ces.2005.02.029]. *Chemical Engineering Science, 60*(14), 3969-3992.

Richefeu, V., El Youssoufi, M. S., Peyroux, R., & Radjai, F. (2008). A model of capillary cohesion for numerical simulations of 3D polydisperse granular media. *International Journal for Numerical and Analytical Methods in Geomechanics, 32*(11), 1365-1383.

Rognon, P. G., Roux, J. N., Naaim, M., & Chevoir, F. (2008). Dense flows of cohesive granular materials. *Journal of Fluid Mechanics, 596*, 21-47.

Rynhart, P. R. (2004). *Mathematical modelling of granulation processes.* Massey University, Palmerston North.

Saito, Y., Fan, X. F., Ingram, A., & Seville, J. P. K. (2011). A new approach to high-shear mixer granulation using positron emission particle tracking. *Chemical Engineering Science, 66*(4), 563-569.

Salman, A. D., Ghadiri, M., & Hounslow, M. J. (2007). *Particle Breakage*: Elsevier Science.

Salman, A. D., Hounslow, M. J., & Seville, J. P. K. (2007). *Granulation*: Elsevier Science.

Seville, J. P. K., Willett, C. D., & Knight, P. C. (2000). Interparticle forces in fluidisation: a review. *Powder Technology, 113*(3), 261-268.

Sherrington, P. J., & Oliver, R. (1981). *Granulation*. Philadelphia: Heyden.

Sokolovskii, V. V. (1965). *Statics of granular media*. Oxford; New York: Pergamon Press.

Soulie, F., El Youssoufi, M. S., Cherblanc, F., & Saix, C. (2006). Capillary cohesion and mechanical strength of polydisperse granular materials. *European Physical Journal E, 21*(4), 349-357.

Sundaresan, S., Eaton, J., Koch, D. L., & Ottino, J. M. (2003). Appendix 2: Report of study group on disperse flow. *International Journal of Multiphase Flow, 29*(7), 1069-1087.

Tan, H. S., Salman, A. D., & Hounslow, M. (2004). Kinetics of fluidised bed melt granulation - IV. Selecting the breakage model. *Powder Technology, 143*, 65-83.

Tan, H. S., Salman, A. D., & Hounslow, M. J. (2005). Kinetics of fluidised bed melt granulation III: Tracer studies. [doi: 10.1016/j.ces.2005.02.009]. *Chemical Engineering Science, 60*(14), 3835-3845.

Tardos, G. I., Khan, M. I., & Mort, P. R. (1997). Critical parameters and limiting conditions in binder granulation of fine powders. *Powder Technology, 94*(3), 245-258.

Verkoeijen, D., Pouw, G. A., Meesters, G. M. H., & Scarlett, B. (2002). Population balances for particulate processes - a volume approach. *Chemical Engineering Science, 57*(12), 2287-2303.

Weigert, T., & Ripperger, S. (1999). Calculation of the Liquid Bridge Volume and Bulk Saturation from the Half-filling Angle. *Particle \& Particle Systems Characterization, 16*(5), 238-242.

Wildeboer, W. J., Litster, J. D., & Cameron, I. T. (2005). Modelling nucleation in wet granulation. [doi: 10.1016/j.ces.2005.02.005]. *Chemical Engineering Science, 60*(14), 3751-3761.

Xu, Q., Orpe, A. V., & Kudrolli, A. (2007). Lubrication effects on the flow of wet granular materials. *Physical Review E, 76*(3), 031302.

Zhao, H. B., & Zheng, C. G. (2009). A new event-driven constant-volume method for solution of the time evolution of particle size distribution. *Journal of Computational Physics, 228*(5), 1412-1428.

Zhou, Y. C., Wright, B. D., Yang, R. Y., Xu, B. H., & Yu, A. B. (1999). Rolling friction in the dynamic simulation of sandpile formation. *Physica A, 269*, 536-553.

Zhu, H. P., Zhou, Z. Y., Yang, R. Y., & Yu, A. B. (2007). Discrete particle simulation of particulate systems: Theoretical developments. *Chemical Engineering Science, 62*(13), 3378-3396.